SUPERSONIC WIND-TUNNEL —NOZZLE DESIGN AND CONTROL SYSTEM ANALYSIS

BY R.H.T. COX

Submitted to the University of Cape Town,
Mechanical Engineering Department for
consideration of a Master of Science Degree
in Engineering

June, 1972

ACKNOWLEDGEMENTS

The author would like to express his sincere thanks to his advisory committee, Mr. J. Gryzagoridis, Mr. R.M. Stegen and Mr. J.E. Newmarch, for their guidance, help and encouragement at all times and to Mr. S.G. McLaren for his assistance with the analogue computer. He is most grateful to the technical staff, Mr. W.K. Bettesworth, Mr. J. Busbridge, Mr. J.R. Gordon and Mr. D.M. Finlayson, for their patience and the quality of the equipment built in the workshops.

The author is indepted to the Department of Mechanical Engineering for the opportunity to undertake this research and to the South African Council for Scientific and Industrial Research (C.S.I.R.) for the financial assistance that has enabled him to further his education.

Finally, the author is grateful to Mrs.L. Edwards for her offer to type this thesis and to all those who volunteered assistance in checking this work.

ABSTRACT

Symmetrical two-dimensional nozzles were designed for the supersonic wind-tunnel, in the Department of Mechanical Engineering, using both analytical and semi-graphical methods obtained from the theory of Characteristics. These nozzles, designed for an optimum running time of 30 secons, have a Mach number of 2,35. Boundary layer growth was considered by displacing the nozzle contours outwards by the equivalent displacement thickness, while keeping the vertical tunnel side walls parallel.

The five probe pitot calibration results, taken through the central vertical plane in the tunnel test-section, showed Mach number standard deviations about the mean of 0,638% and 1,004% for the analytical and semi-graphical design respectively. These results compare very favourably with those of other wind-tunnels.

Without pressure recovery the critical flow pressure ratio through the tunnel for Mach 2,35 nozzles, is 2,53. Therefore it may be shown that the subsonic diffuser, and the silencer incorporated into it, is about 75% efficient.

The analysis and modification to the existing settling chamber control valve yielded improvements in performance.

1. The maximum fluctuation in settling chamber pressure was kept to within 5,5% for most operating conditions.
2. Critical valve response was achieved by applying a suitable bypass orifice to the damping cylinder - The valve settled down within one second after flow had been initiated.

A proposed variable symmetrical nozzle was examined for the feasibility of its application to the existing supersonic wind-tunnel.

TABLE OF CONTENTS

NOMENCLATURE

Symbol	Property	Units
A	Area	ft^2
C_v	Specific heat at constant volume	$btu/lb_m{}^oR$
C	Acoustic velocity	ft/sec
F	Force	lbf
g_c	gravitational acceleration	ft/sec^2
h	Enthalpy	btu/lb_m
$\dot{M}$	Mass flow rate of air	lbm/sec
M	Mass of air	lbm
M	Mach Number, $\frac{V}{C}$	dimensionless
P	Pressure	lbf/ft^2
R	Universal Gas Constant	$ft\ lbf/lb_m{}^oR$
S	Entropy	$btu/lb_m{}^oR$
T_t	$Temperature_{time}$	$^oR_{secs}$
V	Velocity	ft/sec
V	Volume	ft^3
X, Y	Co-ordinates on the perpendicular X and Y axes	ft
γ	Ratio of specific heats c_p/c_v	dimensionless
π	Constant = 3,1416	radians

Nomenclature applicable to Chapter 1:

C+, C-	Characteristics in the physical plane (left? right?)	-
C*	Critical speed of sound for isentropic flow	ft/sec
l	Distance down nozzle from throat	ft
M*	Critical Mach number $\frac{V}{C^*}$	dimensionless
N	Number of reflections	-
Q	Volume flow rate	ft^3/sec
R_R	Reynolds Number $\frac{\rho v l}{\mu}$	dimensionless
α	Mach wave angle	degrees/Radians
δ	Boundary layer thickness	feet
δ^*	Displacement thickness	feet
δ_{equ}	Equivalent displacement thickness	feet
η_d	Diffuser Efficiency	%
μ	Absolute viscosity co-efficient	$\frac{slug\ sec}{ft}$

ω	Defined by equation 1.16	-
θ	Inclination of vector velocity to X-axis	degrees/radians
I, II	Characteristic Co-ordinates	-, -

Subscripts:

t	Settling chamber stagnation conditions
b	Back or exit conditions
∞	Atmospheric conditions
1	Test Section Conditions
01,02	Stagnation conditions at points 1 and 2
di	Initial storage drum conditions
df	Final storage drum conditions
*	X, Y co-ordinates at nozzle throat
i	" at inflection point
e	" at exit of nozzle
s	" at nozzle inlet.

Nomenclature applicable to Chapter 2:

B	Constant of integration	-
BM	Bending Moment	lbf ft
C	Constant of integration	-
D	Constant of integration	-
E	Modulus of Elasticity	lbf/in^2
f	Deflection of beam	feet
G	Constant of integration	-
I	Moment of inertia	ft^4
$K_{1,2}$	Constants in beam theory	-
l	Length of Beam	feet
$R_{A,B}$	Reactions at beam supports, A and B	lbf
r	Radius of curvature of beam	feet
t	Beam thickness	feet
W	Concentrated load on beam	lbf
$\omega_{1,2}$	Uniform load on beam	lbf/ft

Nomenclature applicable to Chapter 3:

a	Magnitude scale factor	-

$B_{1,2,3,}$	Constants; $C_{1,2,3,4}$ Constants	-
C_{nl}	Non-linear damping coefficient	$\frac{lb\ sec^2}{ft^2}$
C_l	Linear damping coefficient	$\frac{lb\ sec^2}{ft^2}$
E	Bulk Modulus	lbf/in^2
H	constant	-
I	Constant	-
K_1	Valve coefficient of mass flow rate	$\frac{lbm\ ft}{sec\ lbf}$
K_2	Nozzle coefficient of mass flow rate	$\frac{lbm\ ft2}{sec\ lbf}$
k	Stiffness coefficient (spring)	lbf/ft
L	Constant	-
N	Constant	-
n	Time scale factor	-
$\dot{P}$	Rate of change of Pressure	$lbf/ft^2 sec$
$\dot{X}$	Velocity in terms of displacement X	ft/sec
$\ddot{X}$	Acceleration in terms of displacement X	ft/sec^2
α	Defined by equation 3.8	-
ψ	Phase angle-constant	degrees/radians
μ	Static coefficient of friction	dimensionless
τ	Computer unit of time	secs.

Subscripts:

d	Variable storage drum conditions
i	Initial storage drum conditions
s	Settling chamber conditions
sett	Desired stagnation conditions
total	Total initial controlling force on valve
p	Piston properties
V	Valve properties.

by mach lines, whereas in the lattice-point method, the stream properties are found at the lattice points of the mach net.

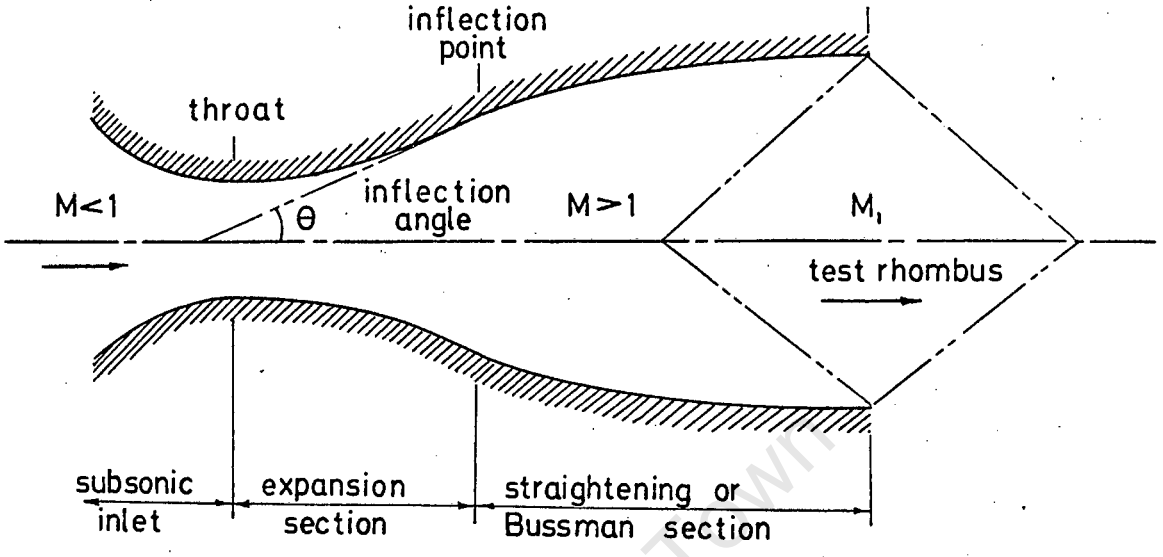

SUPERSONIC NOZZLE

Figure 1

For the very rapid and accurate design of the nozzle contours, especially using a computer, K. Foelsh (1) in 1946 produced an analytical solution. He developed his equations from the theory of characteristics assuming that radial flow exists at the inflection point. (Figure 1). Similarly, Atkin (1) based his analysis on the same principles, but included a straight section at the inflection point.

Boundary Layer Growth

As the motion of both viscous and compressible flows involve extreme mathematical complications, certain simplifying assumptions must be made. Prandtl (1) pointed out that for a fluid of low viscosity, the viscous effects are confined to a narrow band near the solid boundary of the flow field, i.e. in the boundary layer. Outside this boundary layer, the fluid flow can be considered as perfectly isentropic.

Nozzle profiles are calculated assuming inviscid flow; allowances must be made for boundary-layer growth by displacing this potential outline away from the nozzle centreline. There are many papers dealing with generalised boundary-layers, but this approach is often undesirable in estimating the boundary-

which?

layer allowances in supersonic nozzles. Tucker, Ruptash, Shen (1) experimented with boundary-layers in 1952, basing their theory on Von Kármáns (1) momentum equation. Rogers and Davis (4) drew attention to the more satisfactory methods based on Reynold's Number and suggested suitable approximate formulae for turbulent boundary layer growth with moderate supersonic mach numbers.

Altman (5) carried out an investigation on turbulent boundary layer growth to provide the necessary experimental results needed to substantiate the theories compiled by Oosthuizen (5). The results compared favourably, but the limit on the range of Reynold's Number in the test section restricted a complete comparison somewhat.

Testing of Supersonic Nozzles

Numerous publications offer methods of nozzle calibration.

Harrop, Bright, Salmon and Caiger (6) designed and tested non-symmetrical nozzles, i.e. the nozzle contour was formed on one side of the tunnel only, the other forming the centreline. The mach number distribution was measured along this 'centreline' by means of a series of static pressure holes. From these data, they illustrated how the mach number distribution could be improved with slight modifications to the nozzle profile. Their theory of sonic flow at the throat of the nozzle was confirmed experimentally. The results showed the sonic line to be curved; this possibly having an adverse effect on some assumptions made in nozzle theory.

Fallis, Johston, Lee, Tucker and Wade (7) presented more versatile calibrating techniques using pitot and static pressure rakes. They emphasised the greater degree of accuracy of the pitot readings over the static pressure measurements and substantiated it with theoretical analysis.

Supersonic Diffusers

The high stagnation pressures required for supersonic flow has produced a need for a better understanding of the supersonic diffuser and static pressure recovery.

Following the lead of Crocco (8), who in 1935 delved into pressure recovery across shocks in divergent ducts, Lukasiewicz (8) presented a systematic treatment on the design and performance of supersonic diffusers. He illustrated how the critical diffuser (one that just allowed a normal shock to propagate down the tunnel without choking the diffuser throat) enabled the stagnation or settling chamber pressure to be reduced after flow has been initiated. Comparative data, from many of the existing wind-tunnels of that time, were presented. Further pressure energy recovery entailed a variable diffuser so that the throat area could be decreased during the tunnel operation. Maximum recovery was then possible when flow could be reduced to sonic speeds at the diffuser throat. This technique would only be applied to continuous flow wind-tunnels because of the time needed for the diffuser adjustments.

Types of Wind-Tunnel

Supersonic wind-tunnels may be classified into two main types; the continuous flow and intermittent flow type. These again would be sub-classified according to their design and principle of operation.

The phenominal power requirements, initial cost and subsequent running costs of the continuous flow wind-tunnel, make it prohibitive to most institutions. Hence the intermittent tunnel is favoured.

Of the intermittent wind-tunnels, two types are commonly used:

a) Vacuum storage drive allows air at atmospheric pressure to pass through the nozzle into a large evacuated vessel.
b) Pressure storage driver, relying on the flow of air from a high pressure storage vessel through the nozzle to atmosphere. (See Figure 2).

The advantages of the blow-down wind-tunnel over the former are:

1) The stagnation pressures are higher and controllable as well.
2) The reduced storage volume for the same mass transfer of air, leads to a smaller drum size.
3) The compressor aftercooler assists in removing some of the moisture of the air. This, plus the increased air density allows a reduced drying unit size.

4) The overall construction is cheaper.

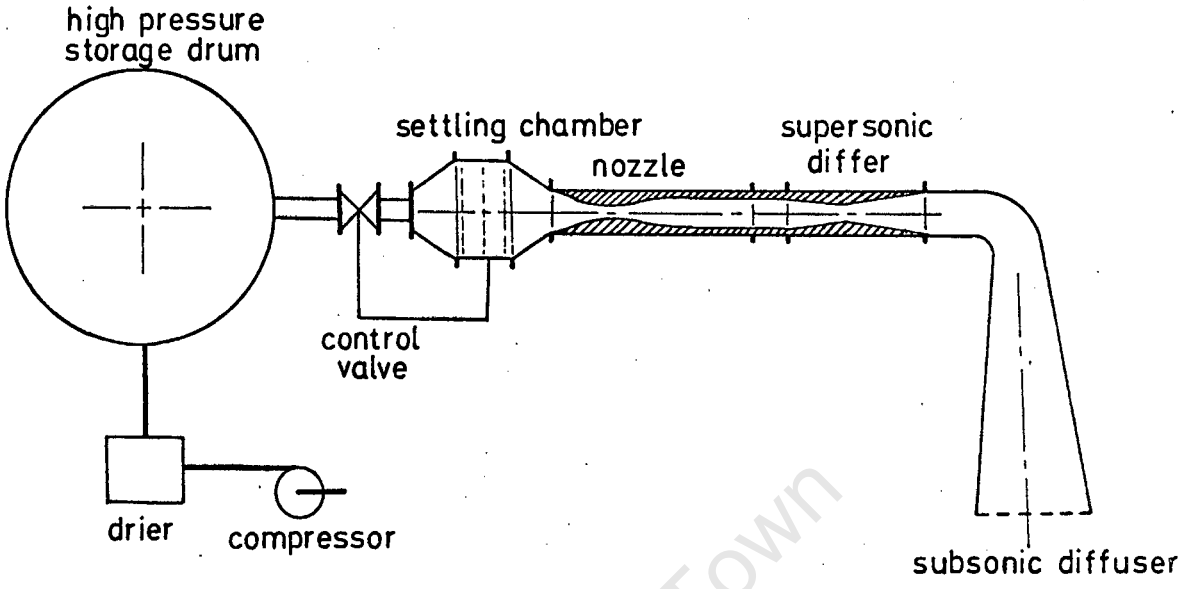

SUPERSONIC BLOW-DOWN WIND-TUNNEL
Figure 2

Settling Chamber Control Valve

In a blow-down supersonic wind-tunnel, the settling chamber pressure must be kept constant while the supply drum pressure gradually falls. The control of this settling chamber pressure is achieved by means of a regulating valve which is preset to a desired stagnation pressure.

Two types of valve are generally available:

1) Butterfly or flap valve.
2) Spool or piston valve.

The latter is not entirely suited to the accurate control of the settling chamber pressure but is much cheaper and more readily available and adaptable than the preferred butterfly valve.

The analysis of a regulating valve automatic system is important for its efficient operation.

In recent years automatic control systems have rapidly been advancing in importance. The applications cover a wide scope, from precision control devises for inertial guidance, to design of massive equipment for control of

the manufacture of steel or other industrial processes. (9)

The theoretical solution of such control systems can become extremely tedious especially if non-linearities are present, as pointed out by Dransfield (9). The analog computer has become a very useful tool in solving these complex control systems. By simulating all the original control properties on the computer the performance characteristics of the system may be quickly and easily achieved. Peterson (10) indicates the limitations of the computer and presents the time and magnitude scaling methods that overcome these difficulties.

CHAPTER 1

SUPERSONIC WIND-TUNNEL DESIGN

EXISTING APPARATUS

The supersonic wind-tunnel in the Department of Mechanical Engineering, University of Cape Town, is intermittently operated by blow-down from a high pressure storage vessel. Figure 1.1 presents a schematic sketch of the system and control.

The air is supplied by a twin cylinder Atlas Corpco air compressor, delivering 130 cu.ft. per minute at 165 lbs. per sq. inch gauge. It takes approximately 20 minutes to pump up the storage vessel to 150 lbs. per sq. inch gauge. The air is passed through a water cooled after-cooler when leaving the compressor and enters into a small receiver.

Moisture is removed as the air is passed through the water-trap and drier. This drier consists of two beds containing about 50 lbs. of silica-gel. These beds, designed to be used alternately, are regenerated by a small blower and heating unit. It is necessary to reduce the moisture content of the air to prevent condensation in the tunnel test-section during a run.

The storage drum has a volume of 165 cubic feet. To maintain a reasonably constant temperature in the tunnel during a run, it is packed with approximately 1,200 lbs. of tin plate offcuts. These act as a thermal storage, giving off heat as the drum temperature falls. Hence, the total decrease in temperature is kept to within $25^{o}F$ for a full run (11).

The control valve is required to effect the rapid release and shut-down of supply air to the wind-tunnel and to maintain a reasonably constant settling chamber pressure. The double seat of this spool valve is necessary to balance the pressures acting across it, while the displacement control is achieved by a pressure differential across the flexible control diaphram.

The wind-tunnel is divided into four main sections:

Settling Chamber

The settling chamber is designed primarly to reduce turbulence in the air stream before it enters the supersonic nozzle. The air flow velocity is reduced sufficiently so that a series of mesh screens and a honeycomb can straighten and dampen out turbulence in the supply air.

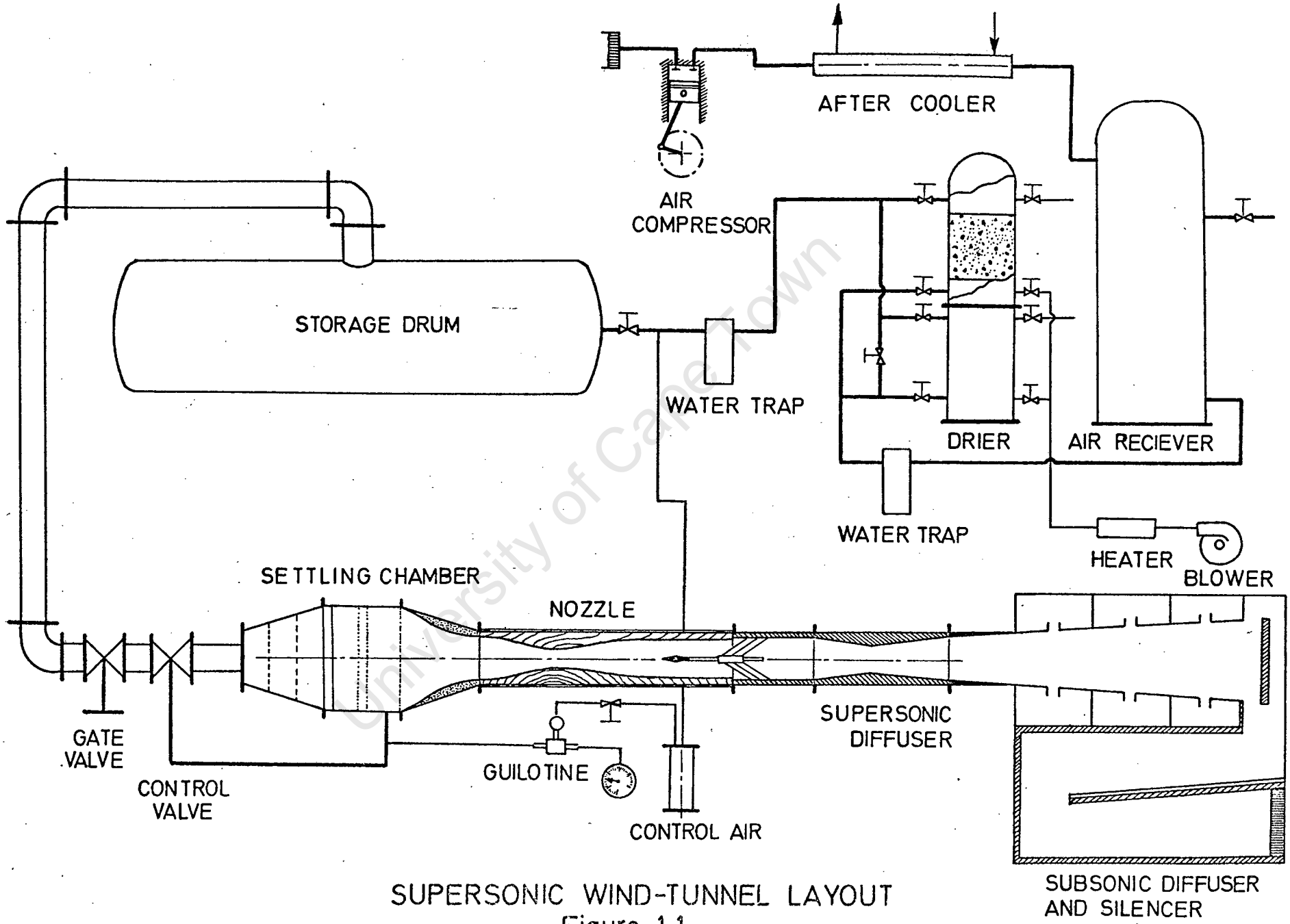

SUPERSONIC WIND-TUNNEL LAYOUT
Figure 1.1

By virtue of the low velocities in the settling chamber, a static pressure tapping located in one of the faces after the screens, offers a satisfactory average value for the total stagnation pressure of the system.

Nozzle

The converging - diverging nozzles are designed to accelerate the air so that when it leaves the nozzle it is uniform, parallel and at the desired supersonic velocity. These two-dimensional nozzles are to be machined from wooden blocks and incorporated in the top and bottom covers of the nozzle box. Because of the character of supersonic flow, the exit mach number is dependant upon the exit to throat area ratio only.

Test-Section

The rectangular test-section, that maintains uniform steady flow, has a nominal cross-section of 4 x 2 inches. The test pieces are supported in the test-section by means of an aerodynamic sting which straddles the tunnel vertically just beyond the nozzle box. The side panels, enclosing the test-section, consist of 1.0 inch thick glass set into steel frames so that flow visualization techniques may be applied.

Diffuser

The diffuser for this tunnel may be sub-classified into three sections:

1) The supersonic diffuser recovers pressure energy by means of a normal shock, induced in the supersonic air flow, by a change in tunnel cross-sectional area.
2) The subsonic diffuser regains static pressure by slowing the subsonic air 'isentropically' in a divergent duct.
3) Incorporated in this subsonic diffuser, is a specially designed silencer that keeps the noise level down.

PART 1
OPTIMUM BLOW-DOWN TIME

1.1 INTRODUCTION

Two methods were applied in the design of symmetrical nozzles for the small blow-down wind-tunnel as defined below.

1) Semi-Graphical Nozzle Design - This design requires the application of the method of characteristics, with the aid of a hodograph, to the field method of graphical construction.

2) Analytical Nozzle Design - The contours are defined by a set of equations derived by Foelsch (1) which are also based on the theory of characteristics.

The running time of the intermittent wind-tunnel is defined as the period of blow-down available before the storage pressure has dropped so low that the regulating valve cannot retain the desired settling chamber pressure. Because of the short running time available, it was advisable that the nozzles should be designed for the optimum time of run. The minimum stagnation pressure required to initiate supersonic flow in these nozzles will be used as a criterion in this estimation.

There are two factors that determine the available run time of the tunnel.

1) The nozzle design mach number determines the test-section to throat area ratio. As the test-section area is nominally kept constant, an increase in design mach number is associated with a decrease in nozzle throat area. Also, the minimum stagnation pressure for supersonic flow increases with increasing mach number. Hence the mass flow rate $\dot{m}$, through the wind-tunnel alters accordingly.

2) The available mass of air in the storage vessel is reduced with an increase in settling chamber pressure.

(See Figure 1.3)

1.2 ASSUMPTIONS

Certain assumptions must be made in order to simplify conditions such that a feasible solution can be obtained in the derivation of run times.

The minimum settling chamber or stagnation pressure will be determined by the degree of pressure recovery across a normal shock in the supersonic test-section and the subsonic diffuser efficiency.

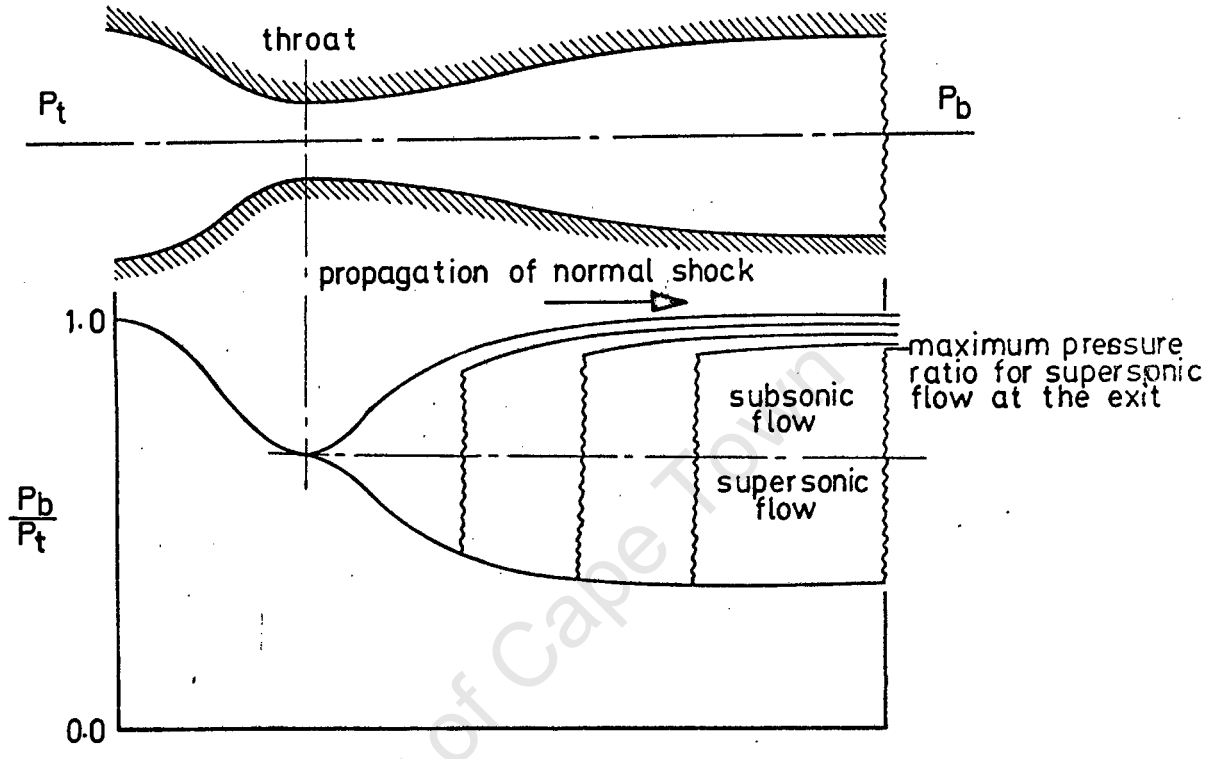

STATIC PRESSURE DISTRIBUTION CURVE

Figure 1.2

As the stagnation pressure increases from atmospheric pressure, subsonic flow initially occurs throughout the whole wind-tunnel. When sonic velocities are reached in the nozzle throat, a normal shock will develop and with further increase in stagnation pressure, will propagate downstream through the tunnel test-section. Once this shock has been displaced to the test-section exit, the stagnation pressure will be the minimum that will retain supersonic flow.

(See Figure 1.2)

A temperature drop of about $25^{\circ}F$ is experienced over a full run period. The initial stagnation temperature may be taken as $65^{\circ}F$ ($545^{\circ}R$).
- Reference (11).

A pressure drop exists between the storage drum and the settling chamber. This is shown to have a magnitude of about 25 lbs. per sq. inch as the run terminates (12). Turbulence, restrictions and duct friction are responsible

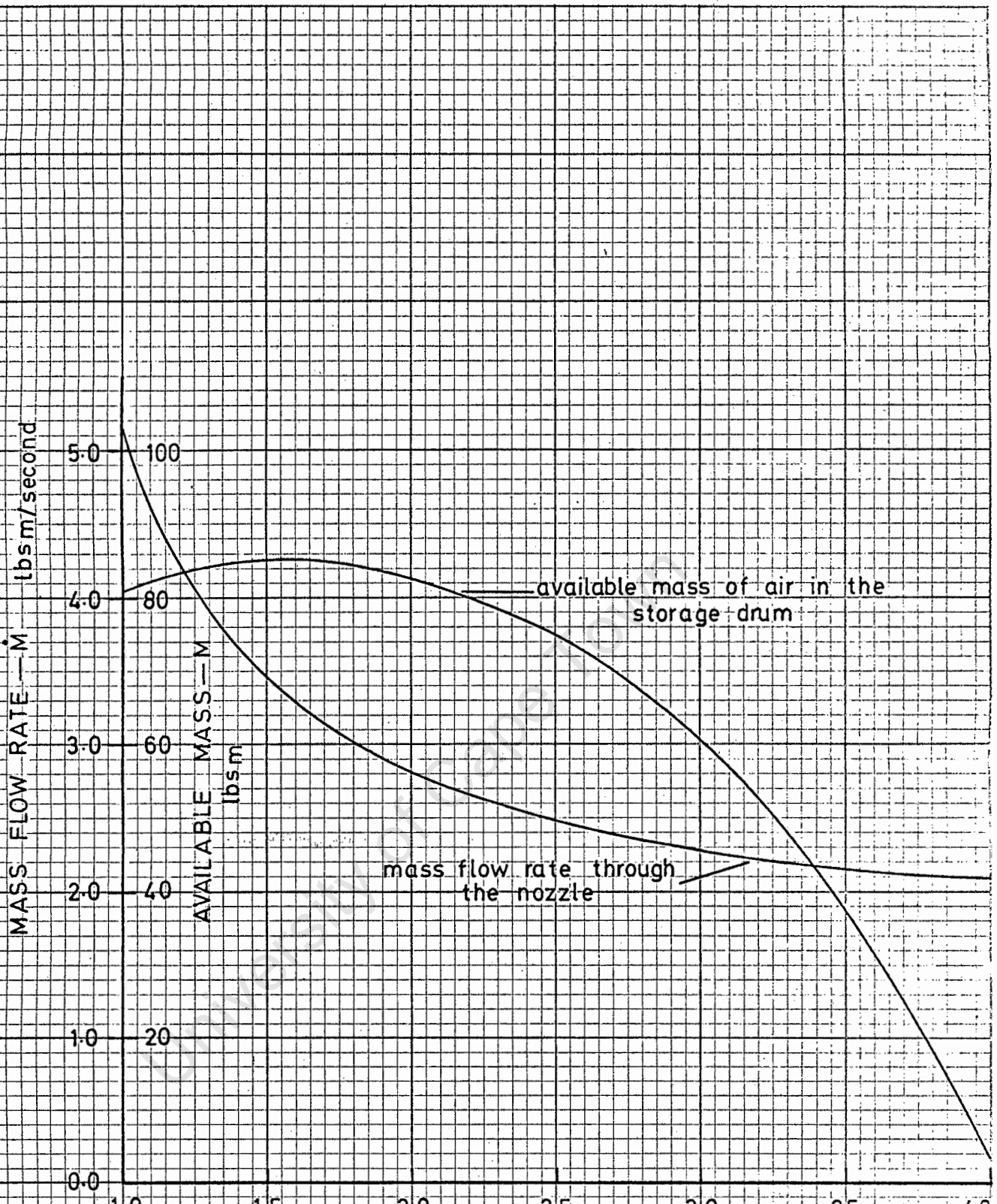

AVAILABLE MASS
AND
MASS FLOW RATE

Figure 1·3

for these losses which may increase with increased mass flow rate.

Both the stagnation pressure and the mass flow rate are assumed constant for the duration of a run.

1.3 OPTIMUM NOZZLE CHOICE

Stagnation Pressure:

The minimum stagnation pressure corresponding to increasing mach number must be determined. Refer to Figure 1.4. For a given mach number M_1, for the nozzle, the static-stagnation pressure ratio P_1/P_t can be determined. Similarly for a shock at that mach number, the static pressure recovery ratio, P_b/P_1, can be determined.

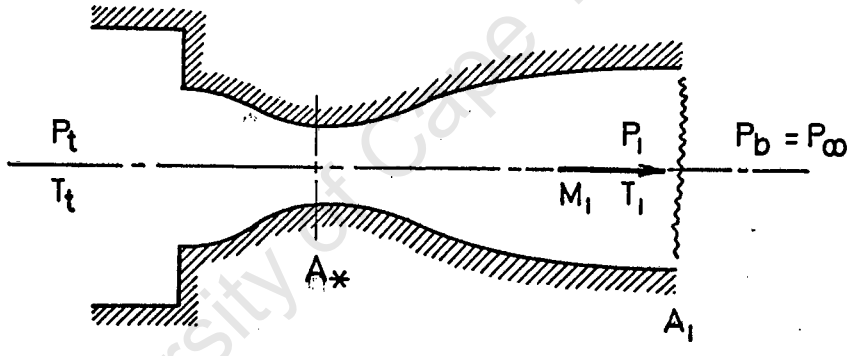

SUPERSONIC NOZZLE
Figure 1.4

Therefore the stagnation pressure can be found in terms of the back or atmospheric conditions.

$$P_t = \frac{P_t}{P_1} \times \frac{P_1}{P_b} \times P_\infty \qquad \ldots\ldots 1.1$$

This minimum stagnation pressure, P_t, for mach numbers increasing from unity, is plotted on Figure 1.6.

Mass Flow Rate:

Mass flow rate of air (13):

$$\dot{m} = \rho . A v$$

$$\therefore \quad \dot{m} = \frac{P_1}{RT_1} A_1 M_1 \sqrt{\gamma g_c RT_1} \qquad \ldots\ldots 1.2$$

Substitute in the known values of the constants and the test-section cross-sectional area, A_1

$$\therefore \quad \dot{m} = 7{,}344 \frac{P_1}{T_1} M_1 \sqrt{T_1}$$

The static pressure and temperature, P_1 and T_1 can be determined for any mach number, M_1 knowing the stagnation conditions. Tables in (13) present these relationships.

This above equation is described on figure 1.3 in terms of increasing Mach number.

Available Mass:

The available mass of air for blow-down is determined by the stagnation pressure required in the settling chamber.

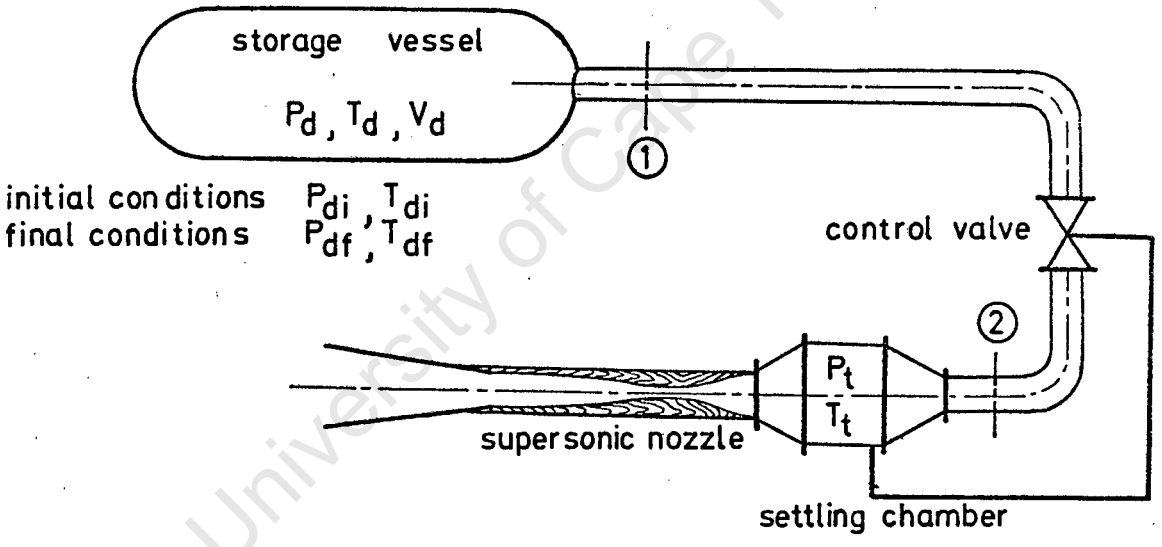

SUPERSONIC WIND-TUNNEL

Figure 1.5

The total pressure loss, P_L, between states (1) and (2) at the termination of the run, is assumed to be 25 lbs per sq.in. Therefore the lower limit of the storage vessel pressure is greater than the settling chamber pressure by this amount.

$$\text{i.e.} \quad P_{df} = P_t + P_l$$

The initial mass in the storage drum is given by:

$$M_i = \frac{P_{di} V_d}{R T_{di}}$$

The final mass remaining in the drum after the flow has terminated is:

$$M_f = \frac{P_{df}\ V_d}{R\ T_{df}} = \frac{(P_t + P_l)\ V_d}{R\ T_{df}}$$

The mass of air available for discharge through the nozzle is given by the difference between the initial and final mass.

$$M_{available} = \left(\frac{P_{di}}{T_{di}} - \frac{(P_t + P_l)}{T_{df}}\right) \cdot \frac{V_d}{R} \quad \ldots\ldots\ldots\ldots 1.3$$

All these are known except for the variable P_t and $M_{available}$. The critical stagnation pressure, P_t, is defined for various Mach numbers, so that the available mass may be plotted on figure 1.3 in terms of Mach numbers.

Optimum Run Time:

The curves plotted on figure 1.3 show that the mass flow rate decreases with increasing Mach number (i.e. The throat area decreases at a much greater rate than the increase in minimum stagnation pressure - see equation 1.2). Also the available drum air mass decreases rapidly to zero above Mach numbers of 3.5.

As the first case indicates an increase in run time, the second denotes a decrease. Hence the optimum running time would occur somewhere between the Mach number limits of 1.0 to 3.5.

The running time, t, is simply determined by dividing the available mass by the mass flow rate through the nozzle.

$$\text{i.e. } t = \frac{M_{available}}{\dot{m}}$$

From equations 1.2 and 1.3:

$$t = \frac{\left(\frac{P_{di}}{T_{di}} - \frac{(P_t + P_l)}{T_{df}}\right) V_d\ T_i}{P_1 A_1 M_1 \sqrt{\gamma g_c R T_1}} \quad \ldots\ldots\ldots\ldots\ldots 1.4$$

This equation is presented on figure 1.6 for increasing Mach numbers.

This curve shows that the optimum running time for this wind-tunnel is about 30 seconds and is satisfied by a nozzle Mach number of 2.35. (Bearing in mind the assumptions of P_{lost} and T_{lost}).

The two symmetrical nozzles, applying the semi-graphical and analytical designs, were produced for this Mach number.

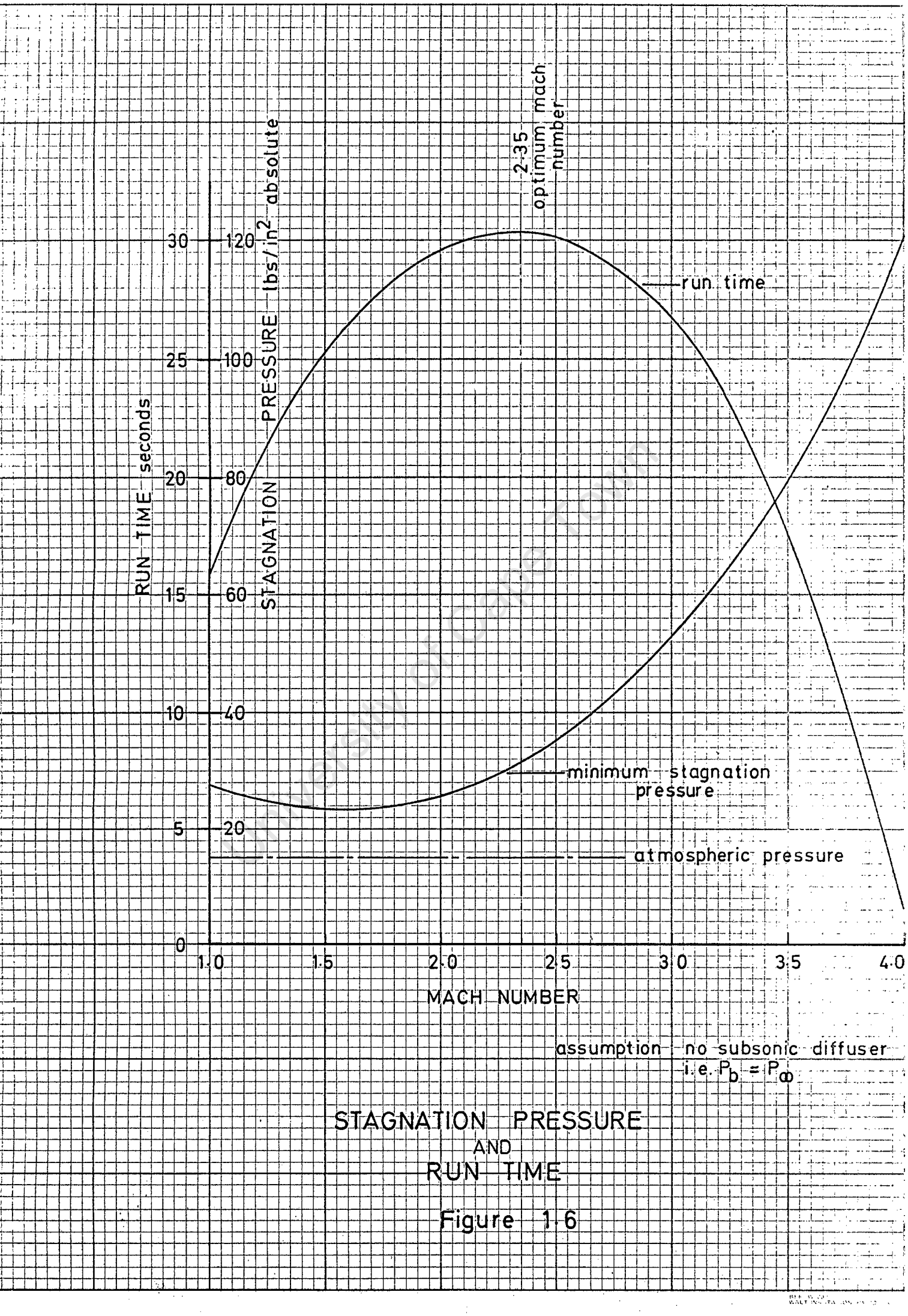

STAGNATION PRESSURE
AND
RUN TIME

Figure 1·6

PART 2
SEMI-GRAPHICAL NOZZLE DESIGN

2.1 THE THEORY OF CHARACTERISTICS

The method of characteristics discussed in this section is limited to two-dimensional, irrotational, isentropic, supersonic flow. Further assumptions are that the flow is steady, the fluid is a perfect gas and that gravity forces are negligible.

From the discussion of the theory of characteristics in appendix 1.2, the following relationship, between Mach number and change in flow direction, has been derived.

For a left-running Mach wave:

$$\theta = -\sqrt{\frac{\gamma+1}{\gamma-1}}\ \arctan\sqrt{\frac{\gamma-1}{\gamma+1}(M^2-1)} + \arctan\sqrt{M^2-1} + \text{constant} \quad \ldots\ldots 1.7$$

Because M increases to infinity at large turning angles in the Prandtl-Meyer flow, it is therefore convenient to put (1) in terms of the dimensionless ratio M^*. M^* is the ratio of the fluid velocity to the acoustic velocity of that fluid at stagnation conditions.

From the adiabatic relationship:

$$M^2 = \frac{2}{\gamma+1} M^{*2} / \left(1 - \frac{\gamma-1}{\gamma+1} M^{*2}\right)$$

Substitute into equation 1.7:

$$\therefore\ \theta = -\sqrt{\frac{\gamma+1}{\gamma-1}}\ \arctan\sqrt{\frac{M^{*2}-1}{\frac{\gamma+1}{\gamma-1} - M^{*2}}} + \arctan\sqrt{\frac{M^{*2}-1}{1 - \frac{\gamma-1}{\gamma+1} M^{*2}}} + \text{constant} \quad \ldots\ldots 1.8$$

This equation can be rewritten in a simpler form where is a function of M^* and the constant of integration, C = (2I - 1 000)

$$\therefore\ \theta_I = -\omega(M^*) + (2I - 1\,000) \quad \ldots\ldots 1.9$$

For a right-running Mach wave:

The derivation is the same as before, but with Mach waves of family I.

$$\therefore\ \theta_{II} = +\omega(M^*) + (2II - 1\,000) \quad \ldots\ldots 1.10$$

The subscript I for θ_I indicates that pressure waves of family I are absent and the process occurs at a constant value of I. Hence all the changes in flow properties take place across the Mach waves of family II. Similarly, this is true for the subscript II whereby all the changes take place across Mach waves of family I.

The complete hodograph plane is given in figure 1.11 for both the left and right running Mach waves. These hodograph curves are drawn out by computer using equations 1.9 and 1.10 (See appendix 1.3 for the flow diagram). They are each identified by a particular value of the constant I or II, as the case may be.

The boundary of this hodograph field is determined by setting M = .

Substitution into the relevant equations, gives:

$$\hat{M}^* = \sqrt{\frac{\gamma+1}{\gamma-1}} = 2{,}45$$

$$\hat{\theta} = \sqrt{\frac{\gamma+1}{\gamma-1}} \arctan(\infty) + \arctan(\infty) + \text{constant}.$$

This maximum change in streamline direction to produce an infinite Mach number, is determined for a constant equal to zero. i.e. For a characteristic wave of 500.

$$\therefore \hat{\theta} = \omega(M^*) = 130{,}5^{o}$$

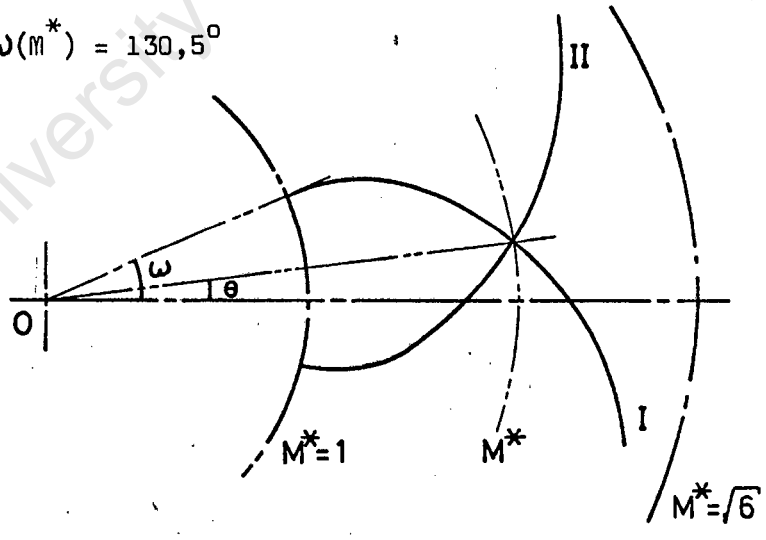

Figure 1.10

This hodograph field describes the conditions anywhere within an isentropic flow field. Each point may be represented by a particular value of I and II, and the flow direction at that point, by θ . (See figure 1.10). We also have the rule that with simple left-running waves, the Mach line at a given point in the physical plane is normal to the hodograph characteristic of the family I at the image point in the hodograph plane.

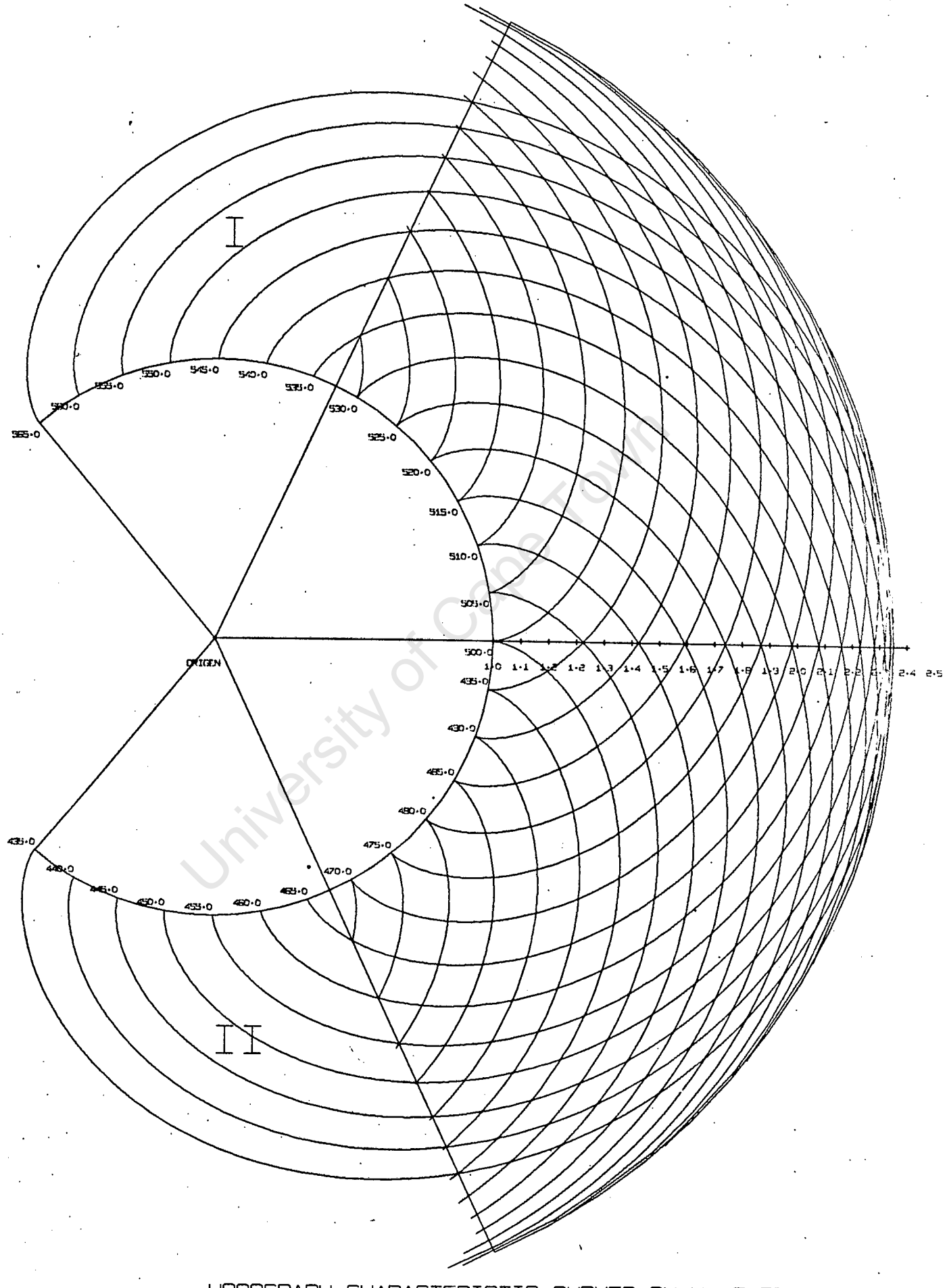

HODOGRAPH CHARACTERISTIC CURVES ON M*, THETA-PLANE

Figure 1·11

II-LEFT RUNNING MACH WAVE;CONSTANT CURVE I

I-RIGHT RUNNING MACH WAVE;CONSTANT CURVE II

2.2 DESIGN OF WIND-TUNNEL NOZZLES

One of the important practical applications of the method of characteristics is the design of two-dimensional supersonic nozzles.

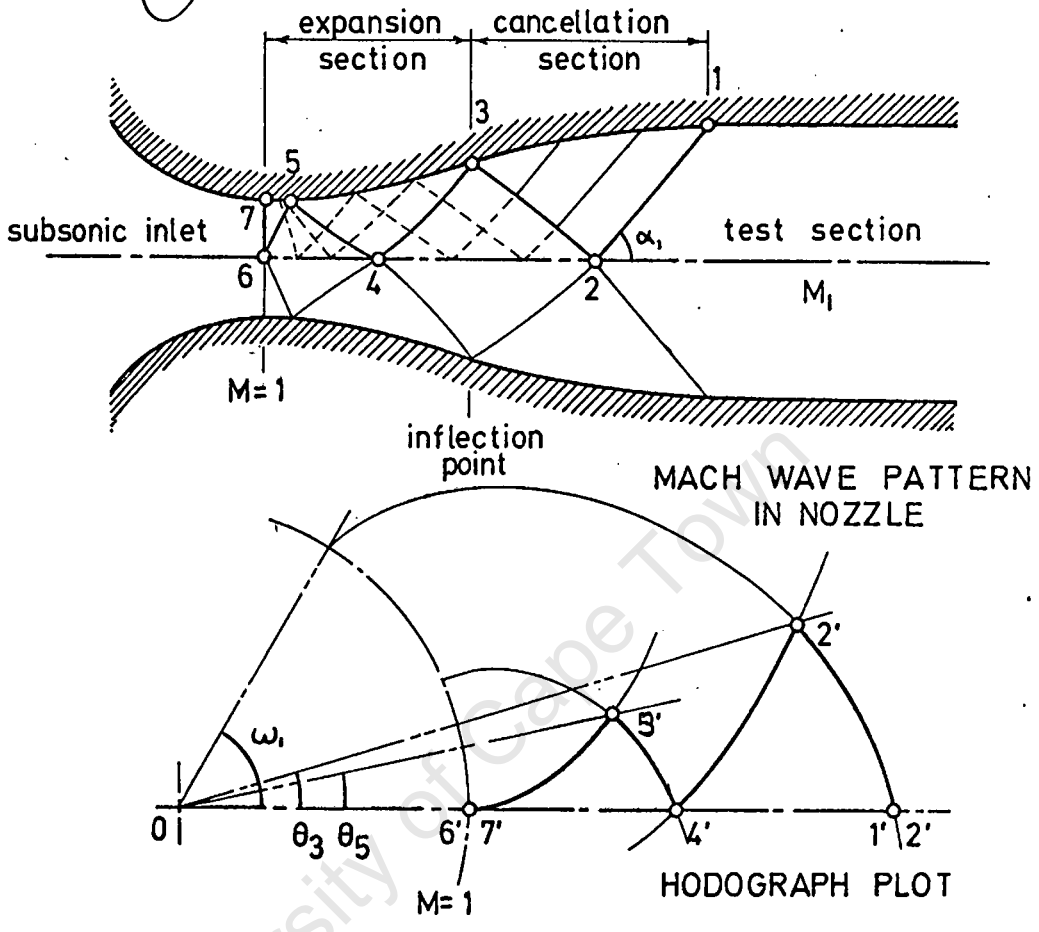

Figure 1·12

The general considerations in the design of a nozzle are illustrated in figure 1.12.

The function of the nozzle is to accelerate the sonic flow at the throat of the nozzle to the designed Mach number in the test-section so that it is uniform and parallel. As the nozzle is symmetrical about the centre-line, only the upper half need be considered:

(i) Expansion Zone:

It is bounded by points 6-7-3-2-6. In this zone, both families of Mach waves are present. Assuming a straight sonic line at the throat. the outward curve of the wall between 7 and 3 generates right-running expansion waves which are reflected from the centre-line as left-running expansion waves. This process of generating Mach waves continues until the desired Mach number is reached at point 2 on the centre-line. The maximum change in flow direction is θ_3 at the inflection point 3.

(ii) Straightening Zone:

This section, bounded by points 3-2-1, consists only of left-running Mach waves. This follows, as only a zone of simple waves can have uniform parallel flow within the Mach lines. Because only left-running Mach waves should exist in this zone, the nozzle walls must be designed to cancel these waves. i.e. The straightening contour must generate positive Mach waves that just cancel out the left-running expansion waves, incident upon it. (The profile then must always be concave).

(iii) Test-Section:

As the Mach line 1-2 is straight and the test-section walls are parallel, it follows then that the flow is uniform, parallel and at the desired Mach number.

An important criterion in the design of nozzles is the choice of the nozzle expansion profile 7-5-3. The development of the Mach wave pattern and the final cancelling profile is controlled by this choice.

Although the sonic line at the nozzle throat is in practice curved (6), for this analysis it is assumed straight and normal to the nozzle axis.

Consider a nozzle limited to a Mach wave pattern of two backward reflections. This system puts certain limitations on the design of such a nozzle. These limitations, derived in appendix 1.4 are given as:

$$0 \leq \omega_5 \leq \frac{\omega_1}{4} \qquad \text{..... 1.12}$$

and

$$1 \geq \frac{|\theta_3|}{\omega_{1\frac{1}{2}}} \geq \frac{1}{2}$$

The two extremes imposed by these equations are:

(i) $\omega_5/\omega_1 = \frac{1}{4}$; $|\theta_3| = \frac{\omega_1}{4}$

This gives $|\theta_3| = |\theta_5| = \frac{\omega_1}{4}$. Therefore the expansion profile is a straight line between the throat and inflection point.

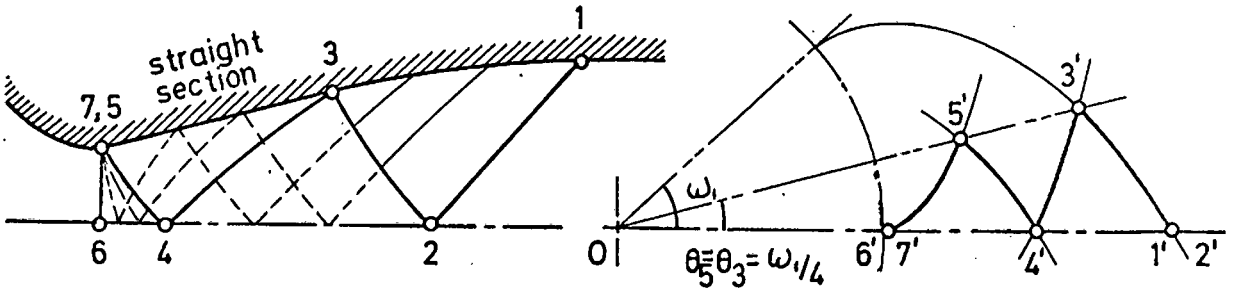

(a) Physical Plane (b) Hodograph Plane

Figure 1·13

(ii) $\omega_5/\omega_1 = 0$; $|\theta_3| = \frac{\omega_1}{2}$

These relationships give point 5 the identical properties as point 7.

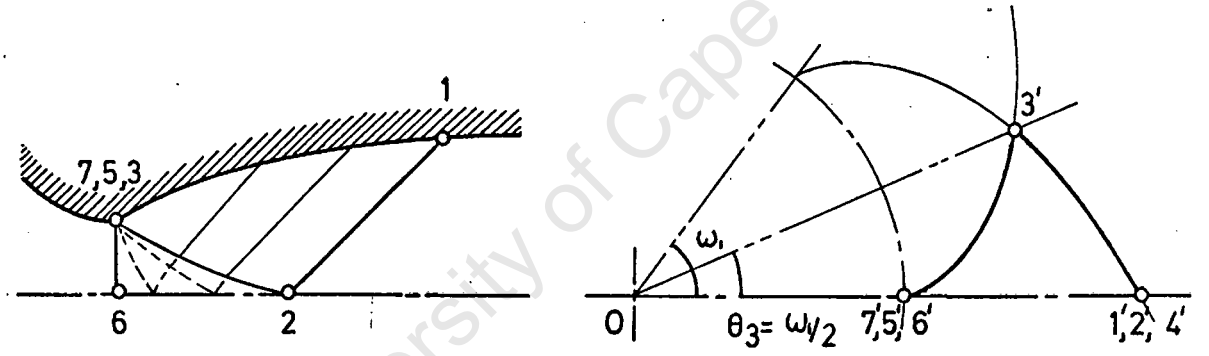

(a) Physical Plane (b) Hodograph Plane

Figure 1·14

Therefore point 3 must coincide with the nozzle throat even though it has different properties to points 5 and 7.

i.e. A sharp corner exists at the throat.

This analysis has been specifically for a double reflection system. A more generalised relationship is given in reference (3).

The limitations imposed on a system of n backward reflections are:

$$0 \leqslant \omega_1/\omega_1 \leqslant \tfrac{1}{2}n \quad \ldots\ldots\ldots\ldots\ldots\ldots\ldots\ldots\ldots\ldots\ldots\ldots\ldots\ldots \quad 1.14$$

and

$$1 \geqslant |2\,\theta_3|/\omega_1 \geqslant 1/n \quad \ldots\ldots\ldots\ldots\ldots\ldots\ldots\ldots\ldots\ldots\ldots\ldots\ldots\ldots \quad 1.15$$

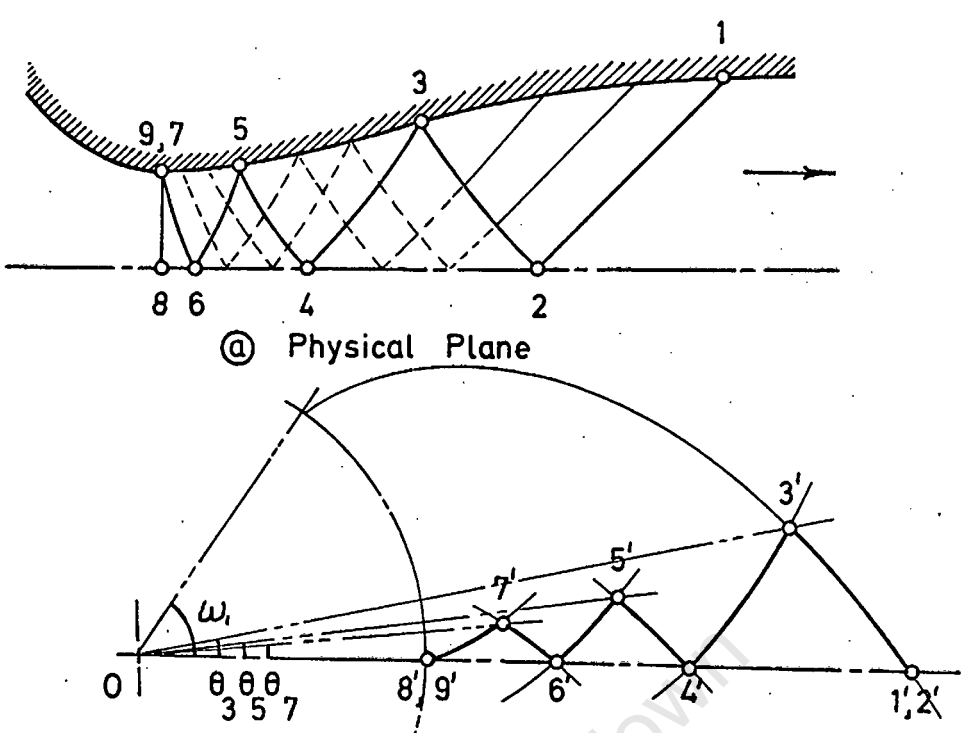

Figure 1.15

The right-hand limits would again give an expansion profile that is a straight line. This time, though, a greater number of reflection would occur (number n).

For a gradually curving expansion section an infinite number of reflections would occur in the proximity of the nozzle throat. Therefore a nozzle of this type may have an inflection angle that is much smaller than the corresponding straight expansion section nozzle.

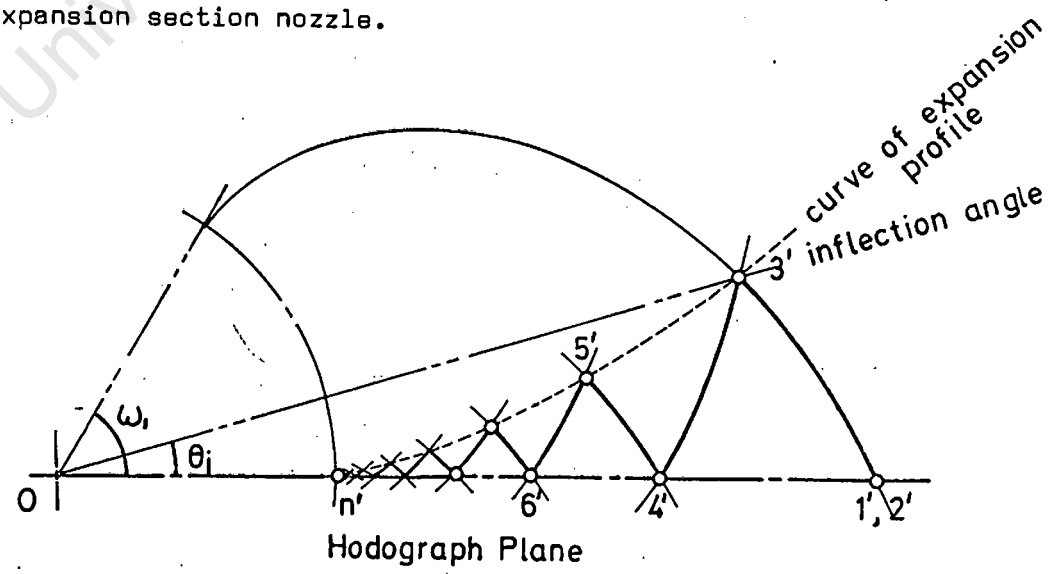

Figure 1.16

The hodograph in figure 1.16 illustrates how the nozzle expansion profile determines the inflection angle. Also this figure shows that accurate

graphical determination of the Mach characteristics, near the nozzle throat, becomes exceedingly difficult.

2.3 APPLICATION OF CHARACTERISTICS TO NOZZLE DESIGN

The nozzle Mach number, M, can be defined by the Mach function $\omega(M^*)$

From equation 1.8:

$$(M^*) = \sqrt{\frac{+1}{-1}} \arctan \sqrt{\frac{M^{*2}-1}{\frac{+1}{-1} - M^{*2}}} + \arctan \sqrt{\frac{M^{*2} - 1}{1 - \frac{-1}{+1} M^{*2}}} \quad \ldots\ldots\ldots 1.16$$

M^* is directly related to the Mach number M. The relation between M and $\omega(M^*)$ is tabulated in (3).

For optimum running time, the semi-graphical nozzle must be designed for a Mach number of 2,35. In order to simplify the construction of the characteristic Mach net, a Mach function, $\omega(M^*)$, of 36° corresponding to a Mach number of 2,3693 is suitable. ✓

The decision to use a sharp cornered, straight expansion section, in the design of the nozzle, was governed purely for the following reasons:

1. The sharp corner initiates the right-running (top symmetrical section) Mach waves and defines the point about which the balance of the construction follows.
2. A straight expansion section is that which gives the minimum expansion angle for a fixed number of reflections.

The length of the nozzle box indicated that a triple reflection construction should be used. The chance of a grave constructional error (or an accumulative error), for this additional expansion length is offset by the improved Mach distribution for a low inflection angle nozzle.

From equations 1.14 and 1.15; applying the right-hand extreme for a triple reflection nozzle:

$$\omega_7 = |\theta_7| = |\theta_3| = \omega_1/2n$$

and

$$\omega_3 = \omega_1(1 - 1/2n)$$

For $n = 3$ and $\omega_1 = 36{,}0^\circ$

$\therefore |\theta_7| = |\theta_3| = 6{,}0^\circ$; $\omega_3 = 30^\circ$ (See figure 1.17).

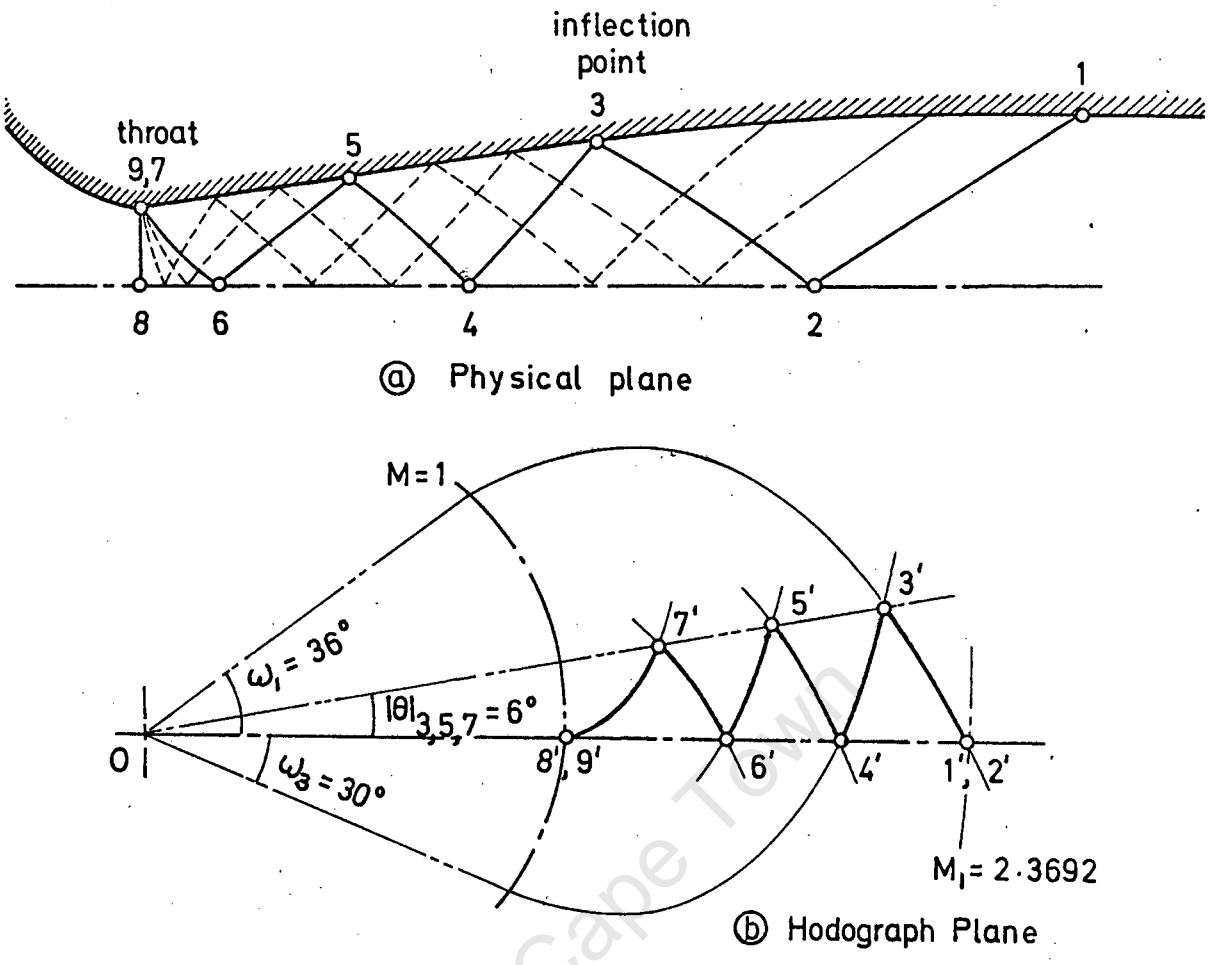

SUPERSONIC NOZZLE DESIGN
– Triple Reflection
Figure 1.17

Field Method of Construction.

This method simply defines the properties of the flow fields bounded by the characteristic Mach net.

Two methods can be applied in finding a solution:

1. The purely graphical solution makes sole use of the hodograph plot. The flow properties are defined by the corresponding hodograph streamlines. The Mach wave angles are then determined by normals drawn to the hodograph streamline joining two field properties.

2. The semi-graphical solution relies on a determination of the hodograph characteristic constants, I an II, that are related to θ and ω in equations 1.9 and 1.10 The Mach angle is directly related to the Mach number M, and therefore the Mach function ω.

The latter method is preferred as a higher degree of accuracy is obtained in the determination of the Mach angle. Application of the hodograph, though, provides a rapid means of constructing the Mach net.

The derivation of the nozzle contour for this thesis, using the field method

of construction, is best described by considering a small portion of the complete characteristic Mach network.

Rules:

Flow across right-running Mach waves will cause the hodograph of the streamline to move along a characteristic of family II. The Mach line is normal to the hodograph characteristic II and lies at an angle $(\theta - \alpha)$ to the horizontal. (See figure 1.18).

Similarly; flow across left-running Mach waves will cause the hodograph of the streamline to move along the characteristic of family I. Again the Mach line is normal to the hodograph characteristic I and lies at an angle $(\theta + \alpha)$ to the horizontal.

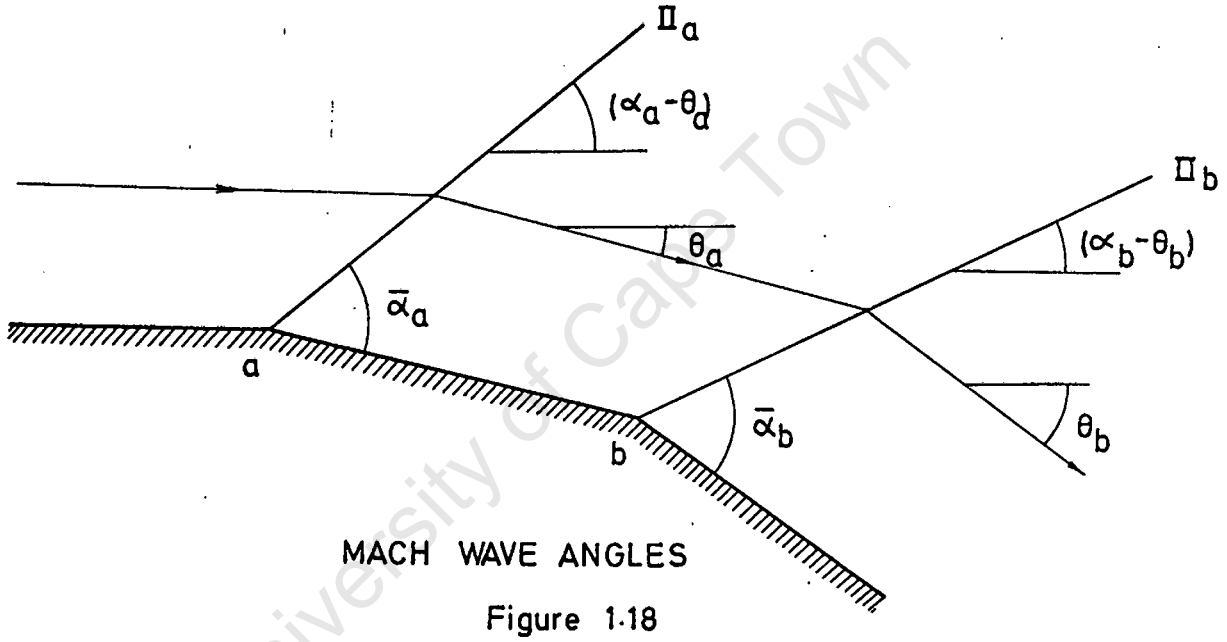

MACH WAVE ANGLES

Figure 1.18

Semi-Graphical Design:

As every field in the Mach net contains flow that has constant velocity and direction within its boundaries, each may be represented on a hodograph plan as a point on the hodograph streamlines. Each of these points may be identified by a particular value of I and II.

Equations 1.9 and 1.10 may be rearranged and written:

$$\theta = I + II - 1\,000 \quad \ldots\ldots\ldots\ldots\ldots\ldots \quad 1.17$$

$$\omega = I - II \quad \ldots\ldots\ldots\ldots\ldots\ldots \quad 1.18$$

Hence given I and II, the stream angle, θ, and the Mach function, ω, can be determined.

Each field, representing steady conditions, is numbered. The only changes in fluid properties take place across finite Mach waves, these are designated by

the field numbers on either side of it.

The first reflection of the Mach wave network is depicted in figure 1.19. The expansion at the corner is governed by a chosen number of six Mach waves of equal strength. The flow direction is turned through one degree by the perturbation potential of each Mach wave until the flow is parallel with the straight expansion surface at 6^{0} to the horizontal axis.

i.e. Flow in fields 1, 2, 3, 4, 5, 6, and 22 have a directional change of one degree respectively.

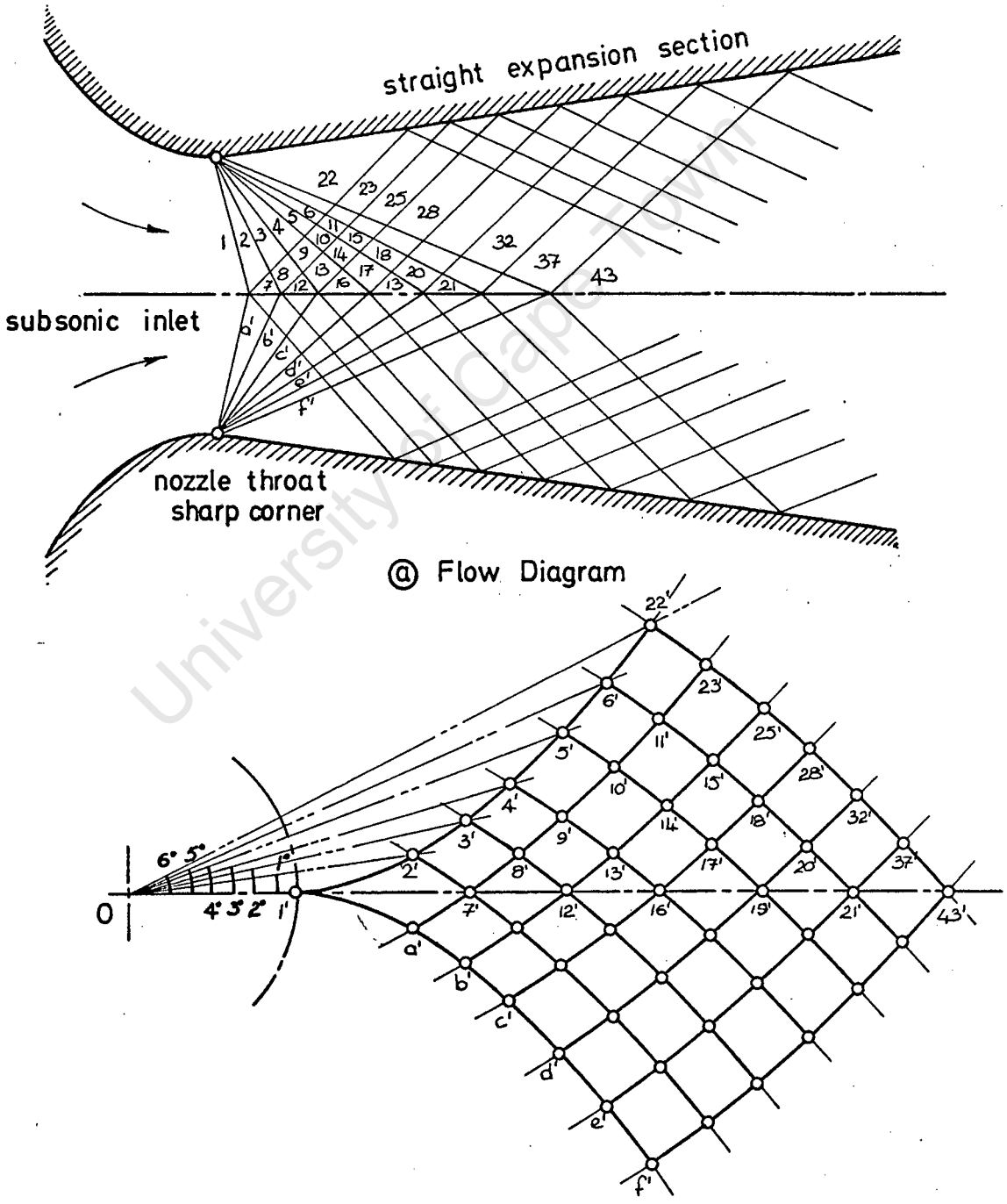

FIRST REFLECTION WAVE PATTERN
Figure 1.19

As the waves are right-running, the flow properties all lie on the same characteristic of family II. In field 1, the flow direction is parallel to the horizontal axis ($\theta = 0$), at a Mach number of unity ($\omega = 0$). Substitution of $\theta = 0$ and $\omega = 0$ into equations 1.17 and 1.18 give the characteristic of family II, a constant value of 500.

Hence knowing the flow direction, θ, and the value of one characteristic curve, or the values of both characteristic curves, (I and II), the other unknowns may be found. The various properties of each field are summarised in table 1.1 (The full tables are presented in appendix 1.5)

For each field, the two properties of the four, I, II, θ and ω, that are found first, are underlined.

Table 1.1 for figure 1.17(b)

Field	I	II	ω degrees	θ degrees	α degrees	$\theta+\alpha$ degrees	$\theta-\alpha$ degrees
1	500	500	0	0	90,00	90,00	-90,00
2	501	500	1	1	67,57	68,57	-66,57
3	502	500	2	2	62,00	64,00	-60,00
4	503	500	3	3	58,18	61,18	-55,18
5	504	500	4	4	55,20	59 20	-51,20
6	505	500	5	5	52,74	57,74	-47,74
7	501	499	2	0	62,00	62,00	-62,00
8	502	499	3	1	58,18	59,18	-57,18
9	503	499	4	2	55,20	57,20	-53,20
10	504	499	5	3	52,74	55,74	-49,74

$\theta+\alpha$ and $\theta-\alpha$ are the Mach wave angles to the horizontal axis of the nozzle for the right-running and left-running Mach waves respectively.

Because the properties within each field are different from the next, the Mach wave angles corresponding to the properties before and after the mean Mach wave are different. A compromise is found by taking the average angle between the fields and using this for the Mach net construction.

(This is done automatically when measuring the mean normal between two field properties in a hodograph plot).

Table 1.2 is arranged so that the left- and right-running Mach wave angles are separated.

Table 1.2 for figure 1.17(a)

Wave	Right-running Mach wave			Left-running Mach wave		
	Upstream $(\theta+\alpha)$	Downstream $(\theta+\alpha)$	Mean $(\theta+\alpha)$	Upstream $(\theta-\alpha)$	Downstream $(\theta-\alpha)$	Mean $(\theta-\alpha)$
	degrees	degrees	degrees	degrees	degrees	degrees
1-2				-90,00	-66-57	-78,29
2-3				-66,57	-60.00	-63,29
3-4				-60,00	-55,18	-57,59
4-5				-55,18	-51,20	-53,19
5-6				-51,20	-47,74	-49,47
2-7	68,57	62,00	65,29			
3-8	64,00	59,18	61,29			
8-12	59,18	55,20	61,59			
4-9	61,18	57,20	57,19			
9-13	57,20	53,74	59,19			

The graphical construction of the Mach net was redrawn to three times the full size of the nozzle. The full solution, consisting of sections I, II, III, IV, V and VI, is given in figure 1.21. The corresponding hodograph plot is presented in figure 1.20.

The disadvantage of the triple reflection construction is that the Mach angle determination is tedious, and the graphical construction requires a high degree of accuracy if an accumulative error is to be avoided.

The hodograph (figure 1.20) plot is an extension of the complete hodograph given in figure 1.11. It is presented so that the characteristic curves of families I and II may be modified to suit any design Mach number. The curves given in this figure may also be applied to the single and double reflection systems:

i.e. A double reflection nozzle would require a 9^{o} inflection angle, while a single reflection nozzle (where the inflection point and throat coincide at a corner) would require an 18^{o} inflection angle.

Figure 1.20 has been reduced from its original size. The large scale diagram may be used to verify the Mach wave angles $(\theta+\alpha)$ and $(\theta-\alpha)$ by measuring the normals drawn across the corresponding characteristic curve. If the speed of construction of the Mach net is of greater importance than accuracy, then this hodograph (or phase plane plot) offers a rapid method of determining the Mach

angles.

(See appendix 1.6, for this hodograph programme)

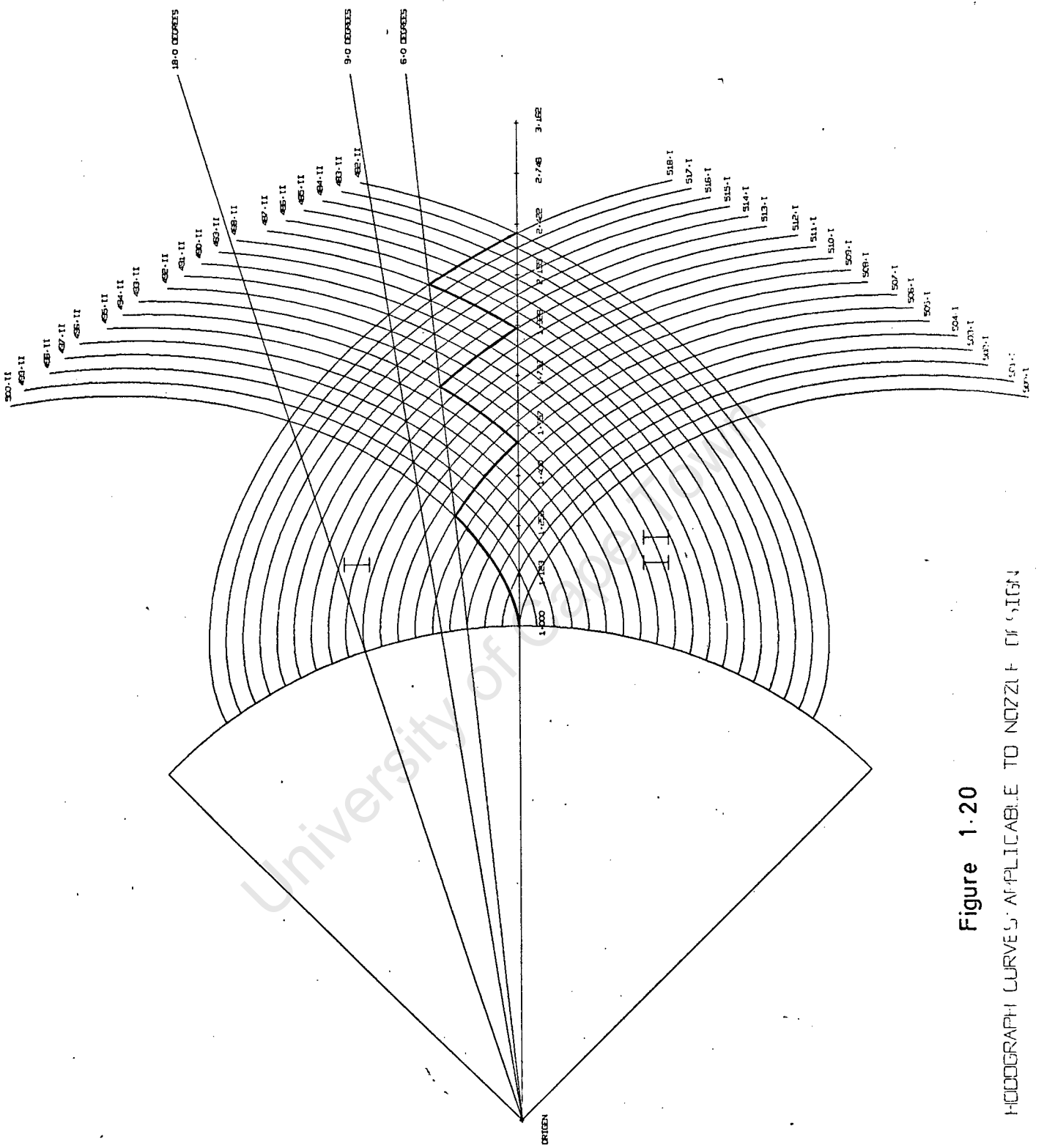

Figure 1·20

HODOGRAPH CURVES APPLICABLE TO NOZZLE DESIGN

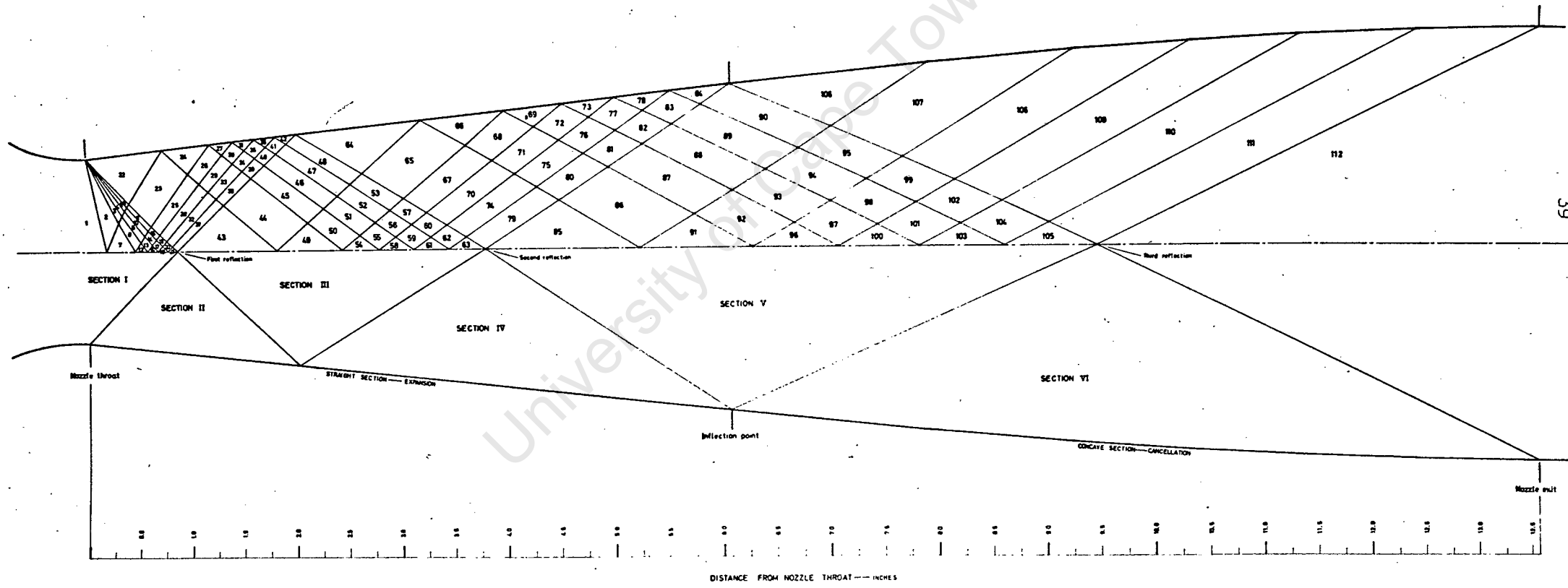

SPECIFICATIONS: MACH NUMBER = 2.3693
MACH FUNCTION = 30°
TEST SECTION AREA = 6 sq.inches
AREA RATIO = 2.3377
INFLECTION ANGLE = 6°
TRIPLE REFLECTION

Figure 1.21 SEMI-GRAPHICAL NOZZLE WALL DIAGRAM

PART 3
ANALYTICAL NOZZLE DESIGN

3.1 FOELSCH'S METHOD

Cancellation Section:

The analytical relations that are derived by Foelsch (1) are based on the theory of characteristics and essentially provide a method of designing a suitable contour to convert uniform radial supersonic flow into uniform parallel supersonic flow.

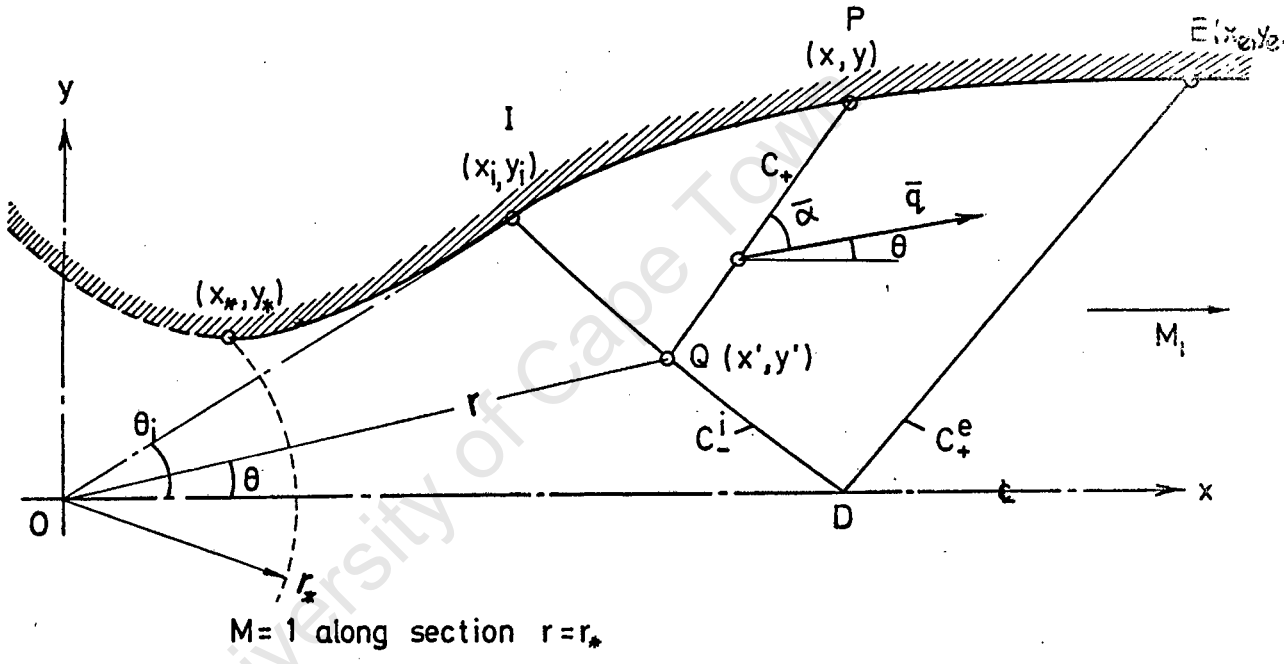

FOELSCH'S METHOD OF TWO-DIMENSIONAL NOZZLE CONTOUR DESIGN

Figure 1.22

Consider the diagram in figure 1.22. The characteristic Mach wave that is reflected at the inflection point is denoted by C_-^i. The flow downstream of C_-^i is swept by a family of straight C_+ characteristics and is finally bound by the characteristic through the nozzle exit (x_e, Y_e), denoted by C_+^e. Beyond this Mach line the flow should be uniform an parallel. The boundary IE should be suitably shaped such that the incident C_+ characteristics are cancelled.

The basic assumption made is that in the region OID, radial source flow exists.

Consider two-dimensional flow of unit width. Therefore, where $r > r_*$ (supersonic region), the streamlines are straight, diverging from the apparent

origin O. From this source, the uniform mass flow per radian of angle can be assumed constant.

The C_+ Mach characteristic QP is of constant perturbation potential. Hence the flow parameters are constant along this line.

i.e. $M = M_P = M_Q$; $\theta = \theta_P = \theta_Q$

$\alpha = \alpha_P = \alpha_Q$; $\rho = \rho_P = \rho_Q$

$q = q_P = q_Q$

The nozzle cancellation profile co-ordinates $(X_1 Y_1)$ may be put in terms of co-ordinates of Q and the characteristic angle $(\theta + \alpha)$.

By equating the mass flow rate across this characteristic wave with that from the apparent origin through angle IOQ, the nozzle co-ordinates may be defined in terms of $\left(\begin{smallmatrix} 2 \\ \cdot \end{smallmatrix} \right)$ ~~~~

The derivation of the equations is given in appendix 1.7.

The following expressions define the nozzle cancellation section in terms of X and Y for the whole field of IDE swept by the C_r characteristics.

$$\frac{X}{Y_*} = \frac{A(M)}{\theta_i} \left\{ \cos\theta + \left[\left(\sqrt{M^2 - 1}\, \cos\theta - \sin\theta \right)(\theta_i - \theta) \right] \right\} \quad \ldots\ldots\ldots \quad 1.28(a)$$

and

$$\frac{Y}{Y_*} = \frac{A(M)}{\theta_i} \left\{ \sin\theta + \left[\left(\sqrt{M^2 - 1}\, \sin\theta + \cos\theta \right)(\theta_i - \theta) \right] \right\} \quad \ldots\ldots\ldots \quad 1.28(b)$$

where $\theta = \omega_1 - \omega$ ..... 1.28(c)

Expansion Section:

The expansion section can be selected arbitrarily as long as the profile satisfies the postulation that radial, uniform flow exists at the C^i characteristic. The conditions imposed upon the expansion profile are:

$Y(X_*) = Y_*$	throat width
$Y'(X_*) = 0$	the slope in the throat is zero.
$Y'(X_i) = \tan\theta_i$	the slope is equal to inflection angle.
$Y''(X_i) = 0$	the rate of change of the slope at the inflection point is zero.

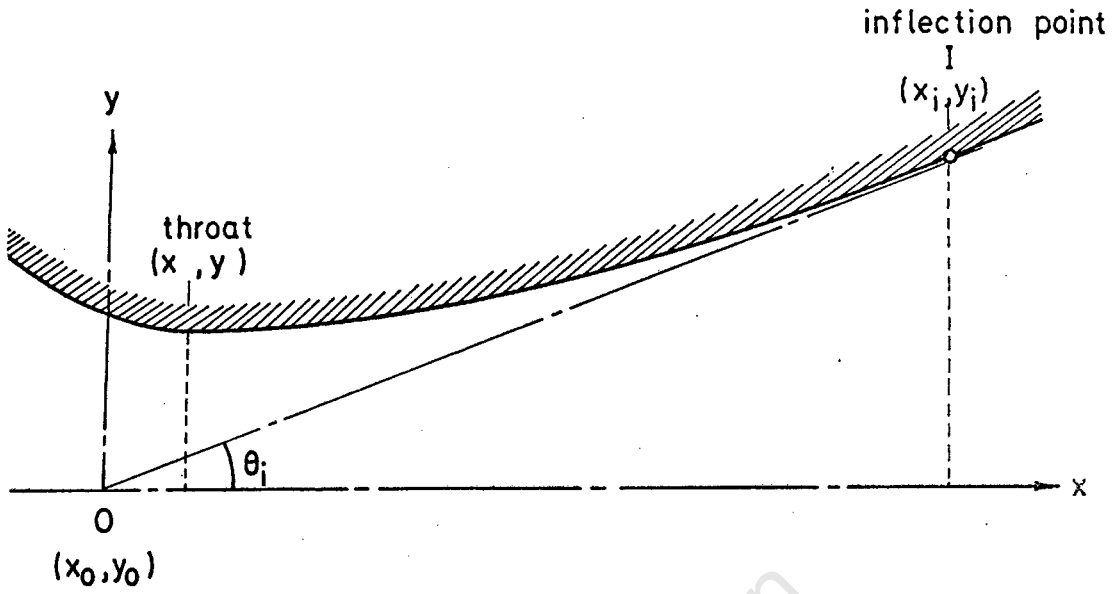

EXPANSION SECTION

Figure 1.24

A cubic equation satisfies these boundary conditions:

$$Y = Y_* + C_1 (X - X_*) + C_2 (X - X_*)^2 + C_3 (X - X_*)^3$$

Differentiating and eliminating the constants by imposing the boundary conditions:

$$\therefore Y = Y_* + \frac{\tan\theta_i}{X_i - X_*} (X - X_*)^2 - \frac{\tan\theta_i}{3(X_i - X_*)^2} (X - X_*)^3$$

$$\therefore \frac{Y}{Y_*} = 1 + \frac{Y_* \tan\theta_i}{X_i - X_*} \left\{ 1 - \frac{X - X_*}{3(X_i - X_*)} \right\} \left(\frac{X - X_*}{Y_*} \right)^2 \quad \ldots\ldots\ldots \quad 1.29$$

The only unknown, after the cancellation section equations have defined X_i and Y_i, is the distance of the nozzle throat to the origin X_*.

Hence, at the inflection point:

$$X = X_i \quad ; \quad Y = Y_i$$

From the above equation:

$$\frac{X_*}{Y_*} = \frac{3}{2\tan\theta_i} \left(\frac{Y_i}{Y_*} - 1\right) - \frac{X_i}{Y_*}$$

Also from equations 1.28:

$$\frac{X_i}{Y_*} = \frac{A(M_i)}{\theta_i} \cos\theta_i \quad ; \quad \frac{Y_i}{Y_*} = \frac{A(M_i)}{\theta_i} \sin\theta_i$$

Hence from these equations:

$$\frac{X_*}{Y_*} = \frac{1}{2}\left(\frac{X_i}{Y_*} - 3 \cot \theta_i\right) \quad \text{..... 1.30}$$

Equations 1.29 and 1.30 define the nozzle expansion section between $X_* \leqslant X \leqslant X_i$.

3.2 SUBSONIC INLET

The purpose of the subsonic inlet is to accelerate the fluid to sonic velocities at the nozzle throat. It must be designed so as to minimise disturbances in the flow stream and essentially create uniform parllel flow.

It has been found (14) that a smooth and gradual acceleration of a fluid will give a good distribution of the velocity profile. There will also be a minimum disturbance to the flow. Therefore any smooth acceleration curve could be satisfactorily applied to the subsonic inlet design.

In this case, a sinusoidal acceleration curve will be assumed over the inlet length (see figure 1.25). The inlet is two-dimensional of unit width.

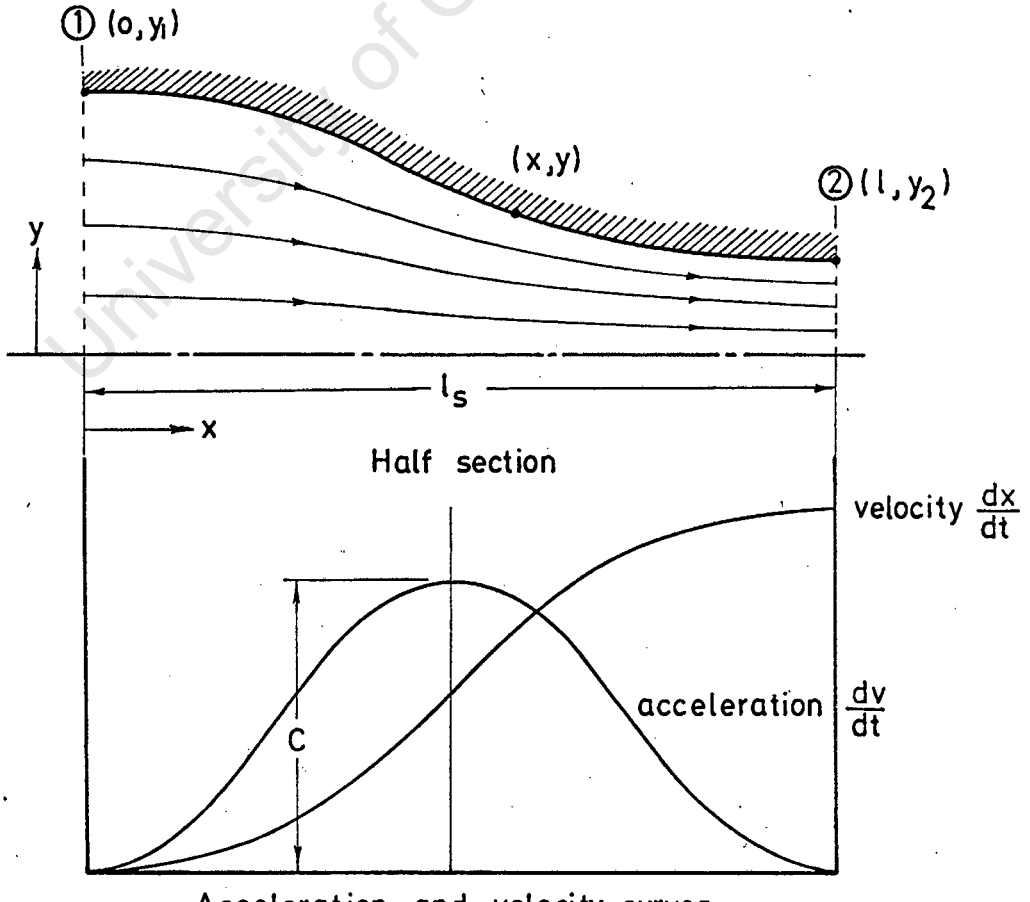

Acceleration and velocity curves

SUBSONIC INLET

Figure 1.25

This sinusoidal acceleration curve is integrated between the inlet boundary (1) and any distance X along the contraction. (The derivation is given in appendix 1.8).

The velocity at point (X, Y) is given as:

$$v^2 - v_1^2 = C\left[X - \frac{l_s}{2\pi} \sin 2\pi \frac{X}{l_s}\right] \quad \text{.....1.32}$$

where $C = \frac{Q^2}{l_s}\left[\frac{1}{Y_2^2} - \frac{1}{Y_1^2}\right]$ 1.33

The maximum acceleration of the flow is determined by the magnitude of this constant C. The following parameters can be changed to reduce this maximum acceleration and the possibility of disturbances in the flow:

1. Increase the inlet length l_s.
2. Reduce the volume flow rate, Q. Because v is fixed at the speed of sound in air, the throat area must be reduced. i.e. Increase nozzle Mach number.
3. Reduce the inlet-throat area ratio, but this is normally fixed by the geometry of the tunnel.

From equations 1,32 and 1.33, the subsonic inlet contour is defined by:

$$\left[\frac{1}{Y^2} - \frac{1}{Y_1^2}\right] = \left[\frac{1}{Y_2^2} - \frac{1}{Y_1^2}\right]\left[\frac{X}{l_s} - \frac{1}{2\pi} \sin \frac{2\pi X}{l_s}\right] \quad \text{..... 1.34}$$

3.3 APPLICATION OF THEORY TO NOZZLE DESIGN

Application of the equations governing the contours of the cancelling, expansion and subsonic inlet sections requires a knowledge of the existing nozzle box dimensions.

The nozzle expansion angle, θ_i, must suit the allowable nozzle length, but at the same time be of satisfactory magnitude. Reference (1) suggests that this angle should be somewhere within the range of $\frac{1}{4}\omega_1$ to $\frac{1}{3}\omega_1$. As far as the production of uniform velocity in the test section is concerned, the smaller this expansion angle, the less critical is the contour design. Unfortunately this results in an increase in nozzle length and additional difficulties in boundary layer growth considerations.

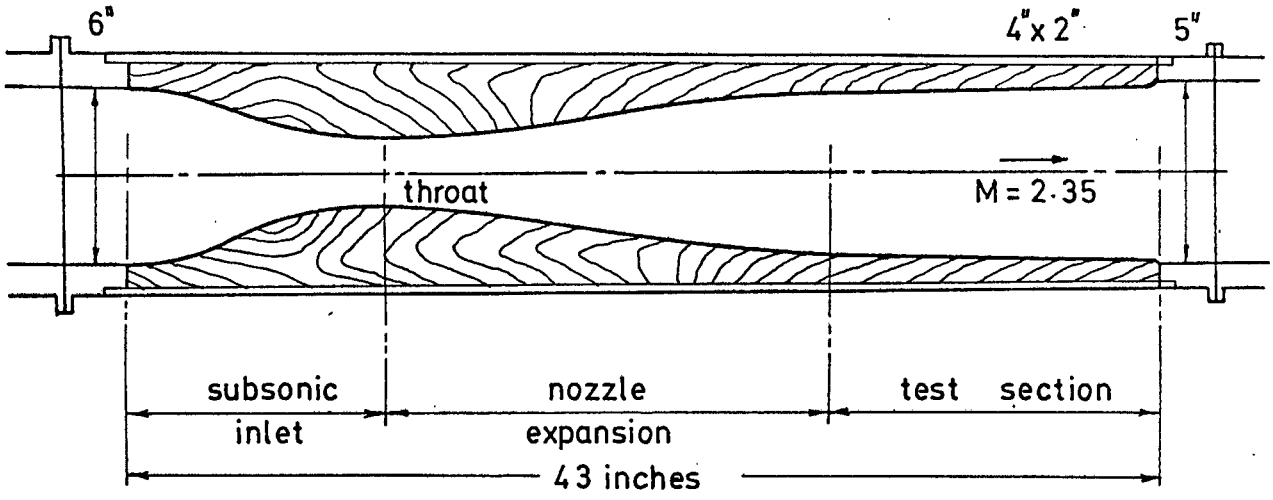

SUPERSONIC NOZZLE

[Figure 1·27]

The nozzle expansion angle was chosen at the lower limit (i.e. $\theta_i = \frac{\omega_1}{4}$) for the following reasons:

1. Because the required construction tolerances on a nozzle of such small dimensions is difficult to achieve, the improved flow distribution, associated with the smaller inflection angle, is very desirable.

2. The inflection angle of this magnitude allows a satisfactory inlet length (15 inches) and test-section length (about 10 inches) (See figure 1.27).

3. The boundary layer growth, although excessive in a tunnel of this size, may be judged relatively accurately from experimental calibrations undertaken previously (5).

Once the nozzle subsonic-inlet length and the nozzle expansion angle has been determined, the equations that define the nozzle profile may be applied.

Referring to figure 1.28, these equations may be applied as follows:

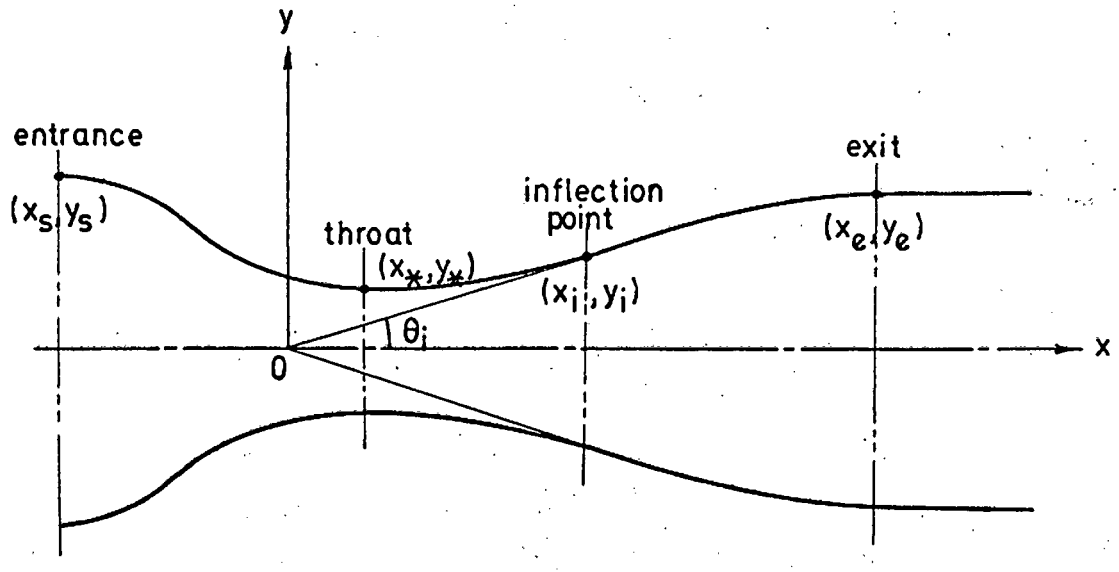

Note : only one half-section need be considered because of symmetry

FIGURE 1.28

Cancellation Section $\quad 0 \leqslant \theta \leqslant \theta_i$

From Equations 1.28:

$$\frac{X}{Y^*} = \frac{A(M)}{\theta_i}\left\{\cos\theta + \left[\left(\sqrt{M^2-1}\,\cos\theta - \sin\theta\right)(\theta_i - \theta)\right]\right\} \quad \ldots\ldots \text{(a)}$$

$$\frac{Y}{Y^*} = \frac{A(M)}{\theta_i}\left\{\sin\theta + \left[\left(\sqrt{M^2-1}\,\sin\theta - \cos\theta\right)(\theta_i - \theta)\right]\right\} \quad \ldots\ldots \text{(b)}$$

where $\theta = (\theta)_i - \omega$ $\quad \ldots\ldots\ldots\ldots\ldots\ldots\ldots\ldots$ (c)

1. Set the nozzle expansion angle $\theta_i = \frac{1}{4}\,\omega_i$.
2. The Mach function, $\omega_i(M)$, (and subsequently θ_i) is determined from the test section Mach number of 2.35.
3. From equation 1.19:

$$A(M) = \frac{A}{A_*} = \frac{1}{M}\left(\frac{1 + \frac{\gamma-1}{2}M^2}{\frac{\gamma+1}{2}}\right)^{\frac{\gamma+1}{2(\gamma-1)}}$$

The throat height, Y*, is obtained from the above relationship knowing the exit Mach number M and the exit height, Ye.

4. Xe is found by substituting all the known values into equation 1.28(a) with θ as zero.

5. By repeatedly inclreasing θ in finite steps between zero and θ_i, and applying equations 1.28(c), 1.19 and then 1.28(a) and (b), the cartesian co-ordinates of (x,y) of the cancellation profile may be found. (for each value of θ, the corresponding Mach function ω is found from equation 1.28(c). The equivalent Mach number M is determined from equation 1.7. This is substituted into equation 1.19 to give the area ratio A(M)).

6. Substitution of $\theta = \theta_i$ into equations 1.28 (a) and (b) gives the inflection point co-ordinates. (X_i, Y_i).

Expansion Section $\quad X_* \leqslant X \leqslant X_i$

From Equations 1.29 and 1.30 respectively:

$$\frac{Y}{Y_*} = 1 + \frac{Y_* \tan\theta_i}{X_i - X_*} \left(1 - \frac{X - X_*}{3(X_i - X_*)}\right)\left(\frac{X - X_*}{Y_*}\right)^2$$

where $$\frac{X_*}{Y_*} = \frac{1}{2}\left(\frac{X_i}{Y_*} - 3 \operatorname{cat}\theta_i\right)$$

1. Substitute all the known values into equation 1.30 to obtain the X co-ordinate of the nozzle throat, X_*.

2. Now these values may be applied to equation 1.29 so that the Y co-ordinate of the expansion profile may be found in terms of the variable X.

3. Again, stepwise decrements of X between the inflection point and the nozzle throat will produce the cartesian co-ordinates of the expansion contour.

Subsonic Inlet $\quad X_s \leqslant X \leqslant X_*$

Let the X-co-ordinate, in terms of the nozzle inlet be X(S).

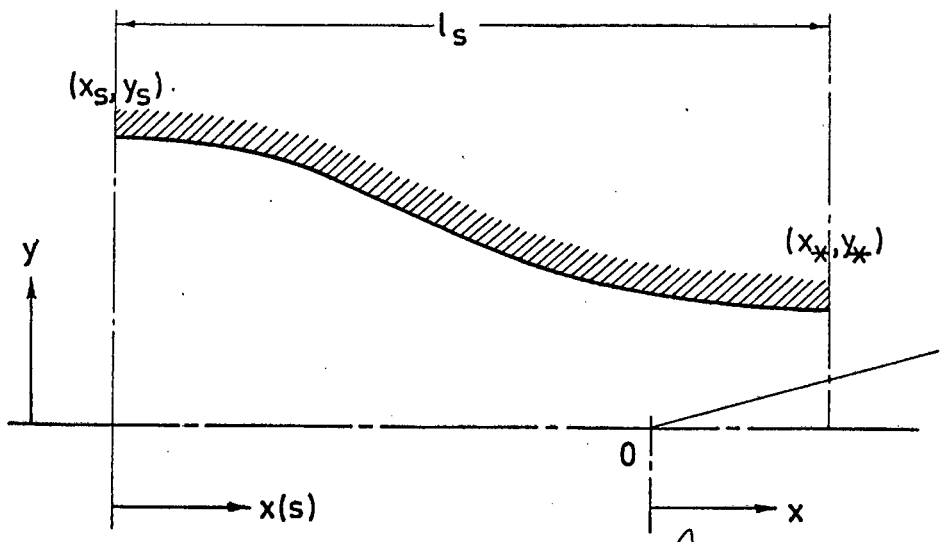

SETTING INLET ORIGEN

Figure 1·29

Therefore, from Equation 1.34:

$$\frac{1}{Y^2} - \frac{1}{Y_1^2} = \left[\frac{1}{Y_2^2} - \frac{1}{Y_1^2}\right]\left[\frac{X(S)}{l_s} - \frac{1}{2\pi}\sin\frac{2\pi X(S)}{l_s}\right]$$

This equation must be rewritten in terms of the origin 0, to bring it into line with the other equations.

Also $Y_2 = Y_*$ Nozzle throat height

$Y_1 = Y_s$ Nozzle entrance height.

From figure 1.29

$$X = X_* - l_s + X(S)$$

$$\therefore X(S) = X + l_s - X_*$$

Substitution into equation 1.34:

$$\frac{1}{Y^2} - \frac{1}{Y_s^2} = \left[\frac{1}{Y_*^2} - \frac{1}{Y_s^2}\right]\left[\frac{X + l_s - X_*}{l_s} - \frac{1}{2\pi}\sin\frac{2\pi(X + l_s - X_*)}{l_s}\right]$$

1. The nozzle entrance height Y_s, the subsonic entrance length l_s, the throat height Y_* and the distance from the nozzle throat to the origin are known.
2. Substitution of these values into the modified equation 1.34, and a stepwise decrement of the X co-ordinate will give the cartesian co-ordinates of the nozzle subsonic entrance.

3.4 NOZZLE CONTOUR SOLUTION

The equations describing the nozzle contour (1.28, 1.29, 1.30 and 1.34) may be solved numerically using a digital computer. The programme that solves these equations is such that all the design parameters, fixed by tunnel geometry and design Mach number, can be varied.

The following instructions may be altered in the program:

1. The design Mach number Me.
2. The ratio of specific heat for a gas .
3. The test-section height Y_e.
4. The subsonic inlet height Y_s.
5. The subsonic inlet length l_s.
6. The inflection angle i.

Each of these parameters occupy one instruction and may be altered independently from each other. Hence the programme may be used for many two-dimensional applications.

Flow Diagram:

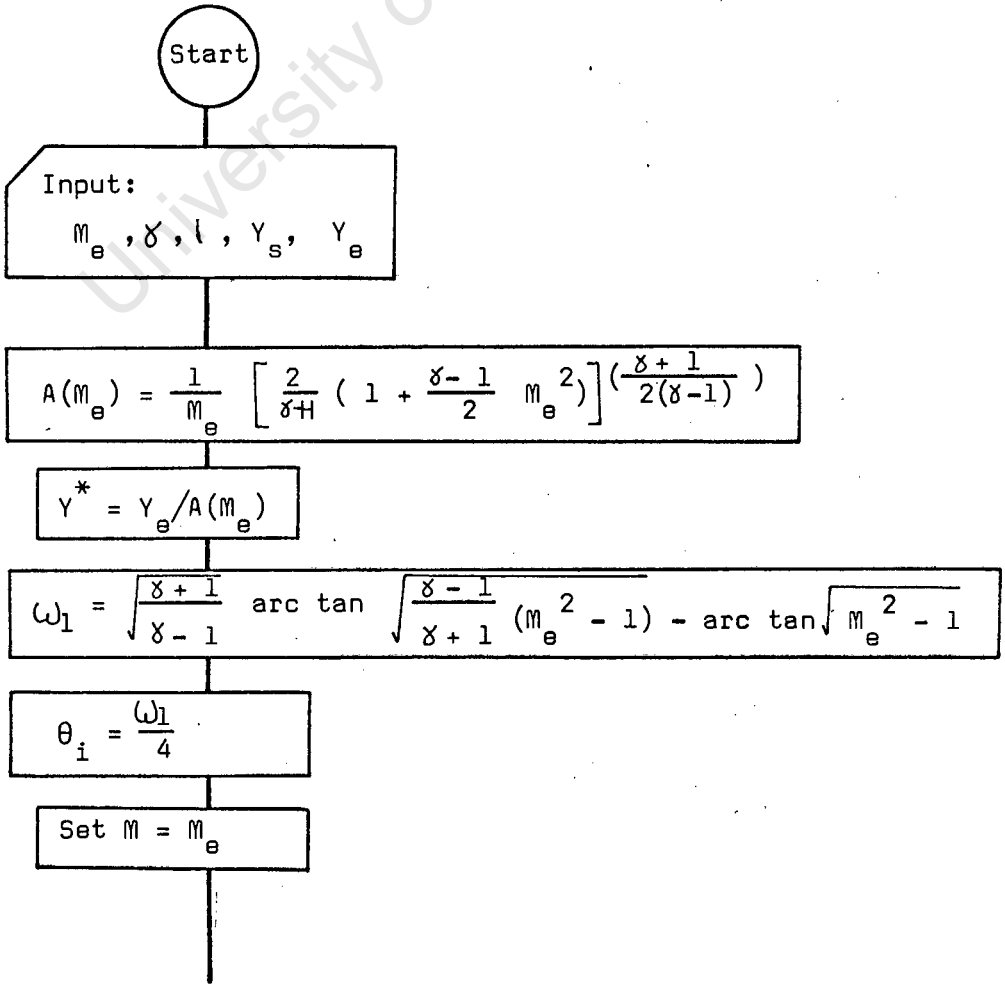

$$A_{(M)} = \frac{1}{M}\left[\frac{2}{\gamma+1}\left(1+\frac{\gamma-1}{2}M^2\right)\right]^{\gamma+1/2(\gamma-1)}$$

$$\omega = \sqrt{\frac{\gamma+1}{\gamma-1}}\arctan\sqrt{\frac{\gamma-1}{\gamma+1}(M^2-1)} - \arctan\sqrt{M^2-1}$$

$$\theta = \omega_1 - \omega$$

$$X = \frac{A(M)\,Y^*}{\theta_*}\left\{\cos\theta + \left[\left(M^2-1\ \cos\theta - \sin\theta\right)(\theta_i - \theta)\right]\right\}$$

$$Y = \frac{A(M)\,Y^*}{\theta_i}\left\{\sin\theta + \left[\left(M^2-1\ \sin\theta + \cos\theta\right)(\theta_i - \theta)\right]\right\}$$

Output: Print X, Y, M, A(M), ω

Plot X, Y.

Is $\theta \geq \theta_i$

No → Set M = M−0.1

Yes

Set $X_i = X$

$$X_* = -\frac{Y_*}{2}\left(\frac{X_i}{Y_*} - 3\ \text{cat}\,\theta_i\right)$$

$$Y = Y_*\left[1 + \frac{Y_*\tan\theta_i}{(X_i - X_*)}\left\{1 - \frac{X - X^*}{3(X_i - X^*)}\right\}\left\{\frac{X - X^*}{Y_*}\right\}^2\right]$$

Output: Print X, Y.

Plot X, Y.

Is $X \leq X_*$

No → Set X = X − 0,25

Yes

$$\frac{1}{Y^2} - \frac{1}{Y_s^2} = \left[\frac{1}{Y_*^2} - \frac{1}{Y_s^2}\right]\left[\frac{(X + l_s - X_*)}{l_s} - \frac{1}{2\pi}\sin\frac{2\pi(X + l_s - X_*)}{l_s}\right]$$

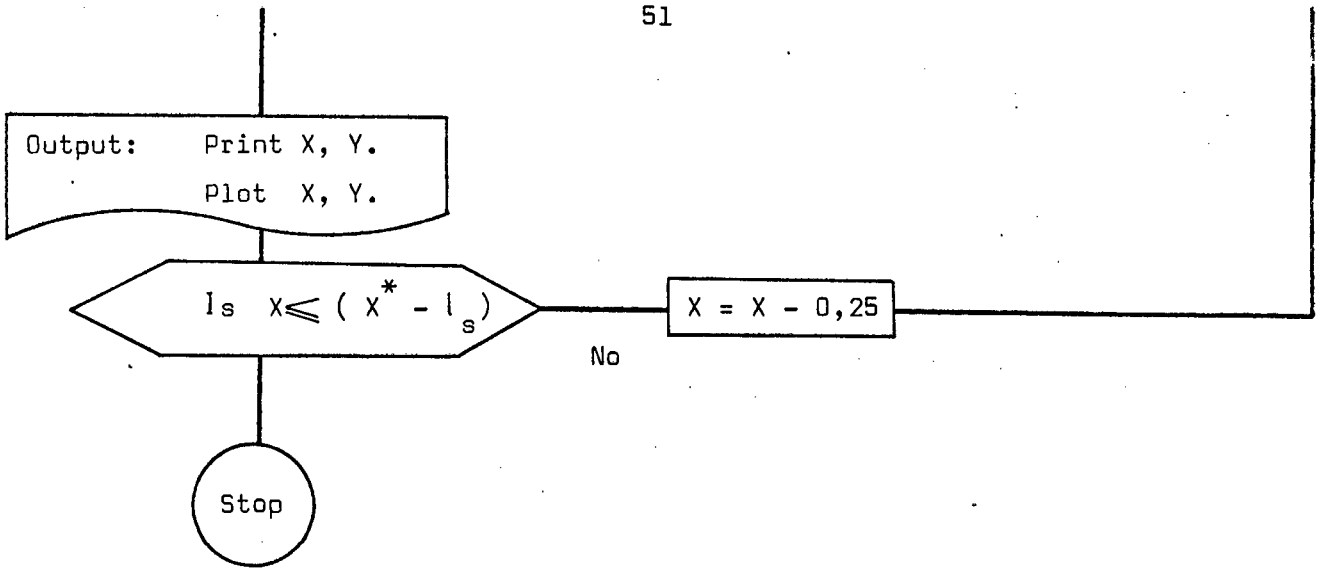

This programme is given in appendix 1,9, while the graphical plots are presented in figures 1,30 a, b, c, d and e for a range of Mach numbers between 2,00 and 5,00.

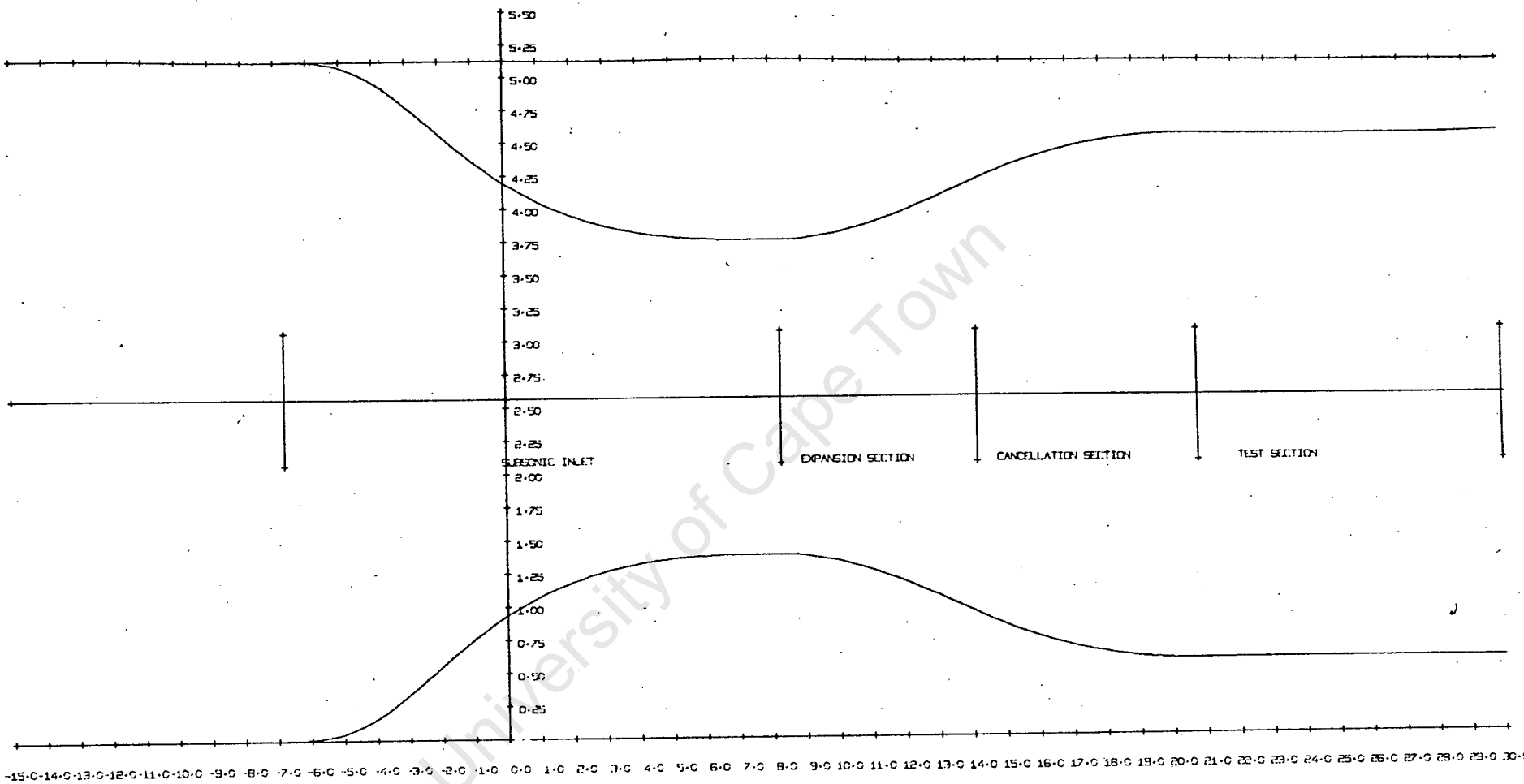

Figure 1·30 (a) SUPERSONIC NOZZLE PROFILE

INFLECTION ANGLE IS 6·61 DEGREES , THROAT GAP IS 2·370 INCHES

UNIFORM MACH N[illegible] 2·00

SCALE HORIZONTAL AXIS HALF FULL SIZE (INCHES)

VERTICAL AXIS TWICE FULL SIZE (INCHES)

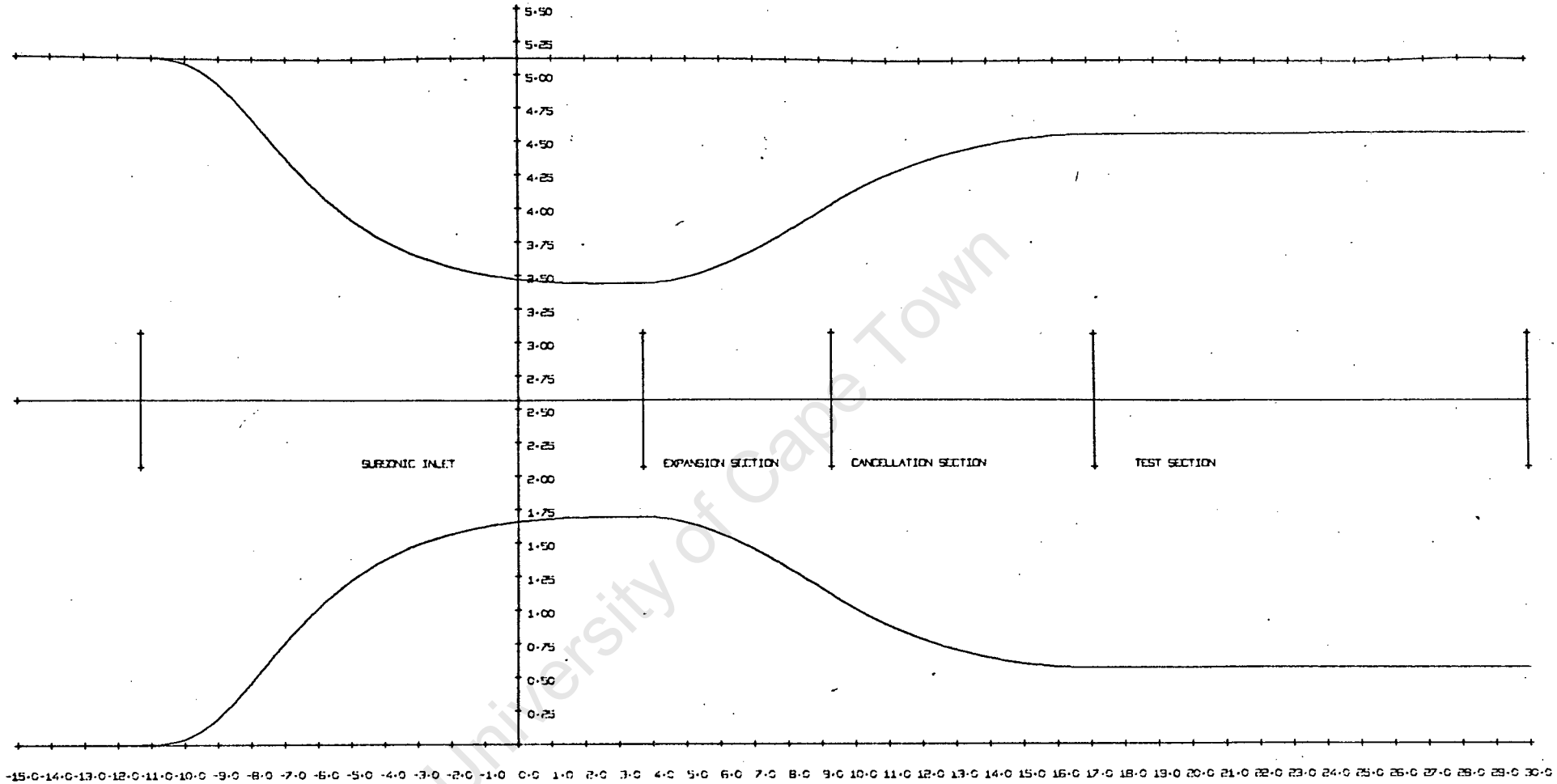

Figure 1·30 (b) SUPERSONIC NOZZLE PROFILE

INFLECTION ANGLE IS 6·30 DEGREES . THROAT GAP IS 1·742 INCHES.

UNIFORM MACH NUMBER IS 2·35

SCALE HORIZONTAL AXIS HALF FULL SIZE (INCHES)

VERTICAL AXIS TWICE FULL SIZE (INCHES)

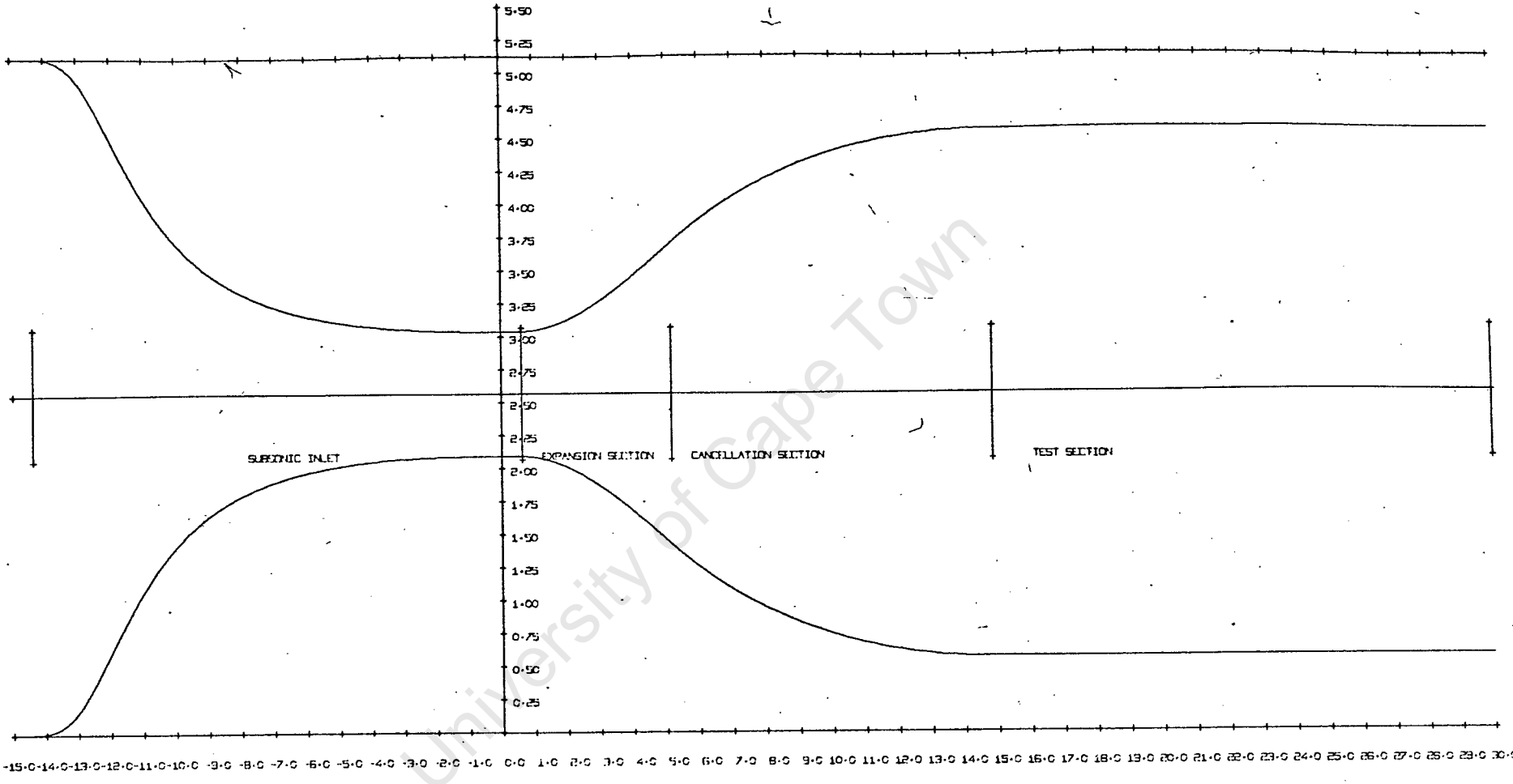

Figure 1.30 (c) SUPERSONIC NOZZLE PROFILE

INFLECTION ANGLE IS 12.47 DEGREES , THROAT GAP IS 0.314 INCHES

UNIFORM MACH NUMBER IS 3.00

SCALE HORIZONTAL AXIS HALF FULL SIZE (INCHES)

VERTICAL AXIS TWICE FULL SIZE (INCHES)

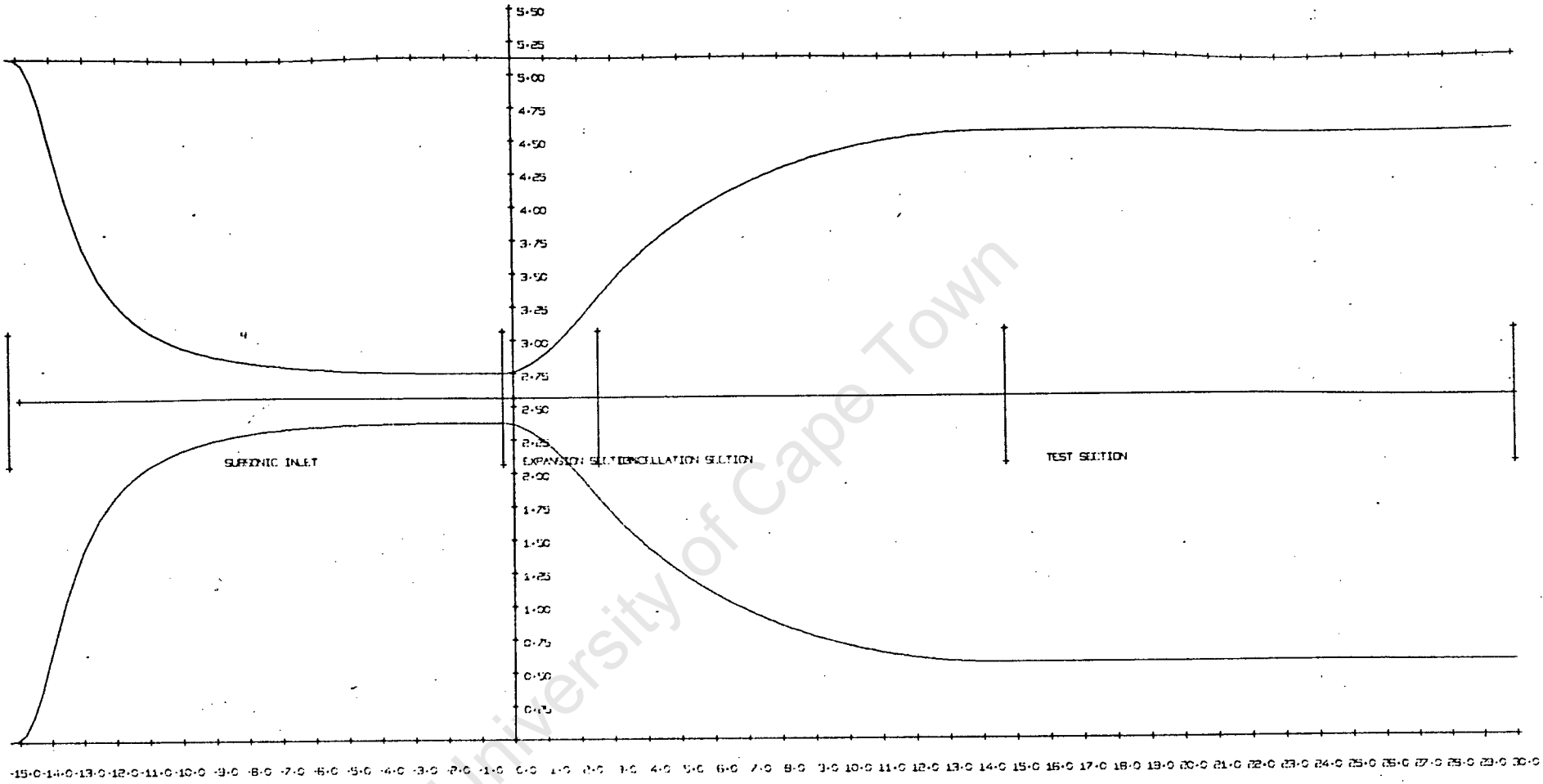

Figure 1·30 (d)

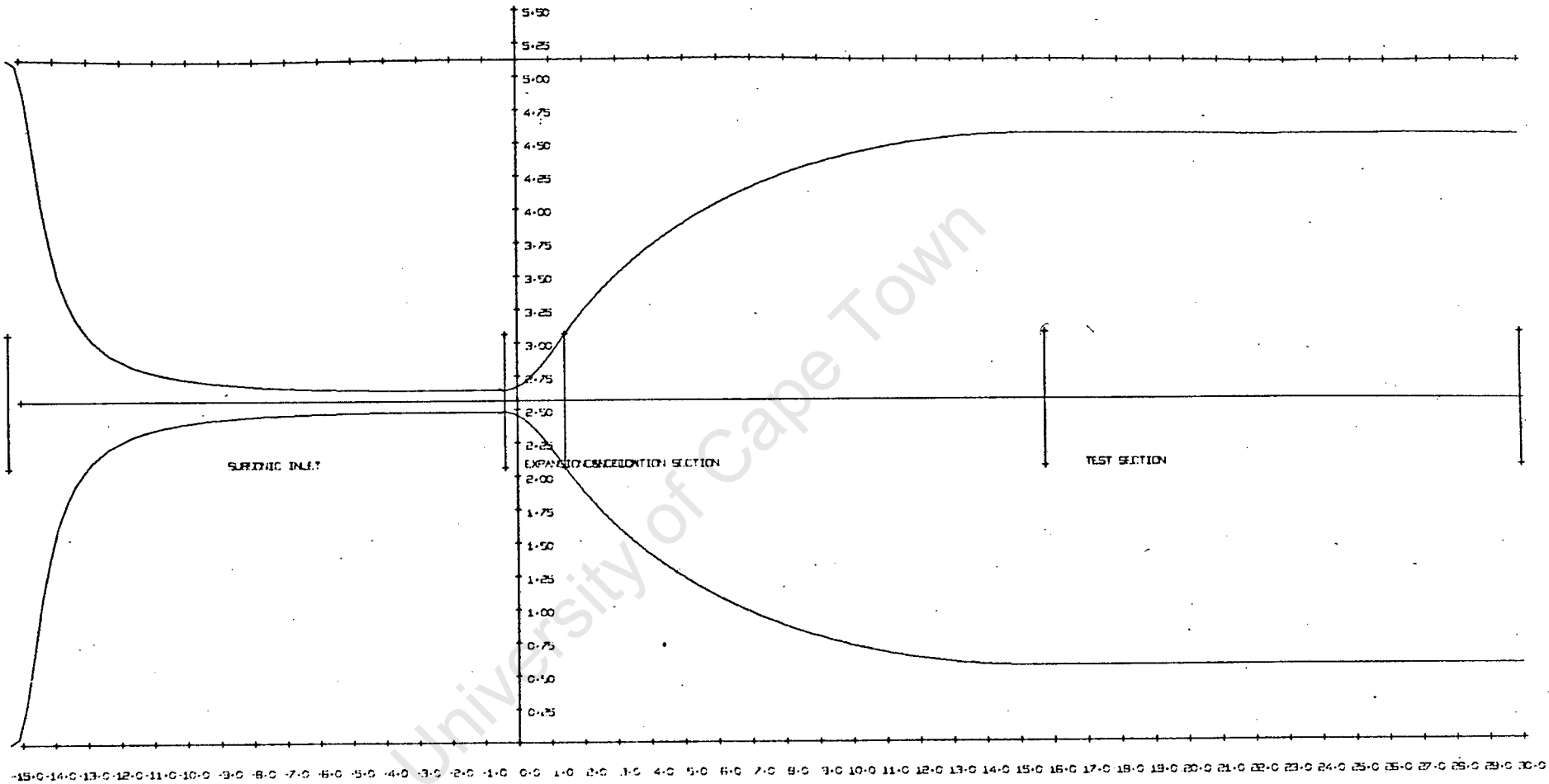

Figure 1·30 (e) SUPERSONIC NOZZLE PROFILE

INFLECTION ANGLE IS 19·28 DEGREES , THROAT GAP IS 0·160 INCHES

UNIFORM MACH NUMBER IN TEST SECTION

SCALE HORIZONTAL AXIS HALF FULL SIZE INCHES

VERTICAL AXIS TWICE FULL SIZE INCHES

PART 4
BOUNDARY LAYER ESTIMATES

4.1 INTRODUCTION

In a real fluid, vixcous effects are present. If the fluid is of low viscosity, these effects are confined to a narrow layer next to the solid boundary. The flow within the boundary layer increases smoothly from zero velocity at the wall to a maximum at the free stream velocity.

It is a reasonable assumption that the flow would be isentropic between the inlet and exit planes with the esception of the small boundary layer region described above.

Since the physically meaningful measure of the boundary layer thickness is the displacement thickness, then the nozzle potential outline for a perfect fluid must be displaced outwards by this amount (see figure 1.31).

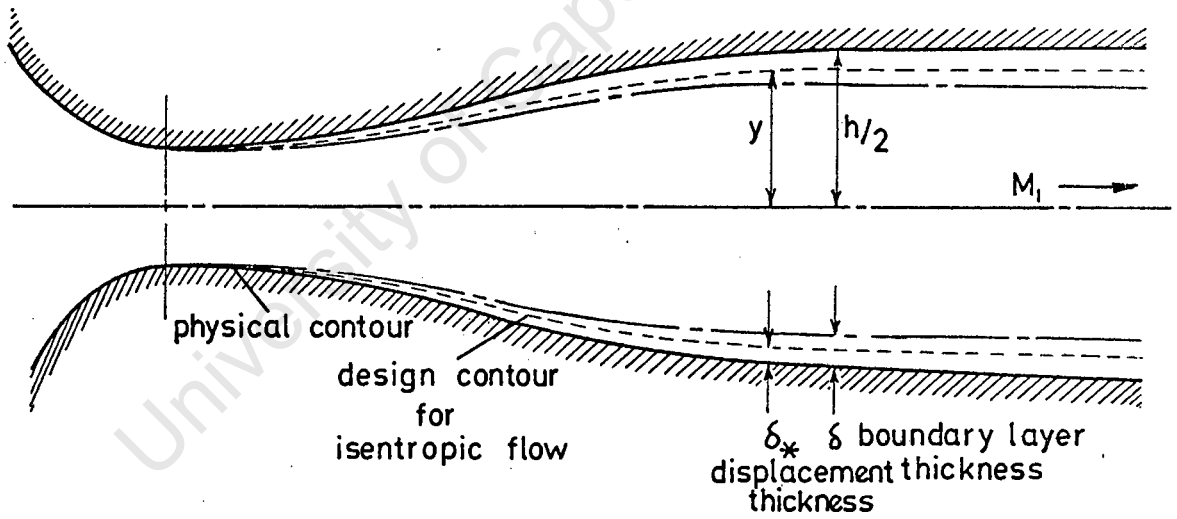

FIGURE 1.31

This allowance in the nozzle contour is dependent upon an accurate estimate of the actual boundary layer thickness. The profile of the turbulent boundary layer is defined as: reference?

$$\frac{U}{U_1} = \left(\frac{Y}{\delta}\right)^{1/N} \qquad \text{.....} \qquad 1.35$$

(See figure 1.31)

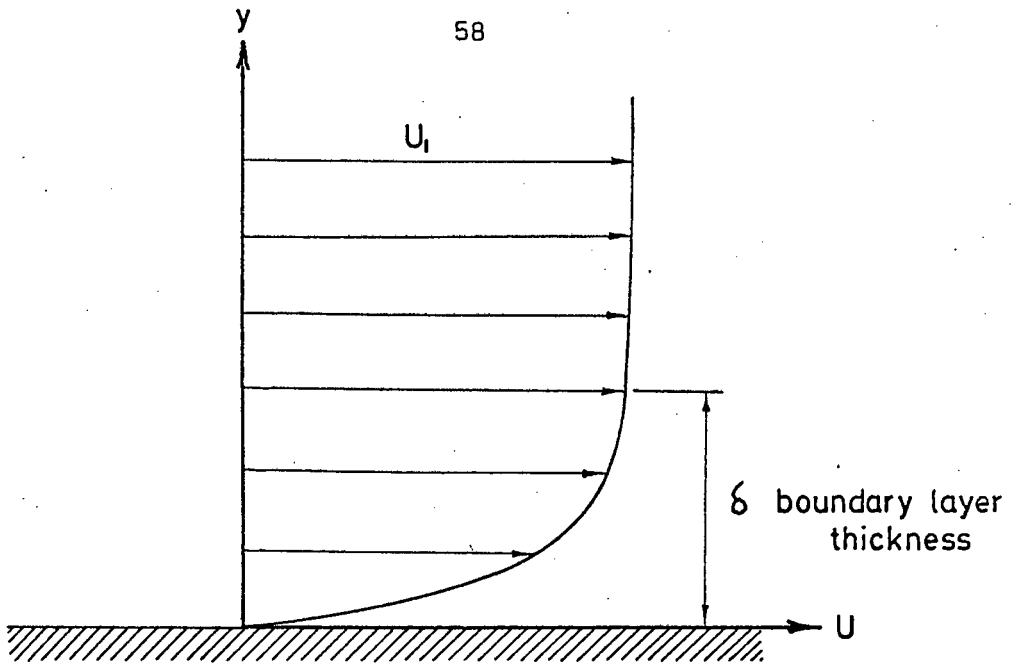

VELOCITY PROFILE

Figure 1.32

Experimental data from (5) and (4) show that the power law index N is approximately 7 for supersonic nozzles of low Mach number.

The displacement thickness is dependent upon the actual boundary layer thickness, the power low index and Mach number. The relationship between these factors was experimentally determined and is presented in (4) as a graph.

For the power law index of 7, the following equation best approximates the relationship between the displacement-boundary layer thickness ratio, G_d, and the Mach number.

$$\therefore G_d = \frac{\delta^*}{\delta} = 0{,}088M + 0{,}07 \quad \ldots\ldots\ldots\ldots\ldots\ldots\ldots \quad 1.36$$

4 2 SIDE WALL ALLOWANCES

Boundary layer compensation is achieved by gradually moving the four tunnel walls away from the nozzle axis by the amount of the displacement thickness increase. Because it is usually necessary to keep the side walls parallel, a satisfactory compromise is achieved by displacing the curved nozzle surfaces still further. Although the flow is in fact undergoing a three-dimensional change due to boundary layer growth on the side walls, the resultant flow pattern is the same as a perfect two-dimensional nozzle (1).

This total effective displacement thickness, δ_{eqv}, on the curved nozzle contours, must be found in terms of the displacement thickness, δ_*, and the wind-tunnel cross-sectional dimensions. These dimensions W and h, are the physical boundaries of the theoretically perfect flow field. (See figure 1.33)

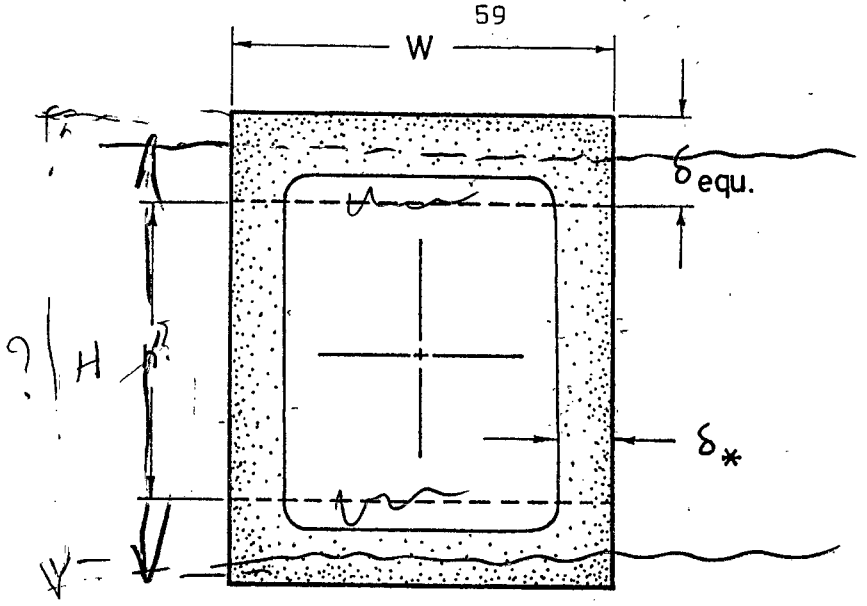

FIGURE 1.33

The effective core area, $A_e = w.h$ $A_e = (W - 2\delta_*)\,h$

The curved nozzle surfaces must be displaced by δ equ to compensate for the boundary layer growth. Because this phenomena occurs on all four walls, the real core area becomes:

$$A_c = (w - 2\delta_*)(h) - 2\delta_* + 2\,\delta\,\text{equ}) \qquad H - 2\delta_{eq}$$

$$= wH + 2w(\delta\,\text{equ} - \delta^*) - 2H\delta^* - 4\delta^*(\delta\,\text{equ} - \delta^*)$$

$4\delta^*(\delta\,\text{equ} - \delta^*)$ may be neglected if the boundary layer is thin.

$$\therefore\ A_c = wh + 2w(\delta\,\text{equ} - \delta^*) - 2H\delta^*$$

The mass flow rate through the effective core area would be the same as through the real core area.

$$\therefore\ A_c = A_e$$

$$\therefore\ \delta\,\text{equ} = \frac{\delta^*(W + h)}{W} \qquad \text{.....} \qquad 1.37$$

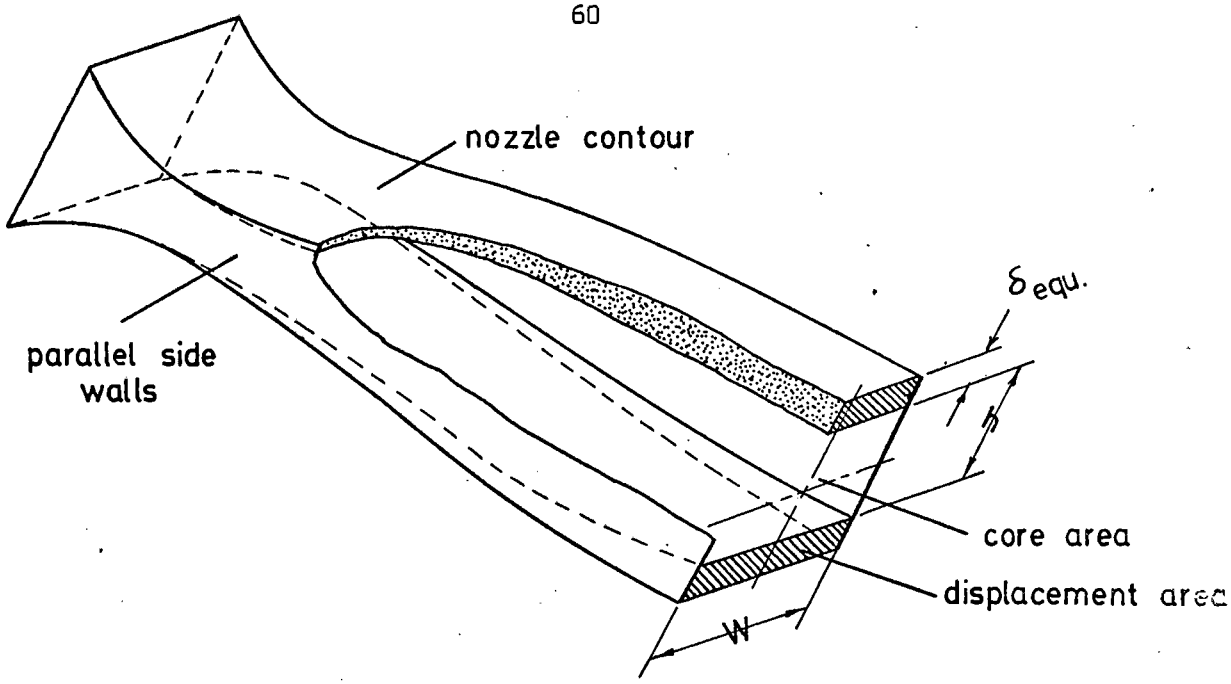

NOZZLE BOUNDARY LAYER GROWTH
Figure 1.34

The boundary layer growth is not necessarily consistent on all four walls of the wind-tunnel.(1). Pressure gradients down the axis of the nozzle and perpendicular across the side walls act on the boundary layer and cause deviations. For example, the transverse pressure gradient causes the boundary layer to thicken along the centreline.

To avoid undue complications in the application of boundary layer equations, these above considerations may be neglected. i.e. Boundary layer growth is assumed linear along the axis of the nozzle and at any cross-section, it is the same on all four walls.

4.3 APPLICATION OF THE TURBULENT BOUNDARY LAYER EQUATION.

In order to determine the displacement thickness, the first step is to fine the rate of boundary layer growth along the nozzle. Unfortunately, no single solution has been found for all the cases of growth in supersonic nozzles because of Mach number variation, nozzle dimensions, pressure gradients and other variables. But, by comparison with experimental data and making basic assumptions on the development of the boundary layer growth, a suitable solution can be found.

The experimental increases in boundary layer thickness, in terms of distance from the nozzle throat and the test-section Reynold's Number, have been grouped together (4). For design Mach numbers below 2.5, the approsimate curve may be represented as:

$$\frac{\Delta\delta}{l} = \frac{0.29}{R_e^{1/5}} \qquad \text{1.38}$$

$$\frac{\Delta\delta}{l} = \frac{0.29}{Re^{0.2}}$$

Here $\frac{\delta}{l}$ is the mean rate of growth of the boundary layer with respect to the distance from the nozzle throat.

This equation implies that the rate of growth is constant throughout the nozzle. It also assumes that the boundary layer starts at the nozzle throat.

This second assumption is not strictly true, except for Mach numbers above 3.0 (4). At the higher Mach numbers, the large favourable pressure gradients restricts the growth of the boundary layer.

Fortunately, experimental evidence was available (5) that indicated that the above equation suitably accounted for this effect within the required Mach number range.

Reynold's Number:

The Reynold's number for the wind-tunnel test-section is given as:

$$R_e = \frac{\rho v l_e}{\mu} \quad \text{.....} \quad 1.39(a)$$

Where:

Air viscosity co-efficient $\mu = \left(\frac{T_1}{T_o}\right)^{0,76} \mu_o$ ..... 1.39(b)

Air density $\rho = \frac{P_1}{T_1 R}$ ..... 1.39(c)

Air velocity $v = M_1 \sqrt{\gamma R g T_1}$ ..... 1.39(d)

Length l_e is the distance from the nozzle throat to the nozzle exit.

Reynold's Number, and therefore the rate of boundary layer growth, changes with stagnation conditions. It is necessary to choose the stagnation pressure and temperature that satisfies the normal working conditions of the supersonic wind-tunnel.

1. Let the operating stagnation pressure be about 10 lb.per sq.inch above the critical minimum.

2. Let the average stagnation temperature during a run be $545^{o}R$ (11).

Equivalent Displacement Increase:

The required outward displacement of the curved nozzle potential outlines, in terms of distance from the nozzle throat, may be obtained by applying equations 1.36 and 1.37 to the turbulent boundary layer equation 1.38. Applying the initial conditions ($\delta = 0$ at $l = 0$) gives:

$$\delta_{equ} = (0.088M + 0.07)\left(\frac{W + (2Y)}{W}\right)\left(\frac{0.29l}{R^{0.2}}\right) \quad \text{.....} \quad 1.40$$

(See also figure 1.33)

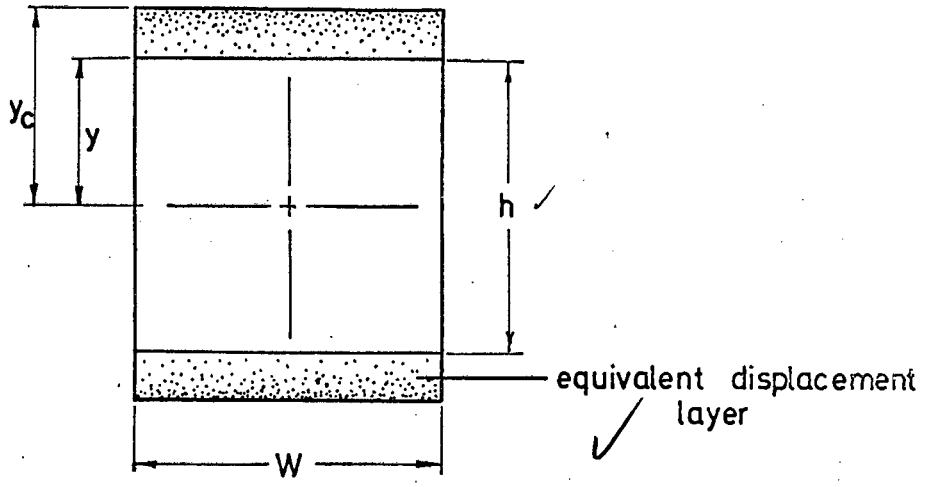

FIGURE 1.35

4.4 BOUNDARY LAYER CORRECTION

The boundary layer correction equation (1.40) may now be applied to the analytical and semi-graphical nozzle design. A digital computer was employed to correct the nozzle contour co-ordinates by the predicted equivalent displacement thickness.

Besides the input of X and Y nozzle co-ordinates, the information following is required for the successful operation of the programme:

1. The design nozzle Mach number, (M).
2. The length from the origin to the exit of the nozzle, (X_e).
3. The length from the origin to the nozzle throat, (X_*).
4. The tunnel width, (W).
5. The throat height, (Y_*) - half for symmetrical nozzle.
6. The stagnation temperature, (T_t).
7. The stagnation pressure, (P_t).
8. Temperature Ratio, (T_1/T_t))
9. Pressure Ratio, (P_1/P_t)) obtained from tables (15).
10. The half height of the nozzle box, (Y_b).

The test section Reynold's Number can be found by substituting the relevant data into equations 1.39 (a), (b), (c), and (d).

At each co-ordinate along the axis of the nozzle, the equivalent Mach number can be estimated from the area ratio, $Y/Y_* = A(M)$.

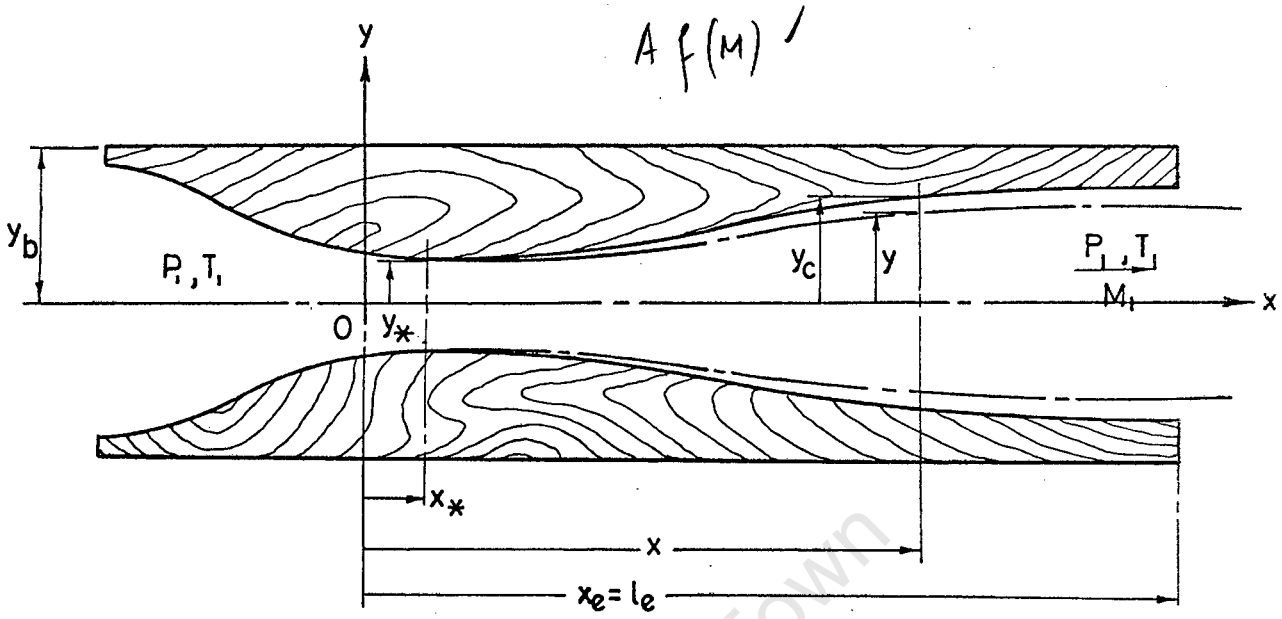

FIGURE 1.36

Rearranging equation 1.19:

$$M = \sqrt{\frac{2}{\gamma - 1}\left\{\left(\frac{\gamma+1}{2}\right)(M_* A(M))^{2(\gamma-1)/(\gamma+1)} - 1\right\}} \quad \text{.....} \quad 1.41$$

This equation may be solved in terms of the area ratio by taking successive itterations until the difference in Mach number on both sides is very small.

For each point, then, along the nozzle outline, the local Mach number M, the Y co-ordinate and the distance from the throat (which is $X - X_*$) may be applied to equation 1.40 together with the nozzle test-section Reynold's Number.

Flow Diagram:

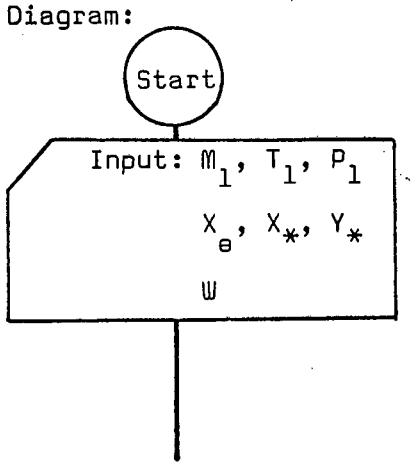

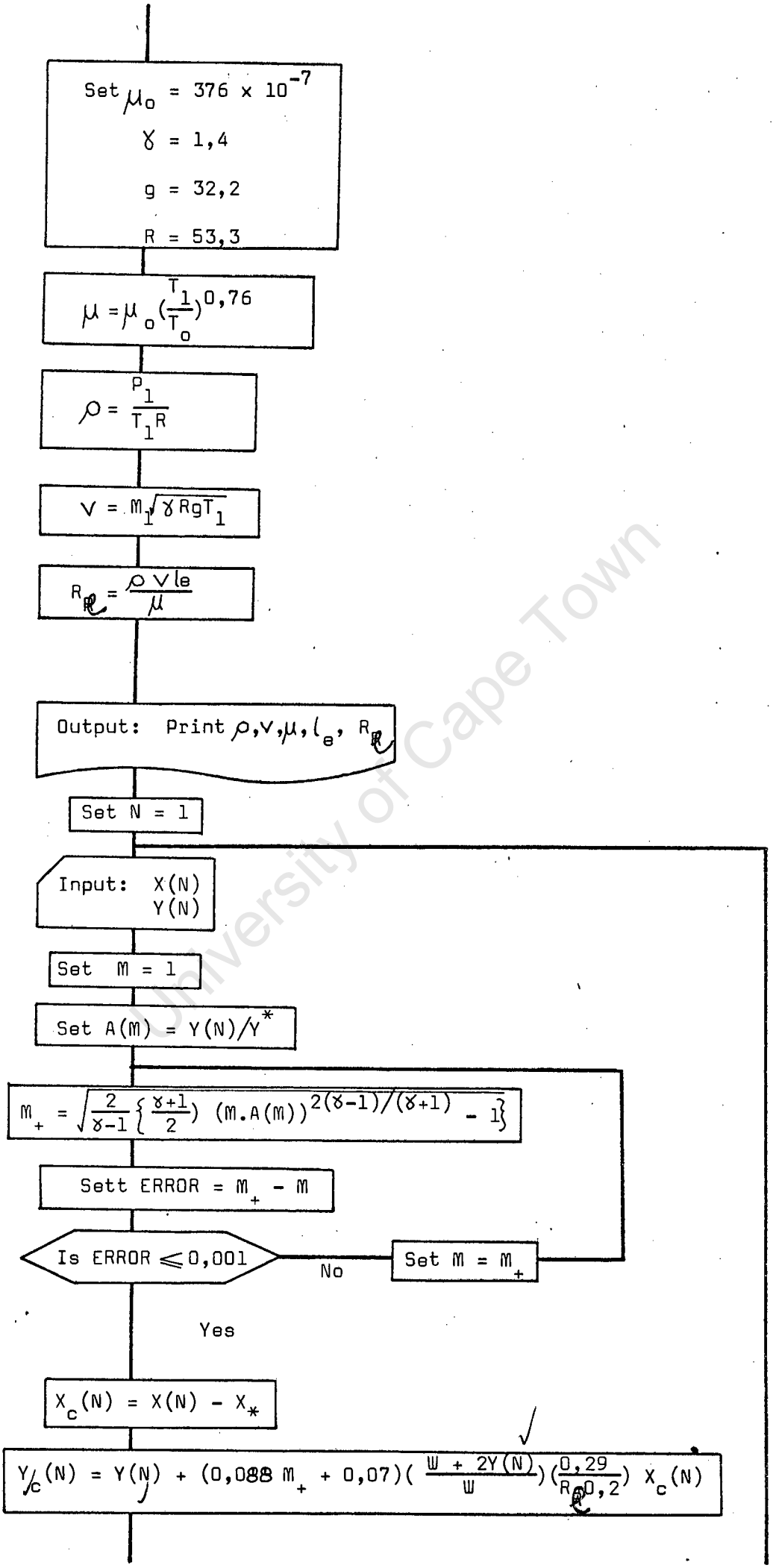

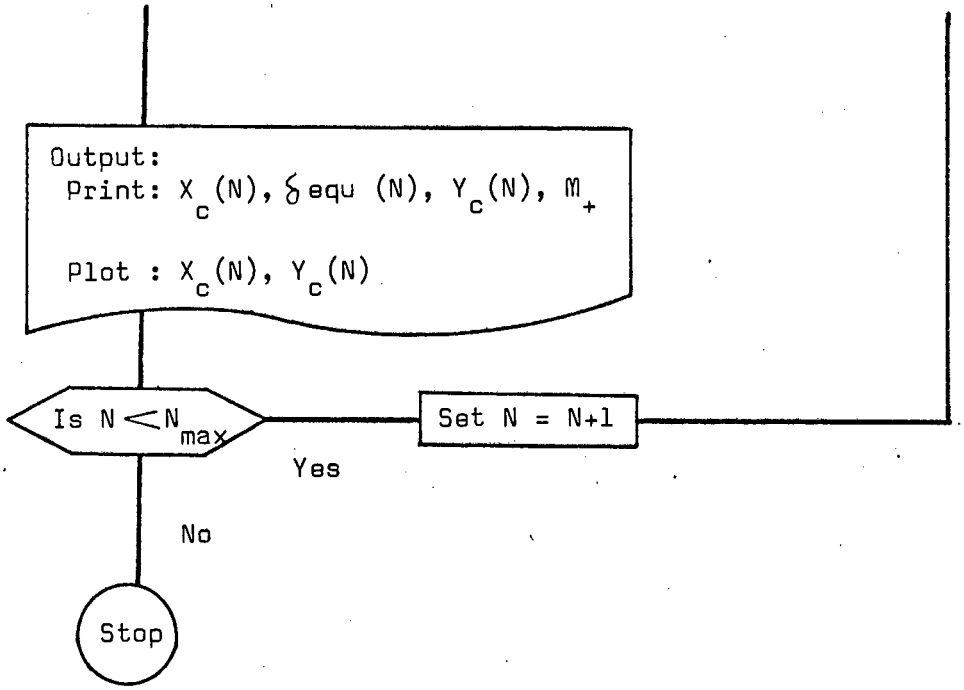

The boundary layer correction output is produced at full size. Figures 1.37 and 1.38 are scaled down versions of this output for the semi-graphical and analytically designed nozzles respectively. It is clearly seen how the nozzle contour changes when the boundary layer growth is taken into account (see figures 1.37 and 1.38, curves (a) and (b)).

Also incorporated in these plots are the final size and shapes of the required nozzle blocks.

The full programme for boundary layer correction is presented in appendix 1.1C together with an explanation of the application of the design parameters.

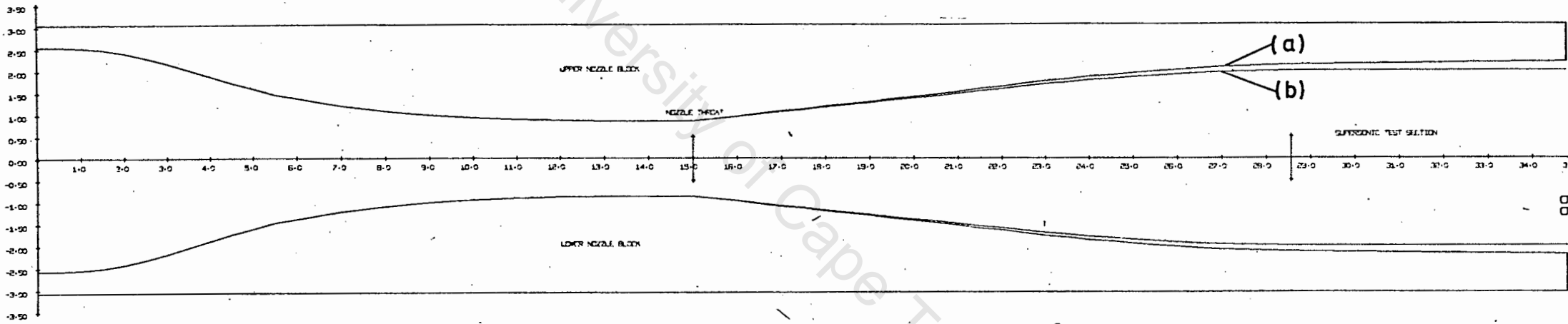

what is a? b?

Figure 1·37

SUPERSONIC NOZZLE PROFILE FOR MACH NUMBER OF 2·3533
WITH BOUNDARY LAYER CONSIDERATIONS

SCALE FULL SIZE · INCHES

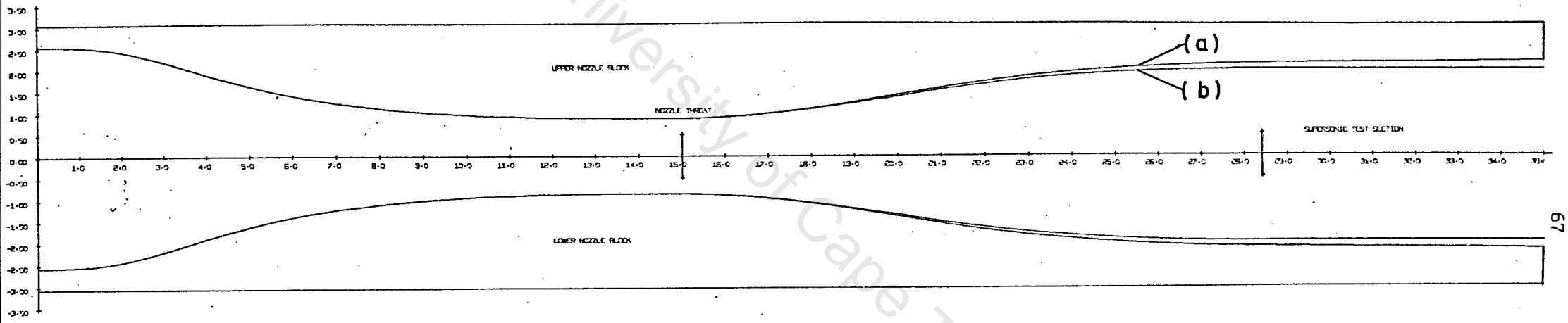

Figure 1.38

SUPERSONIC NOZZLE PROFILE FOR MACH NUMBER OF 2·35
WITH BOUNDARY LAYER CONSIDERATIONS

SCALE FULL SIZE, INCHES

PART 5
NOZZLE PERFORMANCE

5.1 DESIGN OF TESTING APPARATUS

Recording the properties of supersonic flow is achieved in a couple of ways:

(a) Optical Techniques:
   1. Schlieren Method.
   2. Interferometer.
   3. Shadowgraph.

(b) Dynamic Measurements:
   1. Static Pressure Calibration.
   2. Pitot Pressure Calibration.

The optical method is only approximate because the picture represents the integrated effect of disturbances across the width of the test-section. This method is also limited in value by the accuracy in measuring Mach angles. The most accurate determination of the Mach number distribution is obtained from a pitot and static survey of the flow. The following instruments were designed and constructed to achieve a thorough investigation of the flow pattern within the semi-graphical and analytical nozzles.

Static Pressure Plates

Two blanking plates are used to replace the glass side covers of the tunnel. Five rows of pressure holes, set at one inch intervals on one of the plates, are used to record the static pressures down one vertical wall within the tunnel. (See figure 1.39)

Because there are no pressure gradients normal to the wall, any pressures measured in the stationary fluid of the boundary layer is a representation of the free stream static pressure.

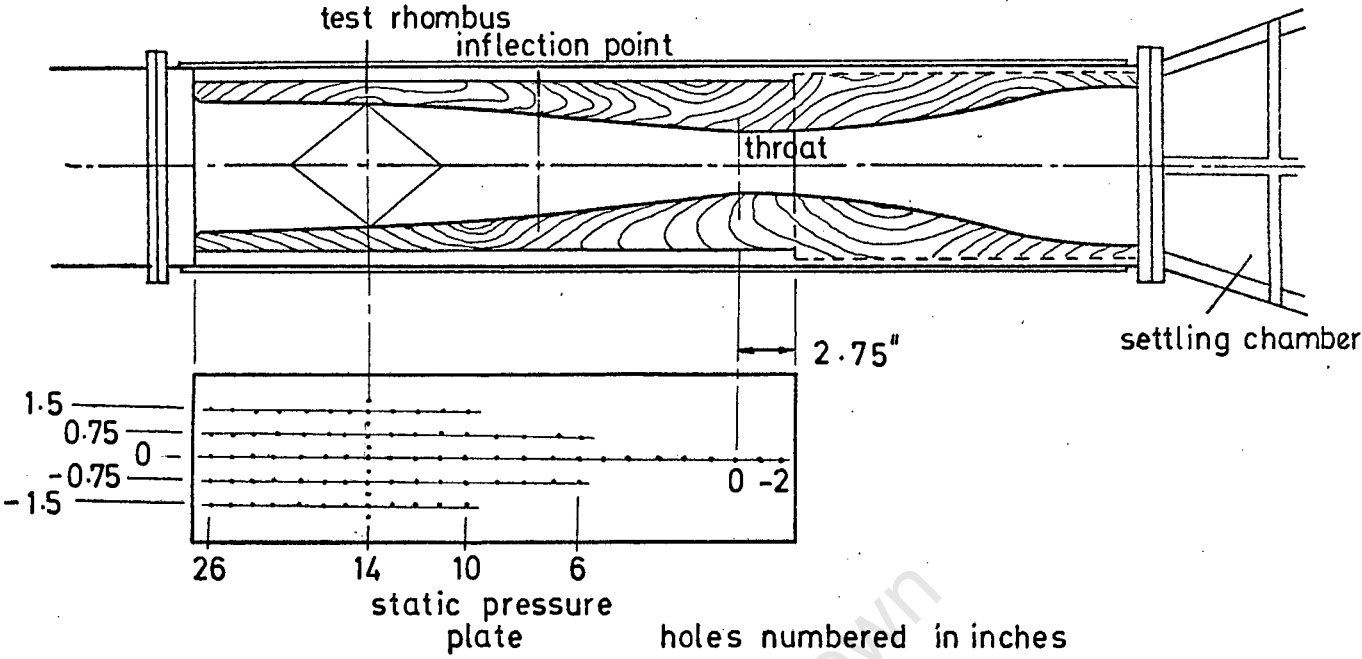

STATIC PRESSURE PLATES
Figure 1·39

The large number of static holes requires that several runs are needed to complete the full pressure distribution. The pressures are measured on a 20 point mercury manometer, the columns held stationary by an air controlled guillotine for post run recording.

Static Probe (Figure 1.41(a))

The free stream static pressure may be measured by introducing a very thin probe with pressure holes located in the surfaces parallel to the flow direction. Great care must be taken to allign the probe with the flow direction so that the fluid disturbances are kept to a minimum.

In the immediate neighbourhood of the probe, owing to oblique shocks and Prandtl-Meyer expansion waves, there are large variations in pressure and flow direction.

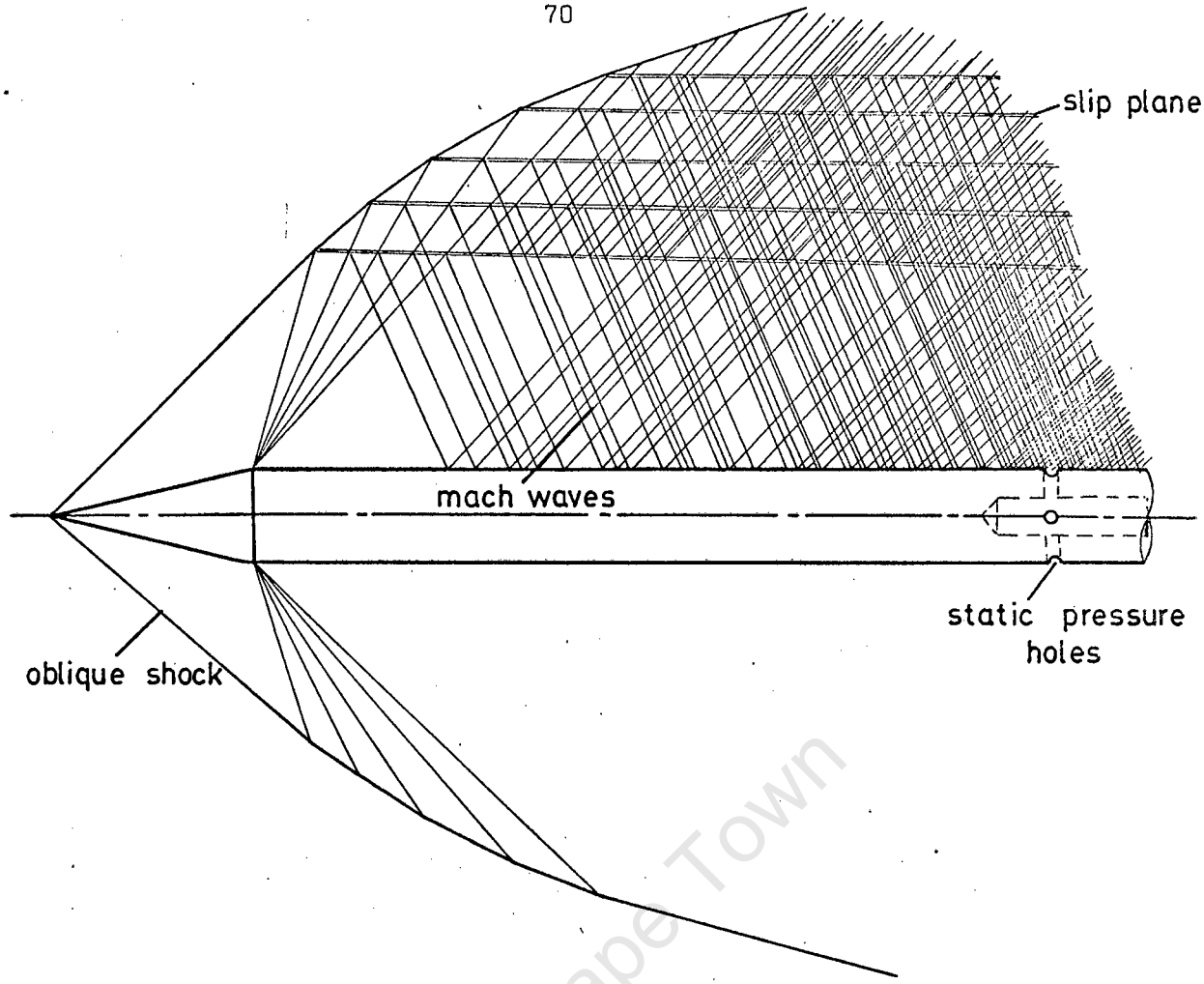

STATIC PRESSURE PROBE

Figure 1.40

However, the compression and expansion waves eventually merge and thereby are mutually weakened. In this discrete wave pattern, the variation in stream properties created along the curved shock is represented by slip planes. Wavelets striking these slip planes are partially transmitted and partially reflected. As more and more waves appear in the field, the non-uniformities are distributed on an ever finer scale. (see figure 1.40). At large distances the flow is, for all practical purposes, uniform and parallel with only an infinitesimal deviation from the free stream condition.

The pressure holes must be at least ten diameters downstream of the sharp conical nose (7).

Pitot Probe and Rake (Figure 1.41(b),(c))

The pitot probe is an instrument that measures stagnation pressure by bringing the flow to rest. In supersonic flow, a normal detached shock exists in front of the blunt nosed probe (see figure 1.42). The stagnation pressure of the fluid measured by the probe would be less than the free stream stagnation pressure.

(i.e. There is an entropy increase across the irreversible shock process)

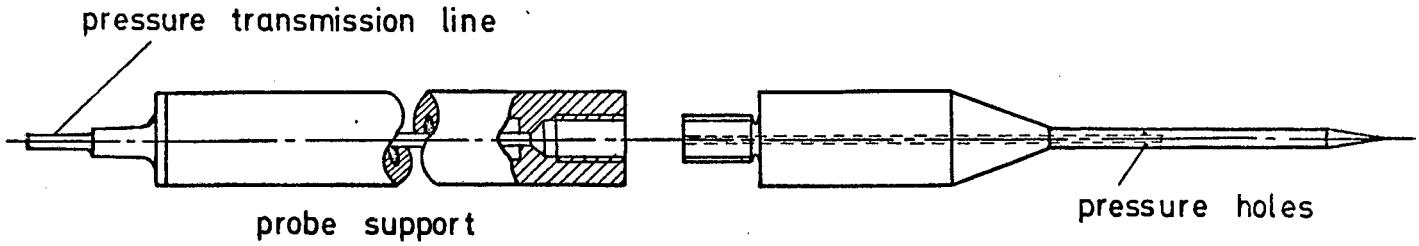

(a) STATIC PROBE

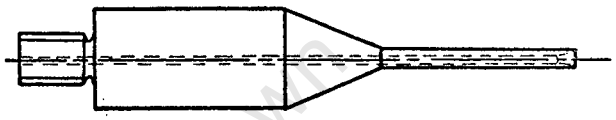

(b) PITOT PROBE

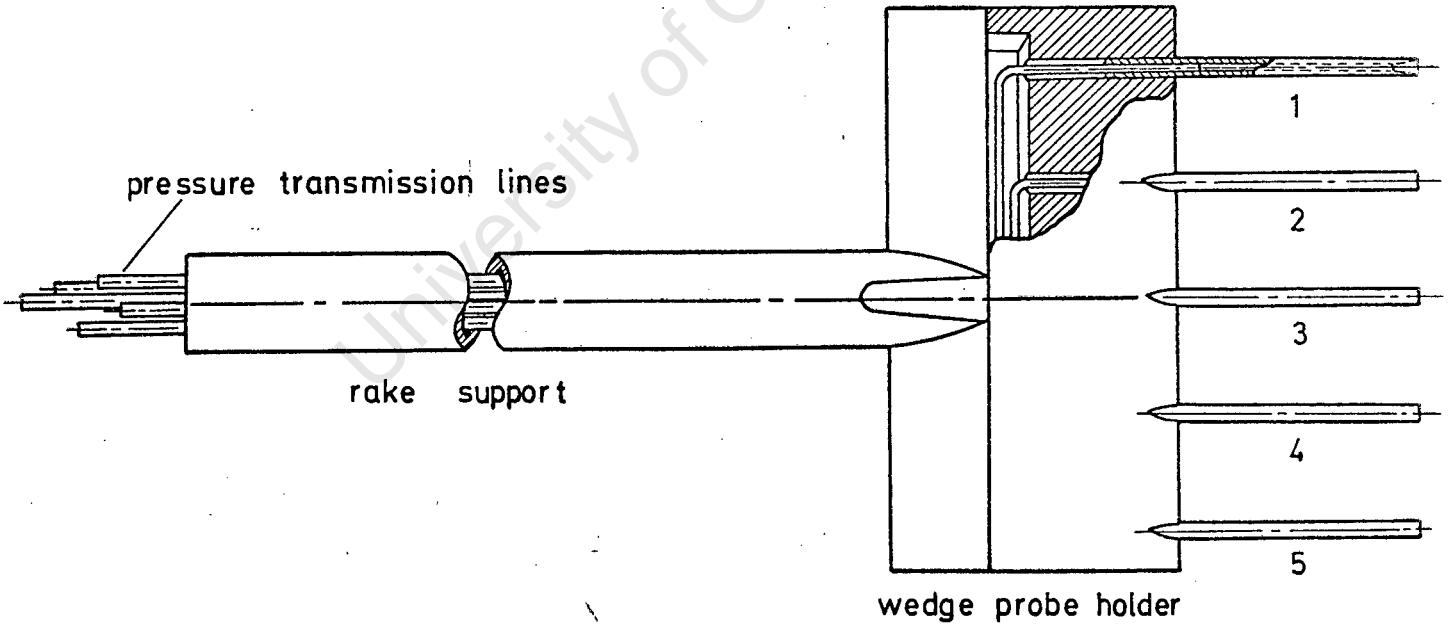

(c) PITOT RAKE

PRESSURE MEASURING INSTRUMENTS

Figure 1·41

Full Size

The relationship between these stagnation pressures, before and after the normal shock, determines the approach Mach number at that point.

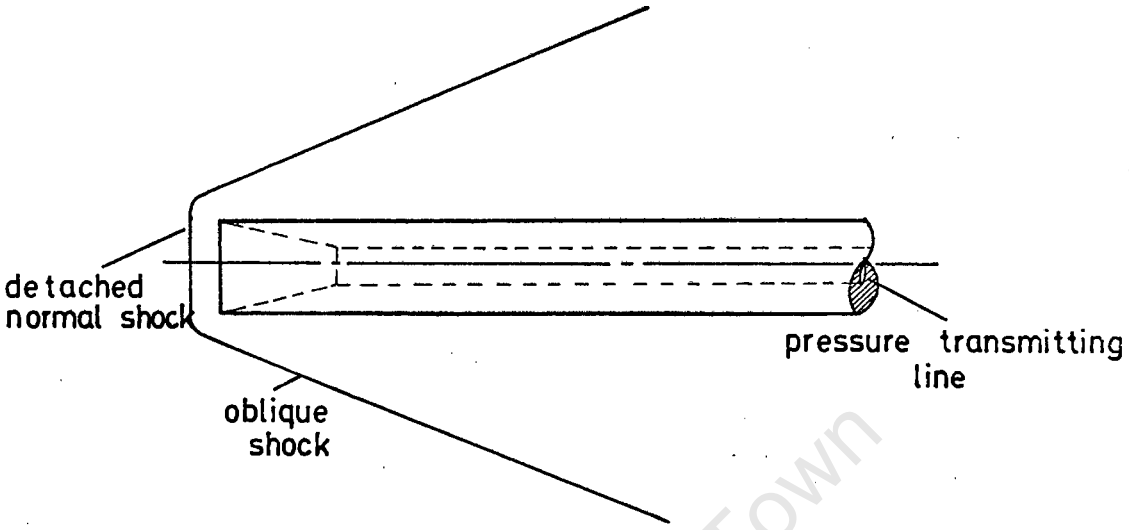

PITOT PRESSURE PROBE

Figure 1.42

The pitot rake has the same principle, but the multiple probes facilitate the traverse off the central axis of the wind-tunnel.

Model Support Sting. (Figure 1,43)

The model and probe support sting was streamlined to prevent chocking before supersonic flow existed in the test-section.

The rigid tubing, to which the probe or models are attached, is secured by lock-nut at the sting. It may be freed to allow a traverse through the wind-tunnel test-section and test-rhombus.

Mach Number Calibration.

The calibration of a set of nozzle blocks for a wind-tunnel consists of finding the Mach number distribution within the whole fluid stream about the tunnel axis. The best method of finding the Mach number distribution is to conduct a systematic pitot and static traverse of the testing region. [ ] ?

Applying some of the isentropic flow relations, it is possible to determine the Mach number from the static pressure (P_1) or pitot pressure (P_{02}) if the stagnation pressure (P_{01}) is known. Or the Mach number can be determined from the Rayleigh Relation if the static (P_1) and pitot pressures (P_{02}) are both known. ✓

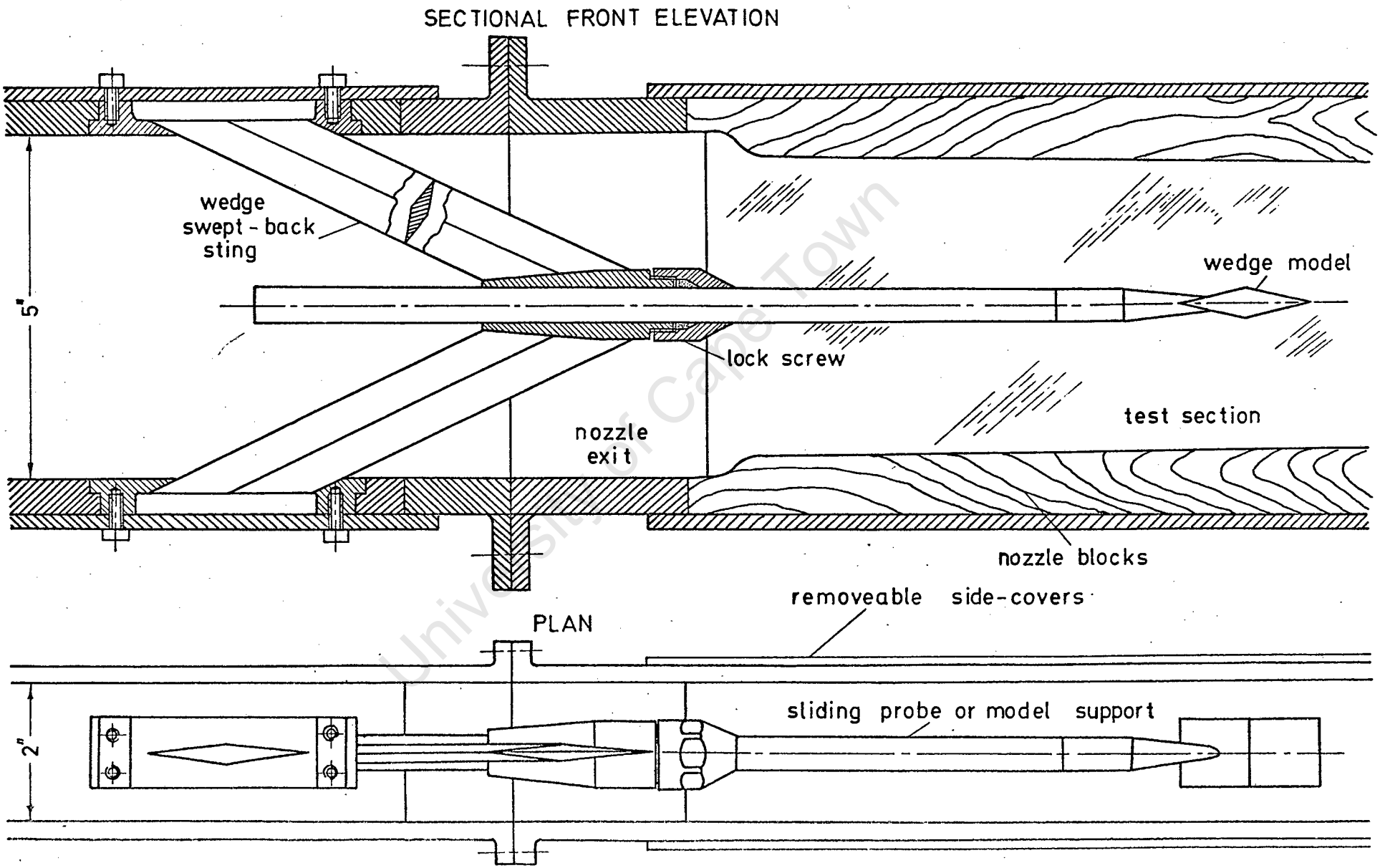

Figure 1.43 MODEL SUPPORT STING Half Full Size

From (7):

$$\frac{P_{01}}{P_1} = \left\{1 + \frac{\gamma-1}{2} M_1^2\right\}^{\gamma/\gamma-1} \quad \ldots\ldots\ldots\ldots\ldots\ldots\ldots\ldots \quad 1.42$$

$$\frac{P_{01}}{P_{02}} = \left\{\frac{(\gamma-1)M_1^2 + 2}{(\gamma+1)M_1^2}\right\}^{\gamma/\gamma-1} \left\{\frac{2}{\gamma+1} M_1^2 - \frac{\gamma-1}{\gamma+1}\right\}^{1/\gamma-1} \quad \ldots\ldots \quad 1.43$$

$$\frac{P_1}{P_{02}} = \left\{\frac{2}{(\gamma+1)M_1^2}\right\}^{\gamma/\gamma-1} \left\{\frac{2\gamma}{\gamma+1} M_1^2 - \frac{\gamma-1}{\gamma+1}\right\}^{1/\gamma-1} \quad \ldots\ldots\ldots \quad 1.44$$

The settling chamber pressure, P_t, is known. This should be a close approximation of the actual wind-tunnel stagnation pressure, P_{01}, because, theoretically, the flow is isentropic through the nozzle. An accurate calibration of the wind-tunnel stagnation pressure, in terms of the settling chamber pressure, may be achieved by using both the static and then the pitot probe and applying Rayleigh's Equation (1.44). ✓

For a more general calibration, either a pitot or static traverse may be undertaken using the settling chamber as a reference. The decision to use a pitot rake instead of a static rake was reached for the following reasons:

1. Pitot readings are not subject to small fluctuations and may therefore be read quite acurately. The static pressure readings are sensitive and are subject to small oscillations (7).

2. Secondly, if the same error is read on both the pitot and static probes for a Mach number of 2.50, then the theoretical ratio of the Mach number error of the static reading to the pitot reading is about 4,4 (7). %?

The determination of the Mach number from the pressure relationships in equations 1.42, 1.43 or 1.44 is achieved numerically by digital computer. The programmes are presented in appendix 1.11.

The programme applying Rayleigh's relation (1.44) also gives the actual stagnation pressure in terms of the settling chamber pressure.

5.2 TUNNEL RUN TIMES

The run times for the blow-down wind-tunnel, with nozzles of increasing Mach number, have been dealt with in Part 1. It is now necessary to examine the validity of these assumptions and confirm the length of blow-down period.

In this case, as only a nozzle of design Mach number 2,35 is to be considered, the run times are to be found as a function of the settling chamber pressure.

Valve Flow Characteristics.

The pressure drop from the storage drum to the settling chamber has been said to be caused by viscous losses, turbulence and restrictions. The latter of these is due to flow through the valve.

The pressure difference across the valve at the termination of the run. (i.e. when the valve reaches its limit of travel) may be found by considering the valve characteristic curve (figure 1.44).

The mass flow rate past the valve in terms of storage drum pressure, may be divided into two regions:

1. Supersonic Range:

For a large enough drum pressure, sonic flow occurs past the faces of the double valve seats. The mass flow rate ($\dot{m}$) is independent to back pressure and may be given as:

$$\dot{m} = 6,99 \; P_d \times X \quad \text{lbm/sec} \quad \ldots\ldots\ldots\ldots\ldots\ldots\ldots\ldots\ldots\ldots \quad 1.45$$

This is derived from equation 1.2 where:

P_d = drum pressure in lb per sq.in.

X = valve travel in inches.

and the constant 699.7

2. Subsonic Range:

For lower drum pressures subsonic flow will be present past the valve seats. Hence the mass flow rate becomes dependent upon back pressure. Applying Bernoulli's Equation for incompressible flow and assuming a discharge coefficient of 0,9:

$$\dot{m} = 1,885 \times X \times \sqrt{45,6 \; P_d(P_d - P_t)} \quad \text{lbm/sec}$$

where P_t = settling chamber pressure in lbs per sq.inch.

The valve flow characteristic curve in figure 1.44 is presented when the valve travel is at its extreme (i.e. X = 0,25 inches). The flow termination conditions, for nozzles of Mach number 2,0, 2,35 and 3,0, are shown to fall within the subsonic region of the curve.

The magnitude of the pressure loss across the valve, at run termination, is only of the order of about 5 lbs per sq. inch for the Mach 2.35 nozzle. Therefore the balance of the pressure loss between the storage drum and settling chamber must be due to the viscous friction and turbulence losses that are dependent

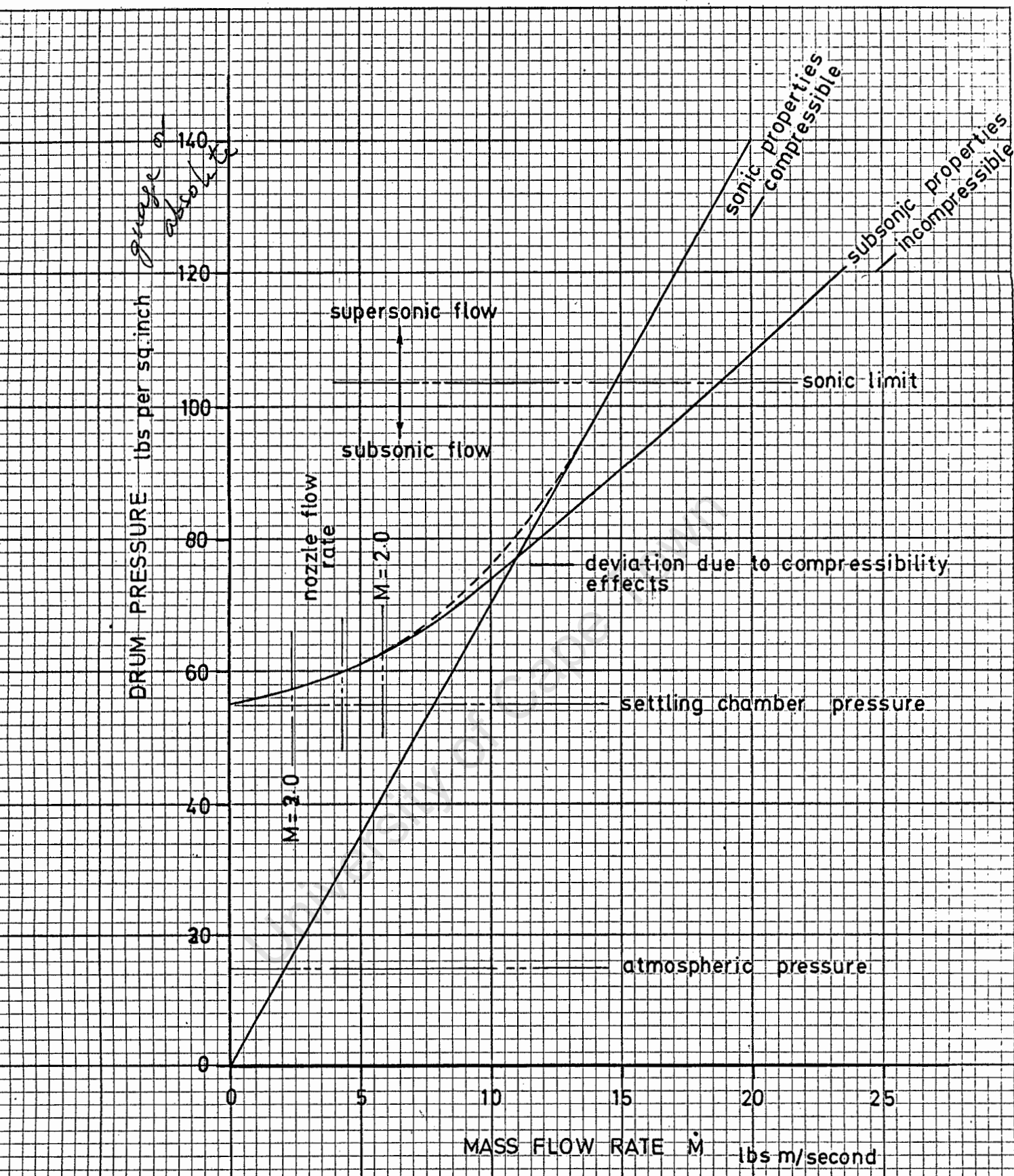

FLOW CHARACTERISTICS THROUGH VALVE

Figure 1.44

upon flow velocity.

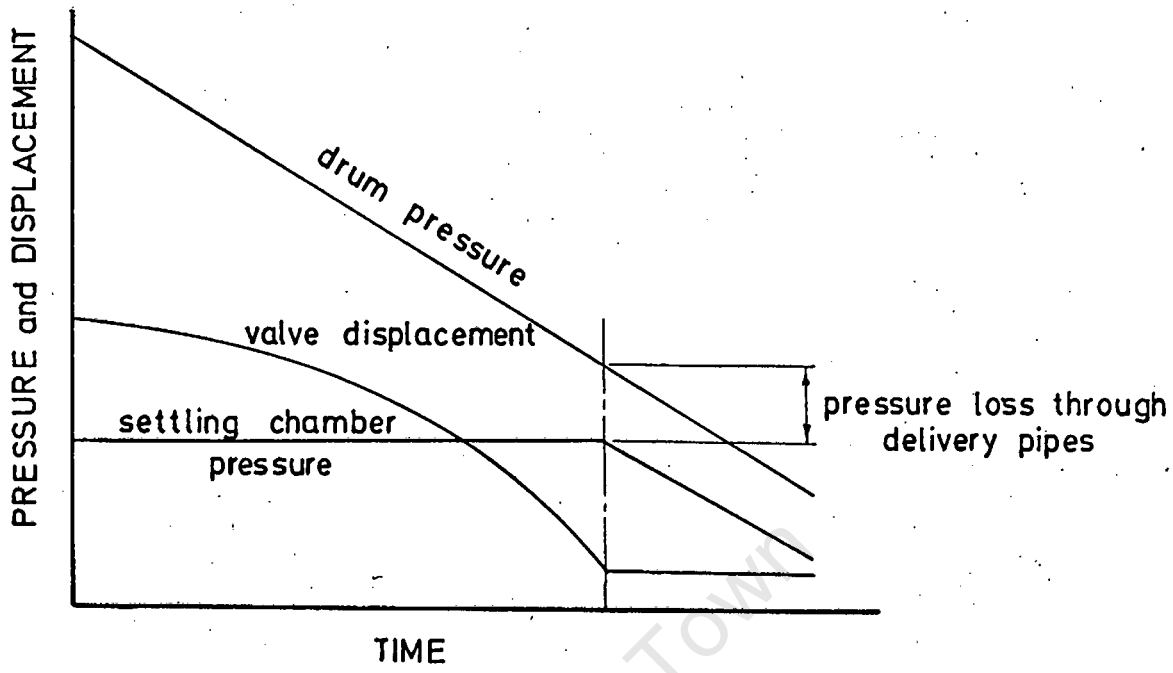

CONTROL VALVE CHARACTERISTICS
Figure 1.45

Blow-Down Time

For the same boundary conditions as in Part 1, but for a nozzle of 2,35 Mach number only, the mass flow rate is given by:

$$\dot{M}_n = 7{,}90 \times 10^{-2} P_s \quad \frac{lbm}{sec} \qquad \text{..... 1.47}$$

Similarly, the available mass of storage air is:

$$M = 0{,}811\ (130-P_s)\ \ lb_m \qquad \text{..... 1.48}$$

These equations are in terms of settling chamber pressure (P_s) in lbs per sq. inch. The run time is found by simply dividing the available mass by the mass flow rate:

$$t = \frac{M}{\dot{M}} = \frac{0{,}811\ (130-P_s)}{7{,}90 \times 10^{-2} P_s} \text{ secs} \qquad \text{..... 1.49}$$

The solution of this equation is given in figure 1.46.

The experimental blos-down period was recorded between flow initiation and run termination when the valve reached irs limit of travel.

The accuracy of these points (see figure 1.46) indicate that the pressure loss assumption and temperature are quite valid for a nozzle of this Mach number.

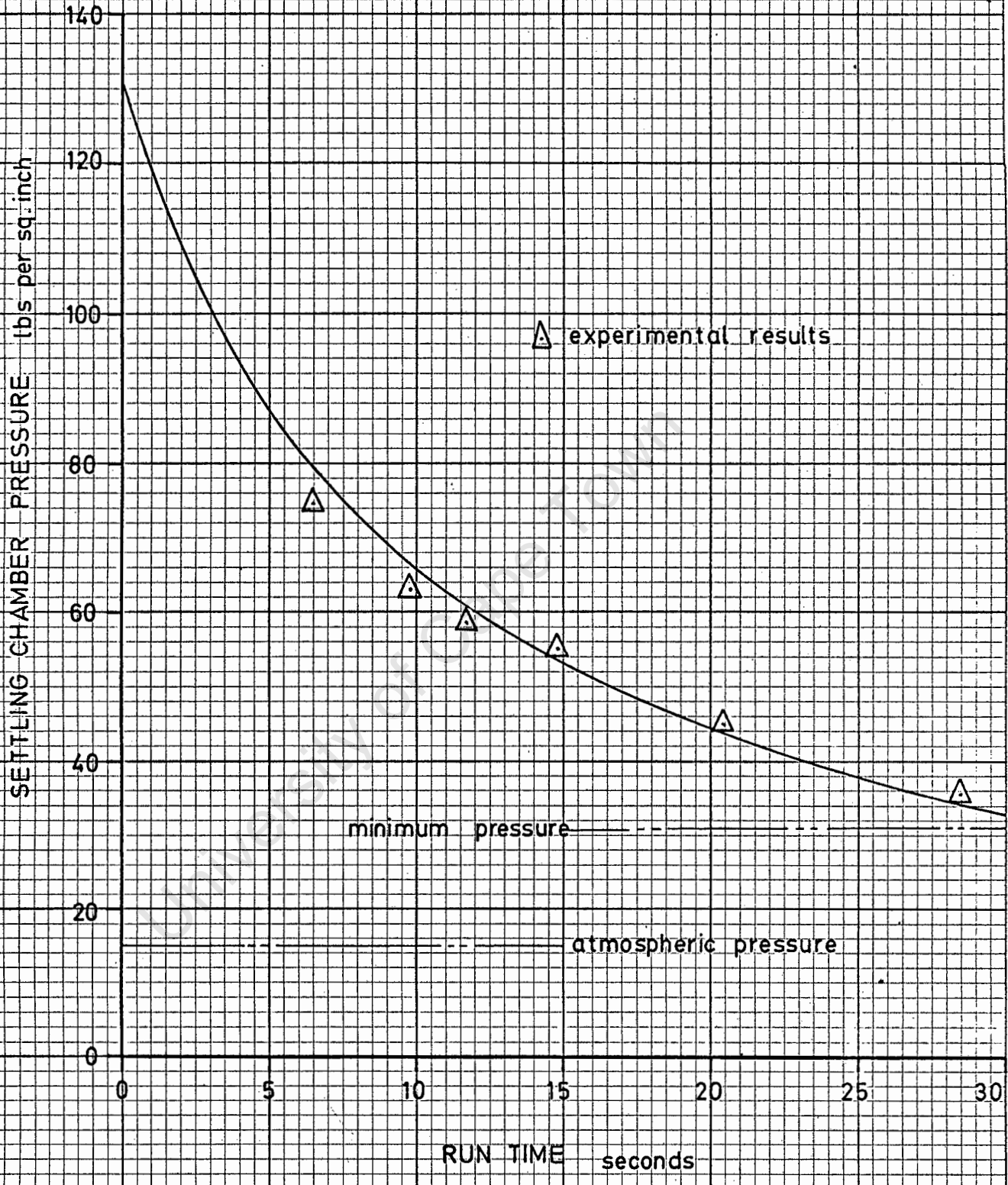

RUN TIME FOR MACH 2·35 NOZZLE

Figure 1.46

A second pitot brought our by these curves is the greater degree of supply pressure loss at run termination for the higher settling chamber pressures. This would be expected because of the increased mass flow rate through the ducting. Conversely, at low settling chamber pressures (when the mass flow rate is reduced) the experimental run times are longer than theoretically predicted.

5.3 CALIBRATION OF SUPERSONIC NOZZLES

The calibration of the supersonic nozzle is required to determine to what extent the experimental data follows the theoretically designed properties of the fluid flow.

Local disturbances are present in the theoretically uniform test-section flow because of the boundary layer phenomena, surface roughness or possible discontinuities in the side walls, limitations in constructional tolerances and design error. The degree of flow uniformity is illustrated by plotting the Mach number distribution within the test-rhombus and test-section. These calibrations are achieved by measuring the static pressure distribution over one of the side walls, or, as in this case, by measuring the pitot pressure distribution within the flow core area using a pitot rake.

Static Pressure Calibration:

Figure 1.47(a) and (b) gives the Mach number distribution superimposed upon the theoretical curves for the analytical and semi-graphical designed nozzles respectively. Each of the experimental traces represents a different position on the side wall. (see figure 1.38); the fluctuation about the mean determines the performance of the design.

These curves are shown to a larger scale in figures 1.48 and 1.49 for each of the five static pressure traversing lines.

Pitot Pressure Calibration:

The pitot calibration is more satisfactory than the static calibration because the Mach number may be determined more accurately even though the same reading error is present in both methods.?? Additionally, disturbances are set up by the presence of the large number of static taps which will possibly affect the readings to some extent.

The calibration results, for the pitot rake traverse through the vertical plane about the nozzle centre-line, are given in figures 1.51 and 1.52.

how about horizontal plane.

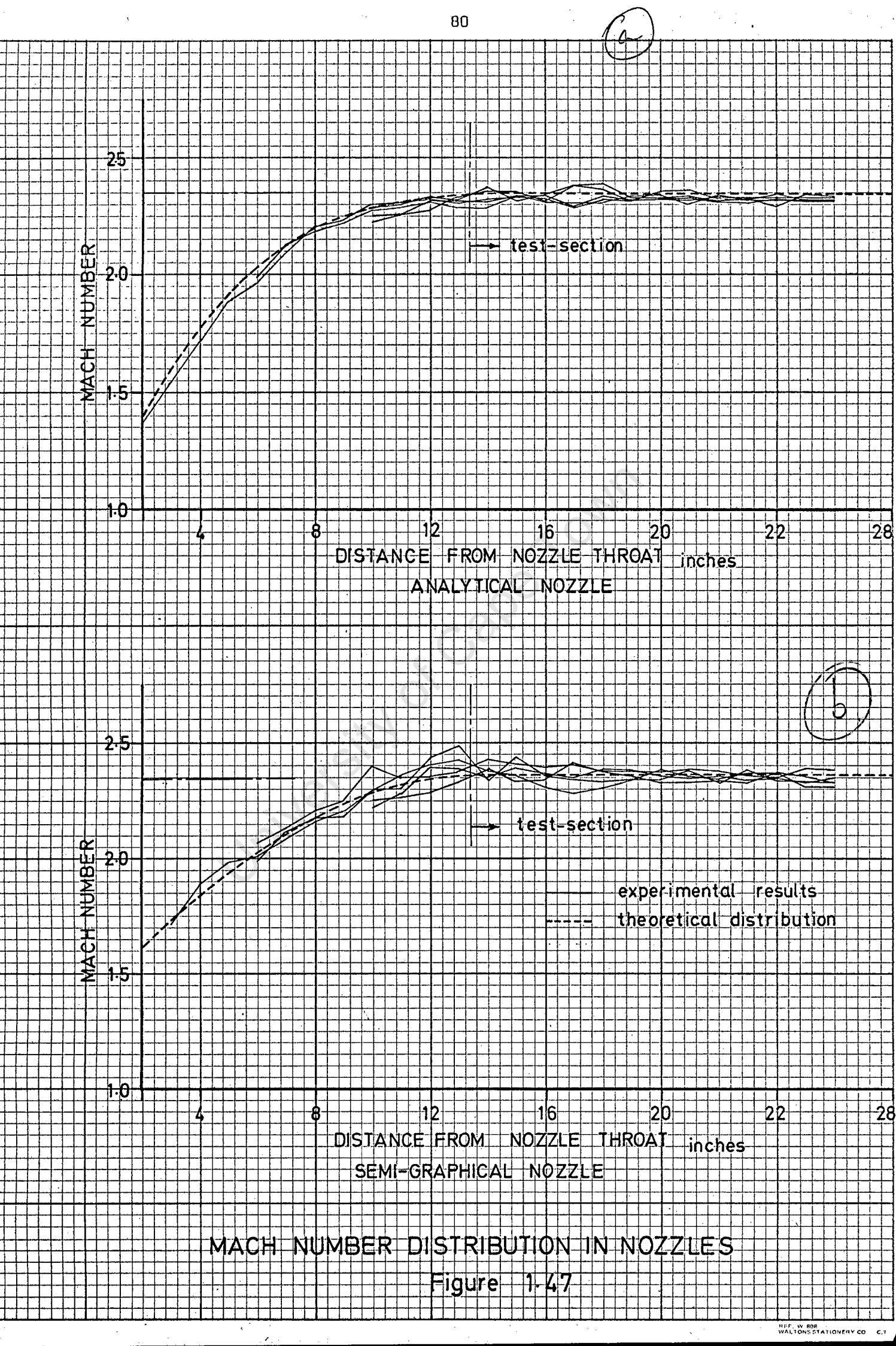

MACH NUMBER DISTRIBUTION IN NOZZLES

Figure 1.47

Calibration Results:

The calibrations in figures 1.48, 1.49, 1.51, and 1.52 have been investigated within the test-rhombus and test-section only. The areas outside these regions are indicated by dashed lines in these figures.

The calibration results are summarised in table 1.3 for both the analytical and semi-graphical nozzle designs.

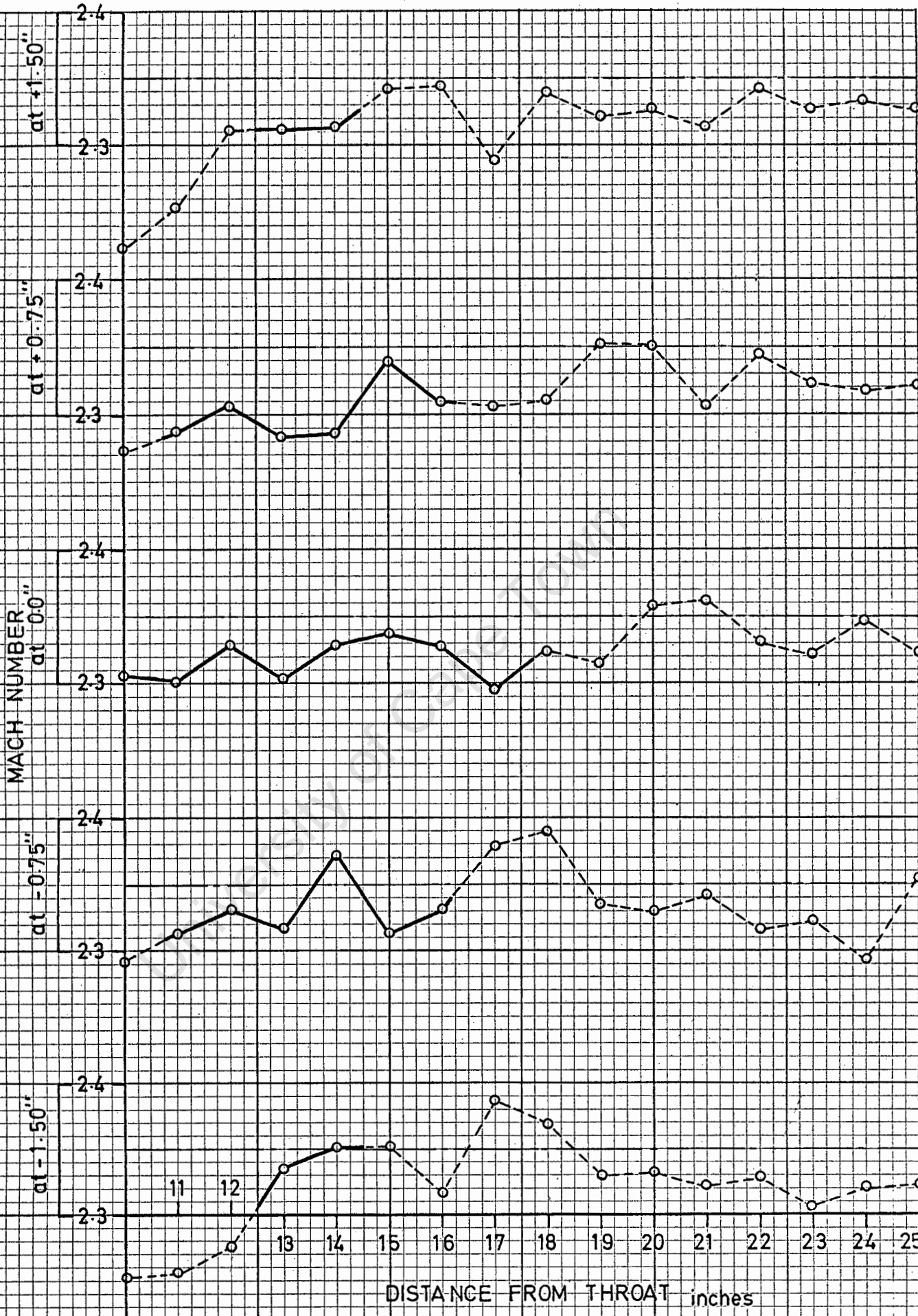

MACH NUMBER DISTRIBUTION FOR STATIC PRESSURE TESTING — ANALYTICAL NOZZLE

Figure 1.48

HFF W 808
WALTONS STATIONERY CO C F

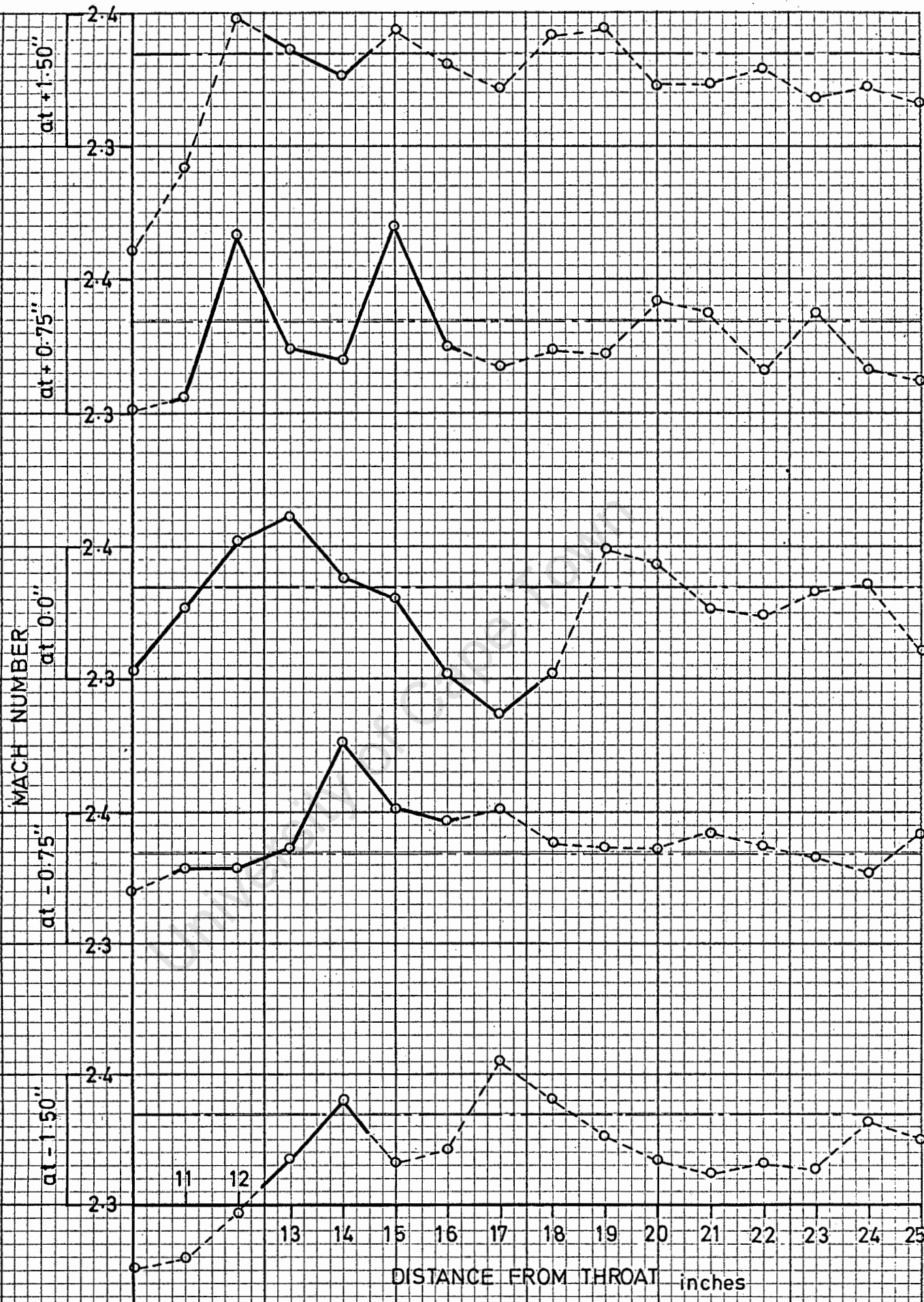

MACH NUMBER DISTRIBUTION FOR STATIC PRESSURE TESTING —— SEMI-GRAPHICAL NOZZLE

Figure 1.49

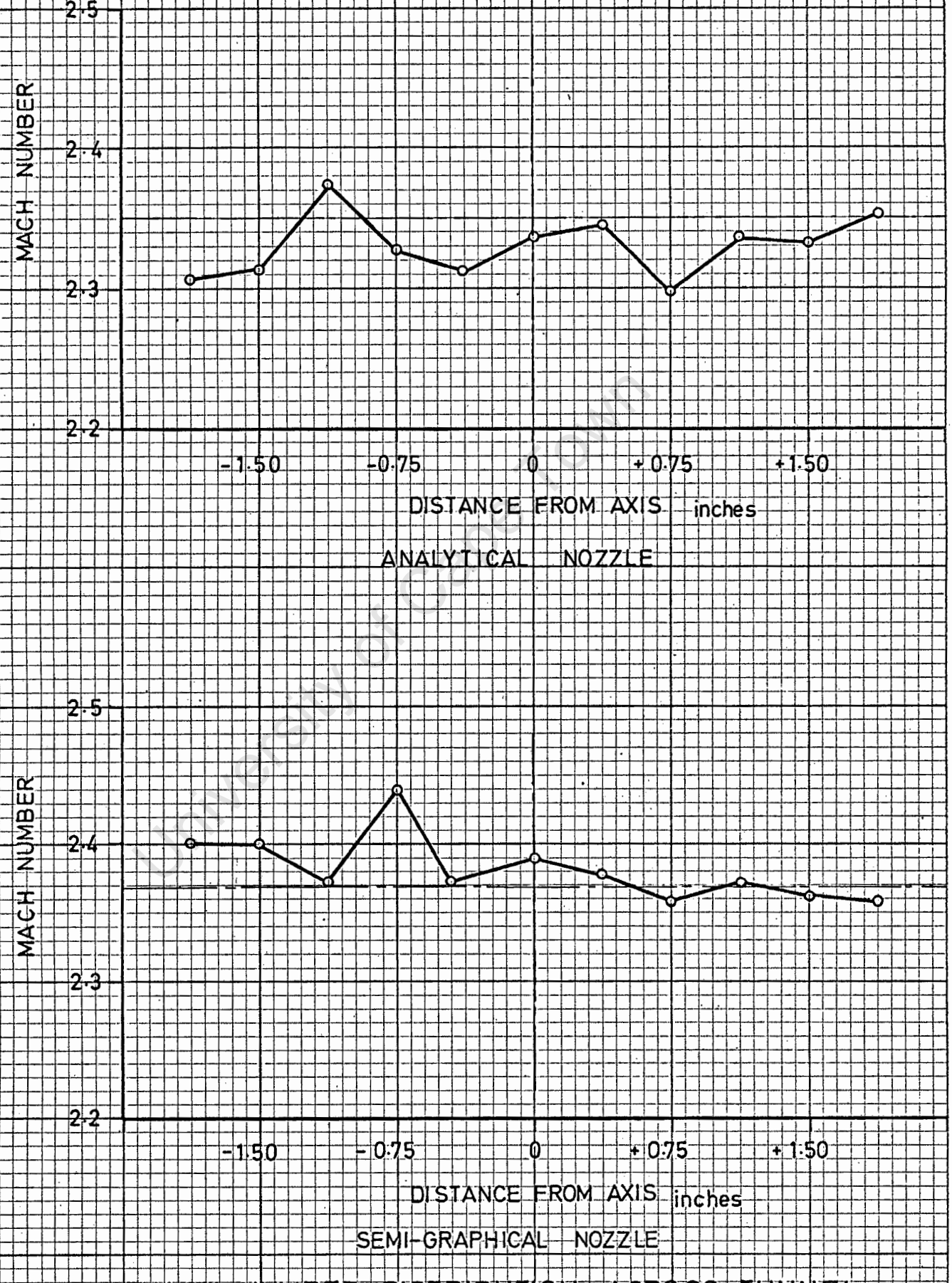

MACH NUMBER DISTRIBUTION ACROSS TUNNEL AT NOZZLE EXIT

Figure 1-50

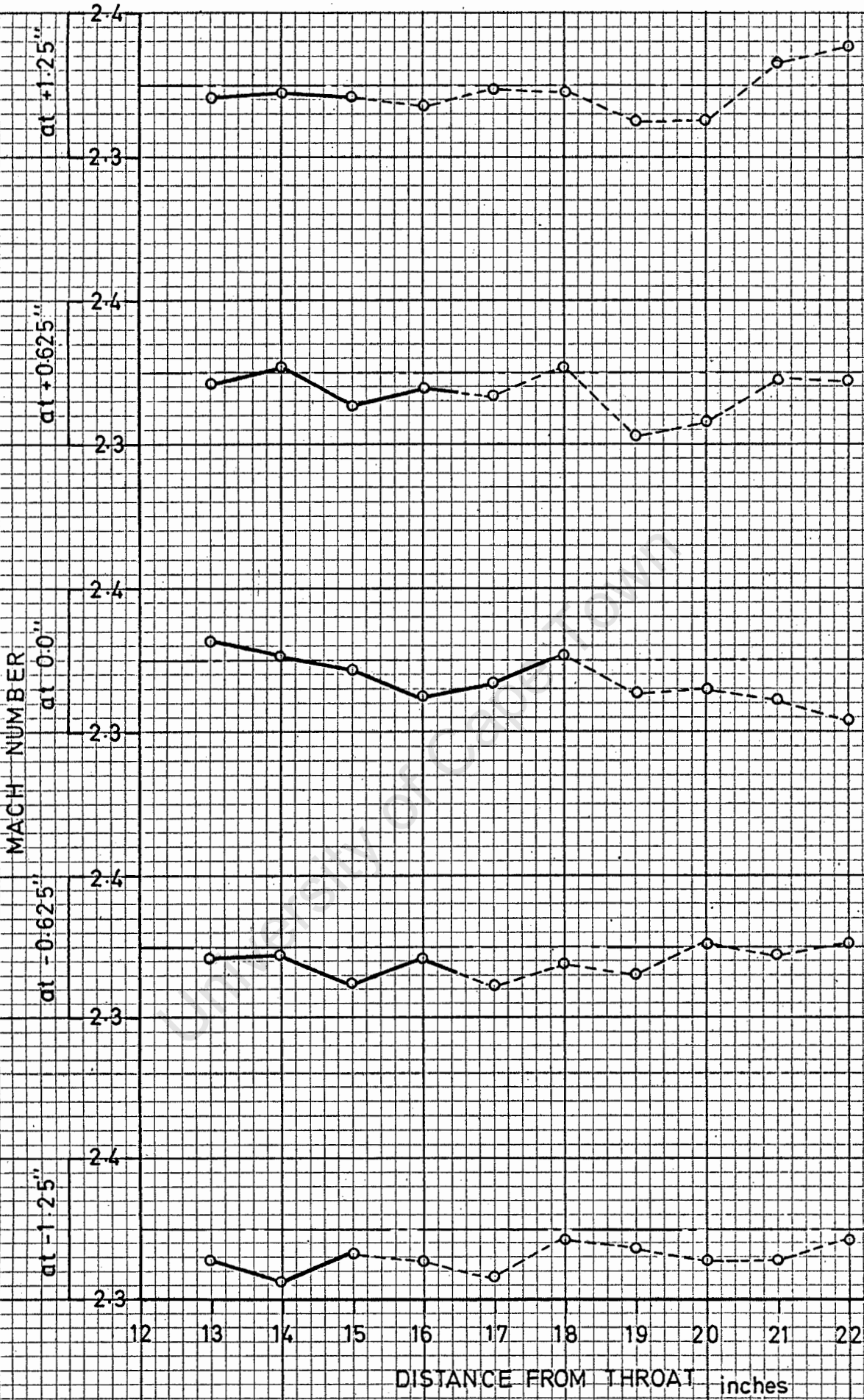

MACH NUMBER DISTRIBUTION FOR PITOT PRESSURE TESTING — ANALYTICAL NOZZLE

Figure 1.51

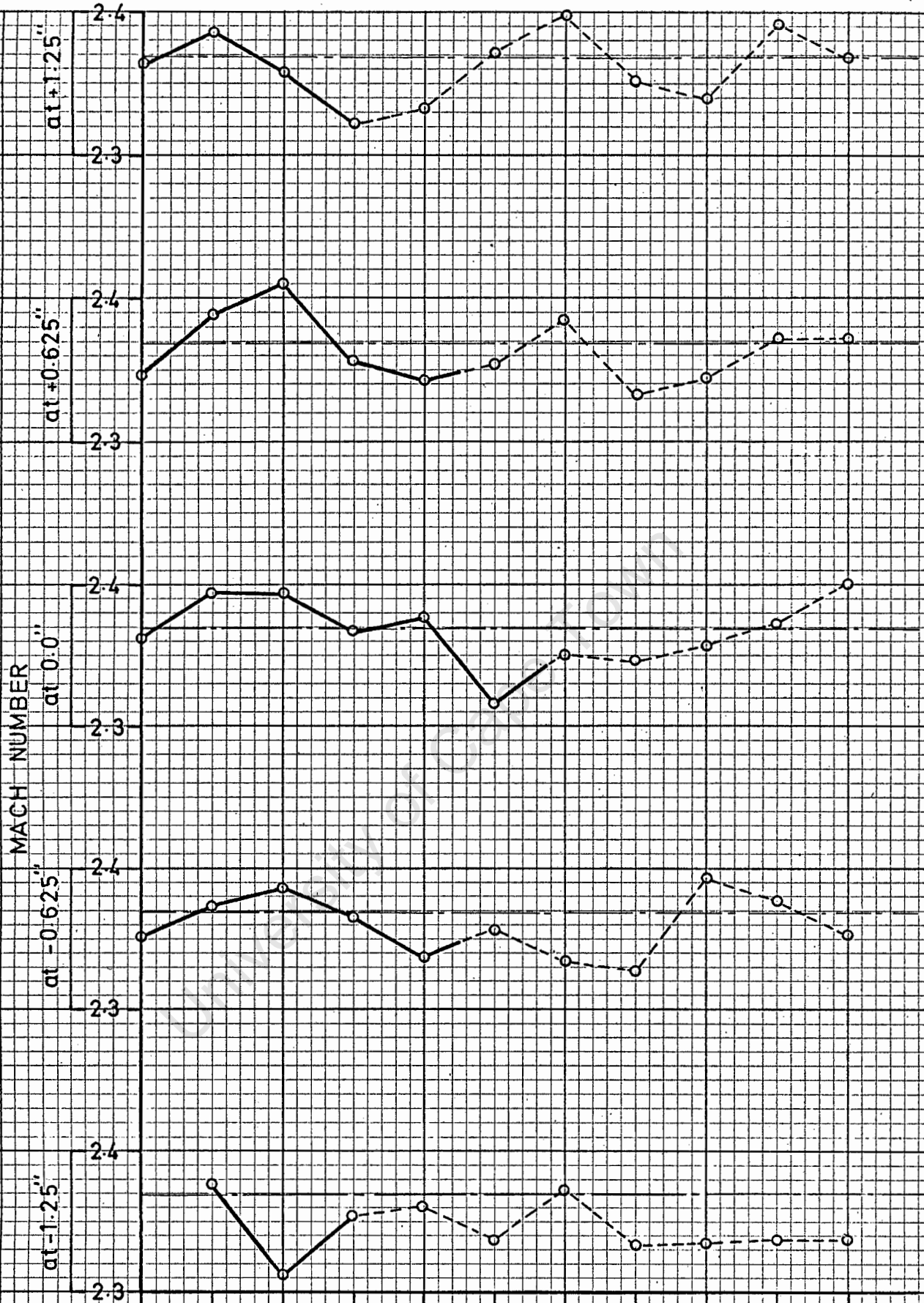

MACH NUBER DISTRIBUTION FOR PITOT PRESSURE TESTING —— SEMI-GRAPHICAL NOZZLE

Figure 1-52

These results are found from:

Mean Mach number; $\bar{M} = \frac{1}{n} \sum_{i=1}^{n} M_i$

Variance; $S^2 = \frac{1}{n} \sum_{i=1}^{n} (M_i - \bar{M})^2$

Standard Deviation; $S = \sqrt{S^2}$

Nozzle	Design Mach No.	Plane	Mean Mach No.	% Deviation from Standard %	Mean Max %
Semi-Graphical	2,3693	Vertical Side Wall (Static)	2,366	1,365	4,056
		Centre Vertical Plane (Pitot)	2,3615	1,004	2,181
Analytical	2,35	Vertical Side Wall (Static)	2,336	0,941	2,641
		Centre Vertical Plane (Pitot)	2,337	0,638	1,797

Stagnation Pressure Calibration:

Some doubt existed as to the reliability of the settling chamber stagnation pressure gauge as a means of measuring the actual stagnation pressure within the wind-tunnel. The necessity of using this gauge as a reference upon which the Mach number is determined, is eliminated when the Rayleigh Relationship (Equation 1.44) is applied. √

This method, of course, involves two runs for each Mach number determination. i.e. The static and pitot probes are used alternately. Precautions are necessary to repeat the exact flow properties over each successive run; otherwise the results will be meaningless.

1. The pre-set stagnation pressure control must not be adjusted for consecutive runs.
2. Each run must be allowed to progress for the same period of time.
3. Sufficient time must be allowed so that disturbances in the flow stream have settled down.

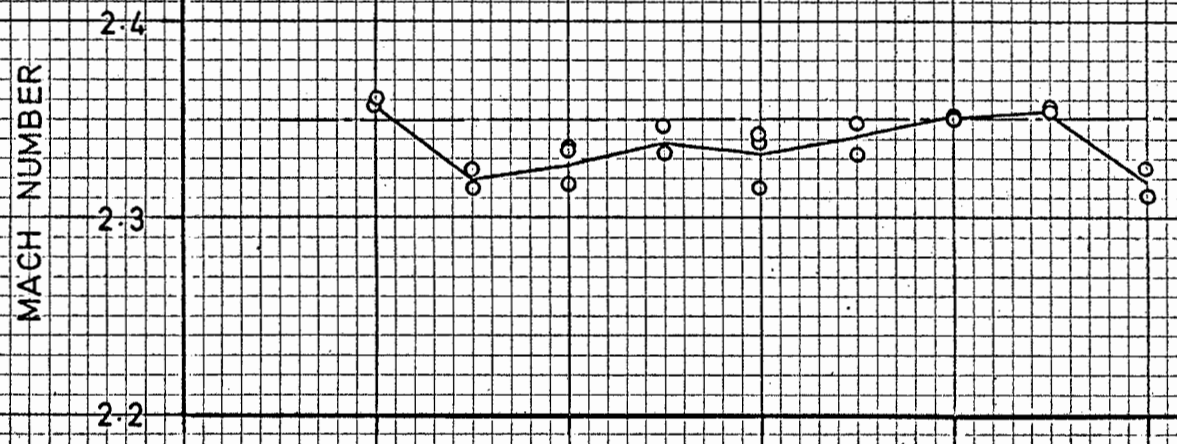

CORRECTED MACH NUBER DISTRIBUTION

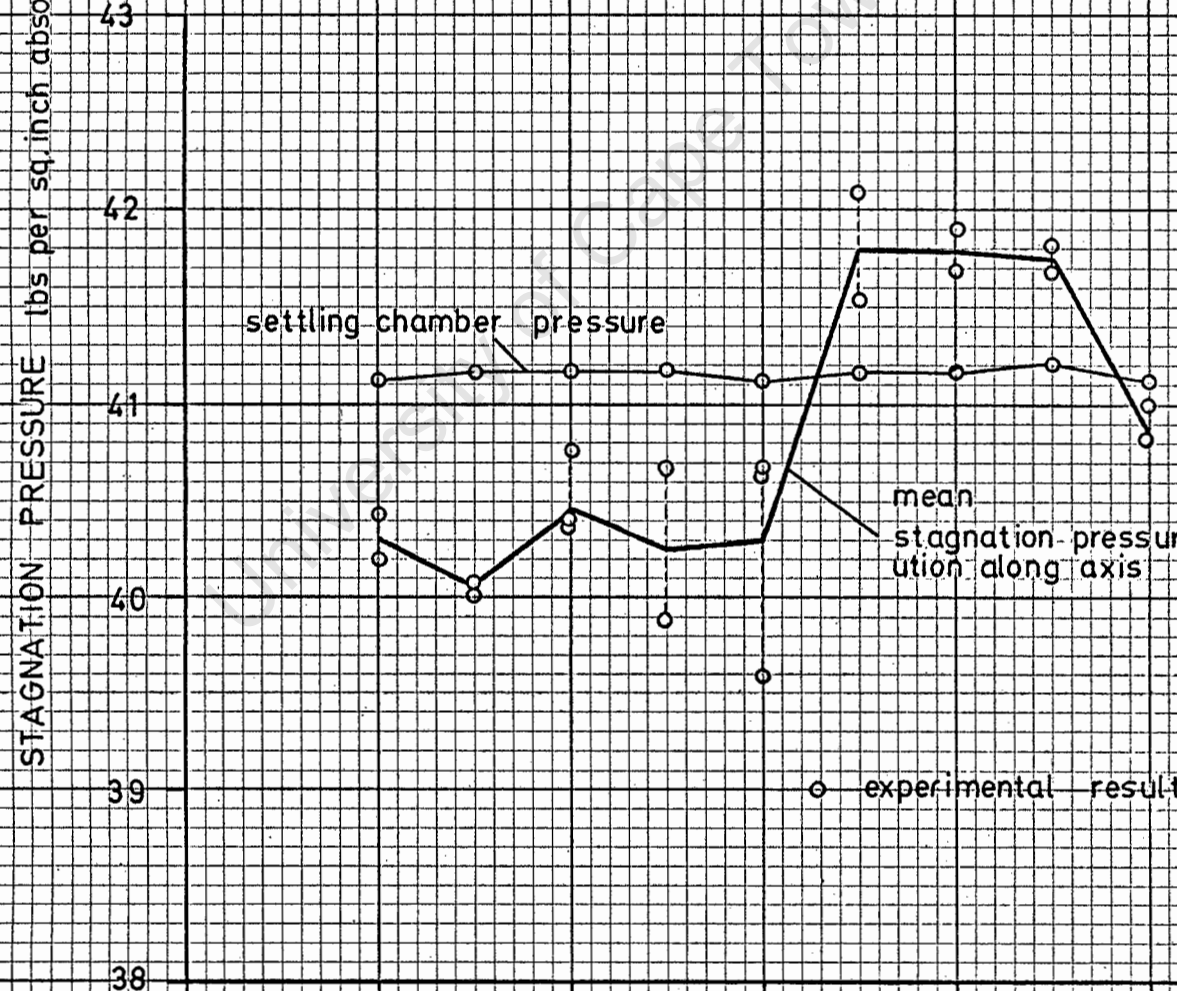

STAGNATION PRESSURE DISTRIBUTION

Figure 1.53

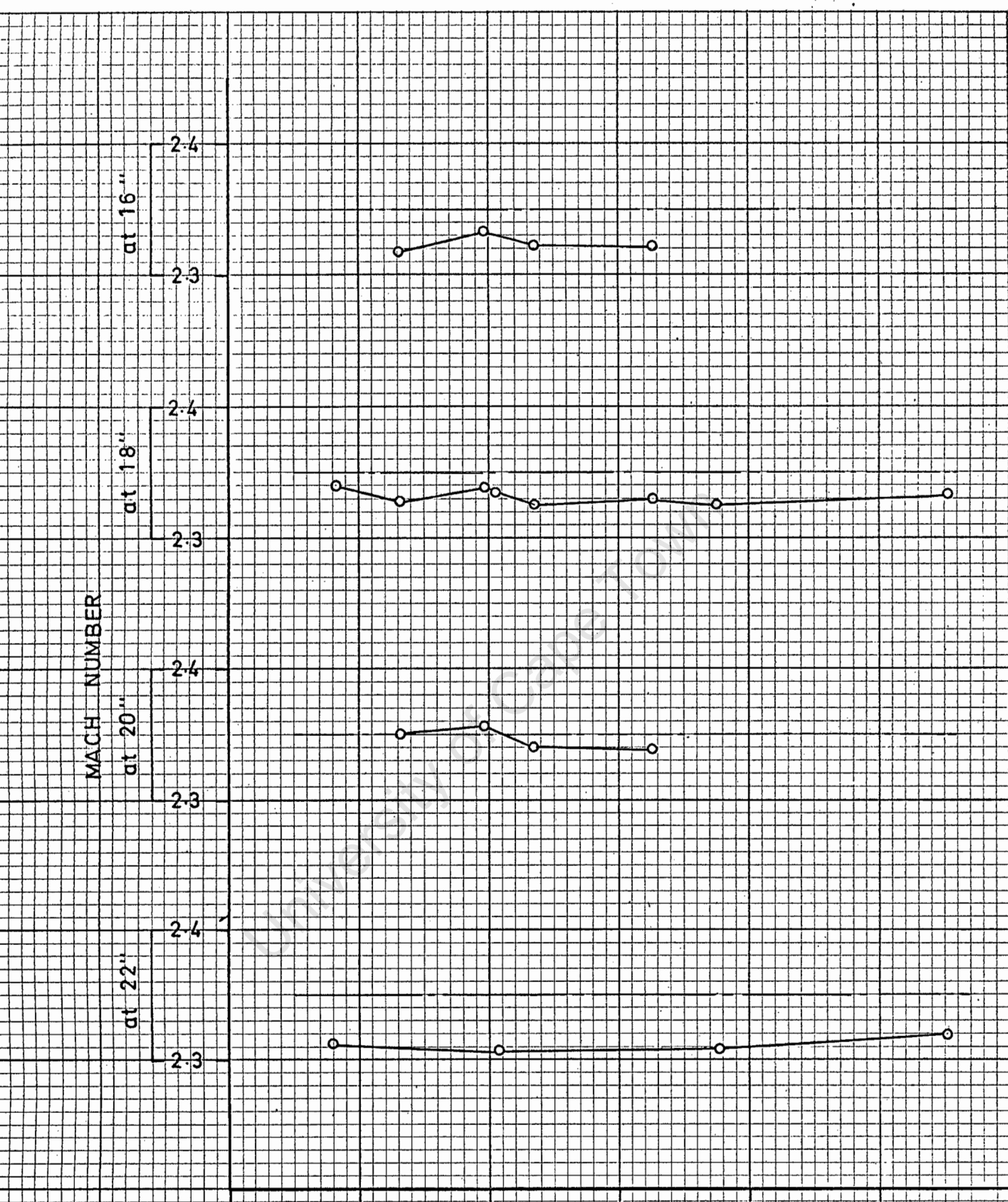

MACH NUMBER DISTRIBUTION FOR PRESSURE TRAVERSE

Figure 1·54

4. The fineness of the pressure transmitting lines, from the measuring probes, act as a damper. Hence great care must be taken in eliminating any leakages or blockages in these lines.

The stagnation pressure calibration tests were undertaken using the analytically designed nozzle only. The procedure may be divided into two parts:

Horizontal Displacement Traverse:

The single pitot and static probes were used to traverse the nozzle centre line between their limits of travel. (i.e. between 14 inches and 22 inches from the nozzle throat). The whole traverse was undertaken for a constant settling chamber pressure. These results were repeated later so that the degree of accuracy of this form of measurement could be assessed.

The Mach number calibration is given in figure 153(a) for the average results in the traverse. The actual stagnation pressures, at the points in question, are determined from equation 1.43; knowing the Mach number (M_1) and the pitot pressure (P_{02}). These results are plotted in figure 1.53(b) together with the measured settling chamber pressure. The deviation of each recorded result about the mean, is the limit of the measuring ability of the apparatus.

Pressure Traverse:

Again, using the Rayleigh relation, the Mach numbers at particular points on the nozzle centre-line were determined for increasing settling chamber pressure. The character of supersonic flow determines that the Mach number at any point remains the same; but the boundary layer, for example, may have some influence upon it.

The calibration results for this traverse is given in figure 1.54.

5.4 CONCLUSIONS

Pitot and Static Calibrations.

The summary of the results of the calibrations, for the analytically and semi-graphically designed nozzles, is presented in table 1.3. The uniformity of the flow within the test-sections compare very favourably with those of similar supersonic wind-tunnesl (see (5), (6) and (7))

The deviation of the flow, within the test-section, from design specifications may be attributed to:

Faults in the design of the cancellation contour of the nozzle.

Incorrect boundary layer estimation.

Constructional disturbances in the surfaces of the four walls of the tunnel.

The first of these would account for the disturbances in the flow velocity that are dymmetrical about the centre-line. The better distribution of flow within the analytical nozzle indicates the dificiencies in the design and the possible limitations of the semi-graphical nozzle.

1. The contour of the semi-graphical nozzle had to be drawn out graphically. Although it was produced to three times its full size, construction errors were bound to occur.

2. The design of the cancellation-section in the analytical nozzle assumed radial flow at the inflection point. This assumption is probably more valid than the straight sonic line in the semi-graphical nozzle ((6) shows this sonic line to be curved)

3. The semi-graphical nozzle incorporated a sharp corner at the throat. The boundary layer, even though it may be thin at this point, will influence the properties of the expansion fan. The analytical nozzle has no such discontinuities in the expansion profile.

4. In order to match the analytical nozzle length, the semi-graphical nozzle was designed for a triple Mach wave reflection pattern. Although the design becomes less critical due to a smaller inflection angle (1), the accumulative error in construction increases.

The incomplete cancellation of the Mach waves in the semi-graphical nozzle is illustrated in figure 1.47(b). At the nozzle exit, the Mach number overshoots. This is then overcorrected by the generation of positive Mach waves. This disturbance is transmitted down the tunnel test-section, but to a much lesser extent further from the initial irregularity. (i.e. The generation of an increasing number of wavelets distribute the non-uniformities on an ever finer scale).

The analytical calibration (Figure 1.47(a)) shows a much smaller transition from the cancellation to the test-section.

The estimation of the rate of boundary layer growth in the supersonic test-section was very satisfactory. No noticeable increase or decrease in the mean Mach number is apparent. (See figure 1.47(a) and (b). In both nozzle designs, though, the average Mach number was slightly below the design specification. This indicates that the rate of boundary layer growth in the expansion and cancellation sections is overestimated by the empirical equation. (i.e. The rate of boundary layer growth has been assumed constant, beginning at the nozzle throat, and independant to the Mach number and pressure).

supersonic flow is such that the Mach number does not change with increasing stagnation pressure. Although it has been shown that this stagnation pressure may vary through the test-section, figure 1.54(b) indicates that this actual stagnation pressure increases in the same proportion as the settling chamber pressure (the variation is still within the limits of the repeatibility of the results).

Therefore the small changes in Mach number, for increasing pressure, are due to boundary layer effects. These changes follow the same trend at each point and are of the order of only 0,7 % from one extreme to the other.

As the stagnation pressure increases the boundary layer thickness throughout the nozzle at test-section decreases (i.e. the Reynolds Number increases). The Mach number rises slightly as the test-sectio-throat area ratio changes. But for supersonic nozzles of low Mach number, the boundary layer at the nozzle throat cannot be neglected (4). Therefore the throat area also increases for increasing stagnation pressure. These two opposing conditions tend to retain the original Mach number - although some discrepancies may occur.

The stagnation pressure variation within test-section may have an adverse effect upon the standard deviation of the Mach number. The two methods of Mach number calibration (i.e. Rayleigh relation and pitot-settling chamber pressure relation) were compared by finding the respective standard deviations along the nozzle centre-line. The results, given in table 1.4, are very favourable even though only a small section of the wind-tunnel has been considered.

Instruments	Design Mach No.	Mean Mach No.	Standard Deviation about Mean.
Pitot-Sett Ch. readings	2,35	2,332	0,588%
Pitot-Static readings	2,35	2,338	0,582%

The uniformity of the Mach number distribution is almost the same in both cases and the mean Rayleigh Mach number approaches the design Mach number more closely.

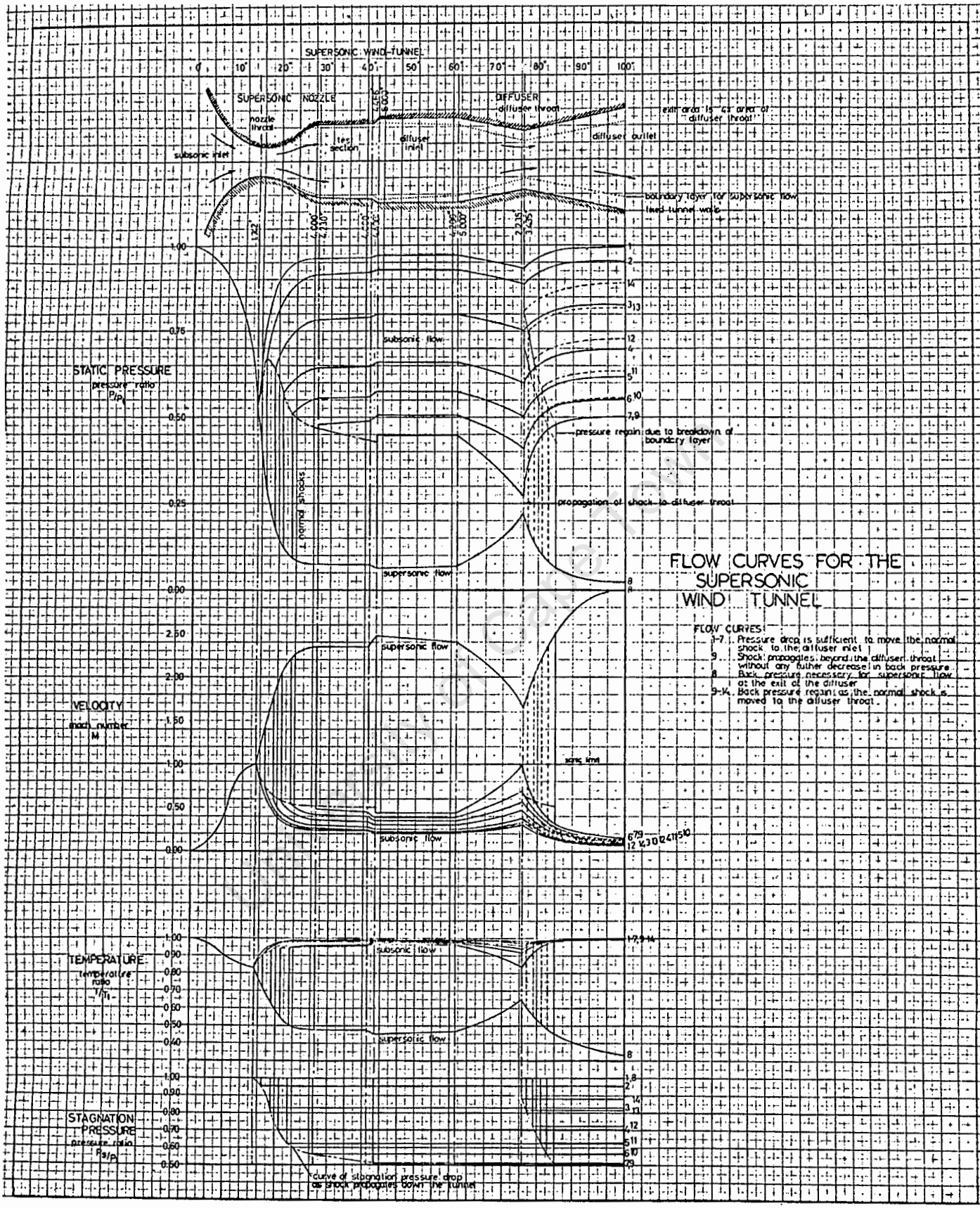
SUPERSONIC WIND-TUNNEL
SUPERSONIC NOZZLE
nozzle throat
test section
diffuser inlet
DIFFUSER
diffuser throat
diffuser outlet
exit area is 6.7 times of diffuser throat
subsonic inlet
boundary layer for supersonic flow
fixed tunnel walls
STATIC PRESSURE
pressure ratio
p/p1
subsonic flow
normal shocks
pressure regain due to breakdown of boundary layer
propagation of shock to diffuser throat
supersonic flow
FLOW CURVES FOR THE SUPERSONIC WIND TUNNEL
FLOW CURVES:
1-7 . Pressure drop is sufficient to move the normal shock to the diffuser inlet
9 . . Shock propagates beyond the diffuser throat without any futher decrease in back pressure
8 . . Back pressure necessary for supersonic flow at the exit of the diffuser
9-14 . Back pressure regain as the normal shock is moved to the diffuser throat
VELOCITY
mach number
M
sonic limit
TEMPERATURE
temperature ratio
T/T1
STAGNATION PRESSURE
pressure ratio
P3/P1
curve of stagnation pressure drop as shock propagates down the tunnel

Figure 1·57

normal shock is much lower.

If the maximum degree of pressure recovery is exceeded, the normal shock in the diffuser throat will instantaneously propagate to the equivalent position in the divergent portion of the nozzle.

6.2 ESTIMATION OF CRITICAL DIFFUSION

Theoretical calculation of the minimum allowable diffuser throat area in isentropic flow is possible, but in practice, this area must be made larger for the following reasons:

1. Boundary layer growth along the walls of the sind-tunnel.
2. Oblique shock-boundary layer inter-reaction in the diffuser contraction and at the model support sting. (See appendix 1.13)
3. Non-uniformity in the flow stream due to the post test-section area change.

(see figure 1.60)

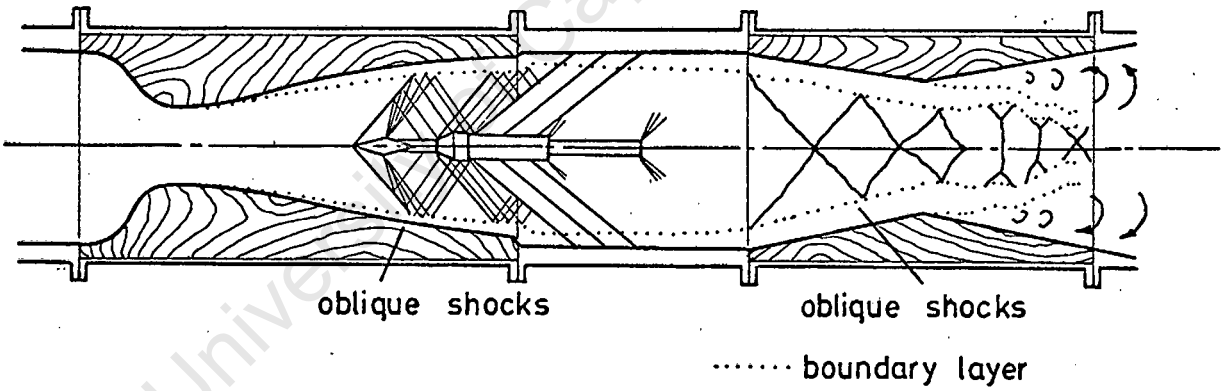

OBLIQUE SHOCK AND BOUNDARY LAYER EFFECTS

Figure 1.60

The critical area of the diffuser throat may be found by determining the theoretical area and then experimentally testing the diffuser. The diffuser throat area may then have to be increased until the normal shock is propagated through the supersonic diffuser.

Theoretical Solution:

Refer to figure 1.61.

The Mach number (maximum) is defined by the area ratio, A_1/A_1^*.

The post shock velocity, M_2, dictates the minimum diffuser throat area ratio, A_2/A_2^*, so that chocking does not occur. i.e. the flow at 2 must, in the limit,

only reach sonic velocity at the diffuser throat.

Therefore, the minimum diffuser-nozzle throat area ratio so that supersonic test-section flow can be achieved is given by:

$$\frac{A_2^*}{A_1^*} = \frac{A_1}{A_1^*} \times \frac{A_2^*}{A_2} \qquad \text{.....} \qquad 1.50$$

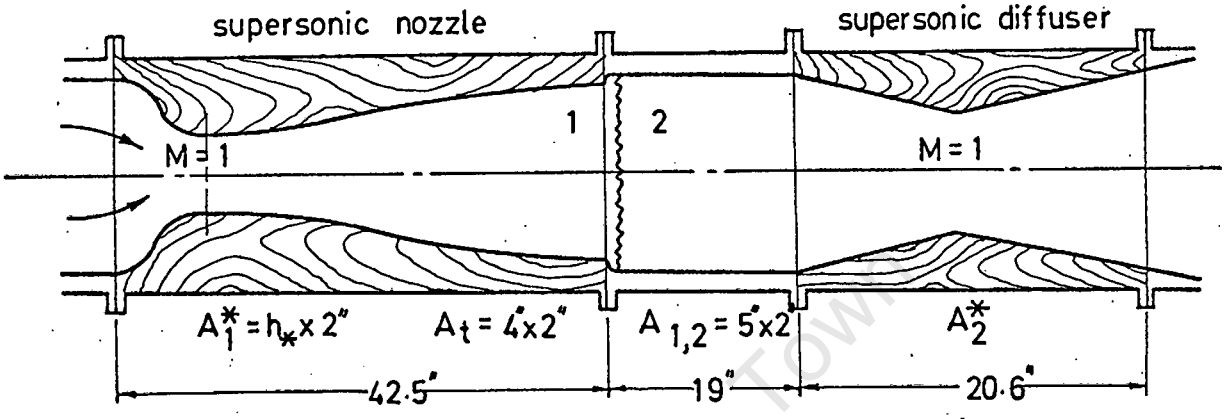

THEORETICAL NORMAL SHOCK DIFFUSION

Figure 1.61

Substituting in the area ratios for a nozzle Mach number of 2,35 and a test-section area of 8 sq.inches from tables from tables (15).

∴ Minimum diffuser throat height = 3,79 inches.

Experimental Solution:

The original diffuser was designed for a critical theoretical diffuser throat area and a suggested inlet contraction angle of 3^0. (8). Because chocking occurred before supersonic flow was effected in the test-section, the throat area had to be increased until the design was satisfactory.

Figure 1.62 gives the final design of the diffuser in relation to the original design.

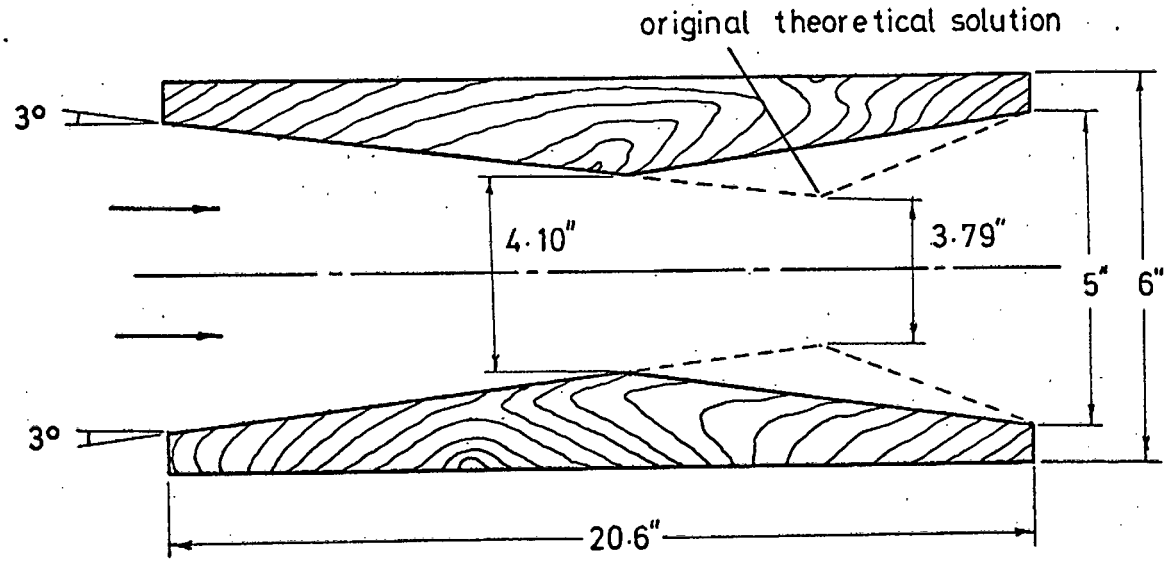

SUPERSONIC DIFFUSER

Figure 1·62

6.3 PERFORMANCE OF THE DIFFUSERS

The enthalpy-entropy diagram for the supersonic wind-tunnel system, with normal shock diffusion, is given in figure 1.65. Although the entropy increase due to boundary layer growth and oblique shock formation has been omitted in the supersonic region of this diagram, it is included in the subsonic stagnation pressure loss.

This stagnation pressure loss in the subsonic diffuser is such that there is a negative static pressure regain between points 2 and 3. Therefore the presence of the subsonic diffuser (and silencer) actually reduces the maximum 'normal shock' efficiency of the tunnel η_1

$$\text{i.e.} \quad \eta_d = \frac{(\Delta h)_s}{V_1^2/2} = 49\%$$

The minimum theoretical stagnation pressure ratios and the diffuser efficiencies, for increasing Mach number, are given in figures 1.66 and 1.67 respectively for the following conditions:

1. Normal shock recovery with a 100% efficient subsonic diffuser.
2. Normal shock recovery with a 0% efficient subsonic diffuser (i.e. The subsonic diffuser, is omitted)

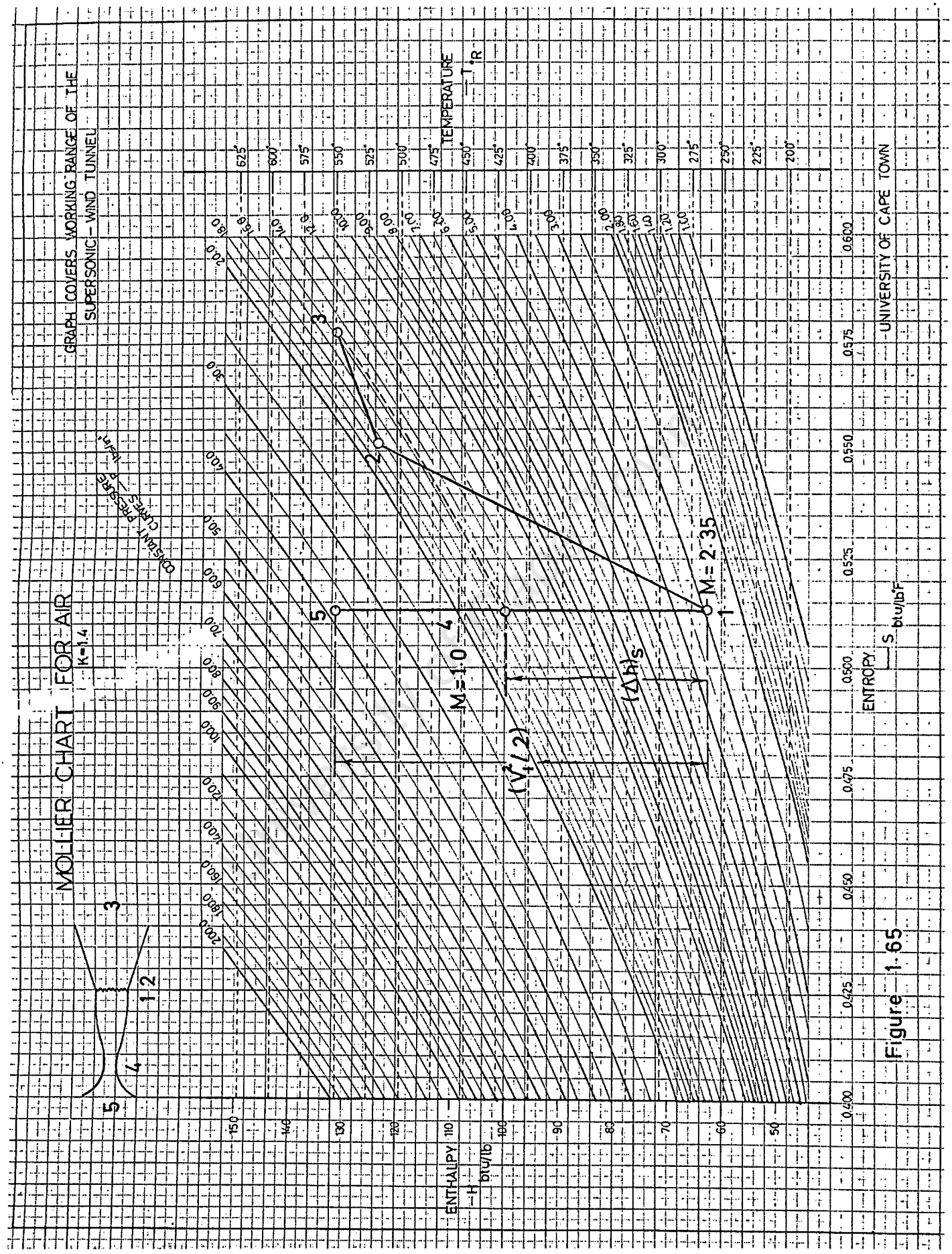
MOLLIER CHART FOR AIR
K=1.4
GRAPH COVERS WORKING RANGE OF THE SUPERSONIC - WIND TUNNEL
CONSTANT PRESSURE LINES
ENTHALPY —H btu/lb
TEMPERATURE —T °R
ENTROPY —S btu/lb°F
M=1.0
M=2.35
$(V_1^2/2)$
$(\Delta h)_s$
UNIVERSITY OF CAPE TOWN

Figure 1.65

3. Complete stagnation pressure recovery for a critical diffuser and a 100% efficient subsonic diffuser.

Normal Shock Diffusion

The experimental minimum stagnation pressure and maximum efficiency for nozzles of Mach number 2.0, 2.35, 2.5 and 3.0, with normal shock diffusion, have been plotted on figures 1.66 and 1.67.

These points appear to follow the same trend as the curves of the zero efficient diffuser, although they lie at about 75% of the maximum diffuser efficiency (see figure 1.67). This trend is expected, because at higher Mach numbers the post shock velocities are reduced and so are the stagnation pressure losses in the ducts. Hence the experimental points approach the theoretically perfect diffuser. Conversely, at low Mach numbers, this velocity is much higher and the stagnation pressure losses in the ducts are increased.

Stagnation Pressure Recovery

Unfortunately, the degree of stagnation pressure recovery is limited for the following reasons:

1. The increase in cross-section area after the test-section implies a further increase in the normal shock strength if it is to pass through this region. Hence the starting stagnation pressure must be higher and the minimum diffuser throat increased.

2. The excessive distance from the nozzle to the diffuser throat, as well as the change in section, aggravates the boundary layer growth. The diffuser throat area must be increased to account for this boundary layer.

3. At low Mach numbers, the maximum possible degree of pressure recovery is small (only a few lbs per sq.in)

The degree of pressure recovery, for the nozzle of Mach number 2.35, is given in both figures 1.66 and 1.67. The efficiency of diffusion is improved to 58%

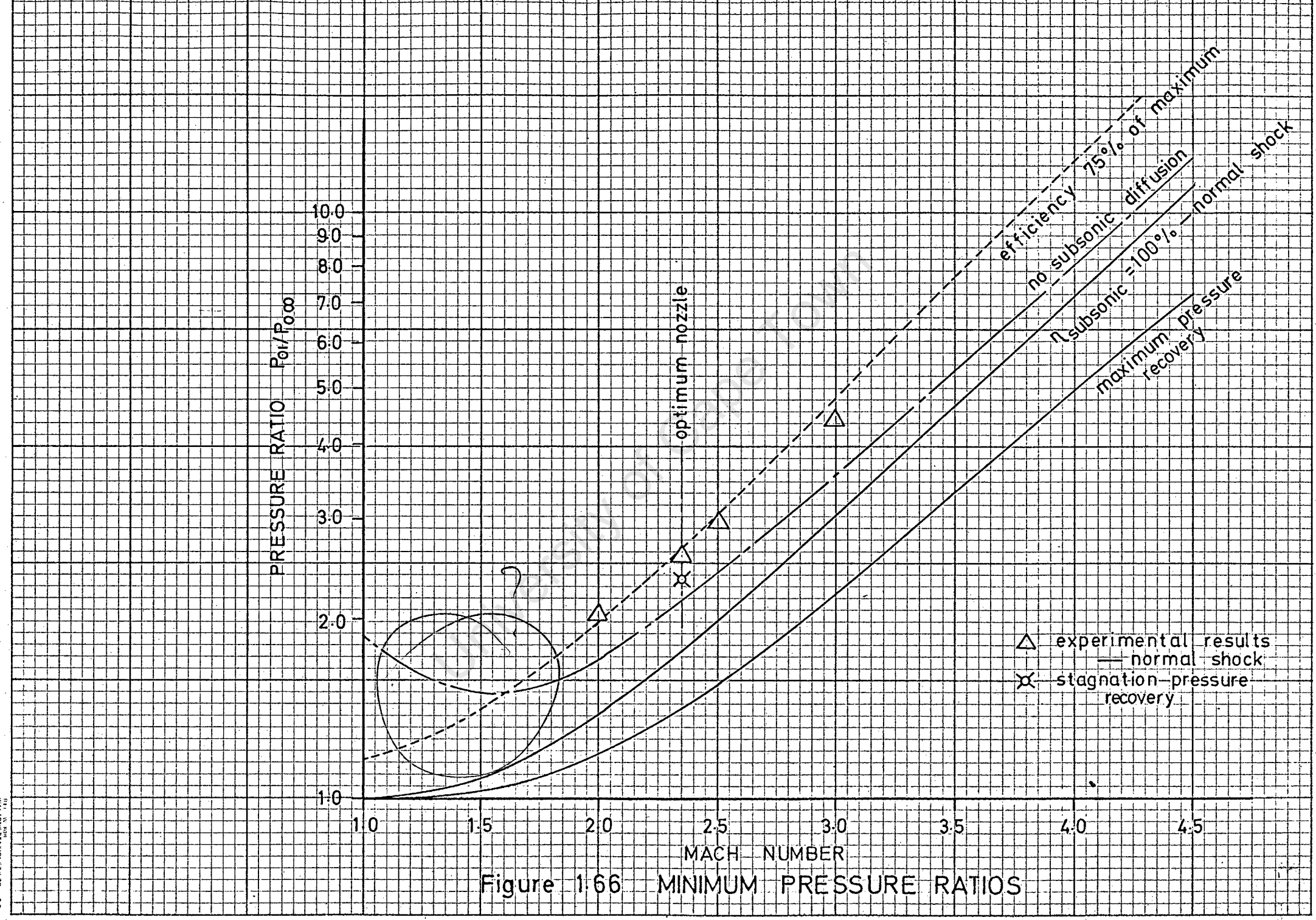

Figure 1·66 MINIMUM PRESSURE RATIOS

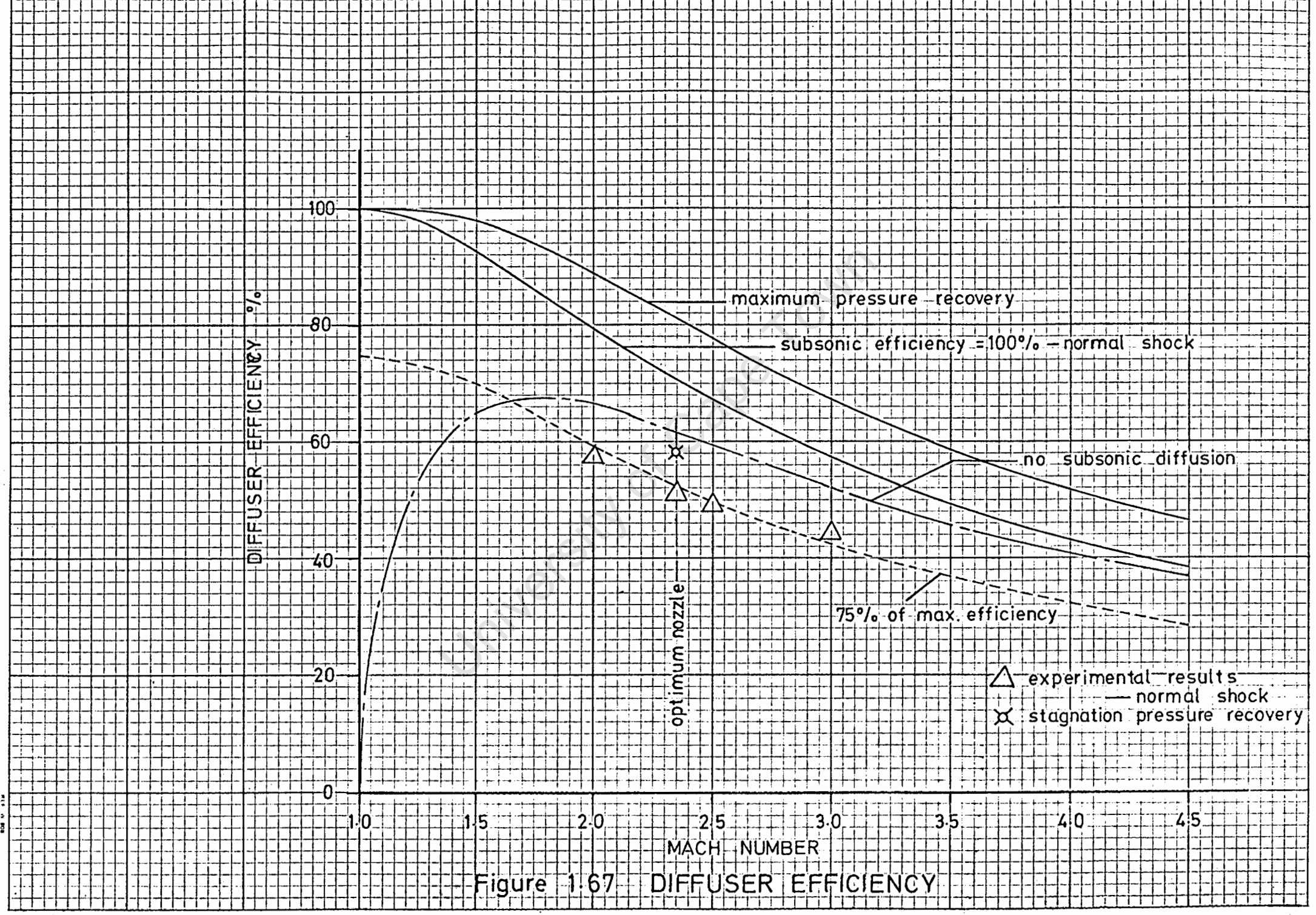

Figure 1.67 DIFFUSER EFFICIENCY

CHAPTER 2

VARIABLE NOZZLE DESIGN

SUMMARY

The variable supersonic nozzle is a necessary component for a versatile supersonic wind-tunnel system. Chapter 2 deals with the design of a suitable nozzle that would satisfy the requirements of the small blow-down wind-tunnel at the University of Cape Town.

Part 1 presents the specifications of the flexible liner structure and the worst possible loading conditions on the surface of thin spring steel plate.

Part 2 deals with the estimation of the maximum bending moment and subsequently the maximum stress in the plate at this worst condition.

The optimum nozzle liner thickness is estimated in part 3 so that the deflection under pressure loading is not excessive and the bending and loading stress is not too great. The final design satisfies the original specifications in strength and flexibility.

PART 1

PRELIMINARY STUDY

1.1 INTRODUCTION

A well designed variable supersonic nozzle offers a much greater degree of flexibility than the fixed black nozzle liners. Firstly, in conjunction with the nozzle profile programme (Chapter 1, part 3.4), the single variable nozzle may cover the whole range of test-section design Mach numbers. Secondly, the design nozzle profile may be readjusted after the initial calibrations to reduce non-uniformities in the flow stream.

In order that the nozzle be incorporated into the top and bottom covers of the nozzle box, the basic design must be simple. The components must also be rigid while still satisfying the boundary parameters of the nozzle design:

1. The subsonic inlet profile will be assumed satisfactory if the contour is smooth and continuous and the curve near the nozzle throat has a large finite radius (1).

2. For a uniform and constant Mach number (and a constant boundary layer growth), the test-section profile is straight.

3. The expansion and cancellation sections of the supersonic nozzle will be adjusted by jacking points at one inch intervals. These jacks are finally 'locked' so that the rigidity of the flexible liners are ensured.

(See figure 2.1).

1.2 SHOCK LOAD ESTIMATES

The criterion in the design of the variable nozzle is the flexible expansion and cancellation sections. The liner must be rigid enough not to deflect excessively under load, but at the same time, it must be sufficiently elastic to take up the required profile.

A severe test of the strength of this liner would occur as a normal shock propagates down the nozzle. The very large pressure gradients associated with a normal shock, maximum at the nozzle exit, would create a turning moment about one of the rigid supports. To find the maximum stress within the liner, the bending moment on the plate must be considered at these extreme conditions. (See figure 2.2).

Assume extreme conditions at:

Design Mach number = 5.0

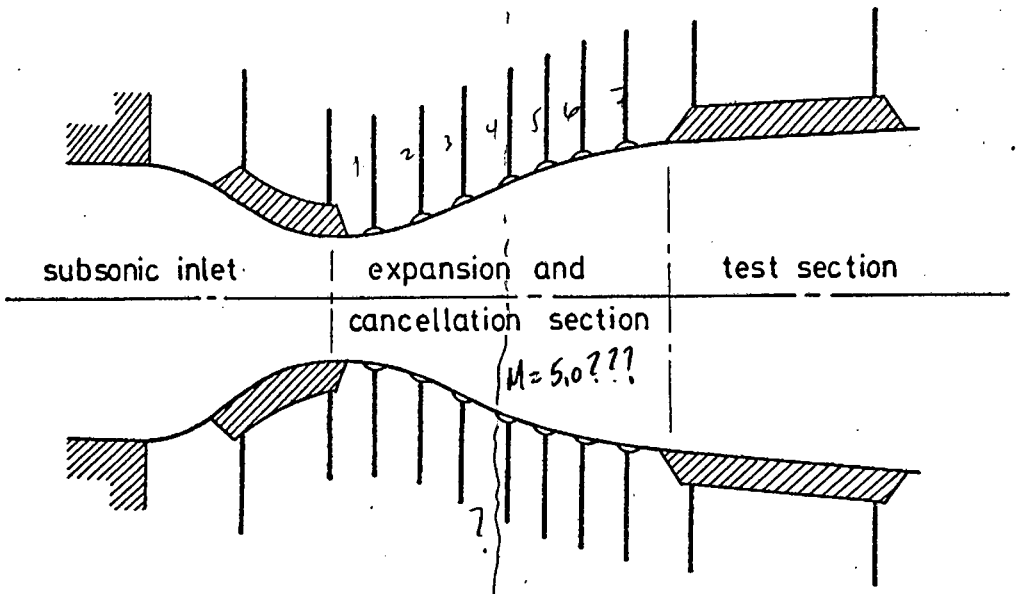

FLEXIBLE NOZZLE PROFILE

Figure 2.1

Maximum stagnation pressure = 80 psig. ✓ ie 95 psia

Atmospheric Pressure = 15 psia.

From tables (15), the free stream static pressure (P_1) is 0,1512 psia and the post shock static pressure (P_2) is 43,8 psia.

$P_1 = (0.189 \times 10^{-2})(95) = 0.1795$ psia

$P_2/P_1 = 29$ ie $P_2 = 5.2$ psia

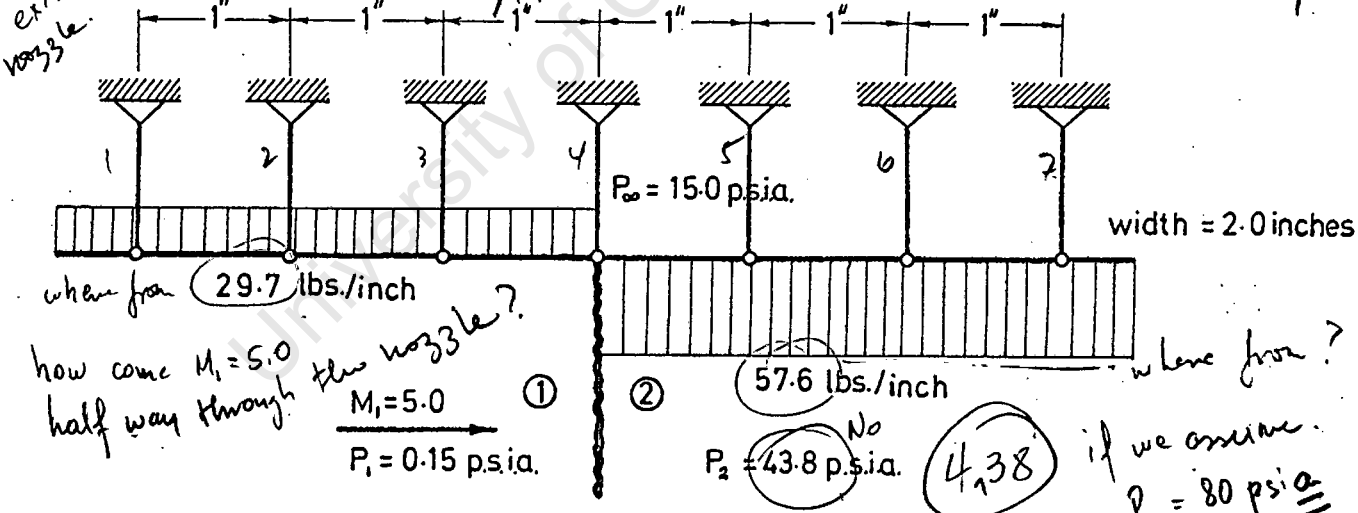

SHOCK LOADING IN NOZZLE

Figure 2.2

The bending moments along the nozzle liner are found by determining the reactions at the rigid supports. This system represents a beam, and the pressures represent uniform loads on its surface.

This system is statically indeterminate because more than two supports are present. The solution may be found by reducing the problem to one that is statically determinate and then applying the law of superposition.

PART 2
DERIVATION OF PLATE BENDING MOMENTS

2.1 APPLICATION OF SIMPLE SYSTEMS

To find the bending moments on the nozzle flexible plate when a normal shock exists, it will be considered as a two-dimensional beam subjected to both uniform and concentrated loads.

how can it be uniform

The normal shock results in a discontinuity in the uniform loading on the plate. The influence of this shock is transmitted through the 'beam', but to a lesser extent further away? Beyond a certain distance, this influence will be minimal and may be neglected. Hence the nozzle plate may be represented by a beam fixed between rigid supports and subjected to a constant uniform load. (See figure 2.3)

meaning what?

do you imply that the normal shock must be treated as a concentrated load if so say it

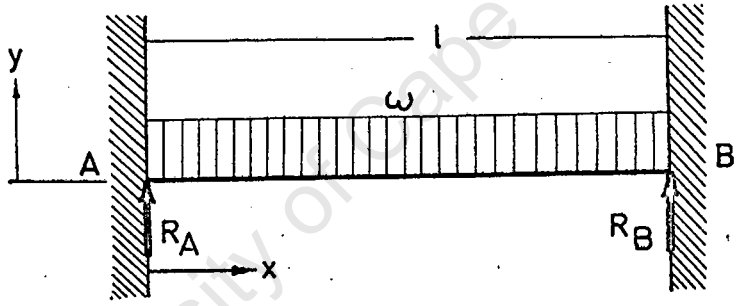

RIGID BEAM UNDER UNIFORM LOAD

Figure 2.3

The loading is symmetrical about the supports and the slope of the liner at points A and B is given as dy/dx = 0

From (16):

$$\text{Bending moment, } BM = -\frac{\omega l^2}{2}\left(\frac{1}{6} - \frac{x}{l} + \frac{x^2}{2}\right) \quad \ldots\ldots\ldots\ldots\ldots\ldots \quad 2.1$$

The maximum deflection is at the centre of the beam:

$$\therefore Y_{max} = \frac{\omega}{EI}\,\frac{l^4}{384} \quad \ldots\ldots\ldots\ldots\ldots\ldots \quad 2.2$$

Nearer to the normal shock, the nozzle liner is subjected to uniform loads of different magnitude that are separated by a step function. In this system, the influence of the shock on the liner will be assumed to extend over seven rigid supports. (Beyond this, the influence of the continuous beam will be small). Because this system is statically indeterminate, it must be reduced to one that has only two rigid supports (See figure 2.4)

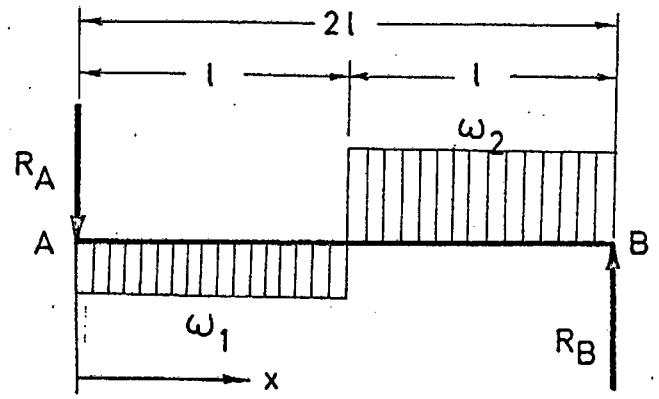

BEAM UNDER UNIFORM LOADS

Figure 2.4

The reaction of the supports are:

$$R_A = \frac{3\omega_1 l}{4} - \frac{\omega_2 l}{4} \qquad \text{..... 2.3}$$

$$R_B = \frac{3\omega_2 l}{4} - \frac{\omega_1 l}{4} \qquad \text{..... 2.4}$$

The deflection equations are given separately for each half of the beam:

$\underline{0 \leq X \leq l}$:

$$EIy = -\frac{\omega_1}{24} X^4 + \frac{R_A}{6} X^3 + \left(\frac{7}{48}\omega_2 l^3 - \frac{3}{16}\omega_1 l^3\right). X \qquad \text{..... 2.5}$$

$\underline{l \leq X \leq 2l}$:

$$EIy = \frac{\omega_2}{24} \cdot X^4 + \frac{K_1}{6} \cdot X^3 + \frac{K_2}{2} \cdot X^2 + C_X + D \qquad \text{..... 2.6}$$

Where $K_1 = \frac{-\omega_1 l}{4} - \frac{5\omega_2 l}{4}$

$K_2 = \frac{l^2}{2}(\omega_1 + \omega_2)$

$C = -\frac{\omega_2 l^3}{48} - \frac{17\omega_1 l^3}{48}$

$D = \frac{\omega_2 l^4}{24} + \frac{\omega_1 l^4}{24}$

The derivation of these equations is given in appendix 2.1.

The pressure loads on the beam must be carried by the rigid supports. These

supports are at one inch intervals and any one may be represented as a concentrated load in a simple determinate system. An example of this system subjected to a single concentrated load anywhere on the beam is given in figure 2.5.

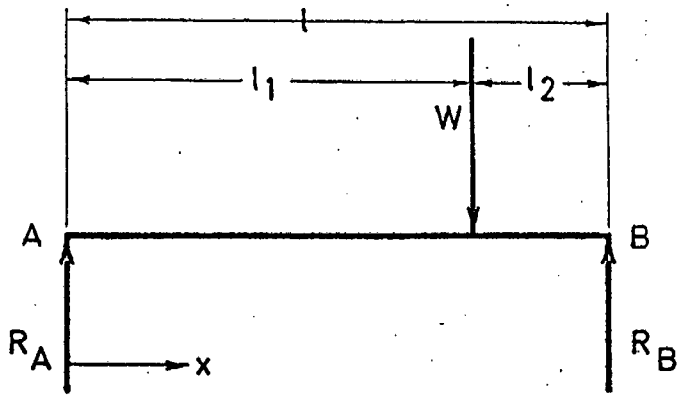

BEAM UNDER CONCENTRATED LOAD

Figure 2.5

The reactions at the supports are:

$$R_A = W(1 - \frac{l_1}{l}) \quad \text{.....} \quad 2.7$$

$$R_B = W \frac{l_1}{l} \quad \text{.....} \quad 2.8$$

As before, the deflection is defined by two equations to cover the whole length of the beam.

$0 \leq X \leq l_1$:

$$EIy = \frac{R_A}{6} \cdot X^3 + W\left(\frac{l_1^2}{2} - \frac{l_1 l}{3} - \frac{l_1^3}{6l}\right).X \quad \text{.....} \quad 2.9$$

$l_1 \leq X \leq l$:

$$EIy = -\frac{W}{6}\frac{l_1}{l} \cdot X^3 + \frac{W l_1}{2} \cdot X^2 - W\left(\frac{l_1 l}{3} + \frac{l_1^3}{6l}\right).X + W\frac{l_1^3}{6} \quad \text{....} \quad 2.10$$

The derivation of these equations is given in appendix 2.2.

2.2 APPLICATION OF THE LAW OF SUPERPOSITION

The law of superpositon states that if the deflection caused by a load on a statically determinate beam is cancelled out by an opposite deflection due to a load at any point, then this load becomes the reaction of a third support (17)

This law may be applied to the considered length of nozzle liner to find the reactions at the seven rigid(or jack) supports. (See figure 2.6).

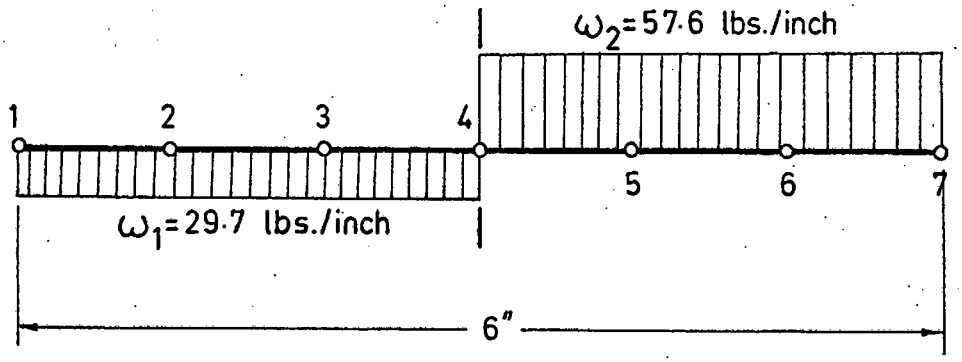

UNIFORM LOAD DISTRIBUTION

Figure 2.6

This beam is statically indeteriminate to the fifth degree. Remove the supports 2 to 6 so that the beam is statically determinate and then apply equations 2.5 and 2.6 to find the deflection curve of the beam under uniform loads ω_1 and ω_2 (see figure 2.7).

Similarly, applying concentrated loads at each of the support points 2 to 6 on the statically determinate beam respectively, the deflection curves may be found from equations 2.9 and 2.10 in terms of the concentrated load W. (See figure 2.8).

The sum of the deflections at the five points, where the concentrated loads are applied, must cancel out the deflections at the same points due to the uniform loads. Then, the law of superposition, the loads required to produce the cancellations become the reactions of the five supports.

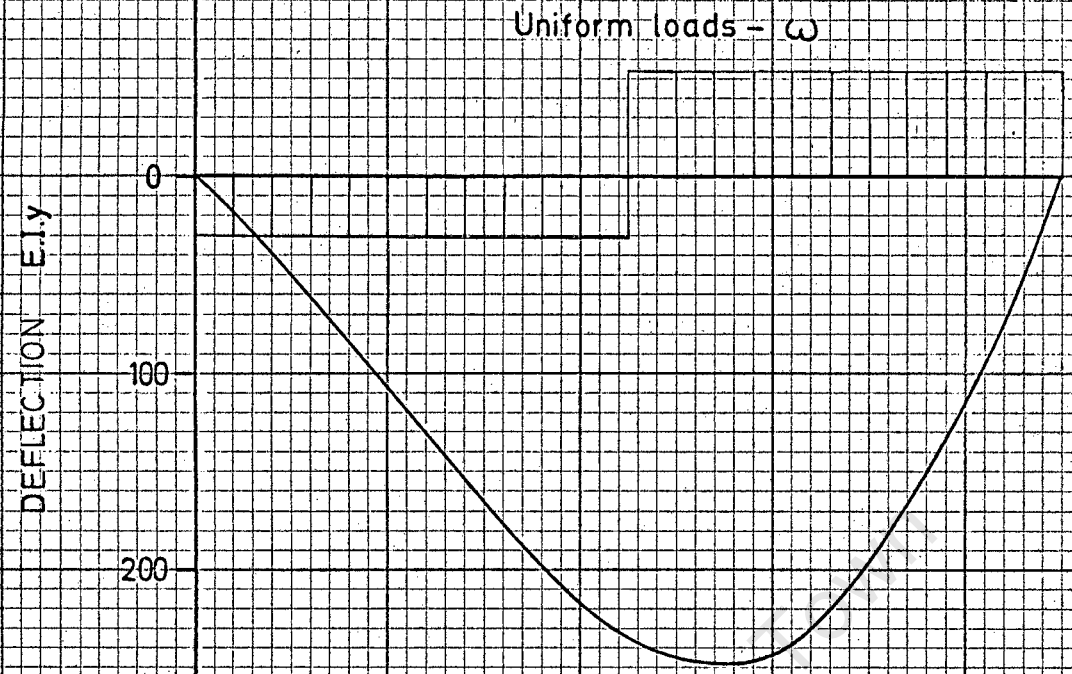

Figure 2·7

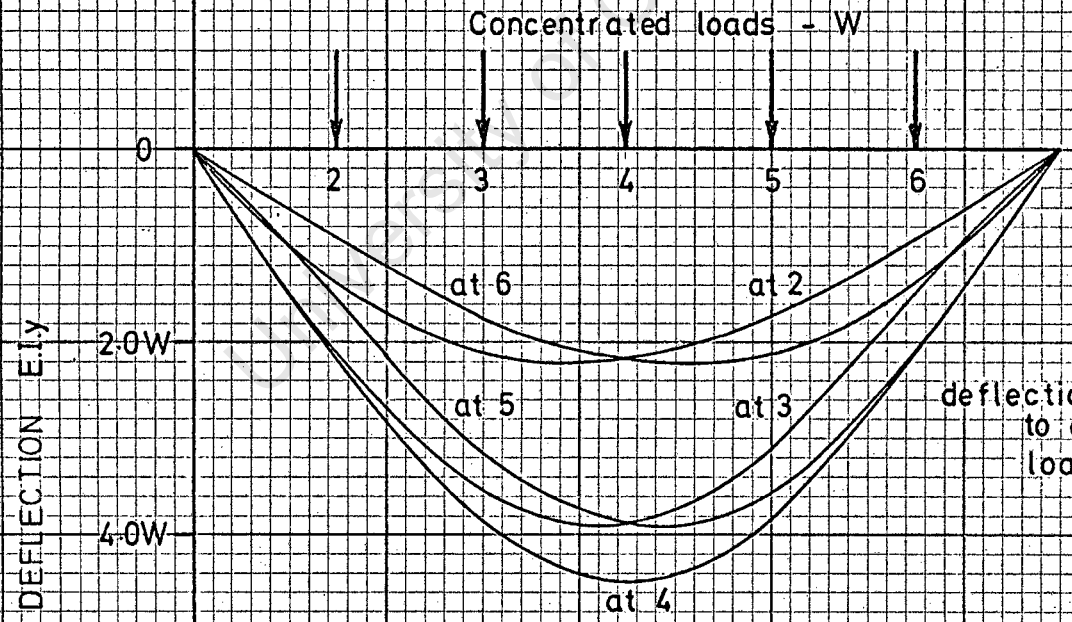

Figure 2·8

DEFLECTION DIAGRAMS

TABLE 2.1

Concentrated loads at :	Deflection at jack points in terms of each cone load : EI_y							Multiple
	1	2	3	4	5	6	7	
Point 2	0	1.39	2.11	2.17	1.72	0.94	0	xW_2
Point 3	0	2.11	3.56	3.83	3.11	1.72	0	xW_3
Point 4	0	2.17	3.83	4.50	3.83	2.17	0	xW_4
Point 5	0	1.72	3.11	3.83	3.56	2.11	0	xW_5
Point 6	0	0.94	1.72	2.17	2.11	1.39	0	xW_6
Defl. due to Unif. load EI_W	0	79.14	164.59	235.41	244.80	159.54	0	

Table 2.1 summarises all the deflections due to the uniform loads and due to each concentrated load. The solution may be determined when the sum of the deflections, at each jack point, is zero.

This may be rewritten in the form of a matrix:

$$\begin{bmatrix} 1.39 & 2.11 & 2.17 & 1.72 & 0.94 \\ 2.11 & 3.56 & 3.83 & 3.11 & 1.72 \\ 2.17 & 3.83 & 4.50 & 3.83 & 2.17 \\ 1.72 & 3.11 & 3.83 & 3.56 & 2.11 \\ 0.94 & 1.72 & 2.17 & 2.11 & 1.39 \end{bmatrix} \begin{bmatrix} W_2 \\ W_3 \\ W_4 \\ W_5 \\ W_6 \end{bmatrix} = \begin{bmatrix} 79.14 \\ 164.59 \\ 235.41 \\ 244.80 \\ 159.54 \end{bmatrix}$$

This matrix is solved numerically using a digital computer. The instruction programme for its solution is given in appendix 2.3

The output is given as:

W_2 = -32,2928 lbs

W_3 = -34.1568 lbs

W_4 = +13,7290 lbs

W_5 = +60,5596 lbs

W_6 = +65,7175 lbs

These now become the reactions at the rigid supports 2 to 6 respectively when the nozzle plate is subjected to uniform loads 1 and 2. The reactions at the end supports at 1 and 7 are found by applying equations 2.3 , 2.4, 2.7 and 2.8. The results are summarised in table 2.2.

TABLE 2.2

Load Distribution				R_1	R_7
Uniform load 1 + 2				lbs	lbs
				-23,625	+107,325
Concentrated load W_2, W_3, W_4, W_5, W_6	W	l_1	l_1/l		
At point 2	-32,29	1"	1/6	-26,911	-5,382
At point 3	-34,16	2"	1/3	-22,771	-11,386
At point 4	+13,73	3"	1/2	+6,865	+6,865
At point 5	+60,56	4"	2/3	+20,187	+40,373
At point 6	+65,72	5"	5/6	+10,953	+54,763
Summation of all the loads at pts 1, 7 due to all the loading.				-11,947	22,093

These results are given in figure 2,9. i.e. The complete loading on the flexible plate is given over seven inches of its length.

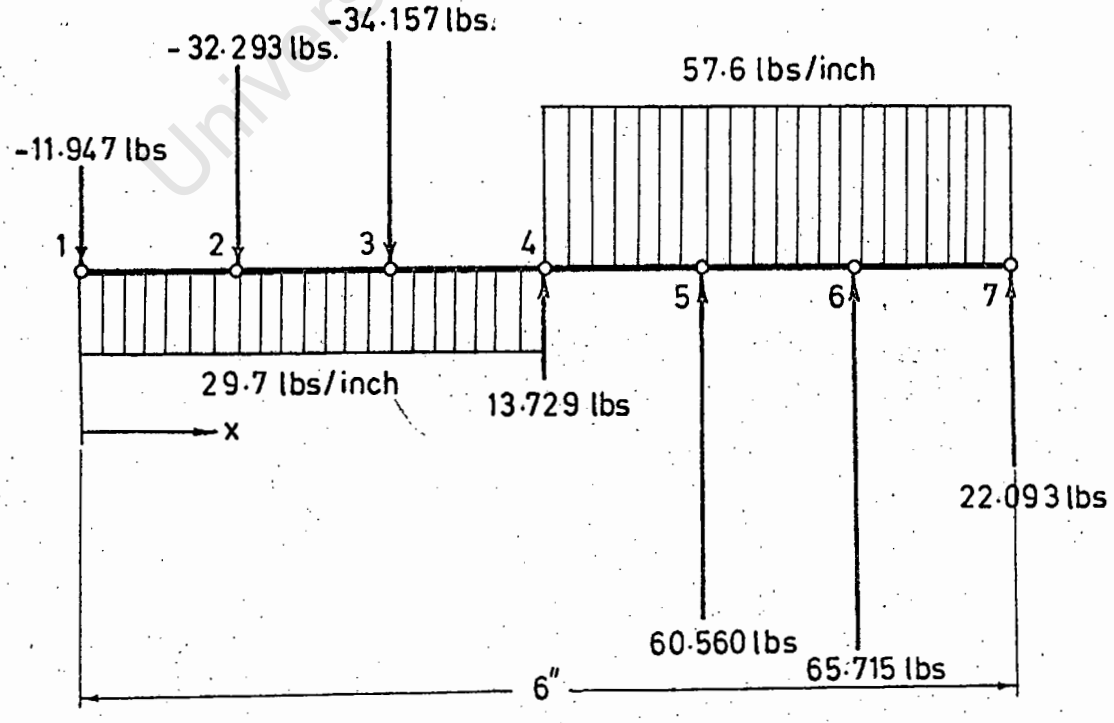

LOAD DISTRIBUTION ON BEAM

Figure 2·9

The bending moment equations for this 'beam' are derived for each of the six sections between the reactionary supports. These are classified into two main sections (from 1 to 4, and from 4 to 7)

$\underline{1 \leq X \leq 4}$

$$BM = \frac{-\omega_1 X^2}{2} - \sum_{n=1}^{4} Rn\,(X-n-1) \qquad \text{2.11}$$

$\underline{4 \leq X \leq 7}$

$$BM = +\frac{\omega_2 X^2}{2} - 3\,(\omega_1 + \omega_2).\,X\,\frac{9}{2}\,(\omega_1 + \omega_2) - \sum_{n=1}^{7} Rn\,(X-n-1) \qquad \text{2.12}$$

Here n refers to the jack support number below the section being considered for bending moments. The number of summations is equal to n in both classifications. i.e. For the section between points 5 and 6, n = 5 and the summation in equation 2.12 is:

$$-R_1(X) - R_2(X-1) - R_3(X-2) - R_4(X-3) - R_5(X-4)$$

The solution to these two equations is given in figure 2.10. Also presented in this figure are the maximum bending moment limits due to either ω_1 or ω_2 only, derived from equation 2.1.

Fortunately, the maximum bending moment due to a normal shock incident upon the nozzle liner surface at a rigid support is not much greater than that due to a continuous?! pressure distribution. (In the order of 10% greater). The irregularity at the ends of the beam is because they have been assumed free, whereas, in fact, the nozzle liner is continuous. This assumption only tends to exaggerate the bending moments at points 1 and 5.

The result of this analysis indicates that there is no loading danger due to shock travel in the supersonic wind-tunnel. Furthermore, because the shock is seldom stationary and that it is distributed over a considerable length (See appendix 1.13), it is unnecessary to overdesign the flexible nozzle liner.

No ?!

the shock is very small A° units in width

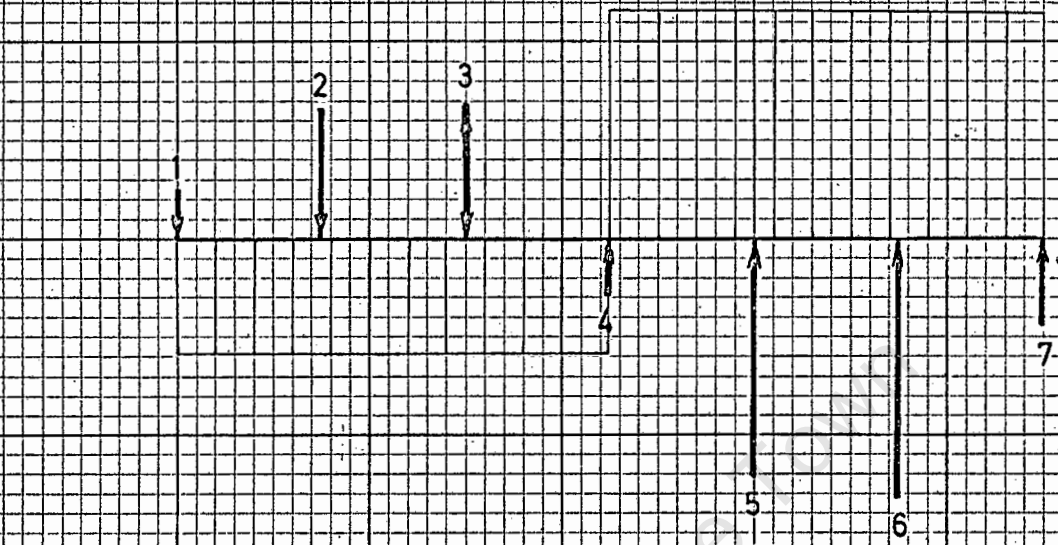

LOADING ON BEAM

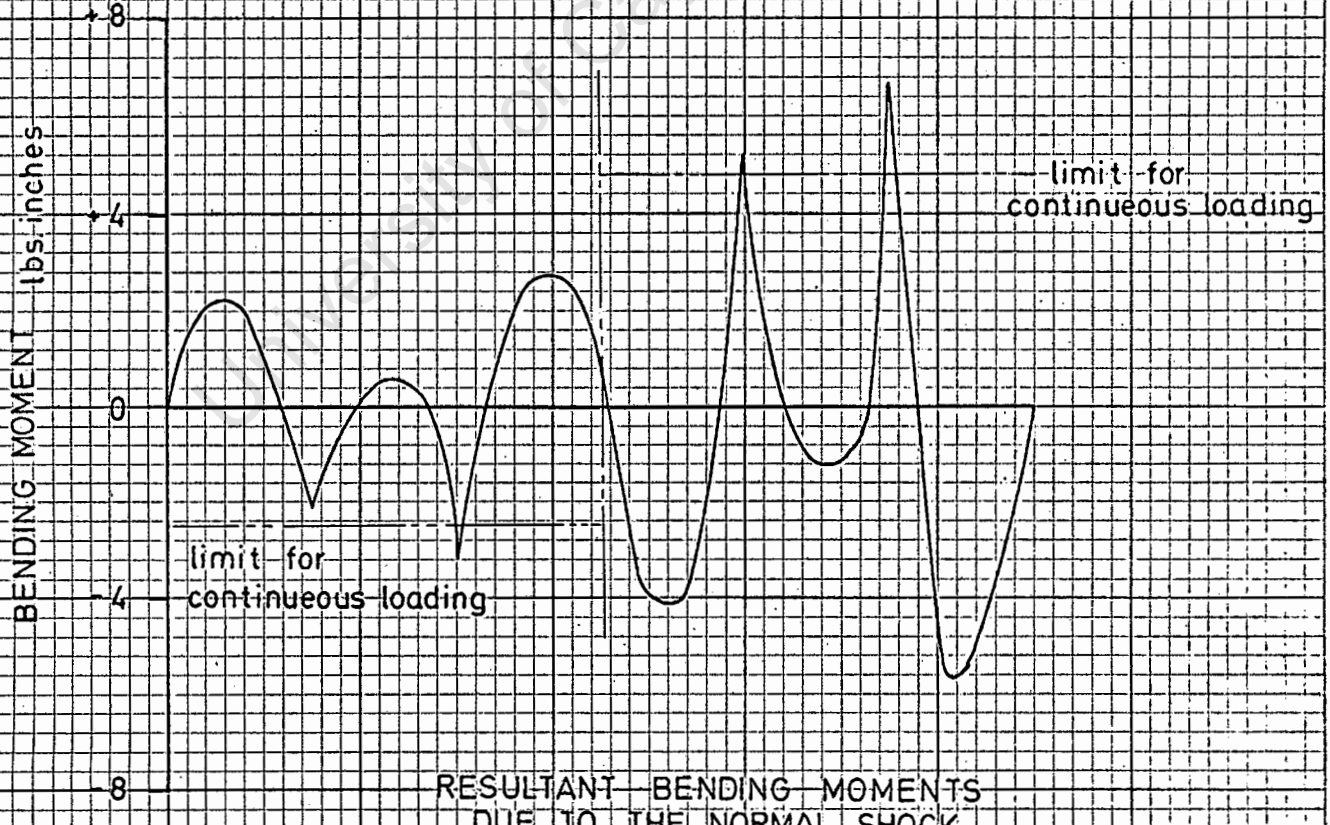

RESULTANT BENDING MOMENTS DUE TO THE NORMAL SHOCK

BENDING MOMENT DIAGRAM

Figure 2.10

PART 3

FINAL DESIGN

3.1 DESIGNING THE FLEXIBLE PLATE

The flexible section of the nozzle liner, between the throat and test-section, must be designed so that it does not deflect excessively under load, but also must retain the desired profile without large restraining forces. These two conditions indicate that the optimum liner thickness must be carefully selected.

Deflection:

Because the pressure distribution along the nozzle line is changing, so will the maximum deflection of the liner between the rigid supports. If this pressure gradient is small over each section, then the liner may be assumed to correspond to the beam ahown in figure 2.3. The maximum deflection is given by equation 2.2 as:

$$Y_{max} = \frac{\omega l^4}{EI\ 384}$$

This maximum deflection is given in figure 2.11, for different nozzle plate thicknesses, in terms of the pressure differences across the liner.

To maintain a reasonable limit to the extent of this deflection, the plate thickness must be greater than 0,030 inches.

Elasticity:

The dimensions of theliner must be such that it does not deform permanently under load. The maximum stress, that the nozzle liner will be subjected to, will be caused by the summation of the bending moments due to pressure loads and that due to bending loads (To form the desired profile)

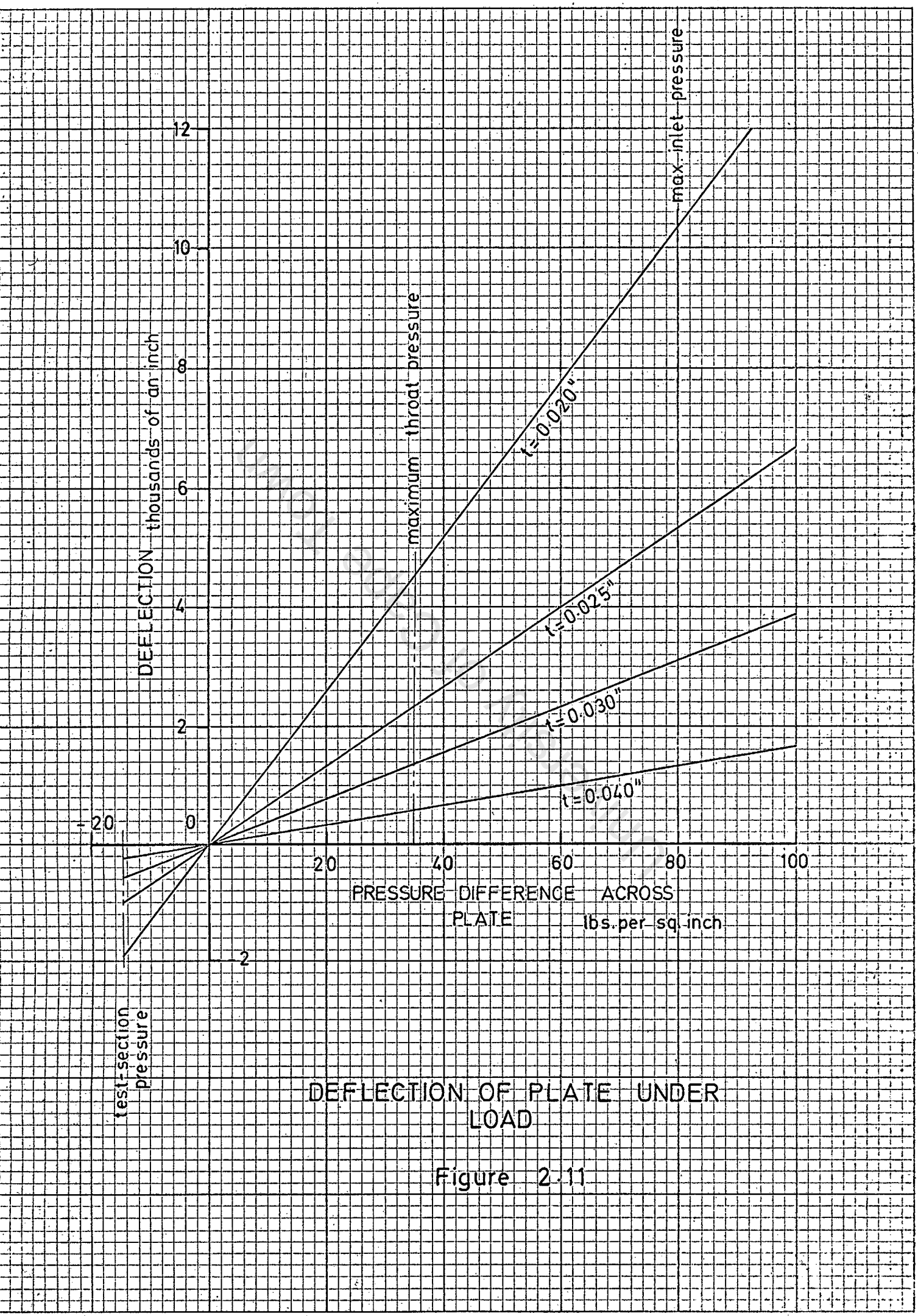

DEFLECTION OF PLATE UNDER LOAD

Figure 2.11

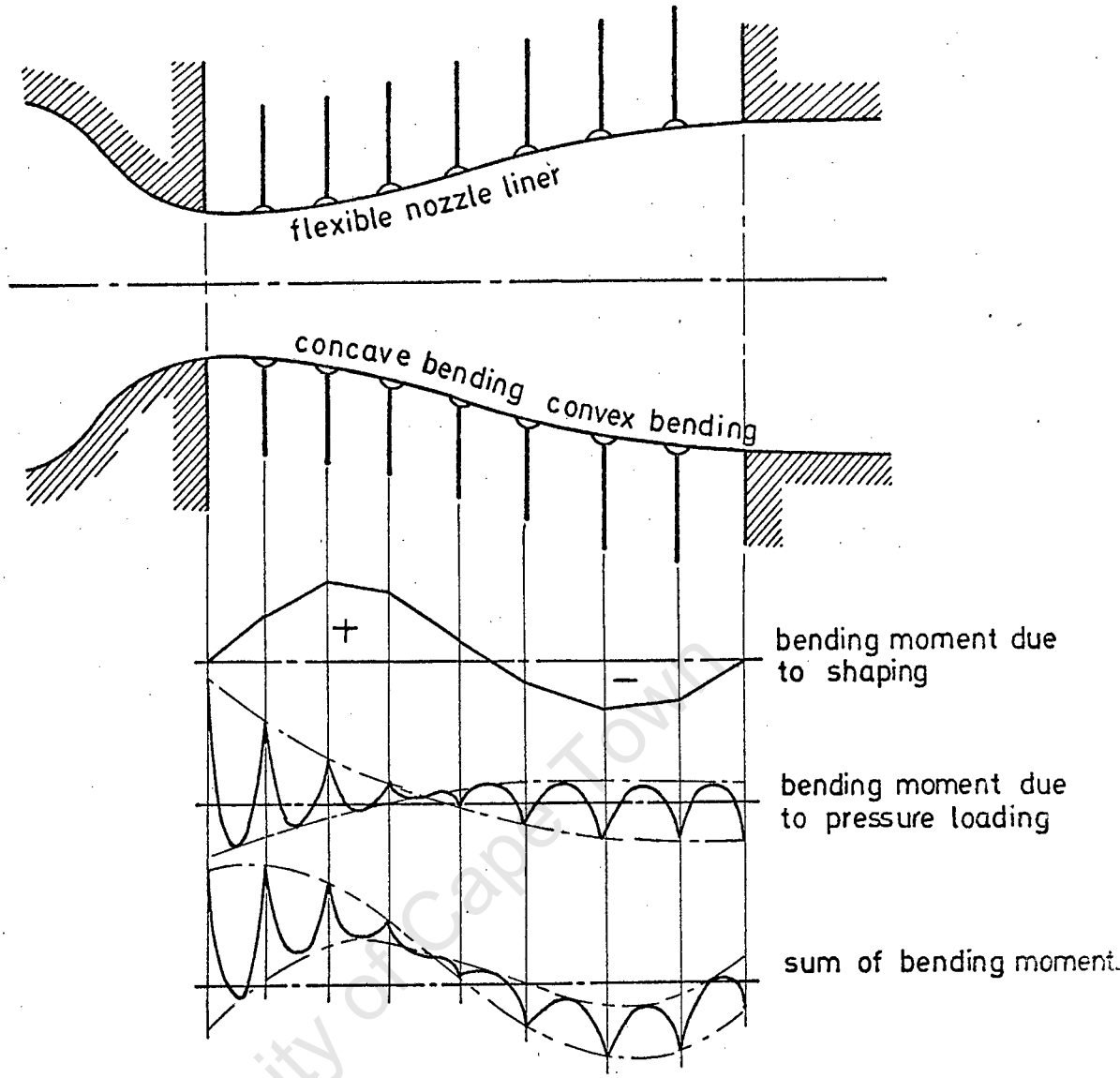

SUM OF BENDING MOMENT DIAGRAMS

Figure 1.12

Figure 1.12 represents the expected bending moments on the flexible nozzle liner and the resultant due to both pressure and bending loads.

To relieve the bending loads to some extent, the nozzle liner may be pre-moulded to the average shape of the nozzles. (i.e. A suitable guide would be the Mach 2.5 nozzle). The resulting bending moments in the actual system must remain within the limits that would produce plastic deformation.

The maximum stress on the flexible nozzle liner is given by:

$$\hat{\sigma} = \frac{B.M}{I} = \hat{y} \quad \text{..... 2.13}$$

Where the moment of Inertia; $I = \frac{wt^3}{12}$ 2.14

A cross-section of the liner is given in figure 2.13; it defines the above dimensions.

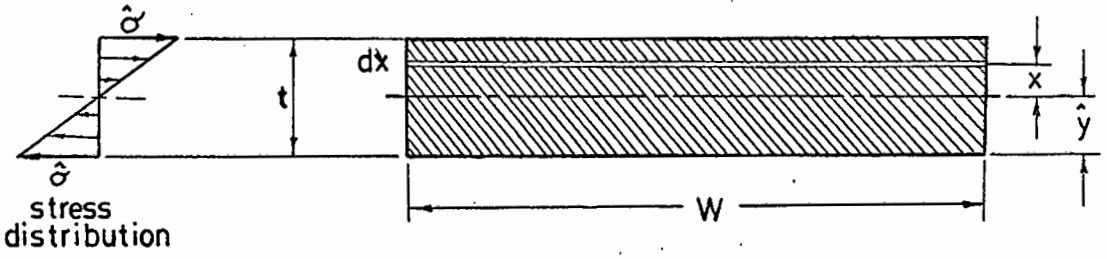

CROSS-SECTION OF NOZZLE PLATE

Figure 2.13

The thickness of the liner, t, must be kept to a minimum so that the loading due to profile forming is not too great. Although it is difficult to predict exactly what the bending moments are in profile forming the nozzle liner (especially as the nozzle is pre-moulded) a guide may be obtained from:

$$r = \frac{EI}{BM} \quad \text{.....} \quad 2.15$$

Where r is the radius of curvature that the nozzle liner will be subjected to. This equation is given in figure 2.14 for different thicknesses of liner plate.

To find a suitable nozzle liner thickness, it must be subjected to extreme conditions: Assume that:

1. The minimum radius of curvature, that the liner will have to be moulded to is 7,5 inches (the resultant bending moment will be less for a premoulded liner).
2. The maximum pressure load at the same section of the liner will be about 40 psia.

The summation of the bending moments due to these two extreme conditions is given in figure 2,15. The maximum bending moment limit for a maximum elastic stress (100,000 lbs/in^2) is derived from equation 2,13. This limit is also given in figure 2,15.

This figure shows that the most satisfactory range in liner thickness, so that the probability of plastic deformation is kept to a minimum is between 0,020 and 0,045 inches.

Any relaxation, in the bending of the liner or the pressure it is subjected to, will reduce the maximum bending moments and the probability of excess stress. Therefore, a nozzle liner thickness of 0,030 inches should be suitable in both strength and ability to resist deflection.

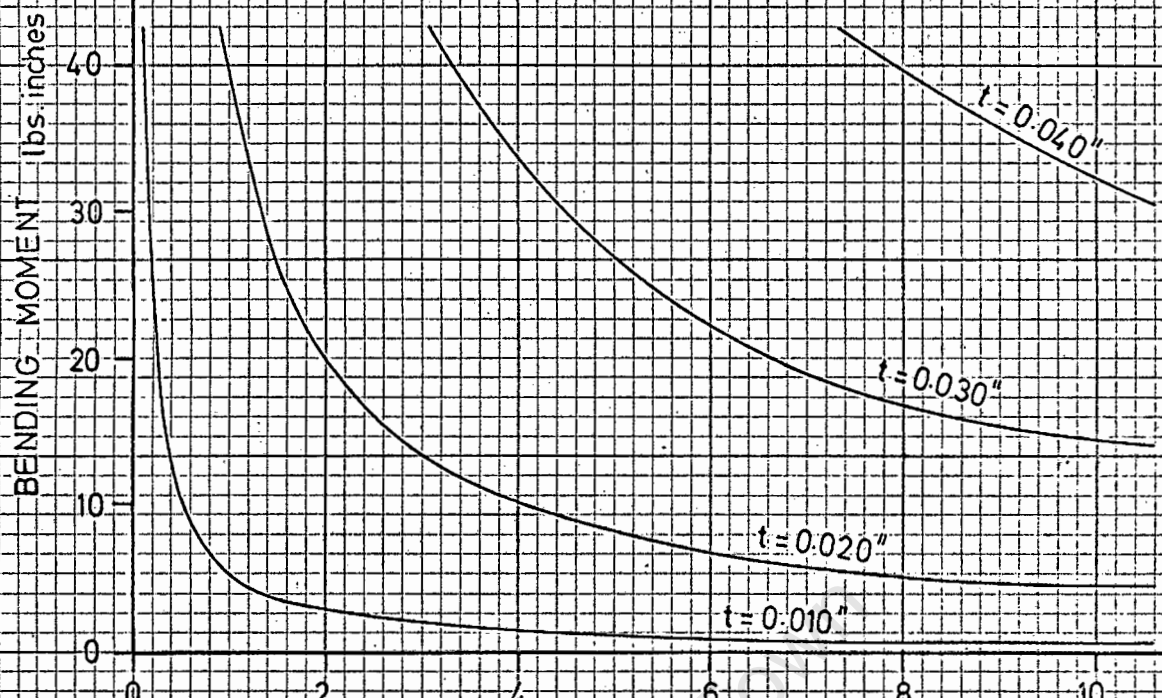

MOMENTS DUE TO BENDING

Figure 2.14

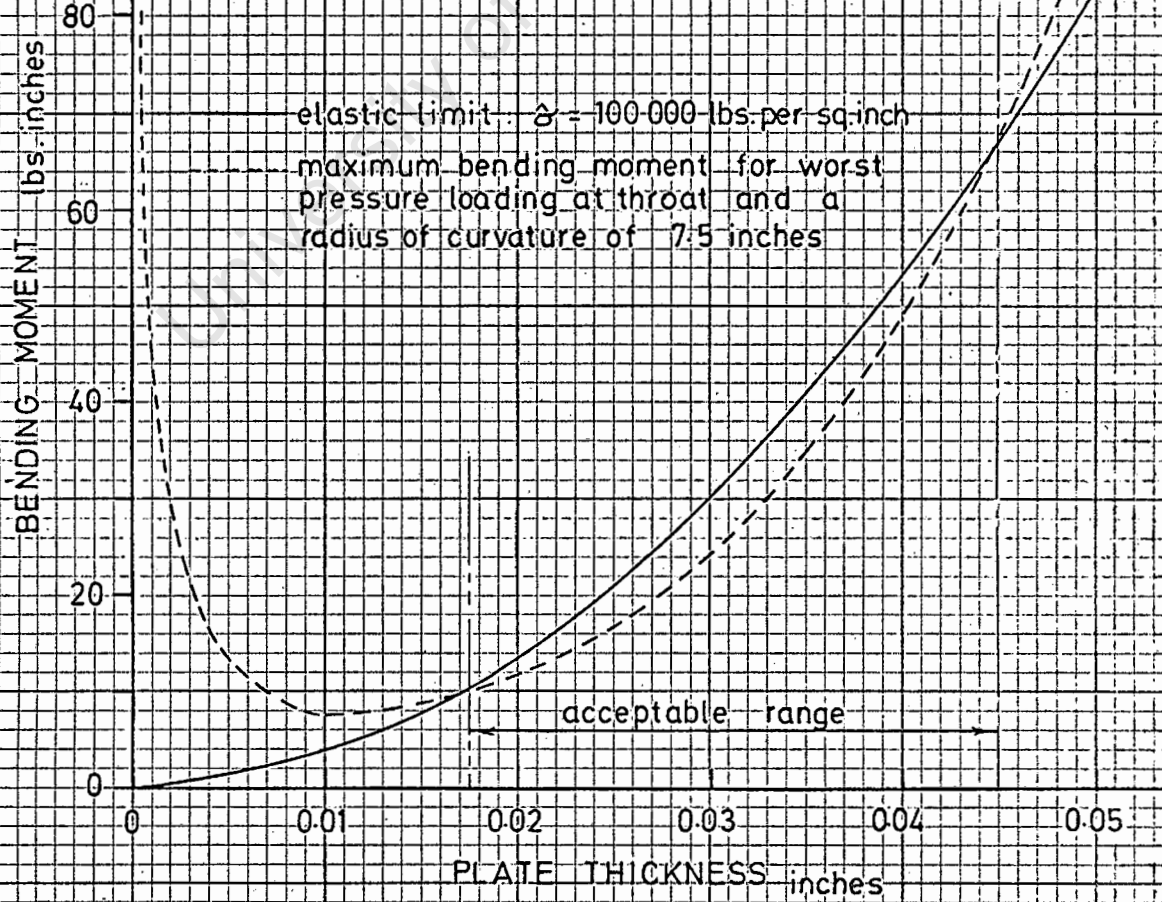

WORST BENDING MOMENT CONDITION

Figure 2.15

3.2 DESIGNING THE VARIABLE NOZZLE.

The final design of the variable nozzle, that satisfies all of the requirements, is given in figure 2.16.

Nozzle Liner

The nozzle liner surface is continuous from the subsonic inlet to the test-section exit. The change in nozzle contour length, due to alterations in design Mach number, are accommodated in sliding grooves at each end. The liner may be attached to the jack supports by spot welding and the surface may then be covered with a thin film of some plastic to remove the irregularities.

Subsonic Inlet

The only condition laid down for this section is that the radius of curvature near the nozzle throat is large. The large positive pressures in the subsonic inlet are carried by a flexible rib which is connected to a horizontal pivot at one point. This pivot arm is necessary to locate the position of the nozzle liner in relation to the nozzle box.

Expansion and Cancellation-Sections

This section is very important in the development of uniform parallel supersonic flow. The flexible liner is located at one inch intervals by adjustable supports which determine the vertical co-ordinates of the nozzle contour. Once the desired nozzle profile has been set, the support is'locked' so that rigidity of the structure is ensured.

Test-Section

The test-section is straight and may therefore be backed by reinforcing. The flexible section of theliner overlaps into this section so that the nozzle length may be increased if necessary.

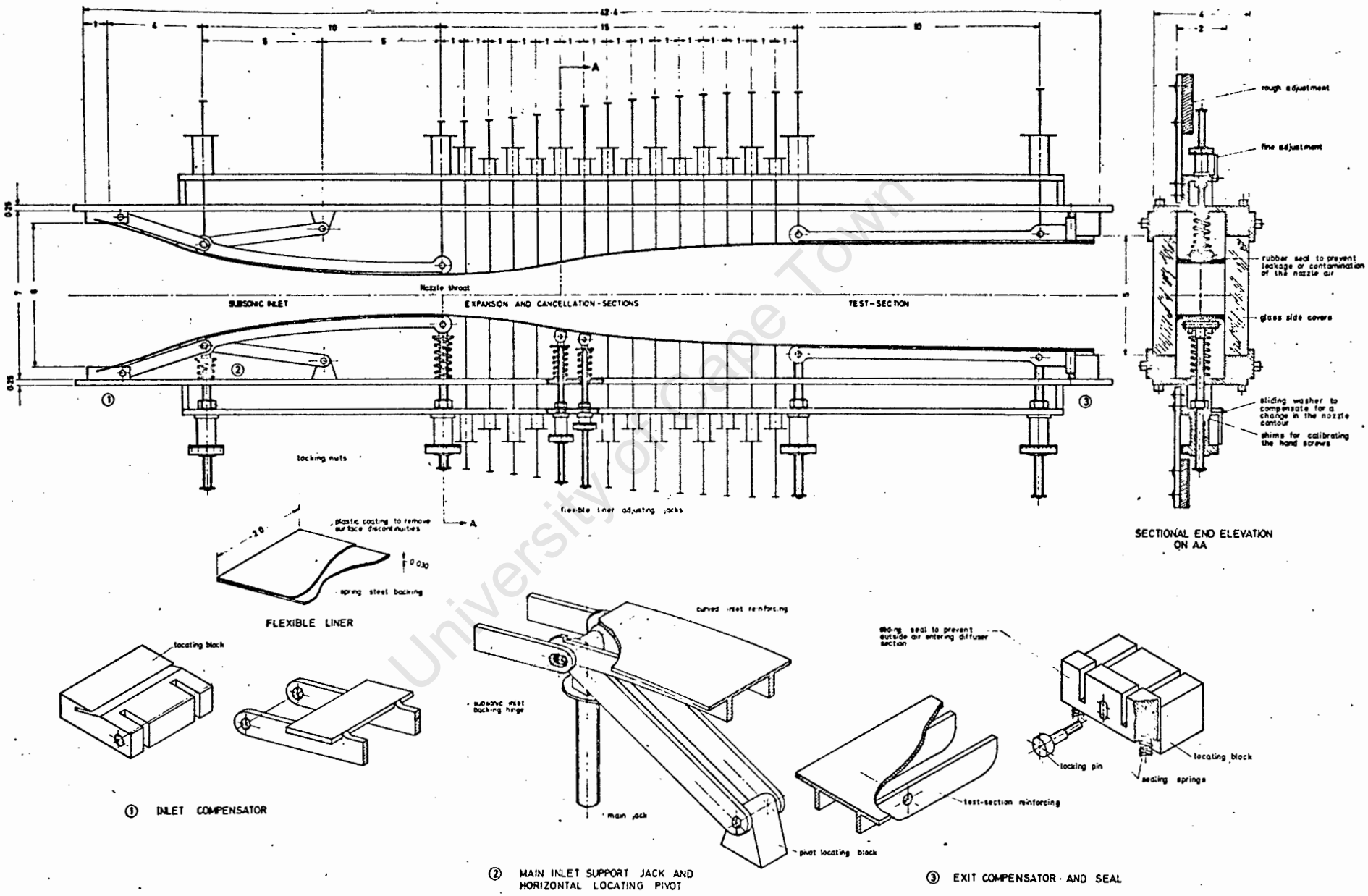

Figure 2·16 VARIABLE SUPERSONIC NOZZLE

ALL DIMENSIONS IN INCHES

CHAPTER 3

CONTROL SYSTEM ANALYSIS

SUMMARY

This chapter deals with the alterations to the control system and the performance analysis of its response.

The limitations of the original control system are discussed in part 1. The necessary improvements are presented together with the test results of the damping cylinder and shut-down piston.

Part 2 presents a comparison of this system with a simple spring system and indicates the possible deviation of the valve response. The control components are analysed and a block diagram is set up to represent the system.

This block diagram is simplified and from it a third order differential equation derived. It is solved, in part 3, using a Laplace transform. These response curves are used to confirm the analogue simulation of the system.

The analogue system is then extended to include the effects of non-linear damping and storage drum pressure decrease (In part 4). The results of this simulation are compared to the performance of the control system in part 5. The differences between the response curves are discussed and the possible reasons as to the causes are given.

PART 1
DESCRIPTION OF SYSTEM AND SOME OF ITS CHARACTERISTICS

1.1 INTRODUCTION

The control valve is required to retain a constant settling chamber pressure although the upstream pressure may be changing. It is also used to initiate flow and to terminate it after the blow-down is complete.

The pneumatic control system for this valve is shown in figure 3.1 and operates as follows:

The desired operating pressure is set on the regulating valve (1) on the control panel. This pressure acts on the upper surface of the flexible diaphragm in the control chamber (2). The settling chamber (3) is connected to the chamber below the valve control diaphragm so that the stagnation pressure acts on the underside of the diaphragm.

The initiation and shut-down of the flow is achieved by means of the shut-down piston(4). Pressure is applied to this piston so that the valve may be lifted against the set pressure. Flow is initiated when the shut-down pressure is released at the controlling two-way switch (5). The valve will open due to the downward force acting on the valve as a result of the set pressure on the diaphragm. The settling chamber pressure will increase until the mass flow rate entering the settling chamber is balanced by that leaving through the supersonic nozzle. This settling chamber pressure acting on the underside of the diaphragm reduces the total controlling force which is defined as the force resulting from the difference in pressure across the diaphragm. When these pressures are equal, the system should be in equilibrium.

During the blow-down period, the reduction in storage drum pressure tends to reduce the settling chamber pressure. The valve compensates for this reduction in the storage drum pressure by opening further until the pressure forces are again in equilibrium. Shut-down of the flow is achieved by re-applying the full control pressure to the shut-down piston.

1.2 FAULTS OF THE ORIGINAL VALVE

The original settling chamber pressure control valve was chosen as a component of the supersonic wind-tunnel because of its cheapness and availability over the more suitable flap valve. Its performance was not entirely satisfactory for the following reasons:

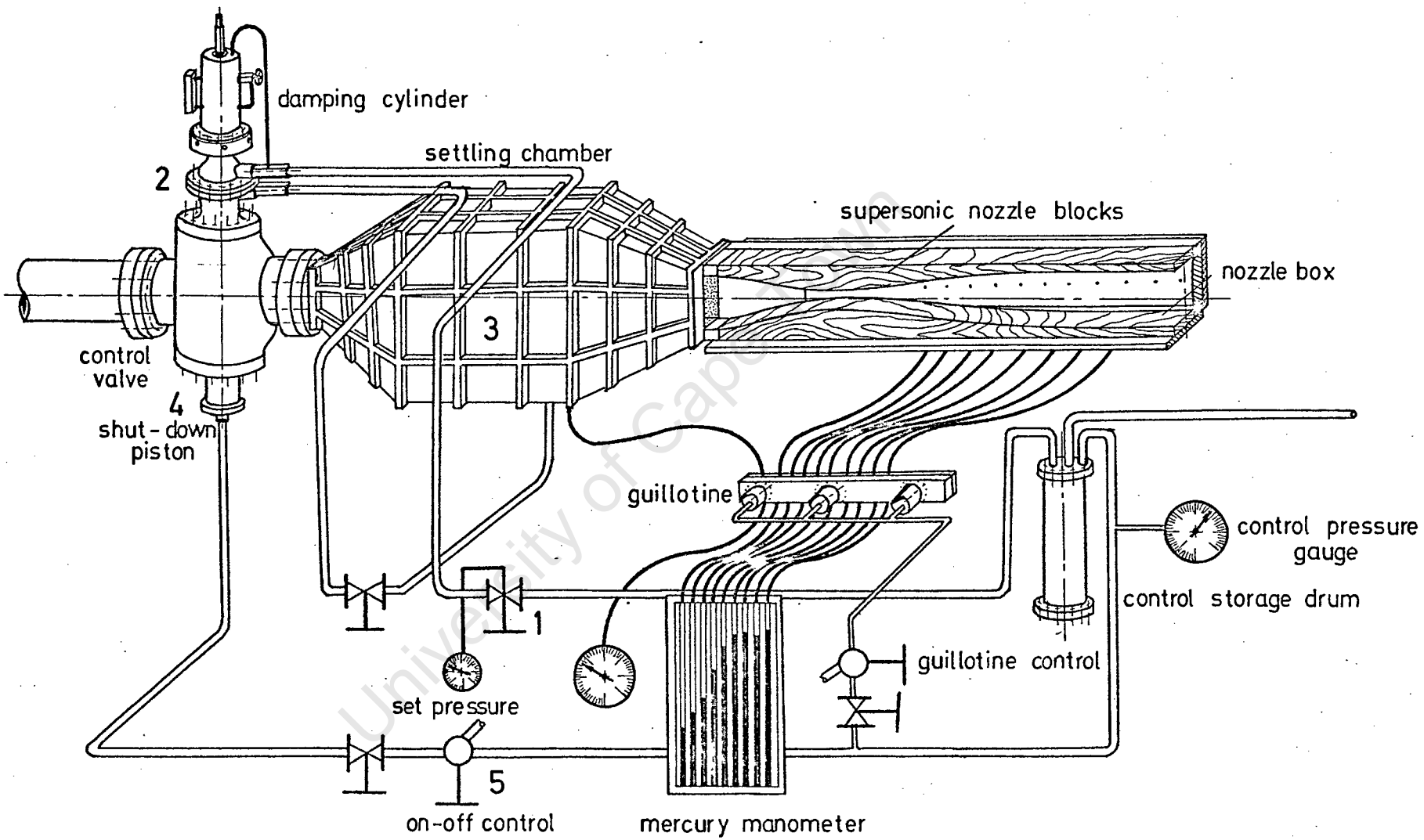

SETTLING CHAMBER PRESSURE CONTROL

Figure 3.1

1. The degree of its control of the settling chamber pressure was limited over a run. The pressure tended to drop with the storage drum pressure (11).

2. The spring control did not offer any form of damping. Consequently, oscillation of the valve, after starting a blow down, continued for some time (5).

3. Leakage of control air into the tunnel led to difficulty in setting-up heat transfer models.

4. Setting up the desired stagnation pressure had to be done manually by changing the preload on the controlling spring. It was unpractical to adjust this pressure during a run period.

1.3 MODIFICATIONS INCORPORATED IN THE CONTROL SYSTEM.

The reduction of these deficiencies in the valve control, with a minimum of alterations to the system, was a straightforward problem.

The spring control was removed and replaced by a pressure control which could be set by remote adjustment. (See figure 3.1). A damping cylinder, shown in fugure 3.2, was incorporated to limit the degree of oscillation of the valve during flow initiation. The motion of the valve is now controlled by the difference in the pressure across the valve diaphragm, the damping forces and the inertia forces. These forces must be in equilibrium at any stage during the valve operation.

A separate sub-unit was incorporated to close the valve against the set pressure. As the shut-down piston, shown in figure 3.2, is subjected to the full control pressure, it has a rubber O-ring seal to prevent air leaking into the tunnel before the run begins. This unit is divorced from the valve so that once the valve has opened fully, the shut-down piston looses contact with the free moving valve and does not further influence its characteristics.

The spool valve is designed with double seats so that any pressure forces on the valve faces, due to the flow of fluid, are balanced and no external forces are necessary to keep the valve stationary. At particularly high pressures this is not so and a certain degree of unbalance is to be expected. This will upset the balance of the pressures across the diaphragm but the degree of this unbalance should be small. The only way to correct this is to apply an external pressure to rebalance the system. This is not warranted for most applications of the wind-tunnel.

The damping cylinder and shut-down piston must be tested so that the damping forces and the static friction may be found respectively. This is necessary for the analysis of the response of the valve control system.

A wkward.

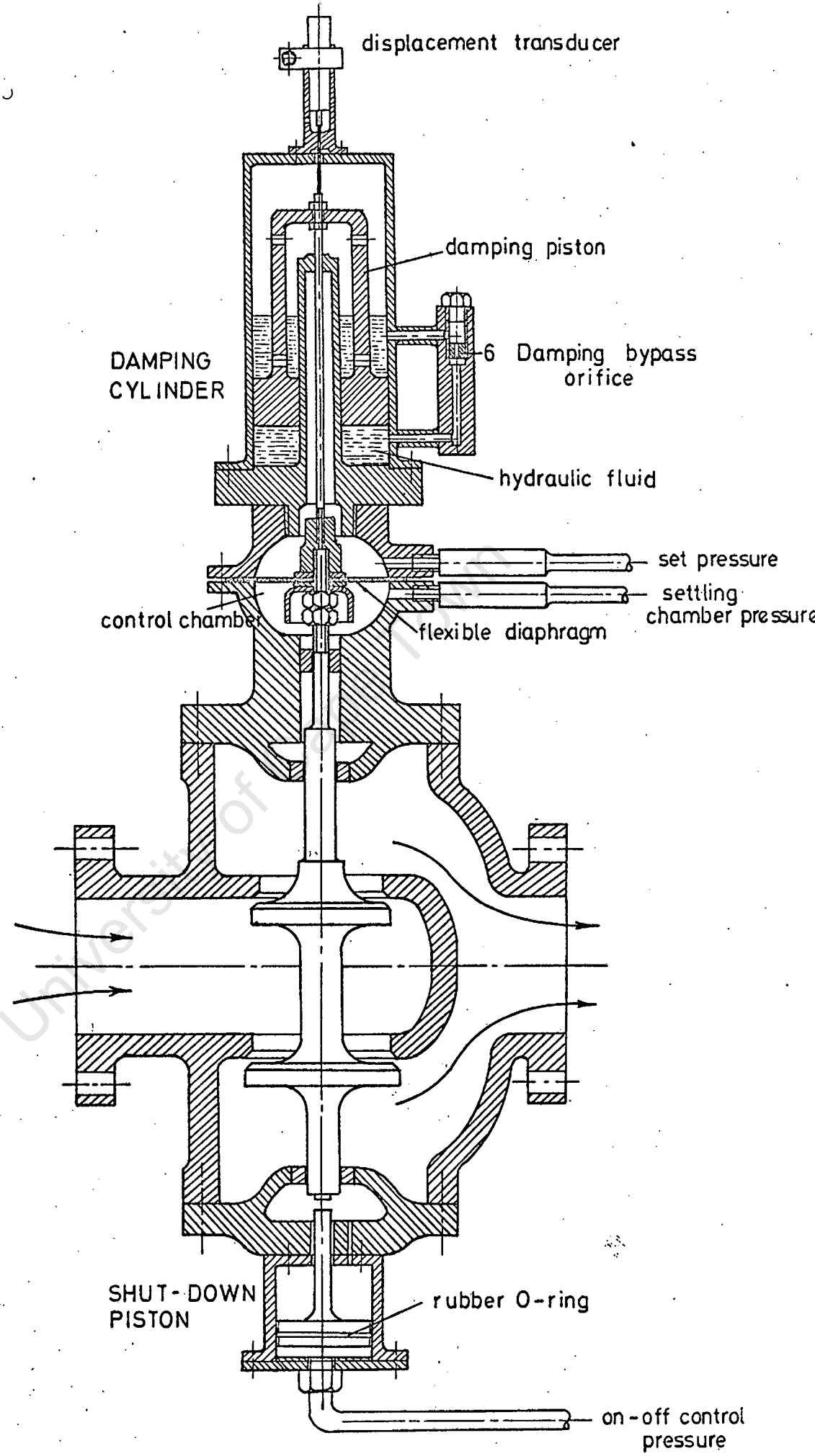

PRESSURE CONTROL VALVE

Figure 3.2

1.4 SHUT-DOWN PISTON

Although the shut-down piston sub-unit does not influence the behaviour of the valve during the tunnel operation, it most certainly will affect its opening characteristics as flow is initiated. for the following reasons:

1. The effective mass of the valve is increased by that of the shut-down piston during the first downwards movement of the valve.

2. The drag on this piston is transmitted to the free valve system.

Once the valve has opened, the increased downstream pressure acting on the upper opposing face of the shut-down piston prevents it from making any further contact with the valve.

The static frictional forces of the piston are easily determined by subjecting it to increasing loads it slips. The application of a lubricant to the rubber O-ring seal resulted in a deviation from the normal static friction characteristics (see figure 3.3). This curve appears to show a transition between static and viscous friction.

The static friction results from the reaction of the rubber seal on the rough cylinder walls. The distortion of this seal due to this reaction

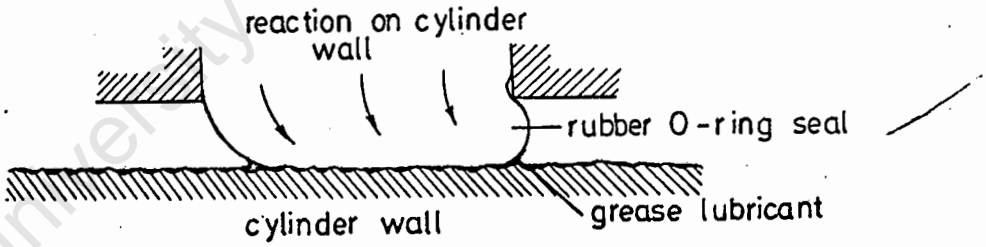

O-RING SEAL
Figure 3.4

in addition to the distortion due to the pressure forces effectively seal the piston against air leakage (see figure 3.4).

The maximum force required to move a body is usually presented as:

$$F = \mu R \qquad \ldots\ldots\ldots\ldots\ldots\ldots\ldots\ldots\ldots\ldots\ldots\ldots \quad 3.1$$

In the presence of a lubricant, such as a grease, the surface roughness of the cylinder is effectively reduced and so is the static friction coefficient . The application of a lubricant also introduces viscous friction which results

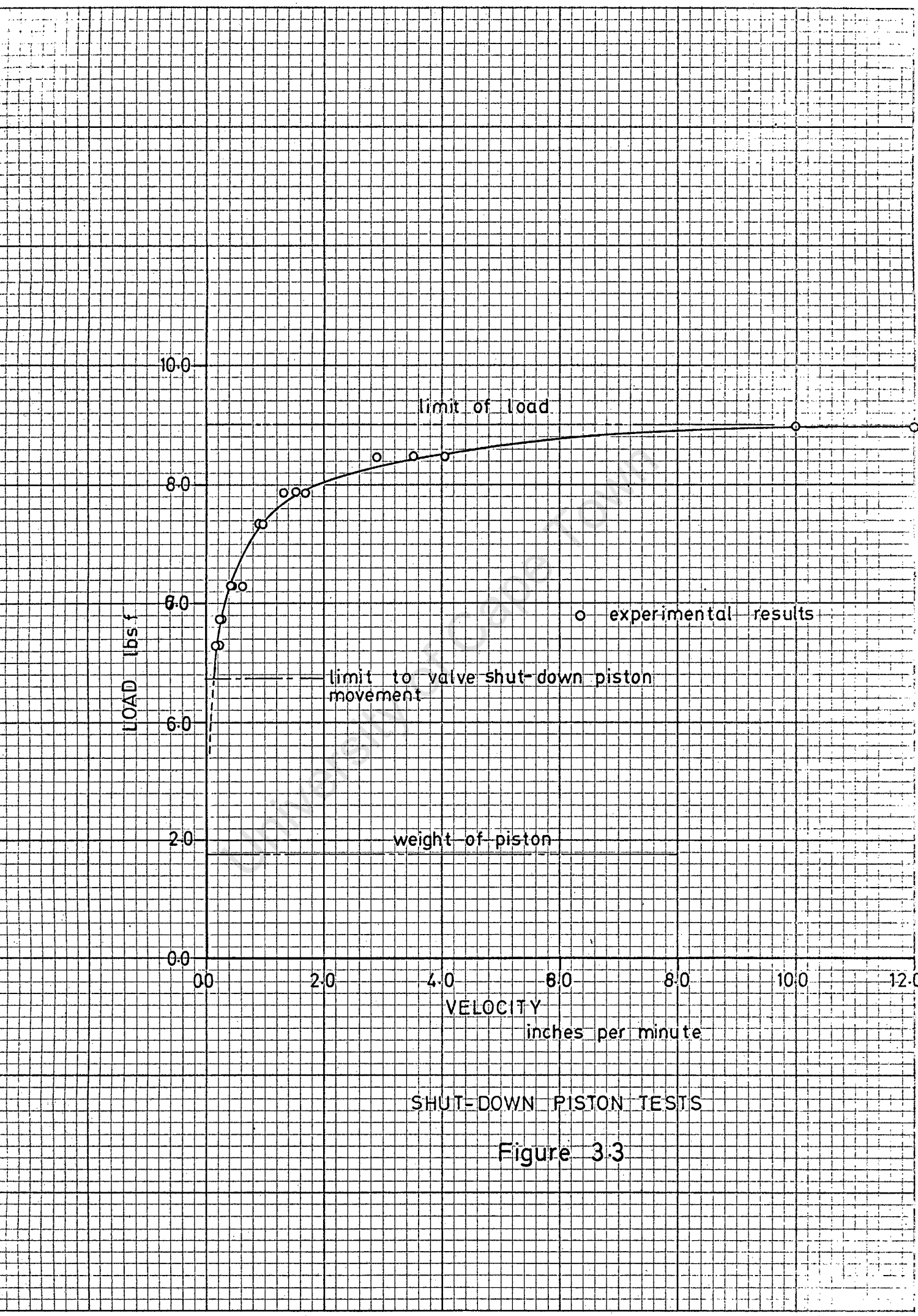

SHUT-DOWN PISTON TESTS

Figure 3.3

in the deviation of the graph. The force thus becomes velocity dependent. At high loads, the static friction law predominates over the viscous friction so that a limit to the drag force is reached.

Although the maximum resistance to movement of this piston is small in relation to the controlling forces on the valve, it may have some influence on the valve response properties.

1.5 DAMPING CYLINDER

The valve damping cylinder was calibrated for different bypass orifices under similar loading conditions experienced during the operation of the valve. The orifice screw is fixed into the damping piston bypass (6) as shown in figure 3.2. The diameter of the orifice determines the magnitude of the damping.

'Velocite' was chosen as the hydraulic fluid because its viscosity is almost independent of temperature changes.

The terminal velocity of the damping piston was measured for a downwards movement by means of a displacement transducer and an oscilloscope. Increasing loads were applied by means of the set pressure acting above the valve controlling diaphragm. These forces resulted in the hydraulic fluid being forced past the damping piston and through the bypass orifice.

The upward motion of the valve has been assumed to have the same characteristics as the downward motion for all practical purposes. It should be noted, though, that the magnitude of the damping force, for an upward movement, is limited to when the pressure below the piston reaches absolute zero. Because the damping cylinder is subjected to the full set pressure, it is unlikely that this limit will be reached.

The viscous force (F_v) is due to the set pressure (P_{set}) acting on the valve diaphragm as well as the weights of the valve and shut-down piston and the drag of the shut-down piston.

$$\therefore \quad F_v = P_{set}.A + (W_v + W_p - F_p) \quad \ldots\ldots\ldots\ldots\ldots\ldots\ldots\ldots \quad 3.2$$

The terminal velocity of the valve was measured for increasing set pressures on the valve diaphragm and increasing bypass orifice diameters. The results of these tests appear in figure 3.5.

These curves appear to be straight lines for very high damping and may be represented as:

$$F_v = C_D \times V \quad \ldots\ldots\ldots\ldots\ldots\ldots\ldots\ldots\ldots\ldots\ldots\ldots\ldots \quad 3.3$$

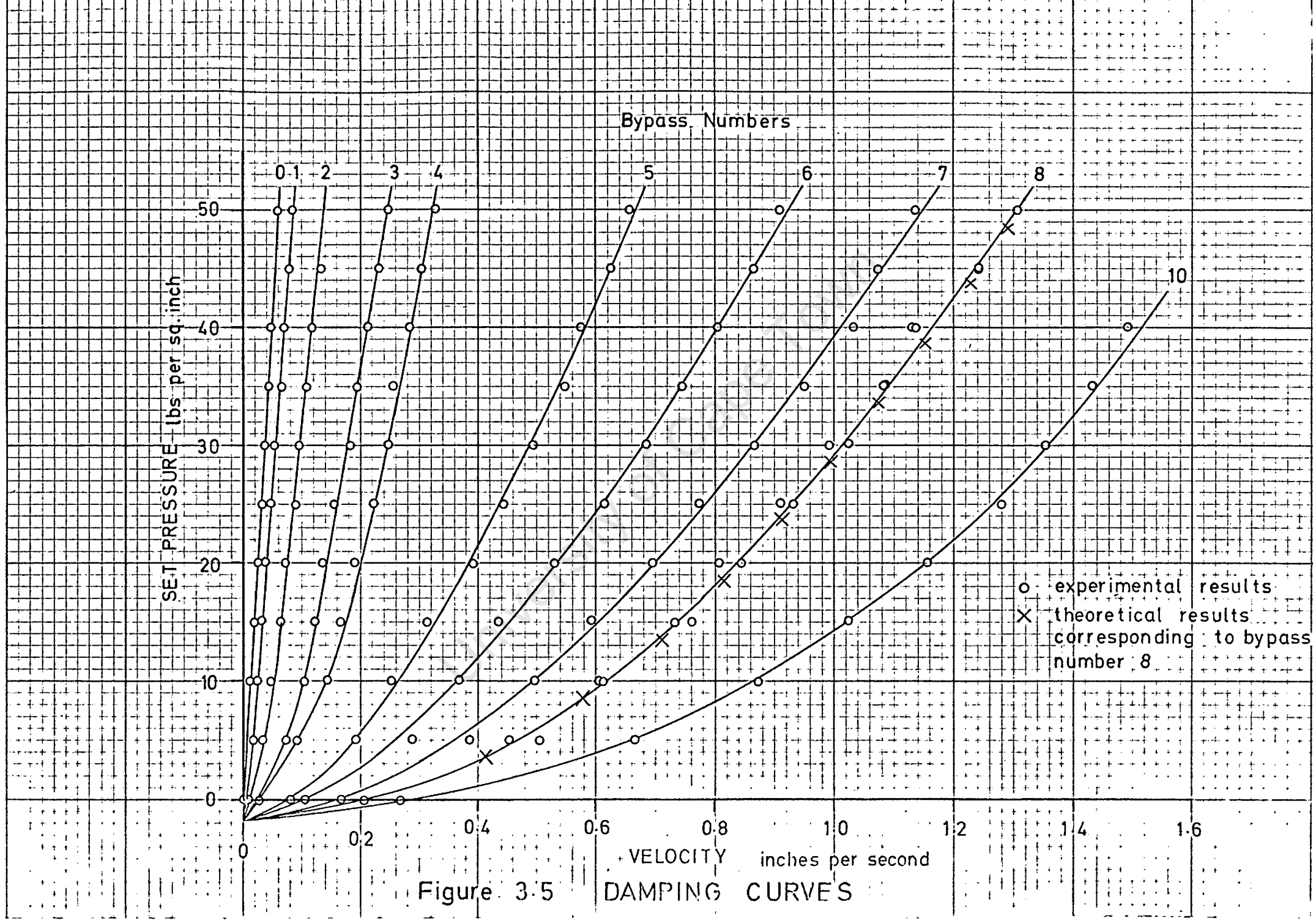

Figure 3.5 DAMPING CURVES

For lower damping, the approximate solution to the non-linear curves may be represented as:

$$F_v = C_{DRL} \times V^2 \quad \text{.....3.4}$$

Discussion of damping curves.

For the closed bypass, the damping curve is linear. The mass transfer of fluid takes place past the damping piston and the flow may be considered laminar. With the inclusion of a small opening, the damping curve is non-linear at low forcing pressures. It is suspected that turbulent flow exists through the bypass orifice and the resistance to flow may be assumed to be roughly proportional to the square of the velocity (18). As the forcing pressure increases, the flow past the piston increases at a greater rate than the flow through the bypass. So that at high forcing pressures, the damping curves appear linear. (see figure 3.6)

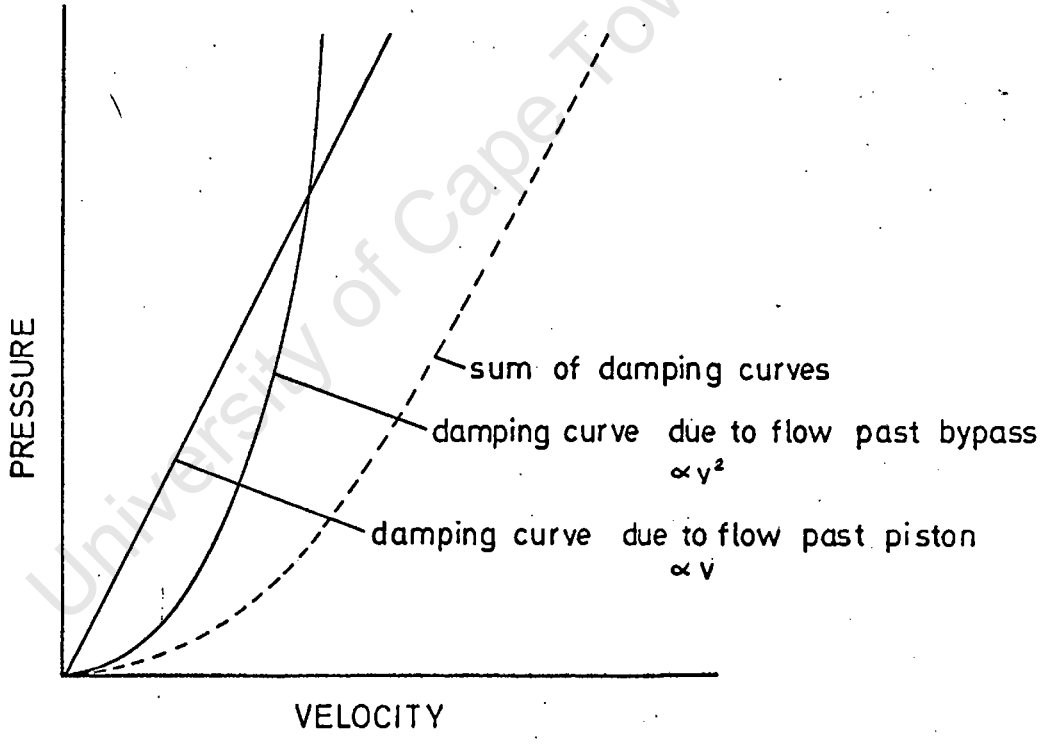

DAMPING CHARACTERISTICS

Figure 3.6

As the damping is decreased further, the laminar flow past the damping piston is exceeded by the mass flow rate through the bypass orifice. Thus the dominant characteristic is turbulent flow.

For high valve velocities, the influence of the inertia of the valve and damping piston becomes apparent from the response curves on the oscilloscope. Figure 3.8 illustrates the difference between the average velocity of the

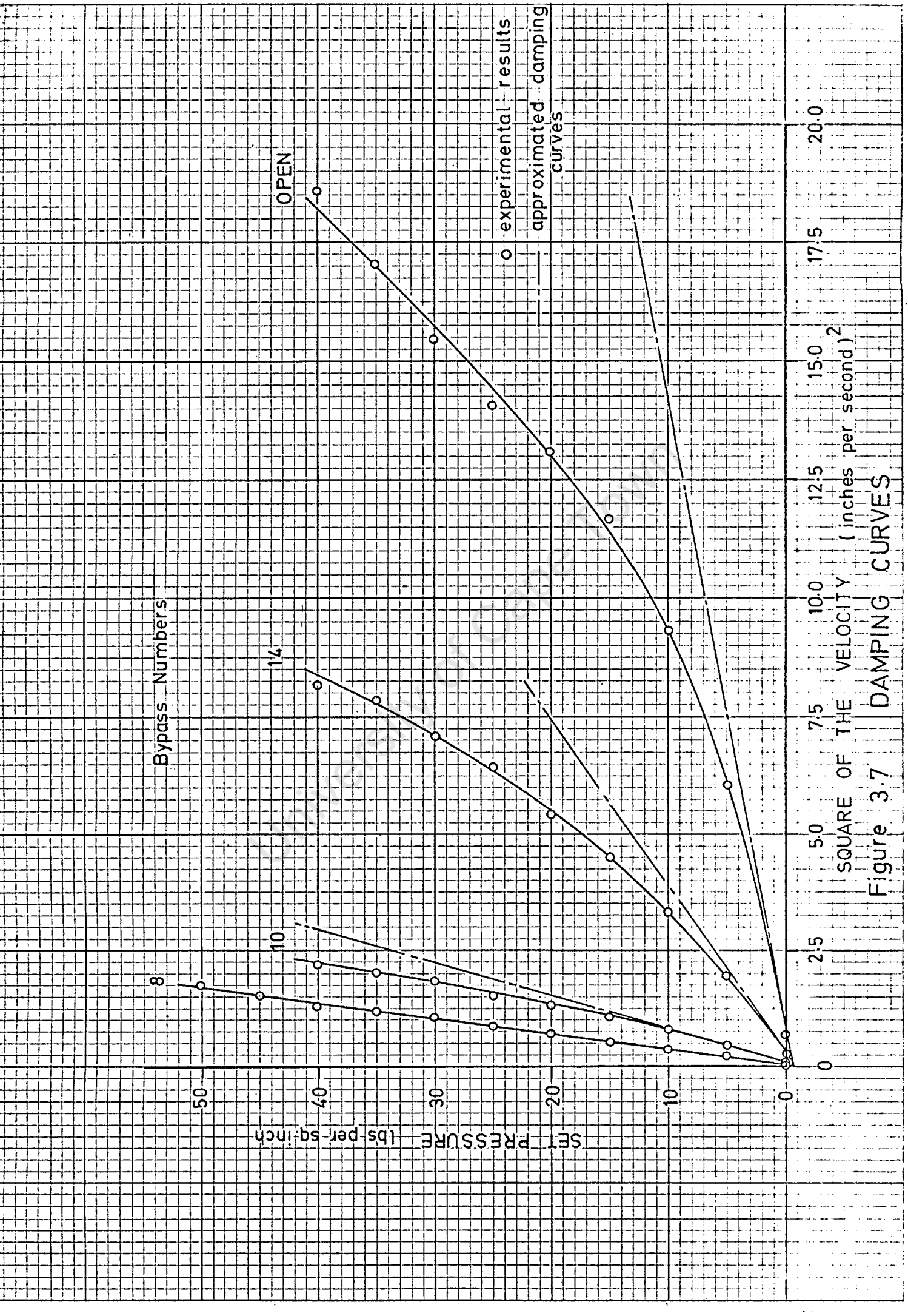

Figure 3.7 DAMPING CURVES

valve between its limits of travel and its terminal velocity. Because of difficulty in measuring the terminal velocity accurately, the square of the average velocity was plotted in terms of the forcing pressure in figure 3.7. These curves show an upward deviation from the expected linear characteristic for damping piston velocities greater than 1.5 inches/second.

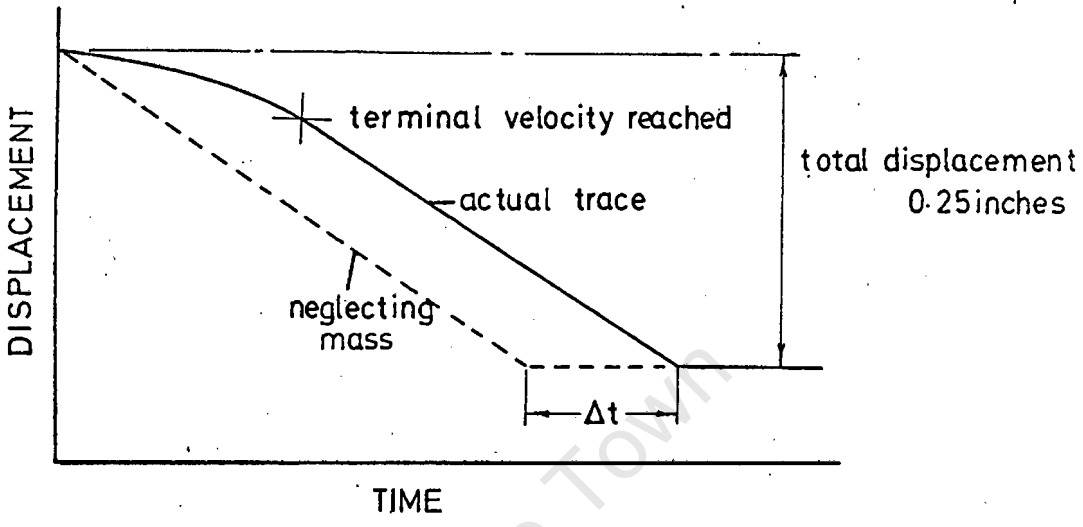

VALVE RESPONSE

Figure 3·8

The terminal velocities were roughly estimated and the straight line characteristics of turbulent damping are superimposed upon these curves.

The damping coefficients for the whole range of bypass orifices are derived as outlined below:

1. Linear damping coefficients are found for the first three bypass numbers 0, 1 and 2 from the straight line that approximates the points of the forcing pressure-velocity graphs.

2. Non-linear damping coefficients are found for the balance of the bypass orifices from the graphs of forcing pressure versus square of the velocity.

These coefficients are presented in appendix 3.1.

PART 2
DERIVATION OF A MATHEMATIC MODEL OF THE CONTROL SYSTEM

2.1 DESCRIPTIVE ANALYSIS

One of the important aspects of the design of the control system, is the study of all the factors that are likely to affect its performance. By comparison with simpler systems, whose response is well known, any problems that are likely to be encountered are brought to the fore.

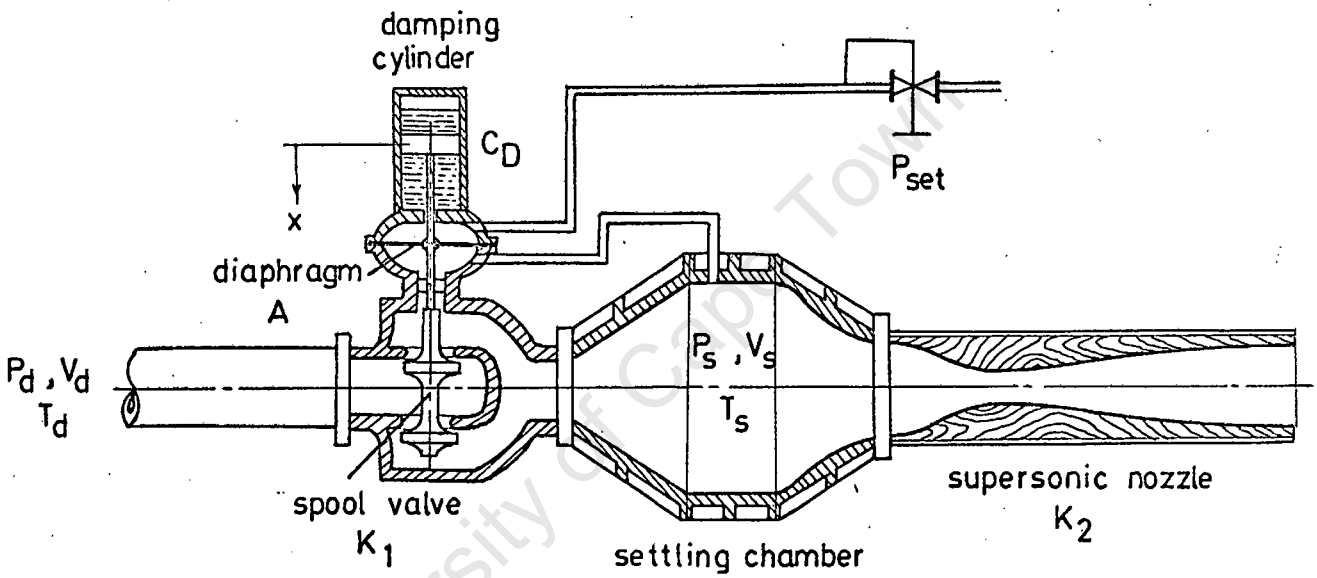

CONTROL LAYOUT

Figure 3.9

The supersonic wind-tunnel settling chamber pressure control system is shown in figure 3.9. Sonic flow occurs past the valve seals during most of the valve operation (see Chapter 1, part 5.2). Hence the mass flow rate past the valve is a function of the upstream pressure and the valve displacement. The mass flow rate through the nozzle is a function of the settling chamber pressure. Therefore, if the storage drum pressure is fixed, and the mass flow rate past the valve is equal to the mass flow rate through the nozzle, then the settling chamber pressure must be proportional to the valve displacement.

The factors influencing the valve motion are:

1. The inertia of the valve.
2. The damping forces (assumed linear).
3. The valve controlling forces (defined as the product of the diaphragm area and pressure difference i.e. set pressure - settling chamber pressure).

This system is similar to that given in figure 3.10.

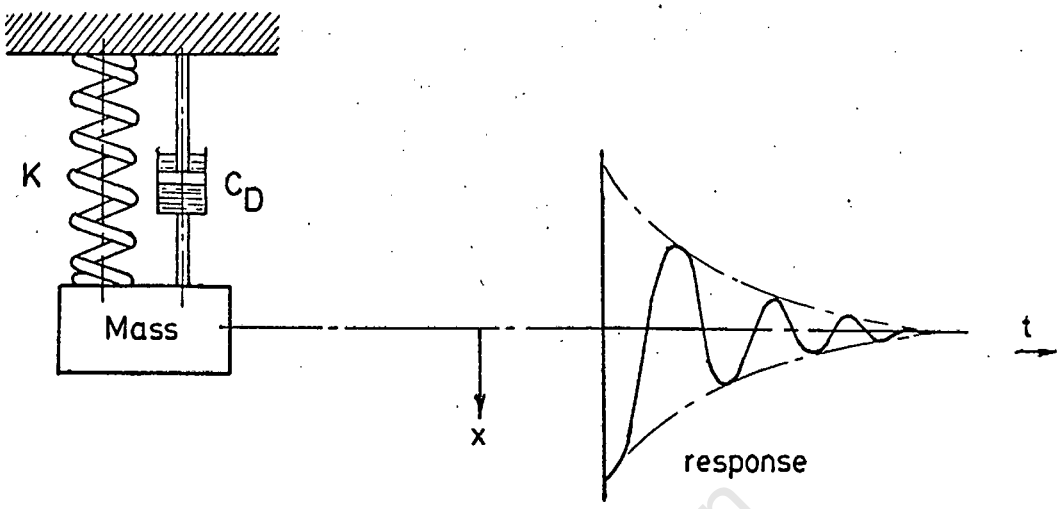

SPRING SYSTEM
Figure 3.10

The solution to this system is well known. The displacement of the valve will be sinusoidal with a decreasing amplitude.

This solution neglects, however, the capacity effects of the settling chamber. There is a time delay between the change in settling chamber pressure and the corresponding change in valve position. (See figure 3.11).

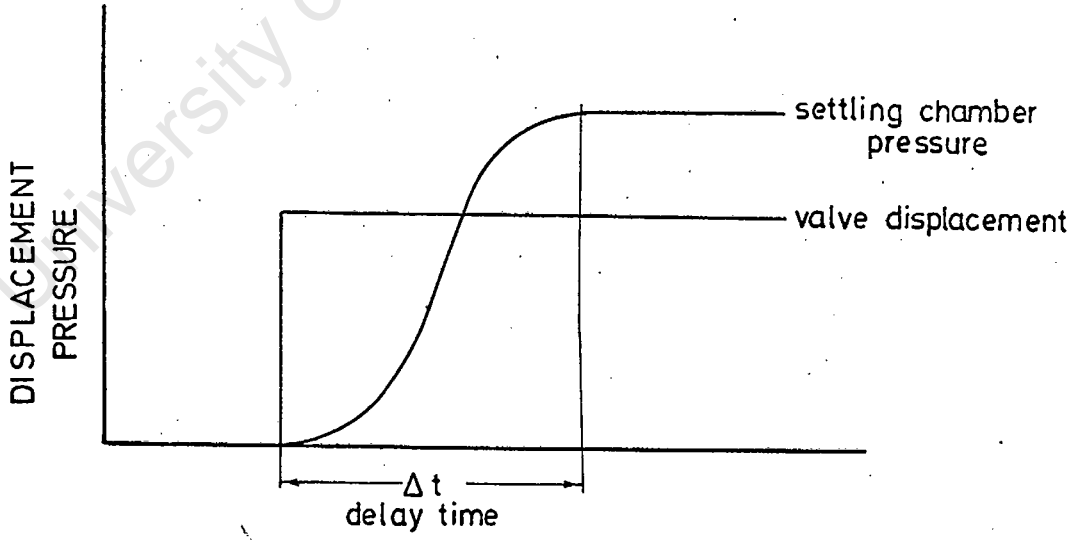

PRESSURE RESPONCE
Figure 3.11

This time delay produces a lag in the application of the force that restores the equilibrium of the valve. If the system has no damping, and a pressure is applied to the upper surface of the diaphragm, the valve will open and overshoot the mean position. Because of the delay in the restoring force, the magnitude of the overshoot X_1 will be greater than the initial displacement X_o (Referring to figure 3.12). Consequently the amplitude of the alternating settling chamber pressure ~~of the alternating settling chamber pressure~~ will

increase with each successive oscillation of the valve, until the valve reaches its limit of travel.

In a self-excited vibration,the alternating force that sustains the oscillation is created or controlled by the motion itself; when the motion stops, the alternating force disappears. Den Hartog (19), terms the effect of self-exitation as negative damping. Because a self-excited system draws from an

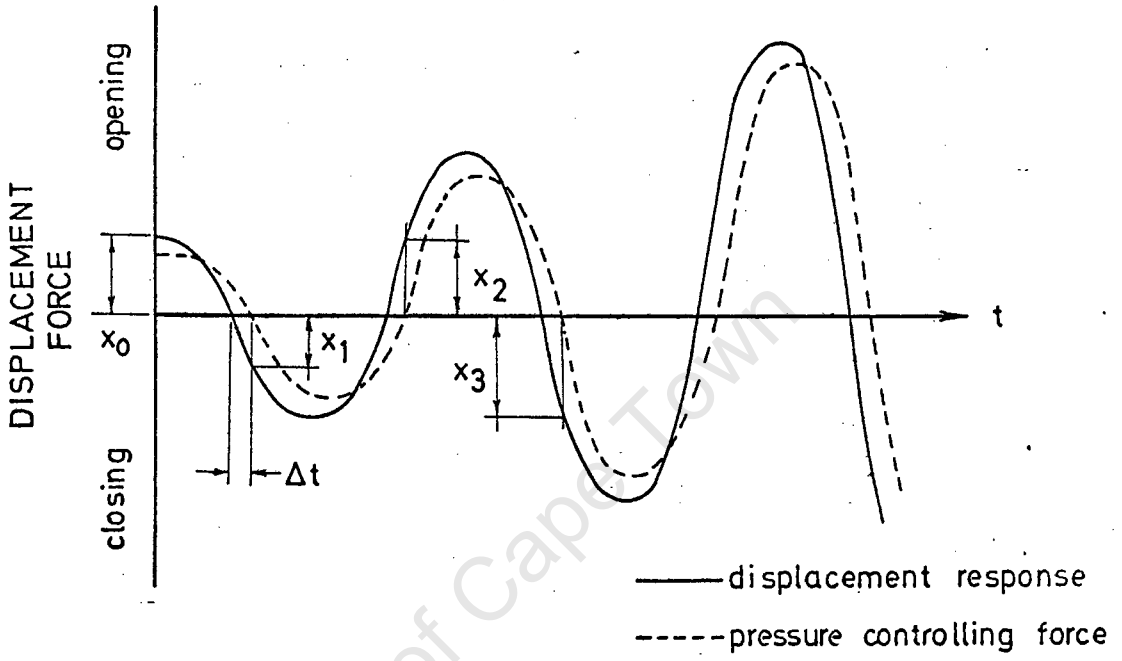

SYSTEM RESPONSE WITHOUT DAMPING
Figure 3.12

external energy source, in this case the pressure potential of the control air, the system may increase in energy. This could result in damage to the control components.

This 'negative' damping must be stemmed by a positive damping system. The degree of this demping defines the characteristics of the valve motion. A normally desirable characteristic is critical damping whereby the valve is brought to rest in the quickest space of time but without any oscillation..

i.e The potential energy due to the controlling pressure across the valve diaphragm and the valve displacement must be balanced exactly by the energy absorbed in the damping cylinder during the initial displacement of the valve.(See figure 3.13).(from closed position to operating pressure).

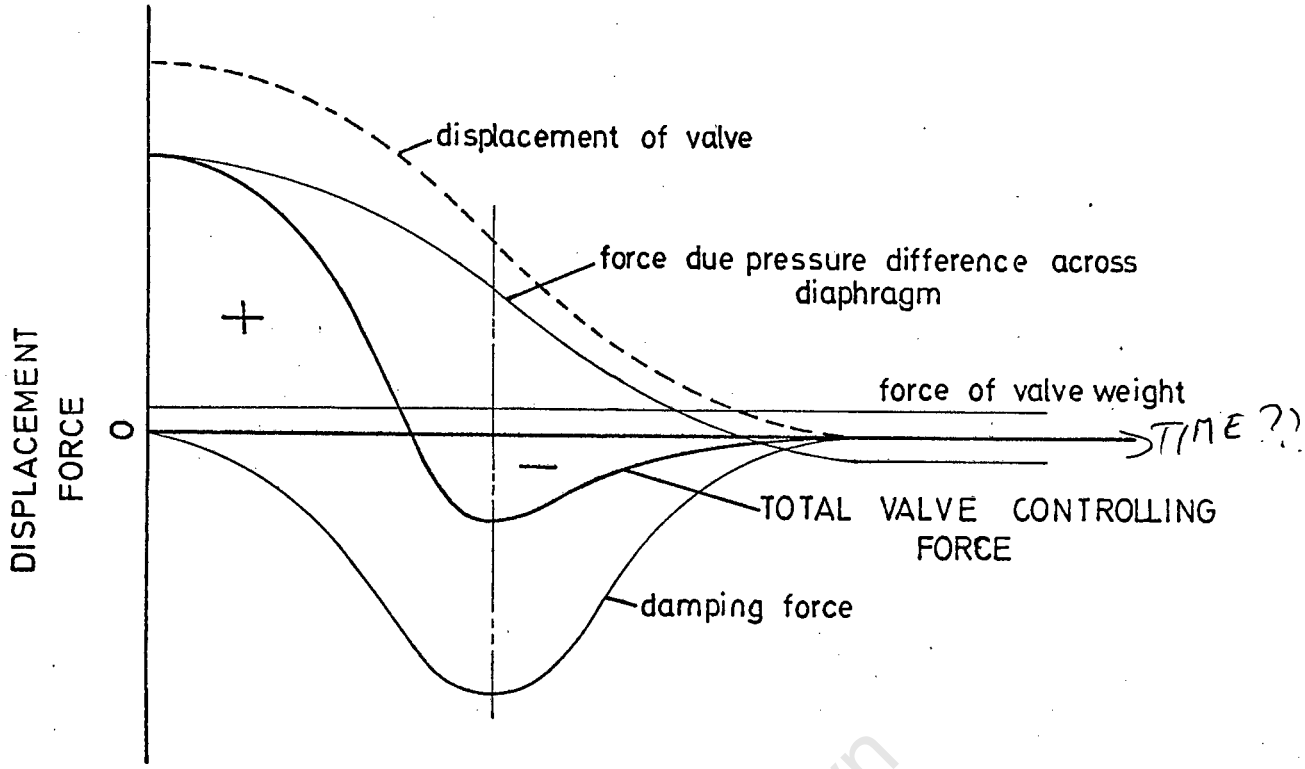

CONTROLLING FORCES

Figure 3·13

An analysis of the control is very limited if based solely on this argument of negative and positive damping. A much more satisfactory method of control analysis involves the derivation of the complete mathematical model.

2.2 ASSUMPTIONS

There are a number of factors that are likely to influence the control. Although their effects should be considered in relation to the final valve characteristics, it is impractical to include them in the control analysis.

The assumptions necessary to simplify the construction of the system block diagram, are listed below:

1. Any unbalance of pressure forces on the valve seat faces are neglected. These forces, which arise from different valve seat diameters and turbulence within the valve body, change with storage drum pressure. Because there are so many variables concerning the magnitude of this force, it can only be found from tests.

2. It is assumed that the damping force is proportional to the velocity at high damping and is proportional to the square of the velocity at low damping (See chapter 3, part 1.5). These are only approximations of the actual curves.

3. The valve controlling force is taken as the product of the pressure difference across the flexible valve diaphragm and the diaphragm area.

4. The mass and the frictional resistance of the shut-down piston, during the initial positive displacement of the valve, are neglected.

5. The pressure difference across the valve is assumed to be such that the air velocity is sonic at the valve seats. The mass flow rate is then only a function of the valve displacement and storage drum pressure.

6. Although the mass flow rate through the nozzle is proportional to the abslute settling chamber pressure, it is necessary to express it in terms of the gauge pressure. This is not an assumption

7. As a result of the Joule-Thomson effect, there is no temperature change across the valve (20). The storage drum and settling chamber air temp is assumed constant at 550°R (11).

8. The time necessary for a disturbance of the valve to effect a change in pressure across the diaphragm is very small (in the order of $0,5 \times 10^{-2}$ secs) and may be neglected. ?

2.3 DEVELOPMENT OF THE BLOCK DIAGRAM

In order to develop the full control block diagram, it is advisable to consider each of the main components of the control separately. The three main sections are:

1. The Valve:

This is influenced by the inertia effects of its mass, the viscous damping and the controlling force on the valve diaphragm. The motion is described by the valve displacement X.

2. The Settling Chamber Capacity:

The capacity effects are influenced by the volume of the settling chamber and the nozzle and valve flow characteristics. (P_s represents the pressure at any given instant of time.)?

3. The Storage Drum:

This external circuit is added to the main control system. It describes the steady decrease in storage drum pressure during the operation of the tunnel.

Valve

Figure 3.14 is the block diagram for the valve. The difference between the pressures acting on either side of the diaphragm give rise to force F_1 which is balanced by the inertia force F_2, damping force F_3 and the valve weight W.

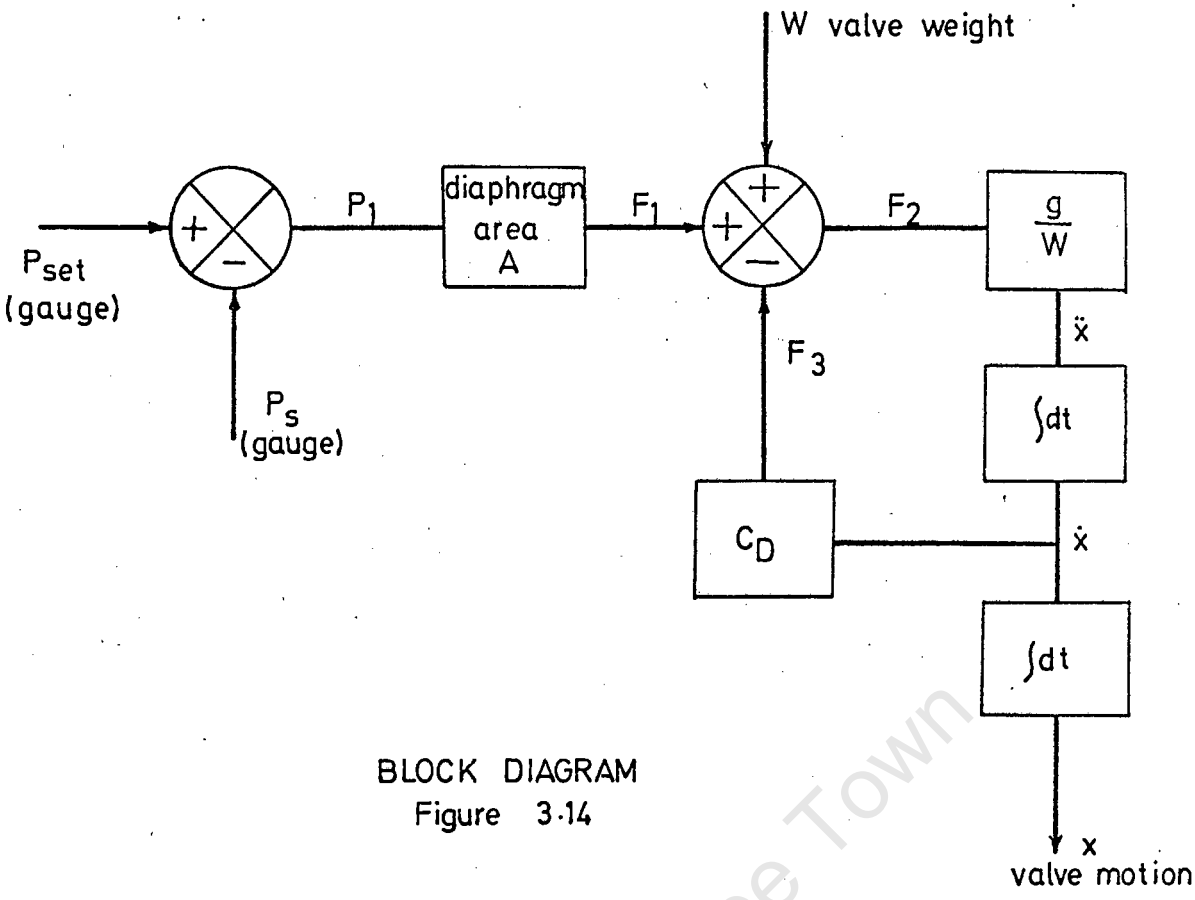

BLOCK DIAGRAM
Figure 3.14

Non-linear damping effects have been neglected in this block diagram. The system can thus be described by an ordinary linear differential equation.

Settling Chamber

The mass flow rate past the valve is a function of storage drum pressure and valve displacement. Hence for a constant storage drum pressure, if the control valve is displaced from the closed position by a step function X, the mass flow rate past the valve will be constant; point 1 in figure 3.15. Initially the settling chamber pressure is zero, so that the mass flow rate through the nozzle is zero. As the air mass builds up in the settling chamber, the pressure and the mass flow rate through the nozzle increase. The settling chamber pressure will follow the nozzle characteristic curve until the mass flow rate into the settling chamber is blanced by that leaving.

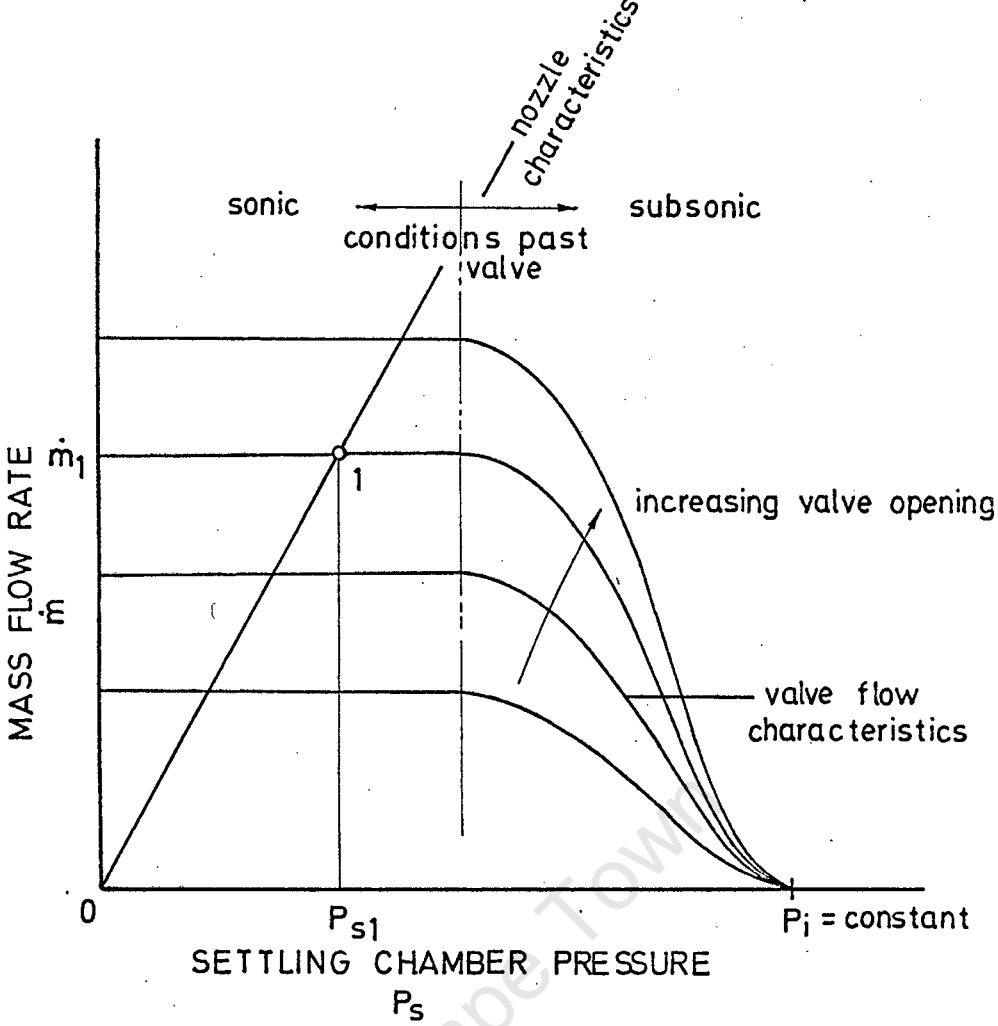

FLOW CHARACTERISTICS

Figure 3.15

The settling chamber block diagram in figure 3.16 indicates the dependency of the settling chamber pressure upon the valve displacement. The increase in mass M, (and hence pressure) in the settling chamber is equivalent to the difference in the mass flow rate into and out of the settling chamber. $(\dot{M}_1 - \dot{M}_2)$

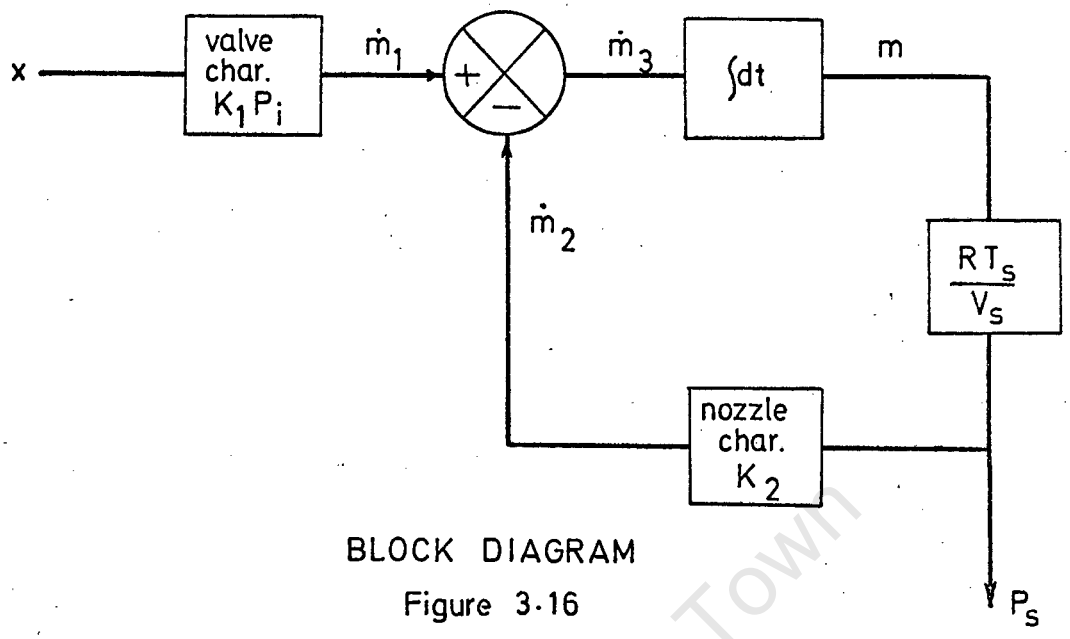

BLOCK DIAGRAM

Figure 3.16

For a constant storage drum pressure, P_i, and mass flow rates into and out of the settling chamber, $\dot{M}_1$ and $\dot{M}2$ respectively, the flow diagram may be simplified too:

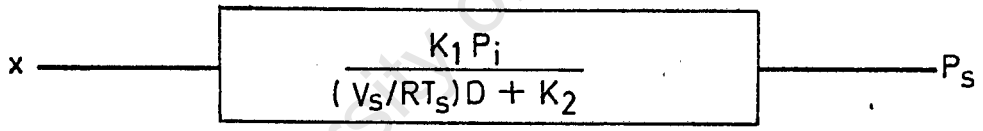

It is convenient to put D as the operator d"dt.

The transfer function is thus:-

$$\frac{P_s}{X} = \frac{K_1 P_i}{(V/RT)D + K_2}$$

Where X is the input disturbance and P_s is the response.

The differential equation is found by cross-multiplication:

$$\therefore \frac{V}{RT} \frac{dP_s}{dt} + K_2 P_s = K_1 P_i X \quad \ldots\ldots\ldots\ldots\ldots\ldots\ldots\ldots \quad 3.5$$

The following is the settling chamber pressure response to a step change in the valve displacement.

By inspection, the particular solution to this equation is found when dP_s/dt is zero.

$$\therefore \quad P_{s1} = \frac{K_1 P_i X}{K_2}$$

The complementary function is obtained when X is equal to zero in equation 3.5. Therefore this equation becomes the characteristic equation of the system being entirely independent of the forcing function.

$$\therefore \quad (D + \frac{K_2 RT}{V}) = 0$$

A solution of this equation is:

$$P_{s2} = Ae^{(-K_2 RT/V)t}$$

Where A is an arbitrary constant. The characteristic function, K_2RT/V, is always positive, so that P_{s2} decays to zero.

The full solution of the differential equation is found:

$$P_s = P_{s1} + P_{s2}$$

$$\therefore \quad P_s = \frac{K_1 P_i X}{K_2} + Ae^{(K_2 RT/V)t}$$

The constant A may be found from initial conditions, viz. $P_s = 0$ at $t = 0$.

$$\therefore \quad P_s = \frac{K_1 P_i}{K_2} \cdot X \cdot (1 - e^{-(K_2 RT/V)t}) \qquad \ldots\ldots\ldots\ldots\ldots\ldots \quad 3.6$$

For steady conditions, when the mass flow rate entering is the same as that leaving, the particular solution holds.

$$\text{i.e.} \quad P_s \longrightarrow \frac{K_1}{K_2} \text{ Pi } X \quad \text{as } t \longrightarrow o$$

(See figure 3.17).

It is interesting to note that the characteristic function, which determines the rate at which the pressure changes in the settling chamber, is only dependent upon the nozzle flow coefficient K_2 and the settling chamber capacity and is independent of the valve flow coefficient K_1 and the storage drum pressure.

It may be shown that for the wind-tunnel, with a Mach 2.35 nozzle, 98% of the total pressure change due to a step change in valve position, occurs in 1.05 secs.

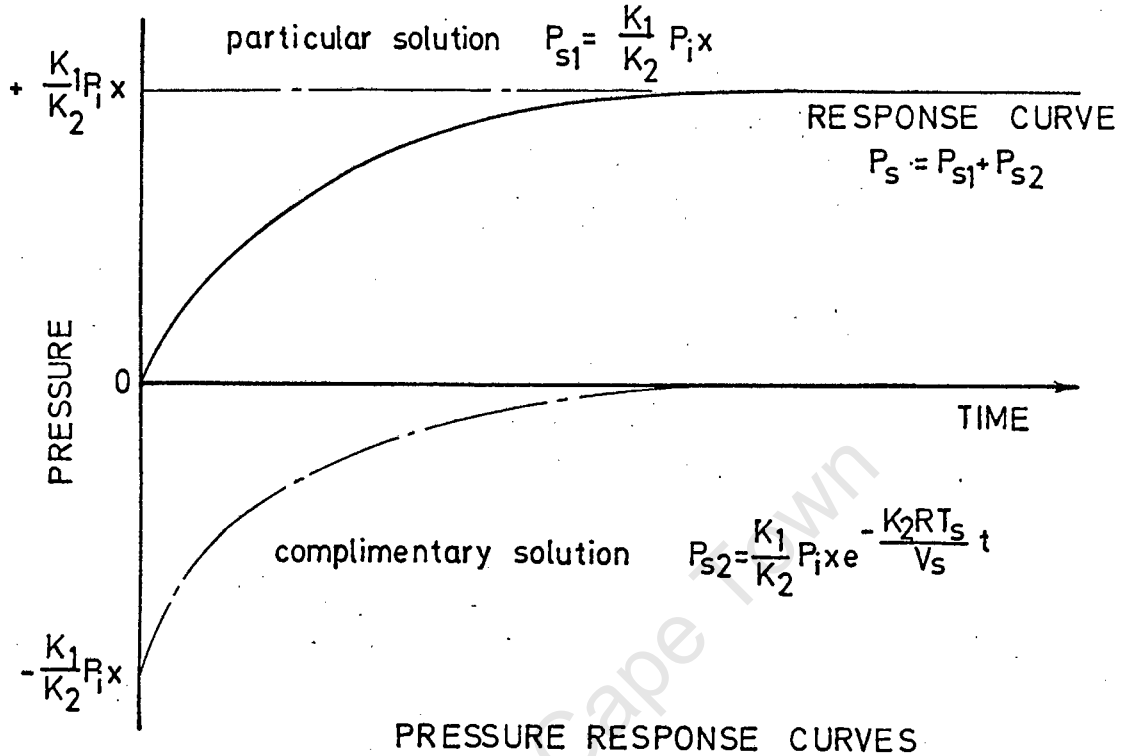

PRESSURE RESPONSE CURVES
for a step valve displacement

Figure 3.17

Storage Drum

This section of the system has only a secondary effect on the response of the valve. It will not effect the initial form of the response. Should any disturbance upset the equilibrium of the valve during a run, the response of the settling chamber pressure will correspond to that of a lower storage drum pressure Pd.

The mass flow rate through the valve $\dot{M}_1$, is a function of the valve opening and the actual storage drum pressure Pd. This actual pressure Pd is the difference between the initial storage pressure P_i and the pressure loss P_1 due to the reduction in mass in the drum. The block diagram is given in figure 3.18.

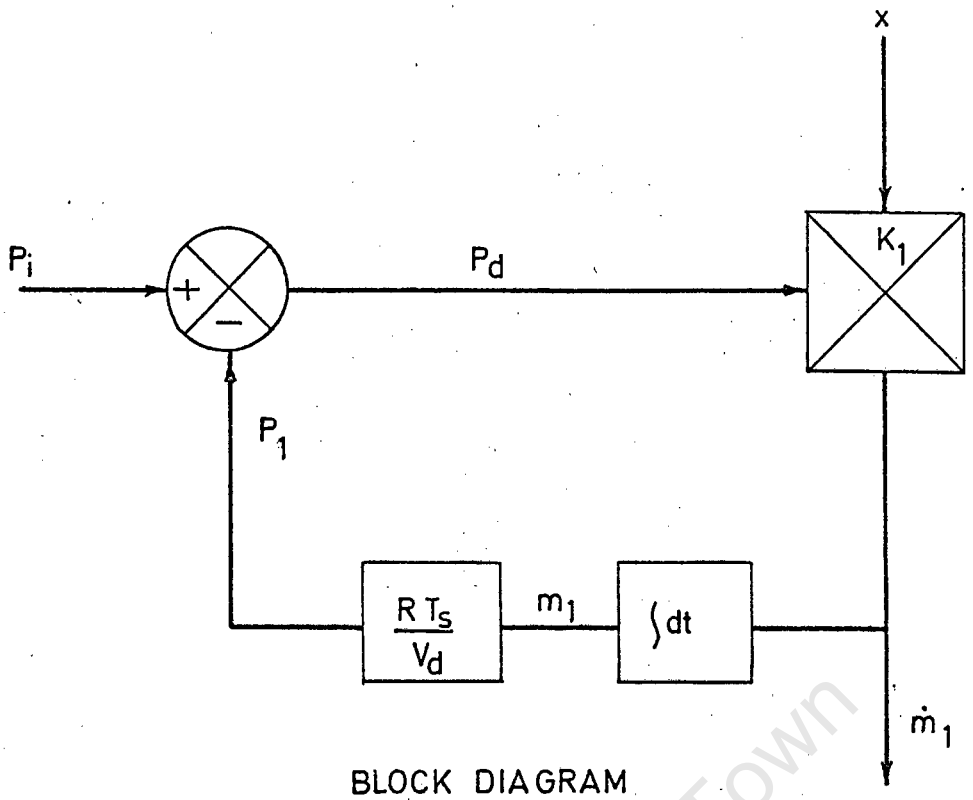

BLOCK DIAGRAM

Figure 3.18

The following transfer function may be deduced from the block diagram:

$$\frac{\dot{M}_1}{X} = K_1\left(P_i - \frac{RT}{V_d}\right)\frac{\dot{M}_1}{D} \qquad \text{3.7}$$

This function does not directly relate the displacement X to the mass flow rate $\dot{M}_1$ because of the appearance of the factor $\dot{M}_1$ on the right-hand side.

Consider the valve displacement for a constant mass flow rate.

$$\therefore \int \dot{M}_1 dt = \dot{M}_1 \int dt = \dot{M}_1 t \quad \text{if } \dot{M}_1 \text{ is constant.}$$

Therefore equation 3.7 may be rewritten as:-

$$\frac{1}{X} = \frac{K_1 P_i}{\dot{M}_1} - \frac{K_1 RT}{Vd}\, t$$

From initial conditions; $t = 0$, $\therefore X_i = \dfrac{\dot{M}_1}{K_1 P_i}$

$$\therefore \frac{1}{X} = \frac{1}{X_i} - \frac{K_1 RT}{Vd}\, t$$

This equation is shown in figure 3.19.

If the initial mass in the storage drum is M_i, then as $X \longrightarrow \infty$ the time taken may be shown to be:

$$t = \frac{V_d P_i}{RT} \quad \frac{1}{\dot{M}_1} = \frac{M_1}{\dot{M}_1}$$

If the valve can only open to three times its initial displacement; it will only be able to retain the constant mass flow rate for 67% of the available run time. How is available run time defined??

The Complete Block Diagram

These three main sections are now coupled together to form a complete model of the system.

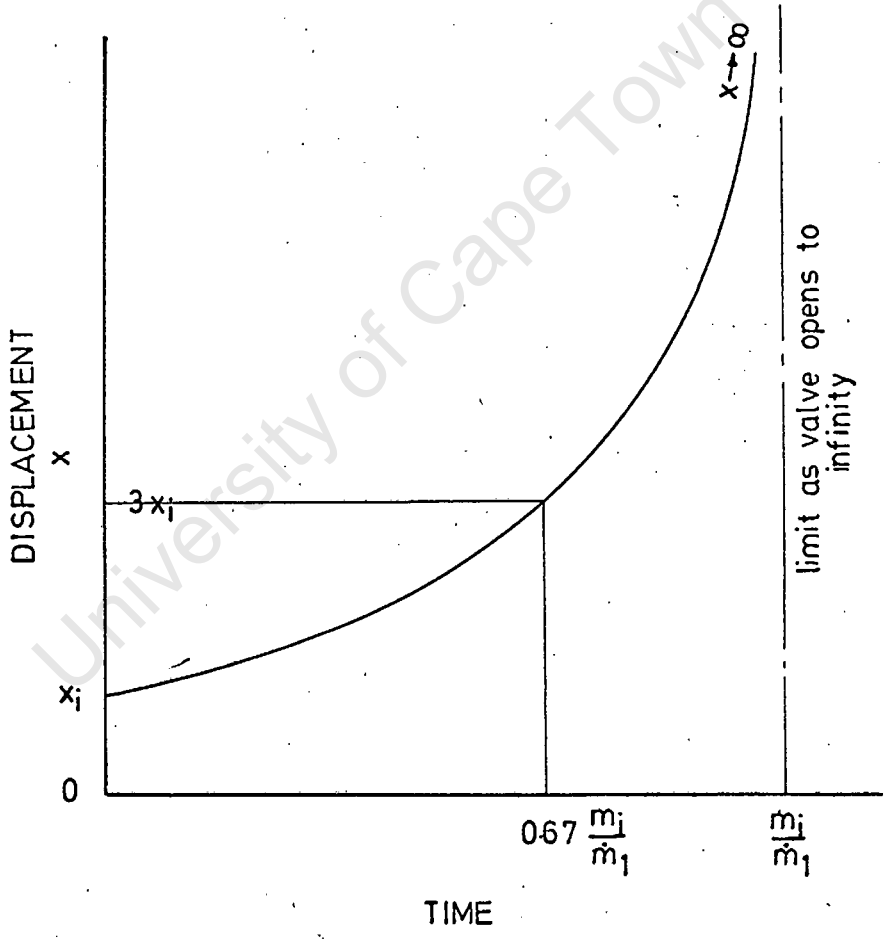

VALVE CONTROLLING RESPONSE??

Figure 3.19

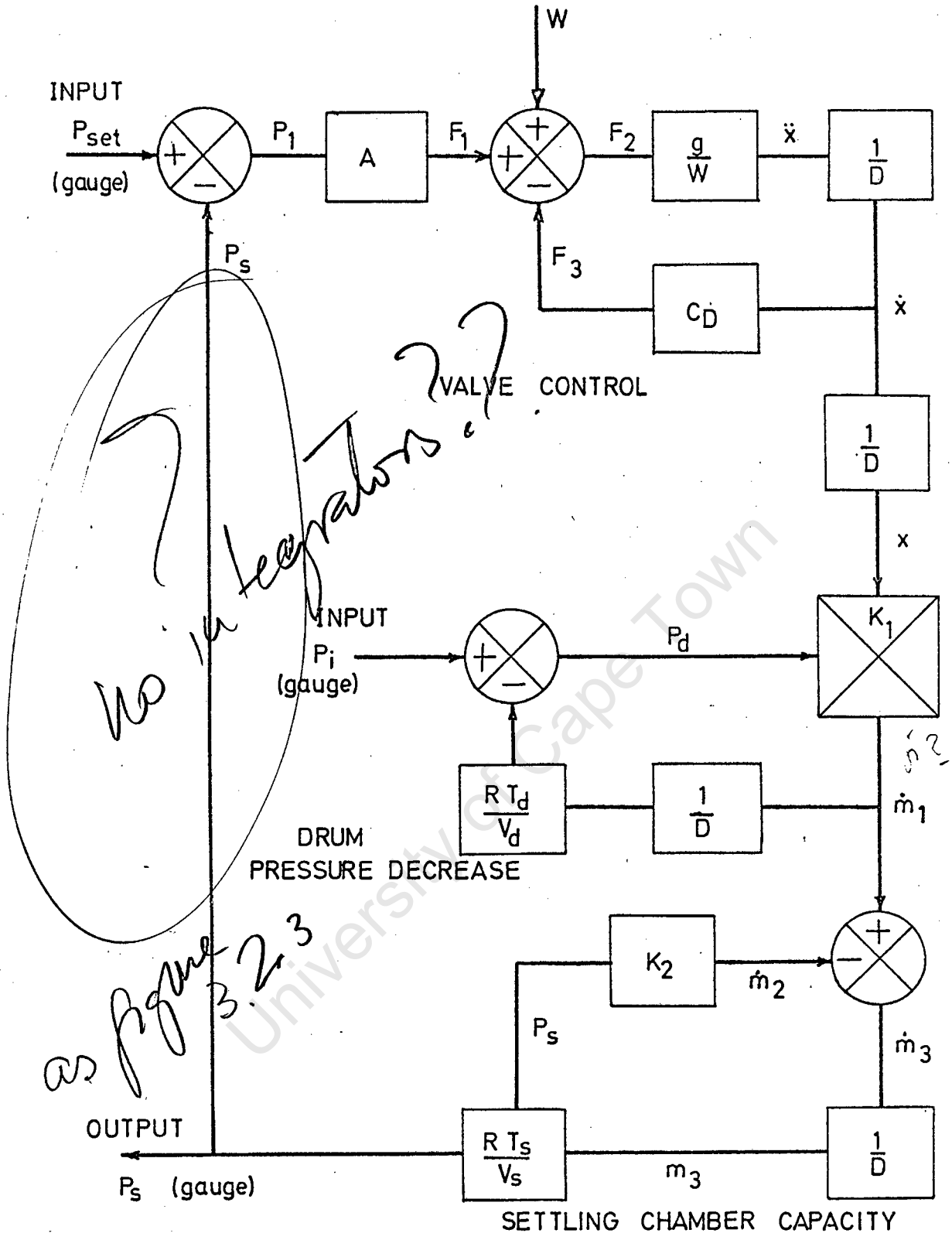

COMPLETE CONTROL BLOCK DIAGRAM

Figure 1·20

Steady conditions will only prevail when the settling chamber pressure is balanced by the set pressure and the equivalent weight of the valve.

PART 3
MATHEMATICAL ANALYSIS

3.1 REDUCTION OF BLOCK DIAGRAM

To determine the response of the control system formulated in figure 3.20, the flow diagram must be simplified and a transfer function deduced giving the settling chamber pressure in terms of 'set' pressure.

The transfer function for the storage drum (equation 3.7) is dependent on the output function $\dot{M}_1$. Fortunately the omission of the block diagram, that which controls the decrease in storage drum pressure, does not alter the initial response of the system and simplifies the differential equation that describes this response.

From figure 3.20

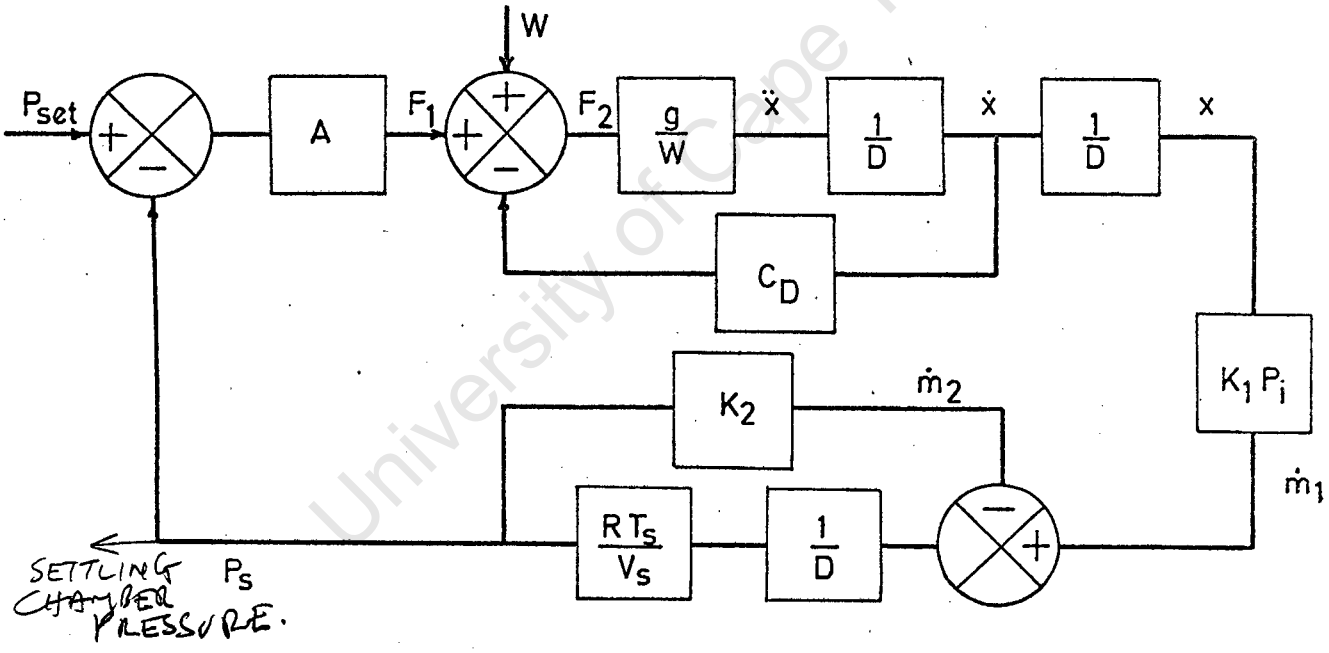

This diagram may then be reduced to that shown below.

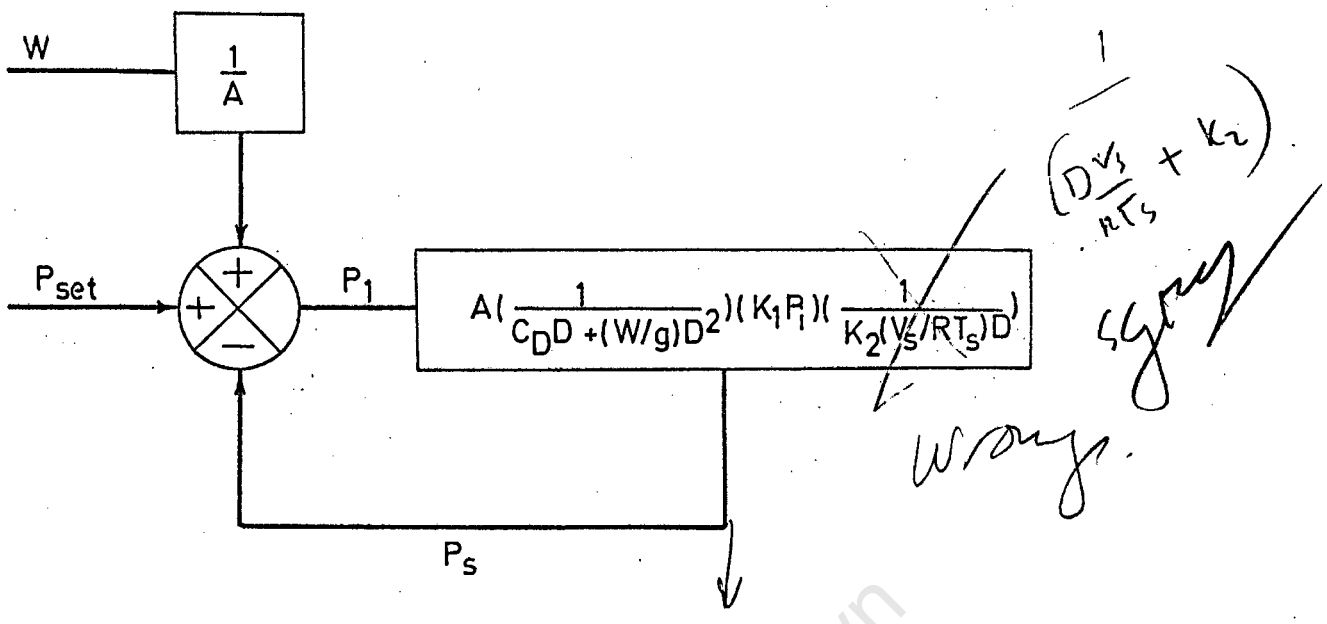

N.B. As W is a constant, it may be omitted as it will not influence the response of the system, but will merely define a new datum.

Let $A\left(\frac{1}{C_D D + (\frac{W}{g}) D^2}\right)(K_1 P_i)\left(\frac{1}{K_2(\frac{V_s}{RT})D}\right) = \phi$

Hence the final reduction yields:

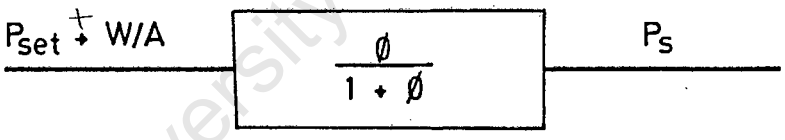

The transfer function may be written as:

$$\frac{P_s}{P_{set} + W/A} = \frac{\phi}{1+\phi} \qquad \text{.....3.9}$$

Note that the effect of the weight of the valve W/A, is not included in the transfer function, but must be included in the input disturbance (N.B. As before, it just changes the datum from which the response is measured).

3.2 SOLUTION OF THE CHARACTERISTIC EQUATION

Equation 3.9 must be put in a form that can be solved.

Rearranging the term gives:

$$\phi = \frac{A K_1 P_i}{(\frac{WV_s}{gRT})D^3 + (\frac{WK_2}{g} + \frac{C_D V_s}{RT})D^2 + (K_2 C_D).D}$$

Let $G_1 = \frac{WV_s}{gRT}$, $C_2 = (\quad + \frac{C_D V}{RT})$

$\quad K_2 C_D$, $C_4 = A$

The [illegible] function [illegible] written as:-

$$\frac{}{P_{set} + \frac{W}{A}} = \frac{}{G_1 D^3} \cdot \frac{C_4}{{}_3D + C_4} \quad \ldots\ldots\ldots\ldots\ldots\ldots \quad 3.10$$

Let $P_{sett} + W/A = P_t$

$$\therefore \quad G_1 P_3 D^3 + C_2 P_3 D^2 + C_3 P_s D + C_4 P_3 = C_4 P_{total} \quad \ldots\ldots\ldots\ldots \quad 3.11$$

The solution of this non-homogeneous linear differential equation is easily found by transforming it to an equivalent algebraic expression by application of the laplace transform. The manipulations necessary to find the solution then become algebraic. On completion, the resulting algebraic function may be transformed to yield a solution in the time domain. The initial conditions are included in the transform process thus eliminating the tedious problem of applying them to the general solution.

The laplace transform of equation 3.10 is given by the following equation if all the initial conditions are zero.

$$\frac{L(P_3)}{L(P_{total})} = \frac{C_4}{G_1 S^3 + C_2 S^2 + C_3 S + C_4}$$

The laplace transform of the sum of two functions is equal to the sum of the separate laplace transforms of the functions

$$\therefore \quad \frac{L(P_3)}{L(P_{total})} = \frac{A}{(1 + K_1 S)} + \frac{B}{(1 + K_2 S)} + \frac{C}{(1 + K_3 S)}$$

Where A, B and C are constants and $-1/K_1$, $-1/K_2$, and $-1/K_3$ are the roots of the third order equation;

$$G_1 S^3 + C_2 S^2 + C_3 S + C_4 = 0$$

If the set pressure undergoes a step change then:

$$L(P_{total}) = H/S \; ; \quad \text{when } P_{total} = H$$

$$\therefore \; L(P_s) = \frac{AH}{S(K_1S + 1)} + \frac{BH}{S(K_2S + 1)} + \frac{CH}{S(K_3S + 1)}$$

The form of solution of this equation is recognised in table 4.2 (9) for laplace transform pairs:

$$\therefore \; P_s = AH(1-e^{-t/K_1}) + BH(1-e^{-t/K_2}) + CH(1 - e^{-t/K_3}) \; \ldots\ldots\ldots \; 3.12$$

This equation can be split up into the particular solution, which is the steady condition of P_{total}, and the complimentary function which is time dependent. The values of the roots K_1, K_2 and K_3 give the form of response and determine the stability of the system.

$$\therefore \; P_s = \underbrace{(A + B + C)H}_{\substack{\text{particular} \\ \text{solution} \\ \theta_{01}}} - \underbrace{H(Ae^{-t/K_1} + Be^{-t/K_2} + Ce^{-t/K_3})}_{\substack{\text{Complementary} \\ \text{function} \\ \theta_{02}}}$$

This equation may be rewritten as:-

$$P_s = P_{total} + B_1e^{-t/K_1} + B_2e^{-t/K_2} + B_3e^{-t/K_3} \; \ldots\ldots\ldots\ldots \; 3.13$$

Where B_1, B_2, B_3 are constants that may be found from initial boundary conditions.

3.3 RESPONSE OF THE SYSTEM

The settling chamber pressure response characteristics may be found by substituting the supersonic wind-tunnel parameters into equation 3.13, and finding the boundary conditions. The degree of damping, the supersonic nozzle Mach number and the storage drum pressure have an influence on this response.

Becuase this theoretical approach is limited to linear damping and a constant storage drum pressure, it will only be used as a guide to the accuracy of the analogue computer.

Roots of the characteristic Equation:

The complimentary function is found from the roots of the characteristic equation:

$$C_1D^3 + C_2D^2 + C_3D + C_4 = 0$$

The mathematical solution to the roots of this cubic equation can be tedious. A satisfactory result was obtained using a small Olivetti desk-top computer. calculator

The programme is discussed and presented in appendix 3.3.

The solution to this above equation is found by eliminating the second term. The real root is determined by the method of tangents:-
The recurrance relation is given as:

$$\gamma_n = \gamma_{n-1} \quad \frac{F(\gamma_{n-1})}{F^1(\gamma_{n-1})}$$

Where γ_n and γ_{n-1} represent two successive approximations to the root and $F^1(\gamma)$ is the derivative of $F(\gamma)$. Once the real root has been found after a number of itterations, the programme calculates the other two roots from the quadratic equation.

The form of the three roots indicate the type of response:

1. Three negative real roots :- $(-r_1, -r_2, -r_3)$

   The system is overdamped. The response will approach the particular solution without any oscillations.

2. One root is negative, two are the same and negative.:- $(-r_1, -r_2, -r_2)$. This is critical damping; the response will approach the particular solution most quickly without any overshoot.

3. One root is negative, two are imaginary with a negative real part:- $(-r_1, -r_2 \pm r_3 i)$. The response is oscillatory about the particular solution, but eventually decays.

4. One root is negative, the real part of the imaginary roots is zero:- $(-r_1, 0 \pm r_3 i)$. The response is oscillatory about the particular solution wihout any decay.

5. One root is negative, the real part of the imaginary root is positive: $(-r_1, +r_2 \pm e_3 i)$. The response is unstable and the system will oscillate about the particular solution with increasing magnitude.

Critical Damping:-
The coefficient G is very small at heavy damping in relation to the other coefficients C_2, C_3 and C_4. Therefore the influence of the first term in the characteristic equation may be neglected for low values of D. (see figure A1 in appendix 3.3. $D \approx 2{,}605$ near critical damping).

Therefore the characteristic equation may be rewritten, only for heavy damping and low values of D, as:-

$$C_2 D^2 + C_3 D + C_4 = 0$$

Therefore the characteristic equation may be rewritten, only for heavy damping and low values of D, as:-

$$C_2D^2 + C_3D + C_4 = 0$$ repeat of previous page

Critical damping occurs when the two roots of this equation are the same. (See point 2 above). For the roots to be the same, the following relation must be satisfied:

$$C_3^2 = 4C_2C_4$$

Substituting in the values of these constants:-

$$\therefore \quad C_{Dcr}^2 - \left(\frac{4V_s A K_1 P_i}{RT_s K_2^2}\right) C_{Dcr} - \left(\frac{4WK_1 AP_i}{gK_2}\right) = 0$$

Substituting in the specifications of the wind-tunnel given in appendix 3.2, the two possible solutions for critical damping may be found:

$$C_{Dcr.1} = -2.995 \ \frac{lbs}{ft} \ sec$$

impossible

$$C_{Dcr.2} = 101,275 \ \frac{lbs}{ft} \ sec$$

The second solution gives the critical damping for the system.

RESPONSE CURVES

Example 1:

For a damping coefficient, $C_D = 100,000 \ \frac{lb}{ft}$ sec, the roots of the characteristic equation are found to be:

$$-173,995 \ , \ -2,605 \pm 0,0$$

Applying boundary conditions (see appendix 3,4) and substituting into equation 3.13 gives:

$$P_s = P_{total} - P_{total} \ e^{-2,605t} \qquad \ldots\ldots\ldots\ldots\ldots\ldots\ldots \qquad 3.14$$

Example 2:

For damping coefficient, $C_D = 10,000 \ \frac{lb}{ft}$ sec, the roots of the characteristic equation are found to be:

$$-17,405, \ -2,605 \pm 7,87i$$

Applying the boundary conditions again (see appendix 3,4), the following

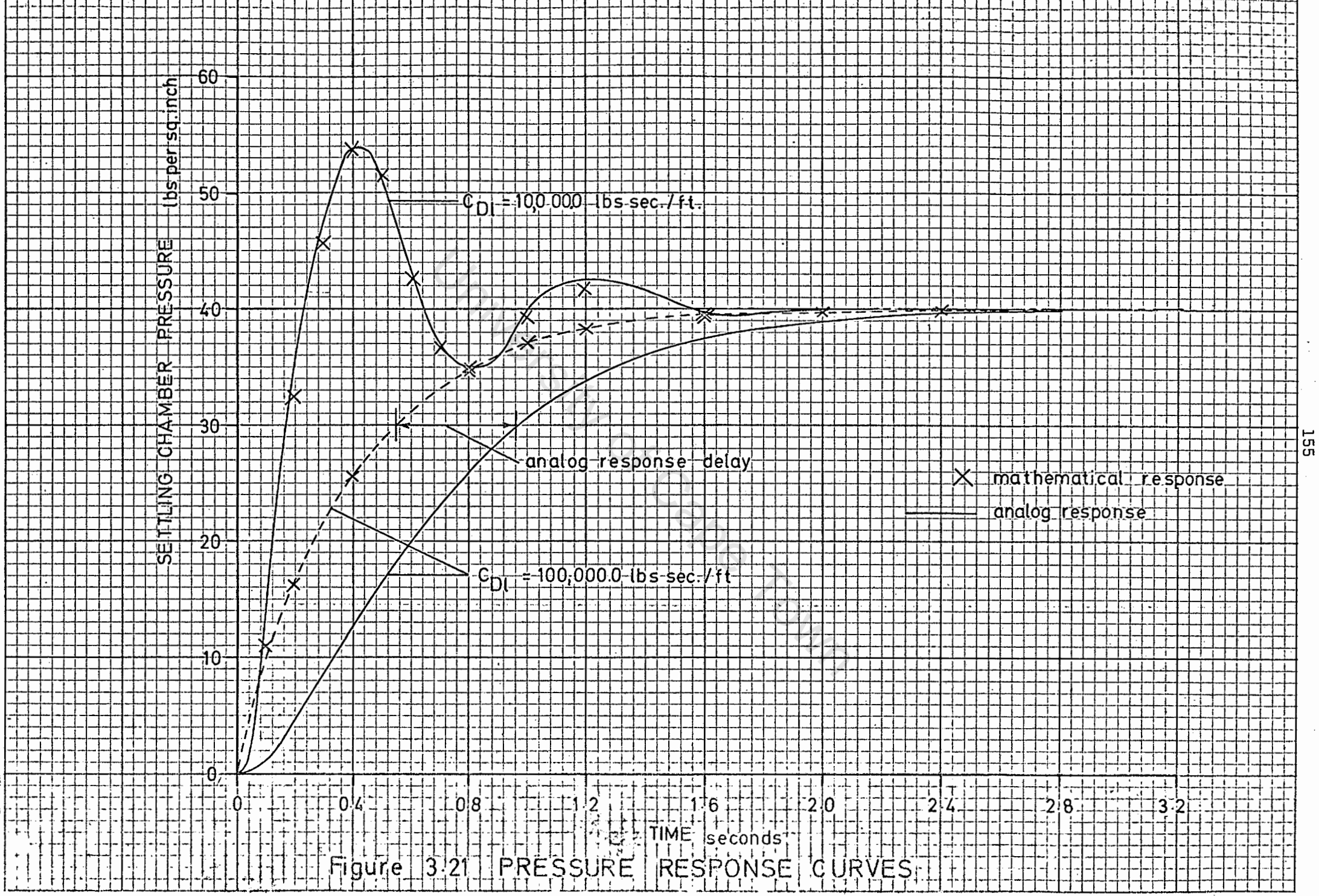

Figure 3·21 PRESSURE RESPONSE CURVES

solution results:

$$P_s = P_{total} - \frac{P_{total}}{0,9494} e^{-2,605t} \sin (7,87t + 71^{o}41') \quad \ldots\ldots\ldots \quad 3.15$$

Similarly, for a step function of P_{total} dqual to 40 lbs per sq.inch, the response curve is presented in figure 3,21 together with its analogue counterpart.

The second example follows the analogue solution perfectly. Unfortunately at the heavier damping, the solutions differed slightly. There was a 10% lag in the response of the analogue simulation. This may be explained by the overloading of the computer amplifiers when a large gain is necessary to simulate heavy damping. (i.e. For large gains, the result is unreliable (10)).

A summary of the roots of the characteristic equation, in terms of the linear damping coefficient, is presented in figure 3,22 for the following changes:

1. Increasing Mach number:
   The frequency of oscillation remains the same (given by the imaginary root), but the rate at which the settling chamber pressure approaches steady state conditions is decreased for the higher Mach nozzle (given by the real root).

2. Decreasing storage drum pressure:
   The rate of decay is the same for any storage drum pressure but the frequency of the oscillation of the response is reduced for a lower drum pressure.

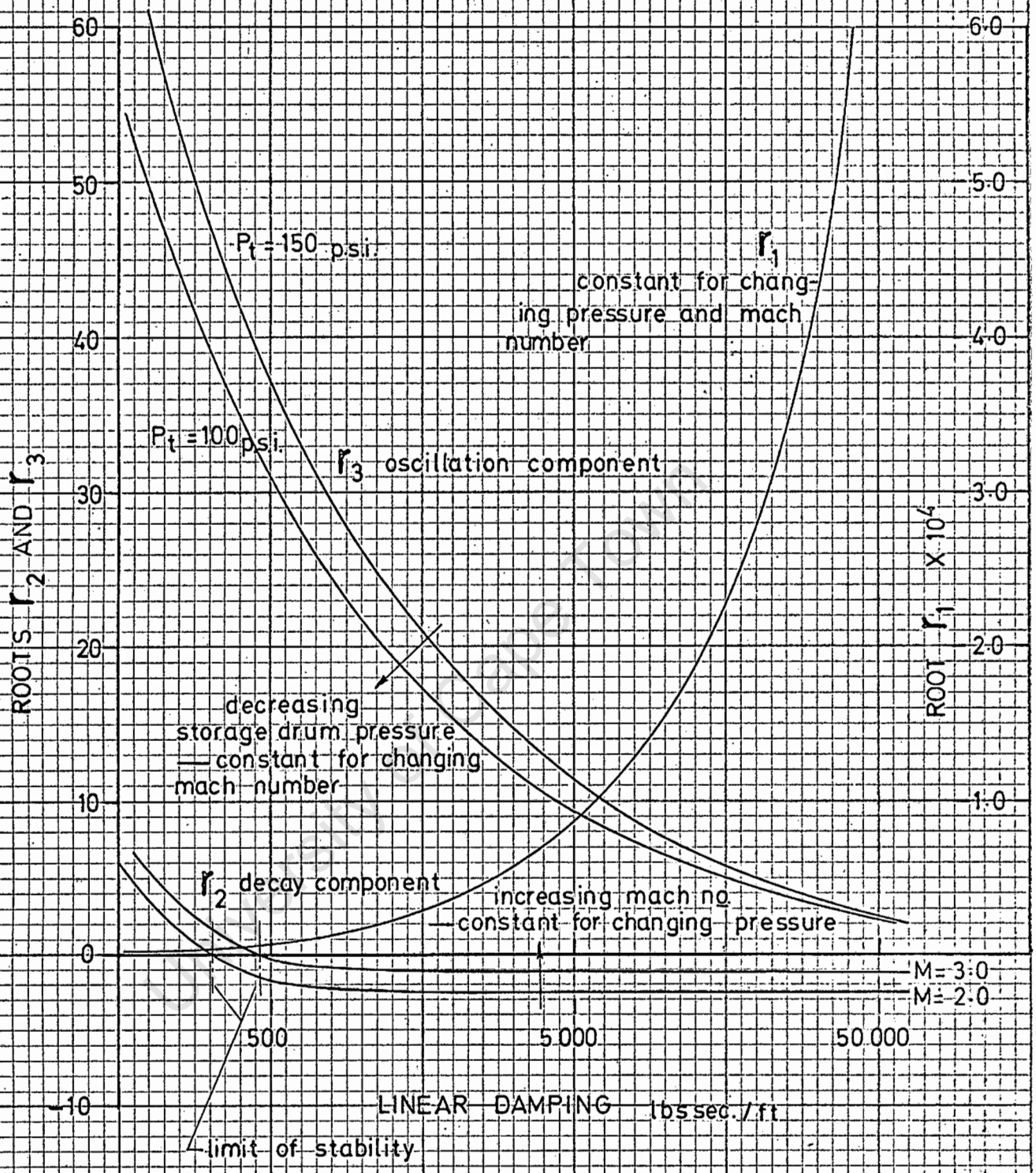

r_1, $r_2 \pm r_3 . i$

ROOTS OF THE CHARACTERISTIC EQUATION

Figure 3·22

PART 4

ANALOG SIMULATION

4.1 INTRODUCTION

Simulation of a control system by an analogue computer may be satisfactorily undertaken if the following points are borne in mind:

1. The variables are governed by the voltage; the limit is set at $\pm$ 10 volts.
2. The plotter is limited by mechanical movement. Time scaling may be necessary to reduce the response rate.
3. Inaccuracies are present when low voltages are used. Hence the maximum voltage should be applied throughout the system. This is achieved by magnitude scaling.
4. The amplifiers in the circuit can become overloaded if the gain is too large.

The advantage in determining the system response by analogue simulation is two-fold; it offers an accurate and quick solution to the complete mathematical model of the system and can handle complex non-linear functions.

4.2 MAGNITUDE SCALING

All the dependent variables, within the computer, are represented by voltages within a certain fixed range. A magnitude scale factor is a constant of proportionality relating the voltage on the computer to the value of the corresponding variable. This scale factor must be chosen so that the voltage representing the maximum possible value of the problem variable will be less than the maximum voltage of the computer.

i.e. $a_x |X|_{max} \leqslant 10$

where a is the magnitude scale factor and $|X|_{max}$ is the modulus of the maximum value of the variable.

The scale factors chosen for all the variables are given in appendix 3.5

The most satisfactory method of magnitude scaling, is to divide the system into a number of summing junctions. The block diagram, shown in figure 3.20, may be rearranged as follows:

1. Valve

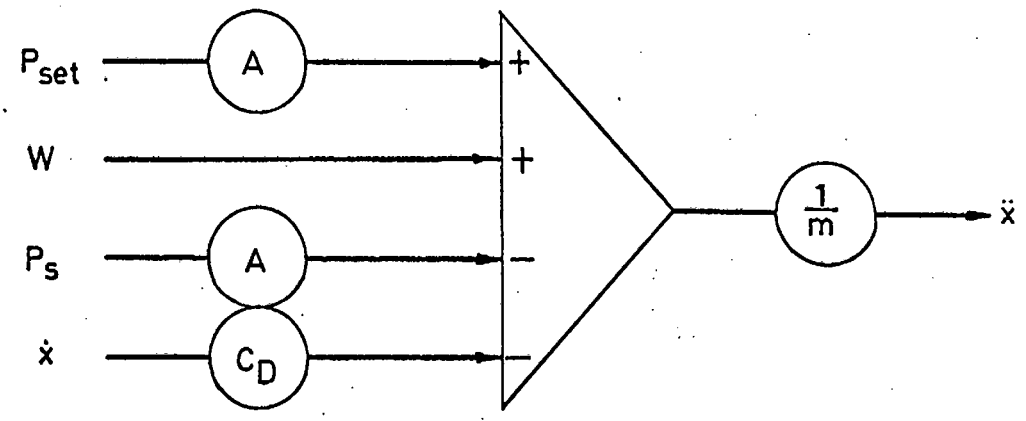

For linear damping, the equilibrium equation may be written as:

$$M\ddot{X} = A.P_{set} + W - A.P_s - C_{Dl}.\dot{X}$$

Magnitude scaling requires that each variable must be multiplied by the magnitude scale factor, a. Magnitude scaling:

$$\frac{M}{0,008}(0,008\ddot{X}) = \frac{A}{0,1}(0,1\ P_{set}) + W - \frac{A}{0,08}(0,08\ P_s)$$

$$- \frac{C_{Dl}}{2.83}(2,83\ \dot{X})$$

$$\therefore\ (0,008\ \ddot{X}) = 1,75\ (0,1\ P_{set}) + 0,258 - 2,19\ (0,08\ P_s)$$

$$-0,492 \times 10^{-2}\ C_{Dl}\ (2,83\dot{X}) \qquad \ldots\ldots\ldots\ldots\ldots \quad 3.16$$

Similarly, for non-linear damping, the equation of equilibrium may be written as:

$$M\ddot{X} = A.P_{set} + W - A.P_s - C_{Dnl}\ (\dot{X})^2$$

Taking into account the fact that the multiplier divides the product of two values by 10 so that the maximum computer voltage is not exceeded:

$$\therefore\ (0,008\ \ddot{X}) = 1,75\ (0,1\ P_{set}) + 0,058 - 2,19\ (0,08\ P_s)$$

$$-1,74 \times 10^{-2}\ C_{Dnl}\ (\ 2,83\ \dot{X}^2) \qquad \ldots\ldots\ldots\ldots \quad 3.17$$

2. Settling Chamber

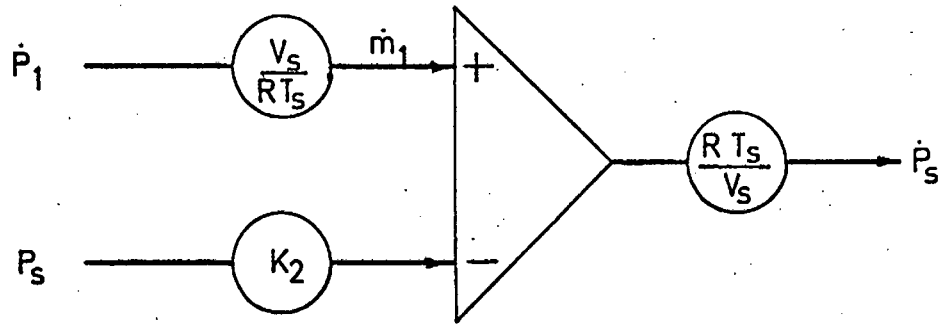

The equation of equilibrium may be written as:

$$\left(\frac{V_s}{RT_s}\right)\dot{P}_s = \left(\frac{V_s}{RT_s}\right)\dot{P}_1 - K_2 P_s$$

Magnitude scaling and simplifying for a nozzle of Mach number equal to 2,0:

$$(0{,}008\ \dot{P}_s) = 10(0{,}0008\ \dot{P}_1) - 0{,}52106\ (0{,}08\ P_s) \quad \ldots\ldots\ldots\ldots \quad 3.18$$

3. Storage Drum Pressure

The addition of this sub-system requires that the two variables of drum pressure and valve displacement be multiplied together.

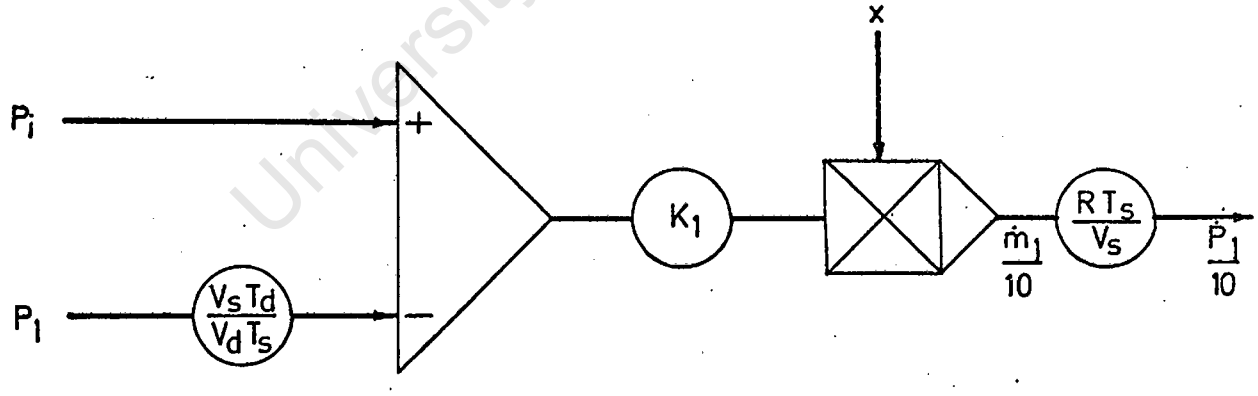

The equation of equilibrium for this summing junction may be written as:

$$\left(\frac{V_s}{RT_s}\right)\frac{\dot{P}_1}{10} = X\left[K_1 P_i - \frac{K_1 V_s T_d}{V_d T_s} P_1\right]$$

Magnitude scaling as before and simplifying gives:

$$(0{,}0008\ \dot{P}_1) = (283X)\ \ 1{,}55 - 0{,}298\ (0{,}0008\ P_1) \quad \ldots\ldots\ldots\ldots \quad 3.19$$

where the initial storage drum pressure is taken as 165 lbs per sq. inch absolute.

4.3 TIME SCALING

The time scale factor relates time in the computer system to time in the actual system.

The mechanical plotter is limited to a maximum speed of one cycle per second for the limit of its travel. Therefore, using the theoretical solution as a guide, the computer system must be slowed down.

If computer time is represented as τ and real time as t:

The time scale factor $n = \frac{\tau}{t}$

The easiest way to time scale the computer system is to multiply the gains of all the integrators by a factor of 1/10. This corresponds to a time scale factor of 10.

4.4 SYSTEM RESPONSE BY ANALOGUE SIMULATION

Applying time and magnitude scaling to figure 3.20 and substituting in the wind-tunnel parameters, gives the analogue computer circuit diagram in figure 3.23.

The constant potentiometer settings are given in the figure. The gains at the amplifiers are indicated at the terminal inputs.

The variable potentiometers may be adjusted to suit the following requirements:

1. The set control pressure:
   P01 is set to 0,175. ($0.1\ P_{set}$)
2. Non-linear and linear damping:
   P02 is set to:
   $1{,}74 \times 10^{-3}\ C_{Dnl}$ fpr non-linear damping.
   $0{,}492 \times 10^{-3}\ C_{Dl}$ for linear damping.
   These figures must be less than one for any particular value of damping. Should they be greater, the gains of amplifiers A1 or A2 are increased.
3. Nozzle Mach number:
   P03 is adjustable for different Mach numbers. The table below gives the settings.

Mach Number	P03 setting
2,0	0,522
2,35	0,384
2,5	0,334
3,0	0,207

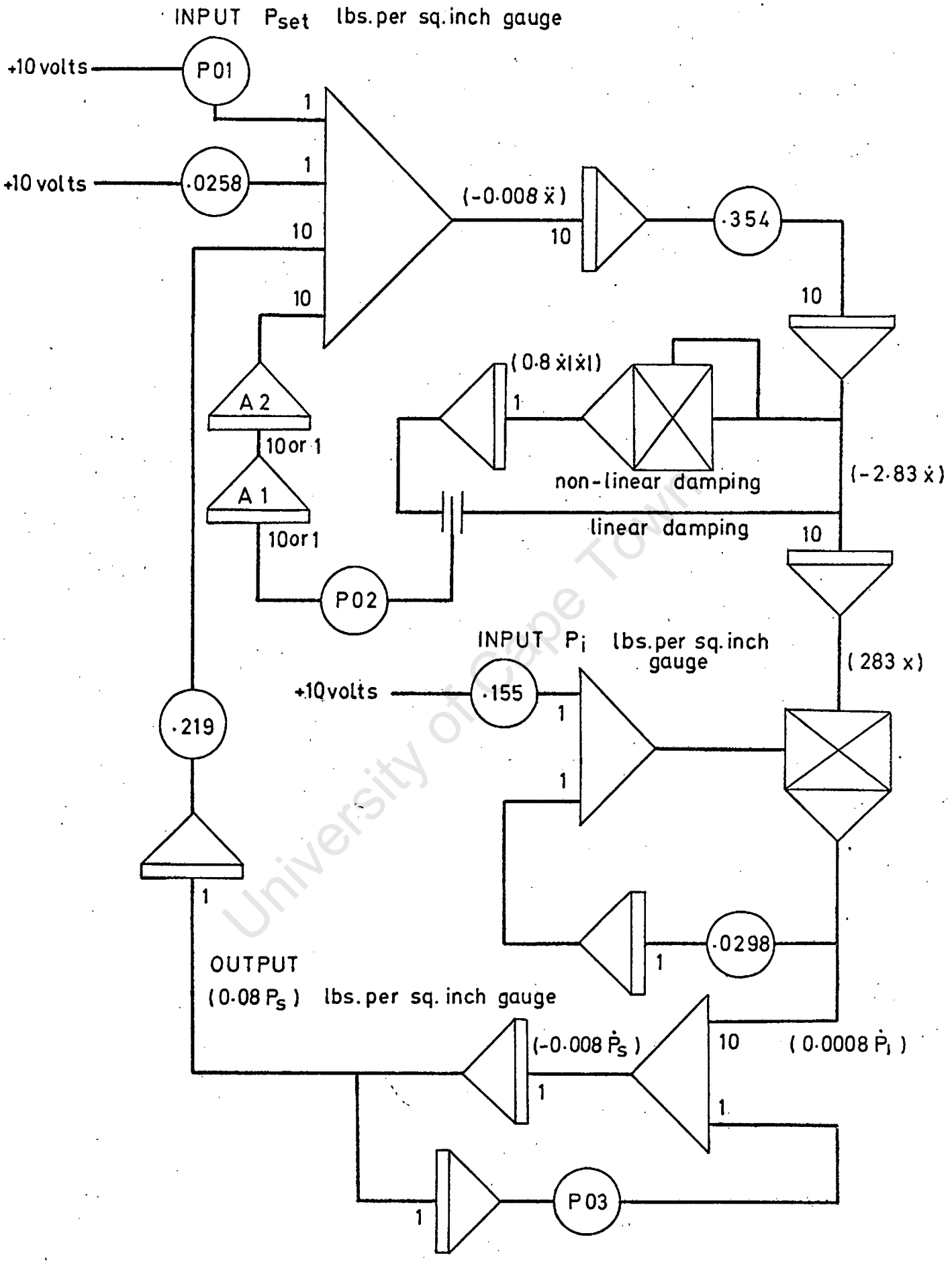

ANALOG SIMULATION FLOW DIAGRAM

Figure 3·23

Response Curves

The predicted response of the settling chamber pressure, by analogue computer, is discussed below. Figures 3,24 to 3,28 present examples of the settling chamber pressure response curves for different set conditions. The valve response is also included in figures 3.24, 3.27 and 3.28. As only one plotter pen is available, the pressure and displacement curves are plotted by taking two consecutive 'runs'.

Figure 3.24 gives the pressure and displacement response curves for a slightly underdamped non-linear system. The damping corresponds to a damping cylinder bypass orifice number of between 4 and 5. The settling chamber pressure oscillates a small number of times before steadying at a short distance above the original set pressure. This difference is due to the valve weight.

The relationship between linear and non-linear damping is illustrated in figures 3,25 and 3.26. With linear damping, the system always reaches the particular solution where the pressure fluctuation ceases (except where the oscillations increase or retain their original amplitude at low damping). With non-linear damping the amplitude of oscillations decreases to a point where hunting occurs. Hunting defines the state whereby the response will oscillate within a limited range without any change in amplitude. The amplitude of this hunting oscillation depends upon the degree of damping and may decrease to zero if the damping is high enough.

If the damping is too high, a sluggish response of the valve will result. Figure 2.27 illustrates how the settling chamber pressure may be caused to deviate from the particular solution if excessive damping prevents the valve from opening quickly enough. At the other extreme, insufficient damping results in oscillations in the settling chamber pressure. (See figure 2.28).

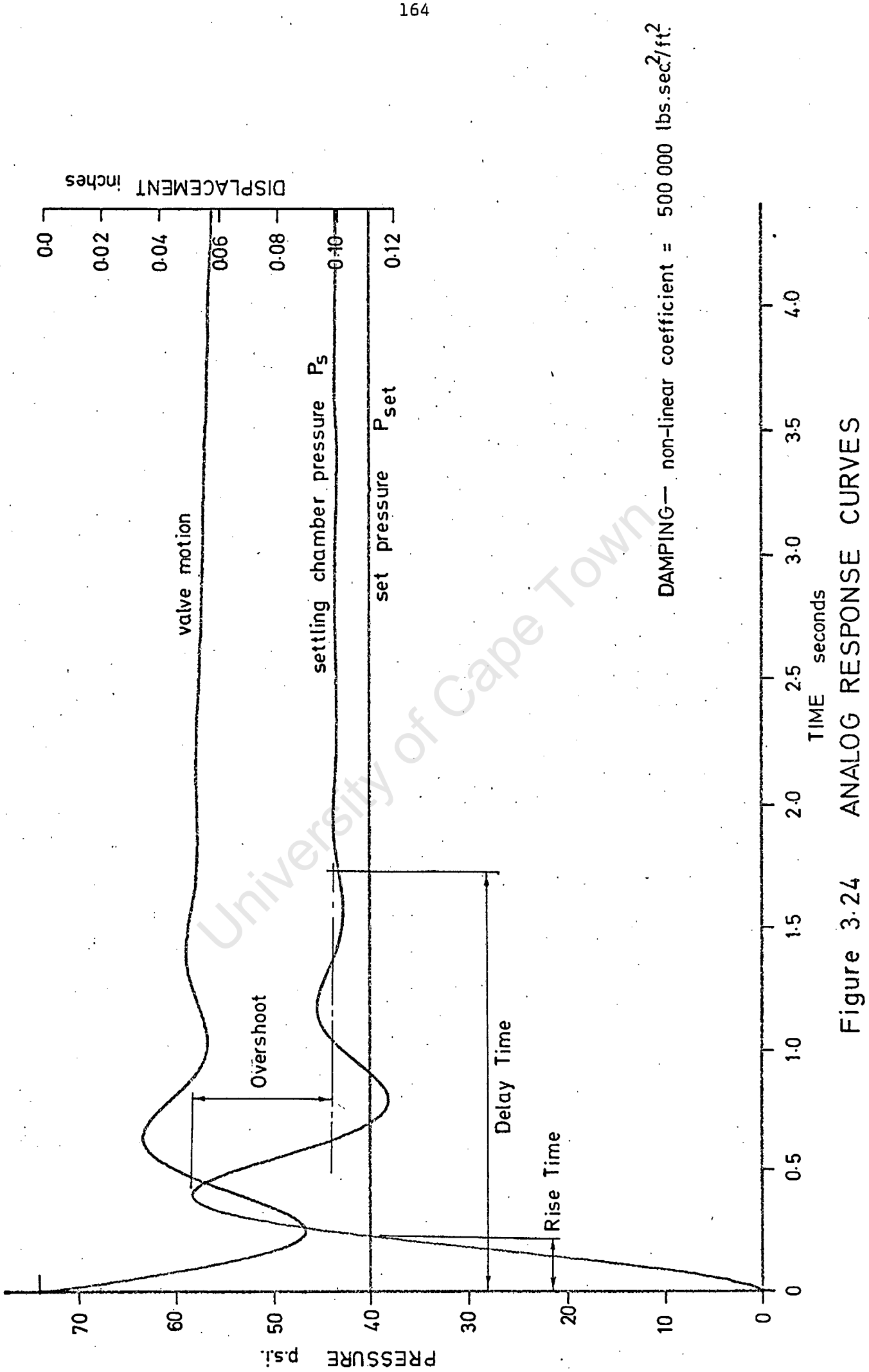

Figure 3.24 ANALOG RESPONSE CURVES

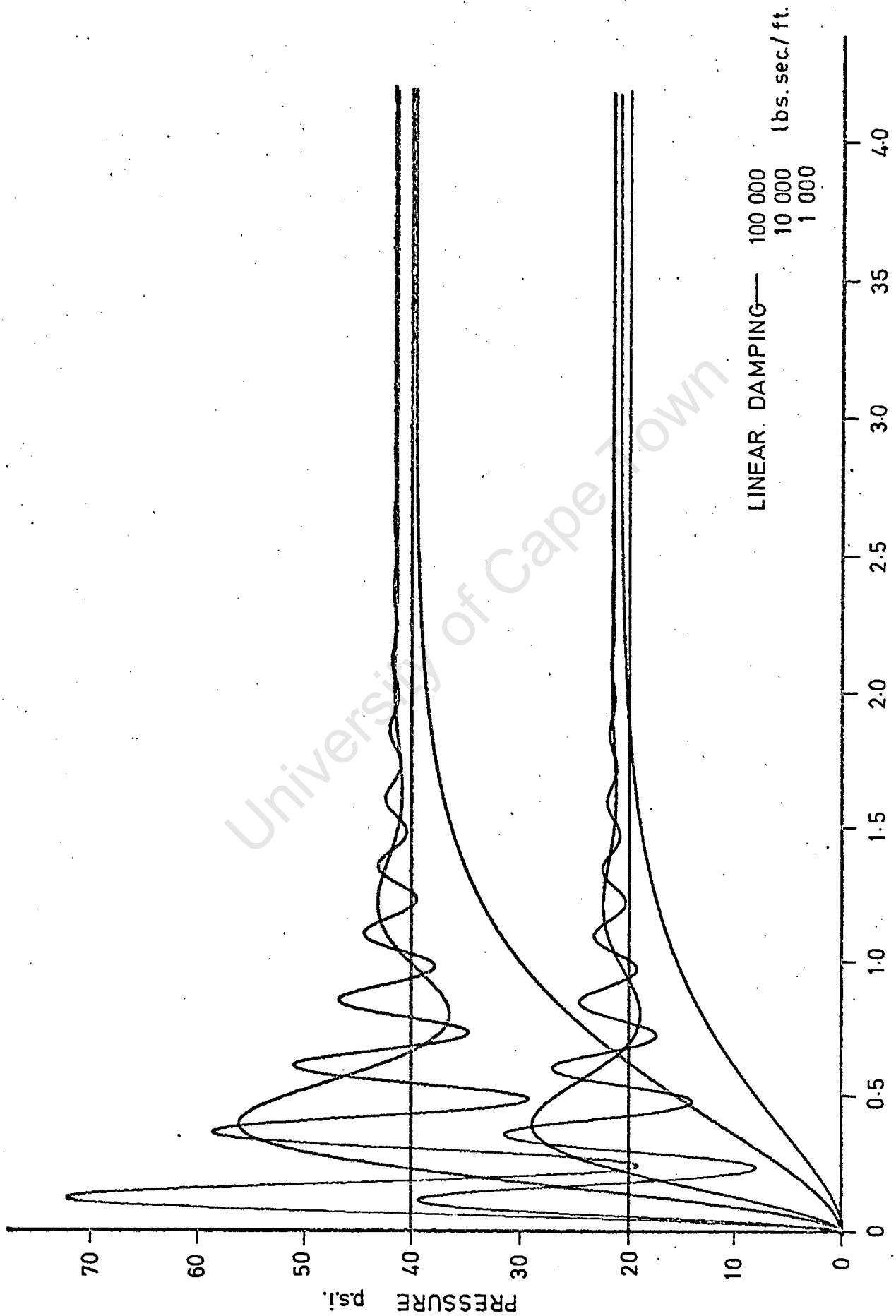

Figure 3·25 ANALOG RESPONSE CURVES

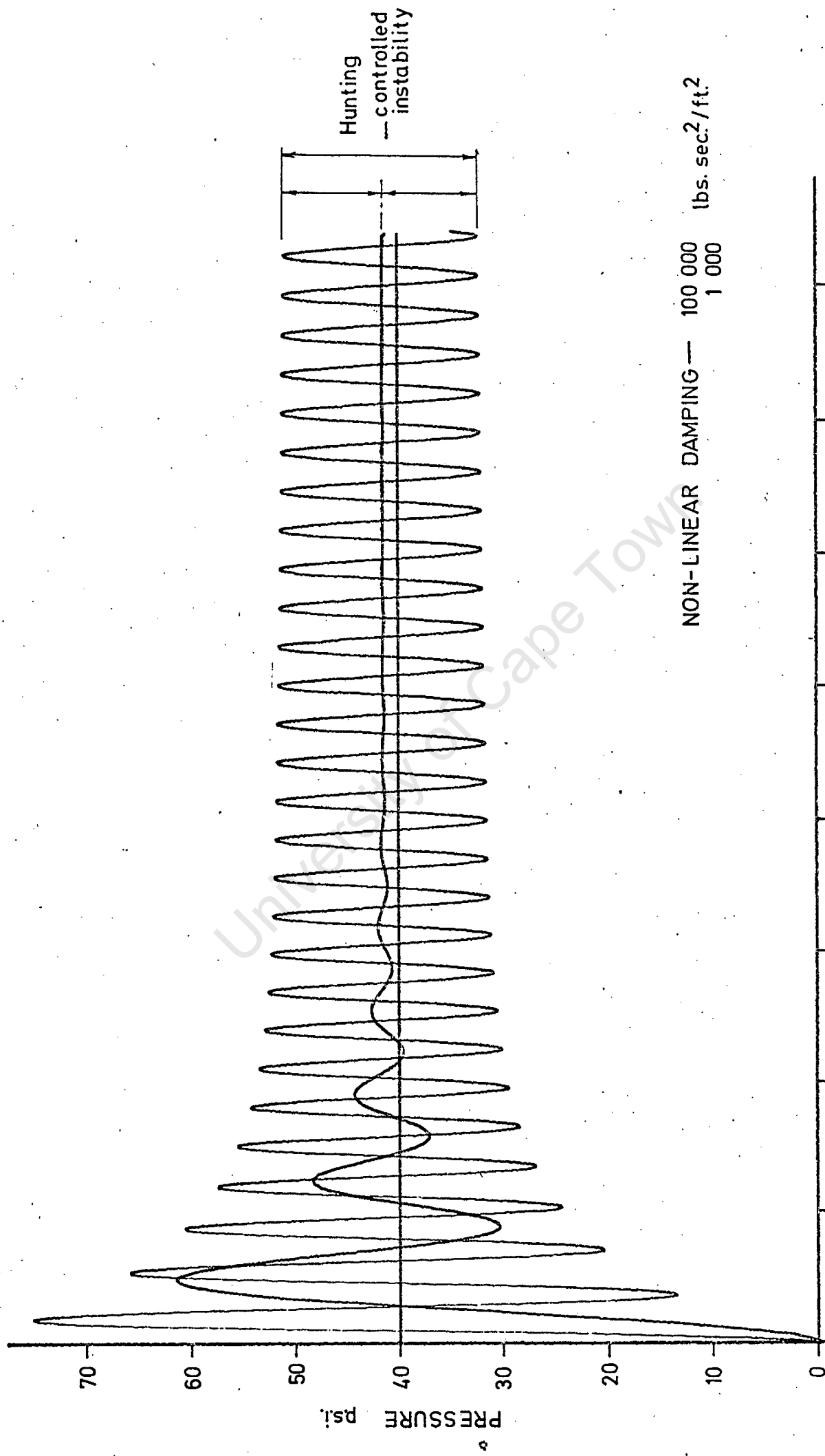

Figure 3.26 ANALOG RESPONSE CURVES

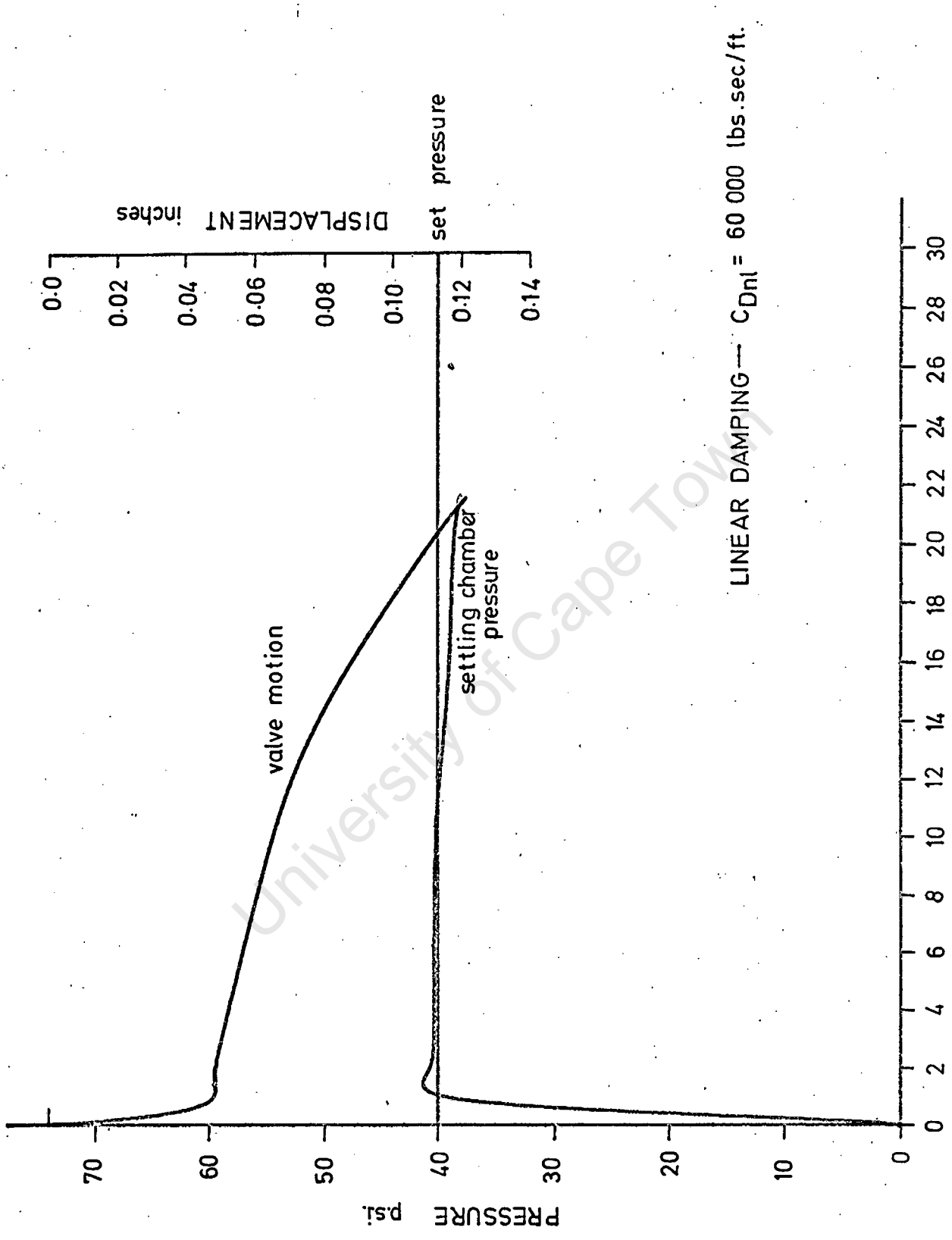

Figure 3.27 ANALOG RESPONSE CURVES

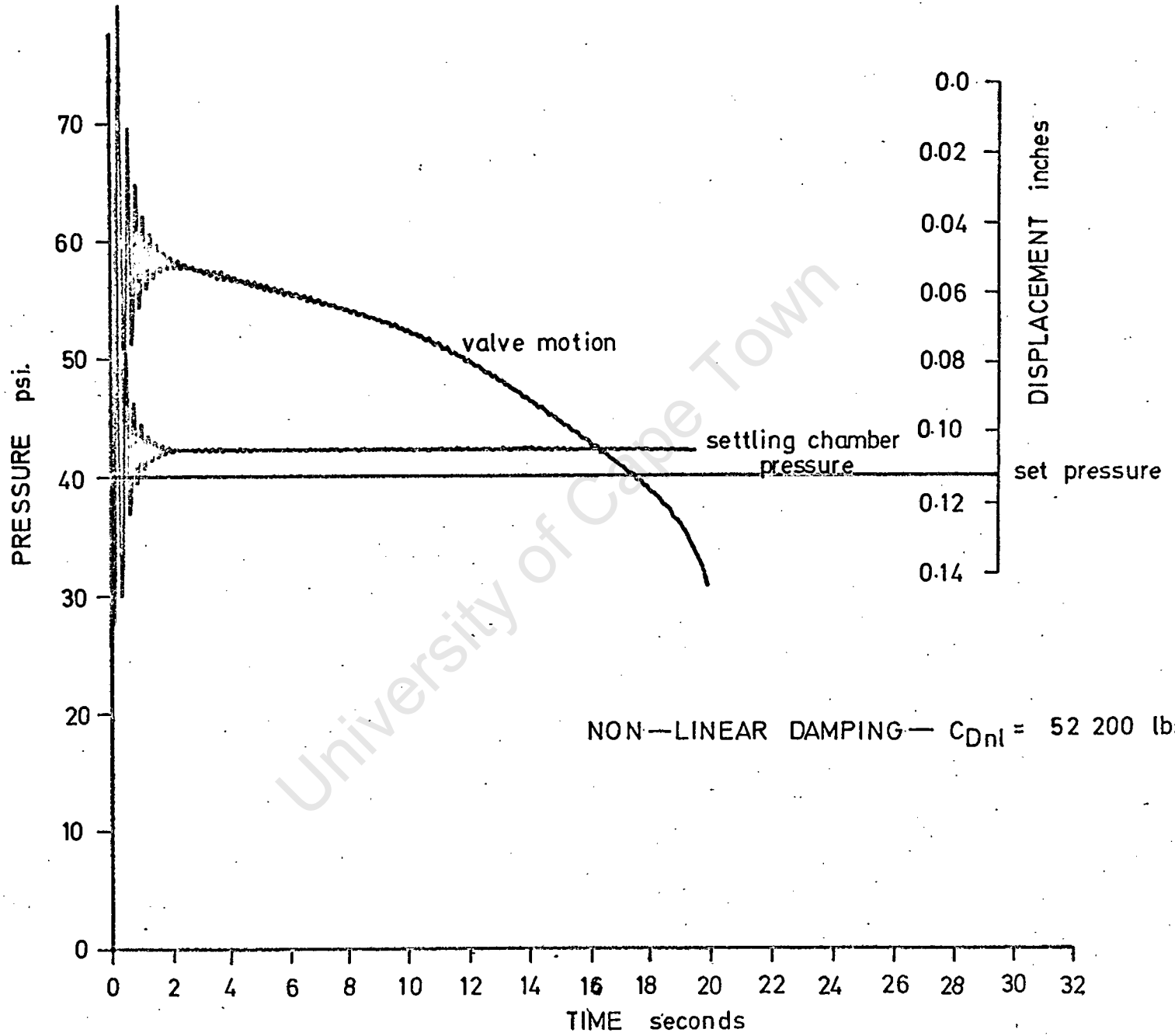

Figure 3·28 ANALOG RESPONSE CURVES

PART 5
EXPERIMENTAL ANALYSIS

5.1 VALVE TESTING PROCEDURE

The apparatus used to test the valve performance, is shown in figure 3.29.

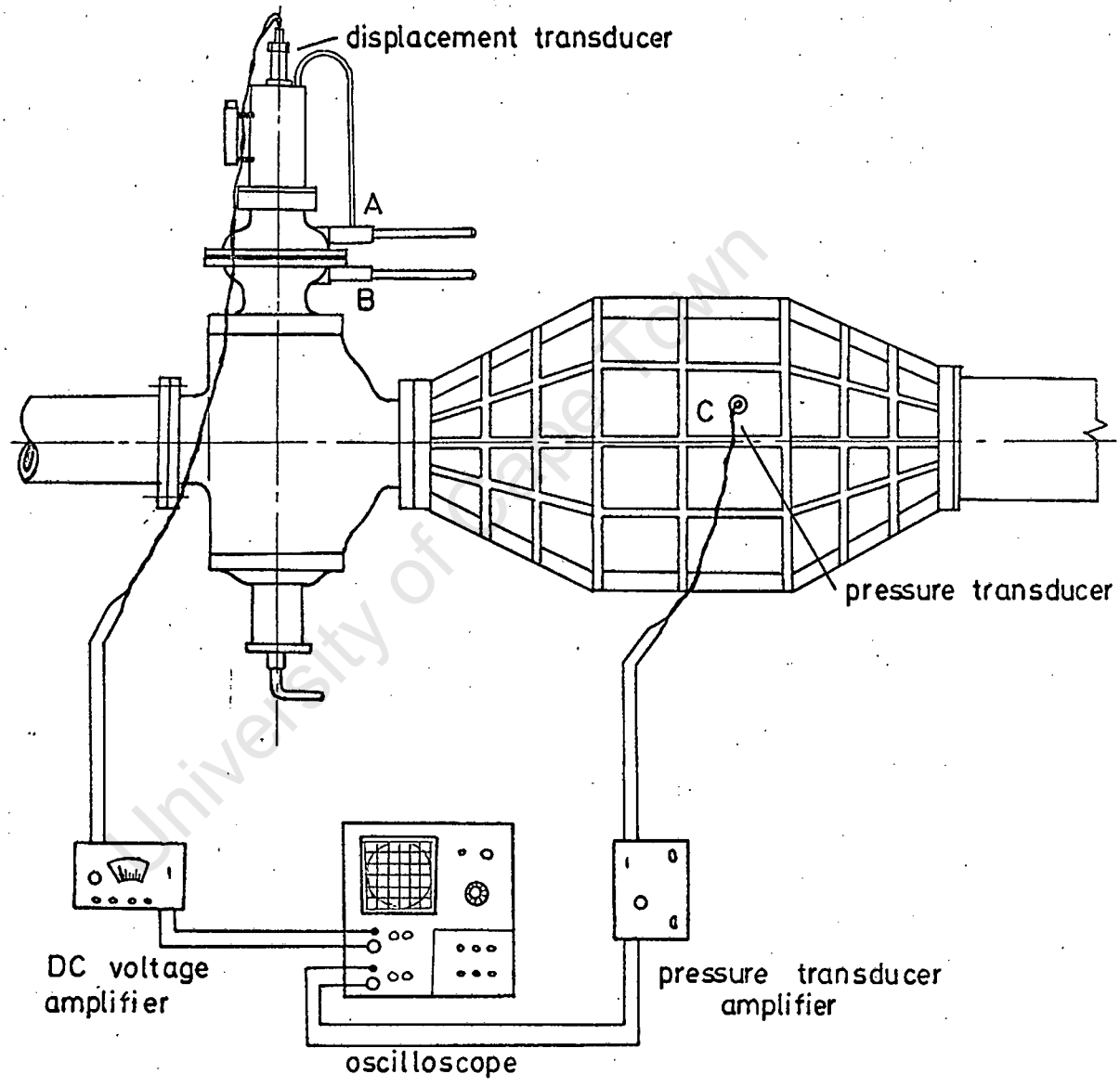

TESTING APPARATUS ARRANGEMENT

Figure 3.29

The valve displacement and settling chamber pressure were recorded by a storage oscilloscope. The automatic trigger was set to start these recordings on the negative slope of the displacement curve.

To test the valve performance under all possible conditions, the same procedure was applied as in the analogue simulation:

1. The damping was varied for a fixed set pressure and nozzle.
2. The set pressure was varied for a fixed damping and nozzle.
3. The nozzle Mach number was increased and the above two points were

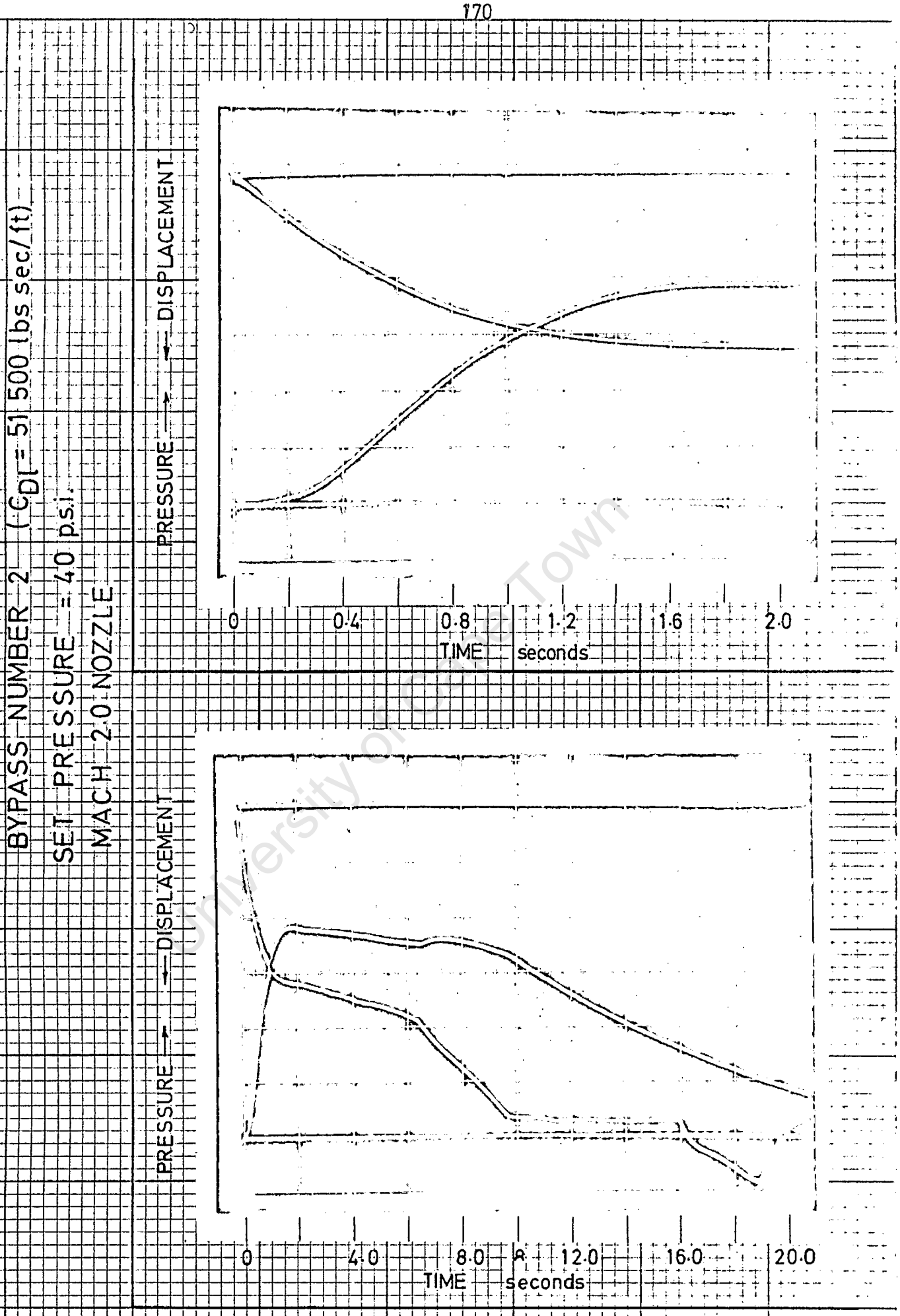

ACTUAL RESPONSE TRACES

Figure 3·30

BYPASS NUMBER 4 (C_{Dnl} = 928·200 lbs-sec^2/ft^2)

SET PRESSURE = 40 p.s.i.

MACH 2·0 NOZZLE

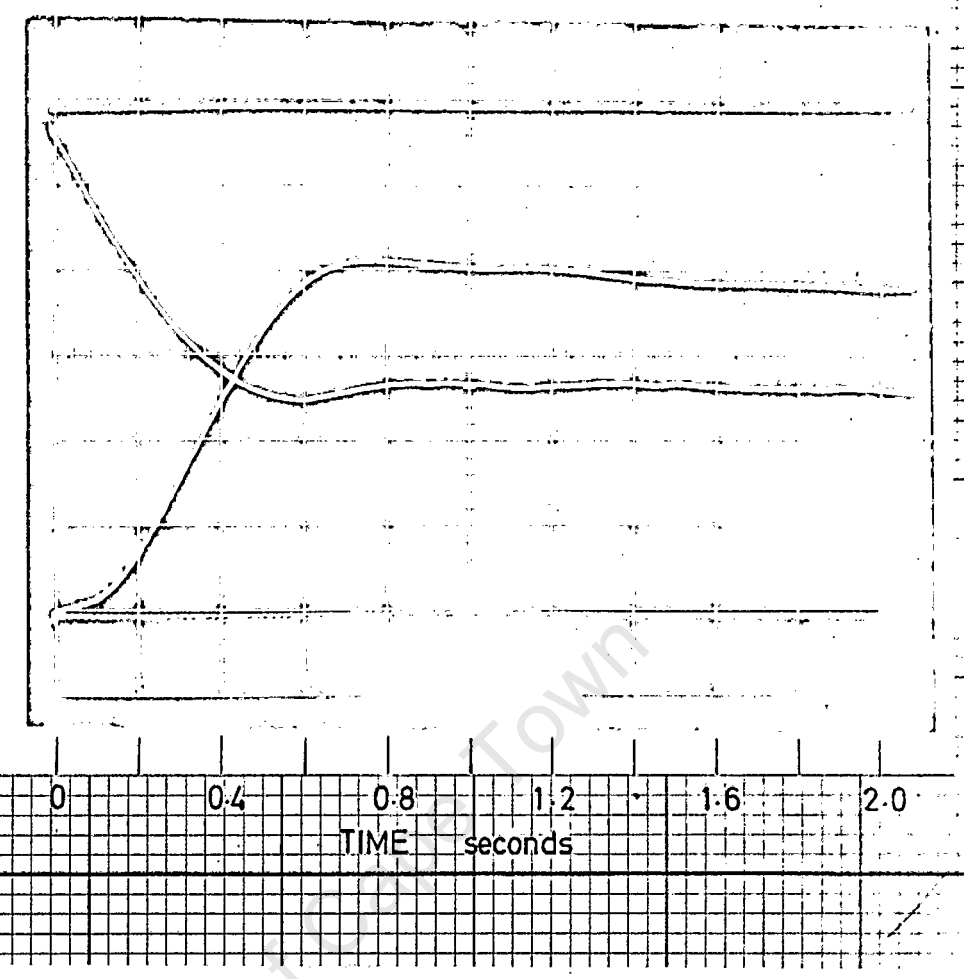

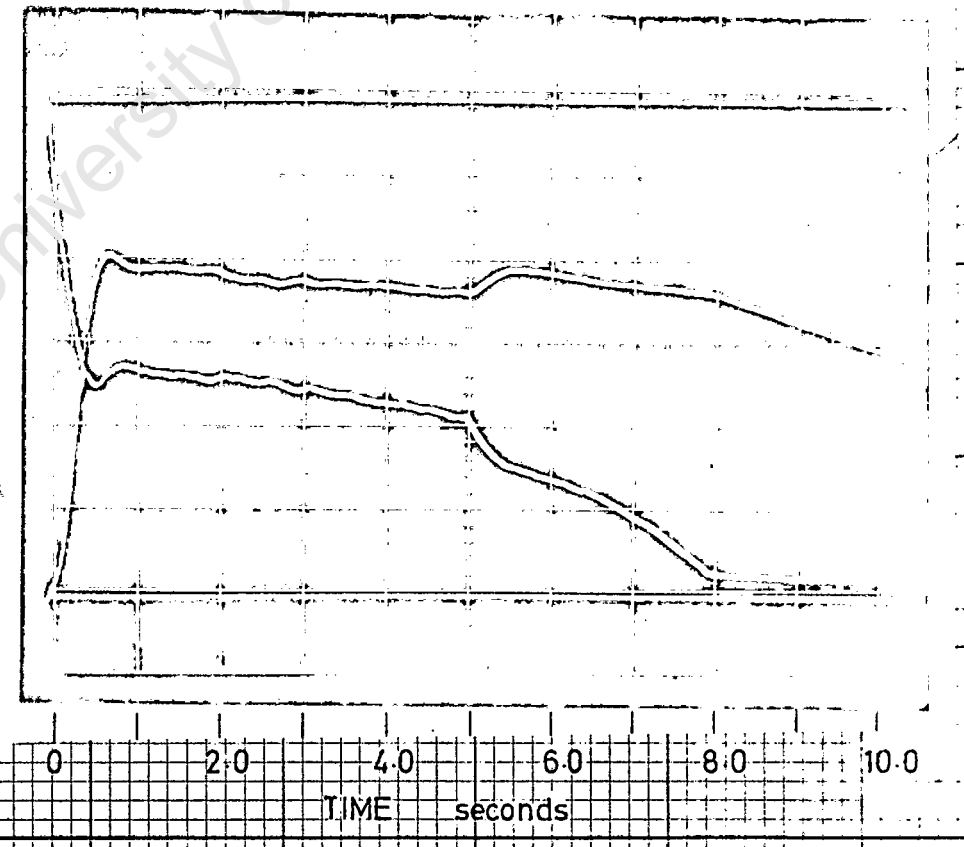

ACTUAL RESPONCE TRACES

Figure 3·31

BYPASS NUMBER 8 (C_{Dnl} = 54 200 lbs sec^2/ft^2)

SET PRESSURE = 40 p.s.i.

MACH 2·0 NOZZLE

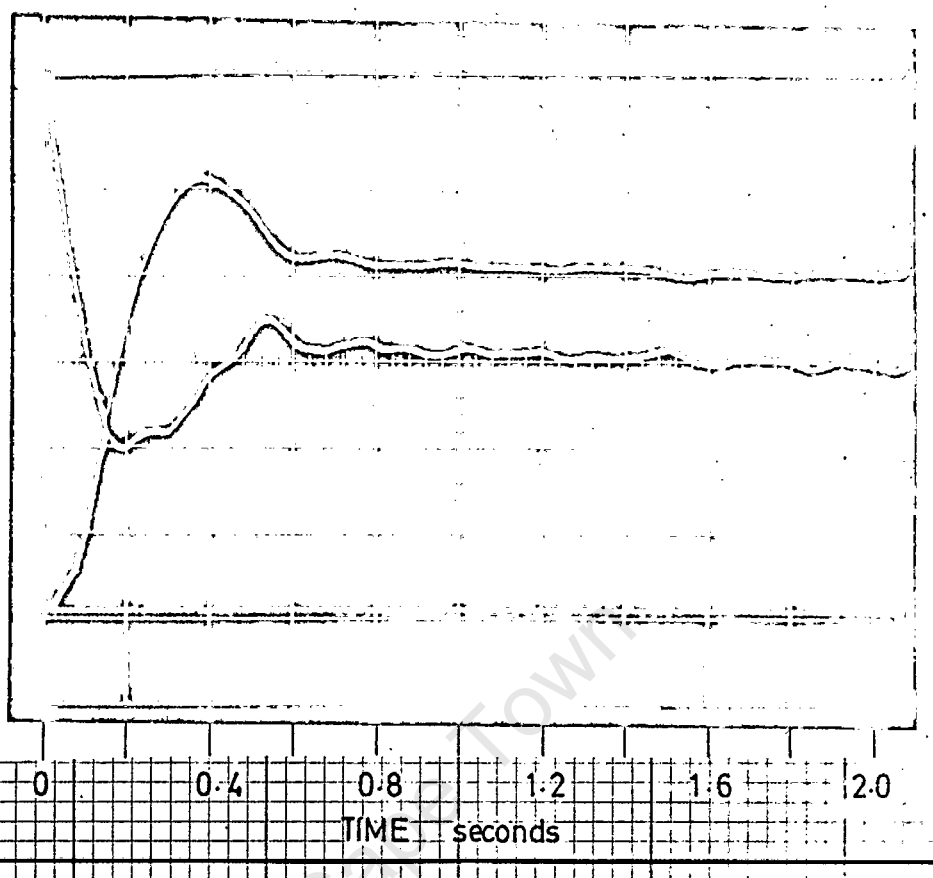

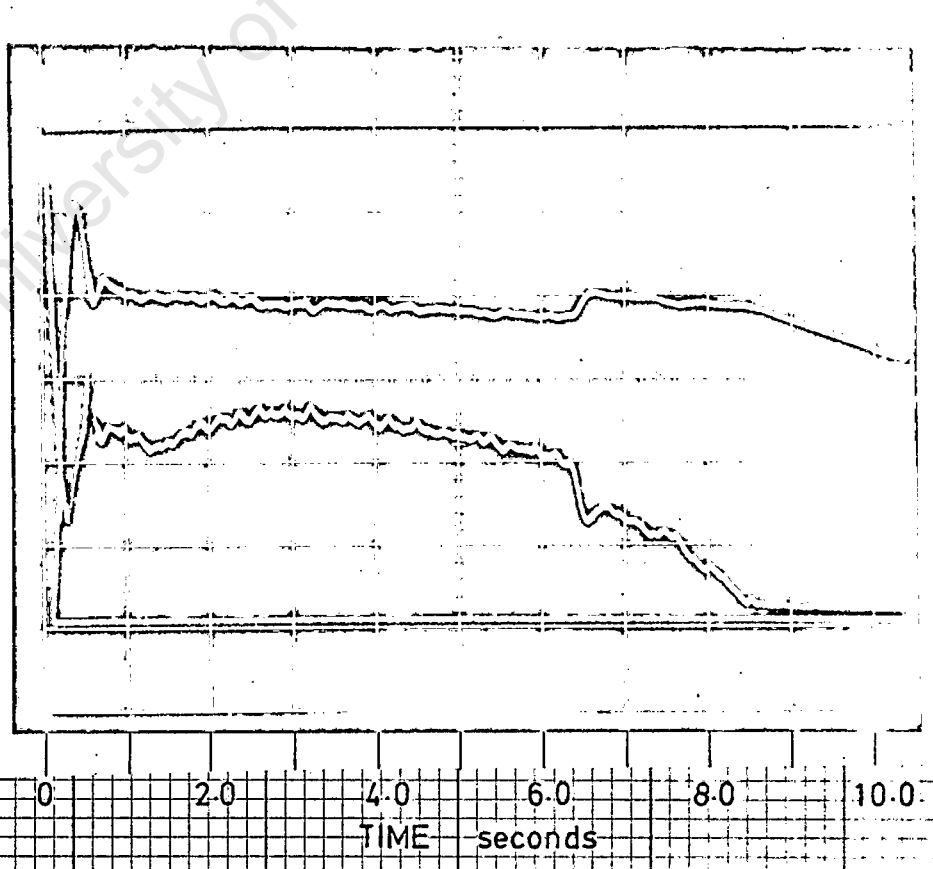

ACTUAL RESPONSE CURVES

Figure 3·32

repeated.

The oscilloscope traces were photographed so that a permanent record could be kept. Examples of these traces are given in figures 3.30, 3.31, and 3.32 for both a short and long time scale. In these cases the set pressure has been fixed and the damping varied for a Mach 2,0 nozzle.

The response curves, in figure 3.31, appear to be essentially similar to the corresponding analogue system in figure 2.24. One basic difference in the pressure response curves, on the long time scale, is the unsteadiness in the real system. (This is most probably due to the unbalance forces on the valve seats).

5.2 ANALYSIS OF VALVE CHARACTERISTICS

The performance characteristics of the actual and simulated settling chamber pressure are summarised in figures 3.33 to 3.39. The theoretically 'perfect' analogue response characteristics are used as the basis of these graphs and the experimental solutions are superimposed upon them. The analogue solutions are necessary to predict the possible performance characteristics of the valve, whereas the experimental results either substantiate or contradict these predictions.

Comparison between actual and predicted system response.

The percentage overshoot of the settling chamber pressure is given in figures 3.33 and 3.34. The point at which the percentage overshoot decreases to zero (i.e. critical damping) is the same for both the actual and simulated systems. - this applies to both the Mach 2.0 and 3.0 nozzles. For lower damping, the percentage overshoot is much less than predicted and the values measured on the wind-tunnel are also somewhat random. This is confirmed in figure 3.34 for increasing settling chamber pressure. Although the percentage overshoot of the actual system is not as great as that of the simulated system, it tends to approach the simulated solution as the pressure increases.

These observations indicate that at both heavier damping and higher settling chamber pressures, the solutions approach the expected curves the deviations, at lower damping, could be due to the fact that the shut-down piston and the valve unbalance, due to flow through the valve, have been neglected in the theoretical analysis.

Firstly, the forces that tend to unbalance the valve would have some effect in controlling its acceleration and the subsequent pressure response curves. Secondly, the additional mass of the shut-down piston, during the initial

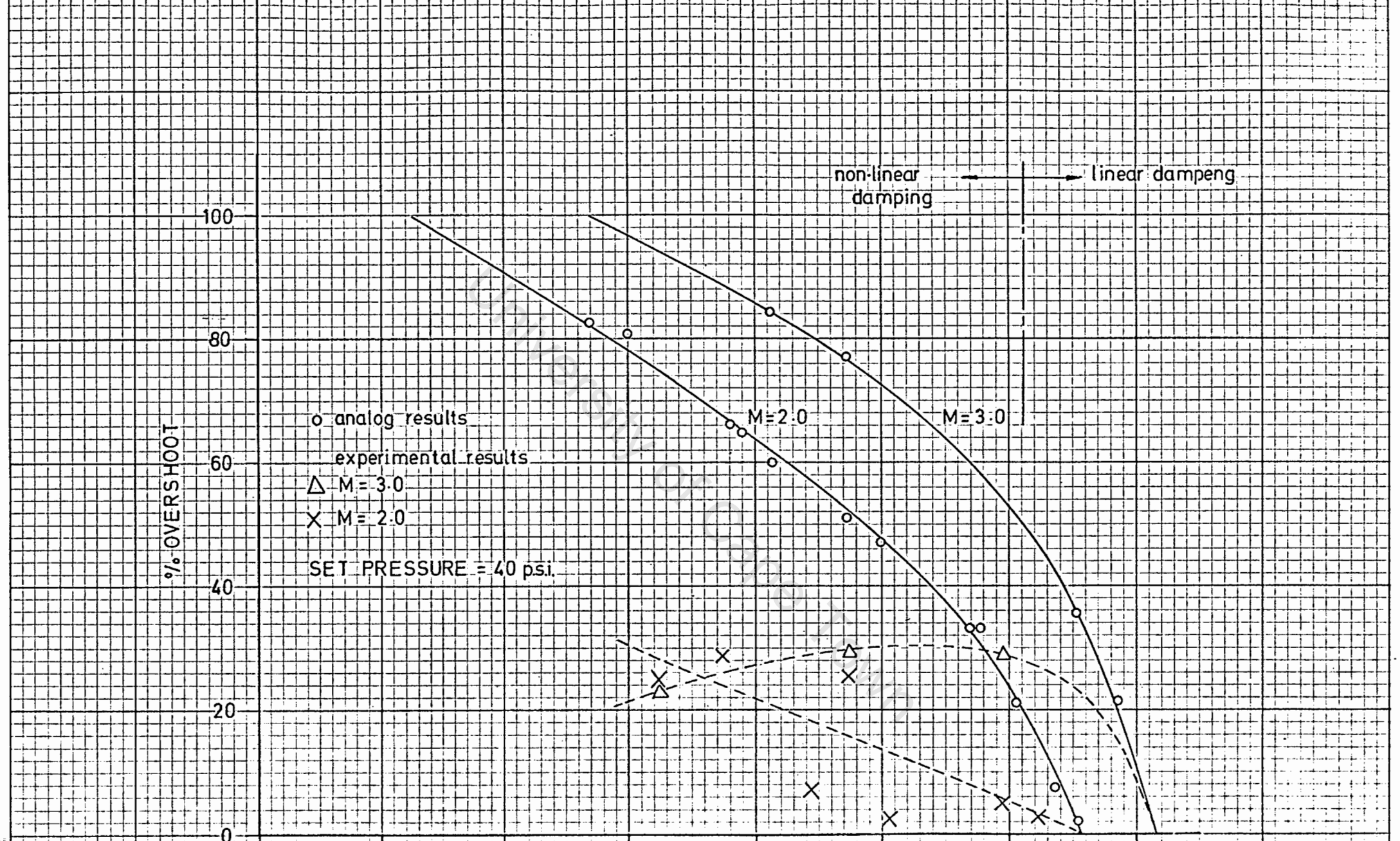

Figure 3.33 RESPONSE OVERSHOOT

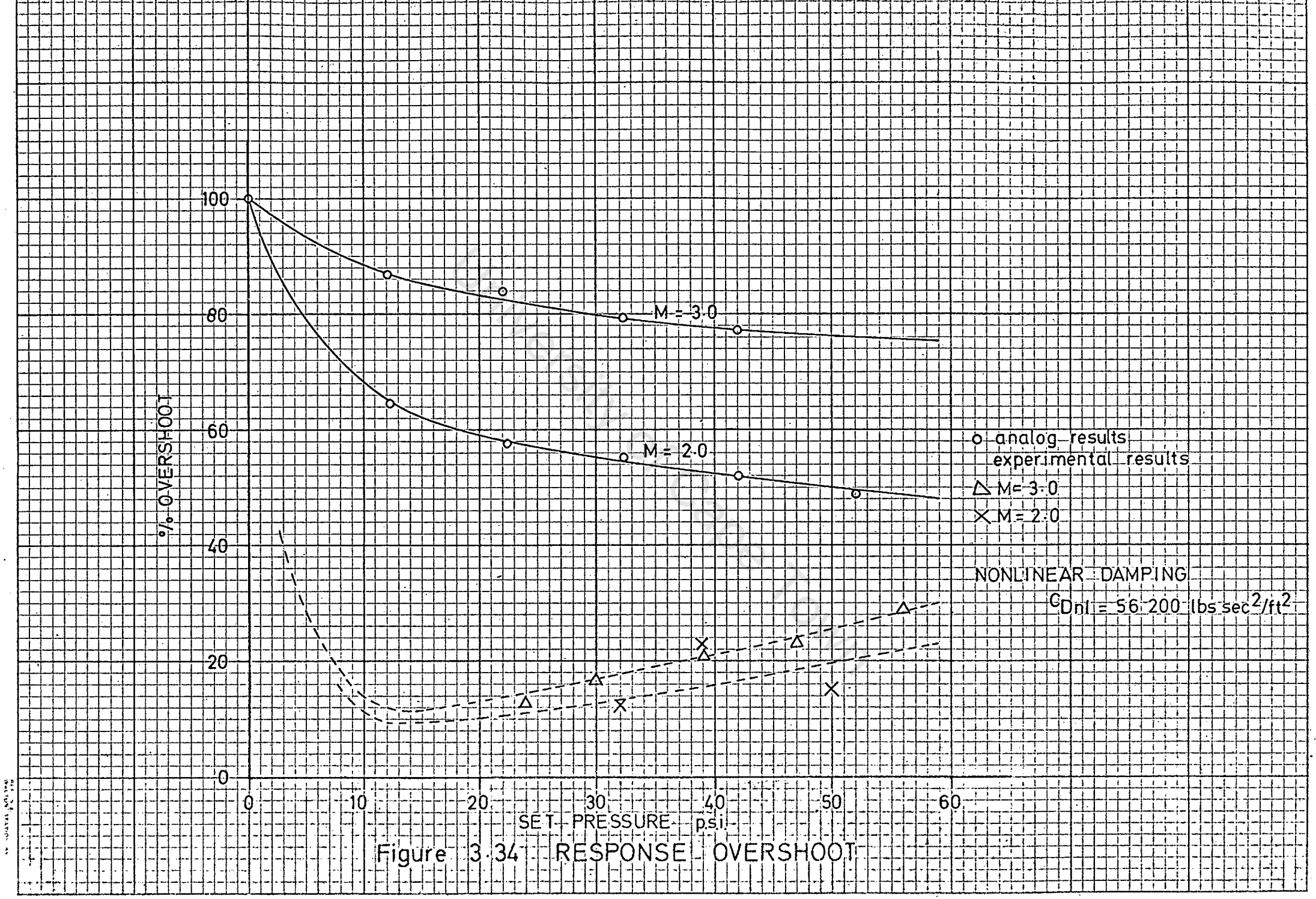

Figure 3·34 RESPONSE OVERSHOOT

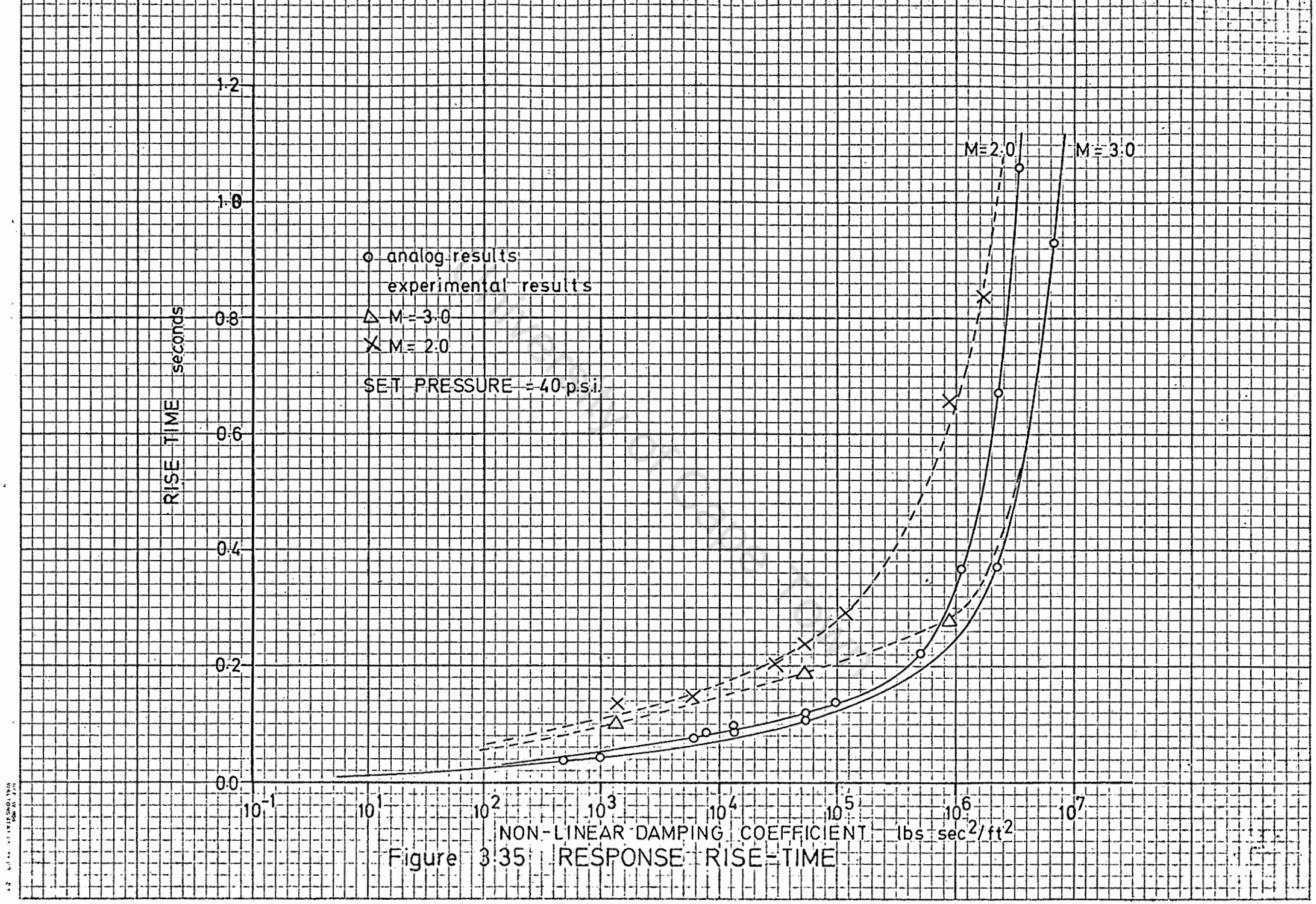

Figure 3·35 RESPONSE RISE-TIME

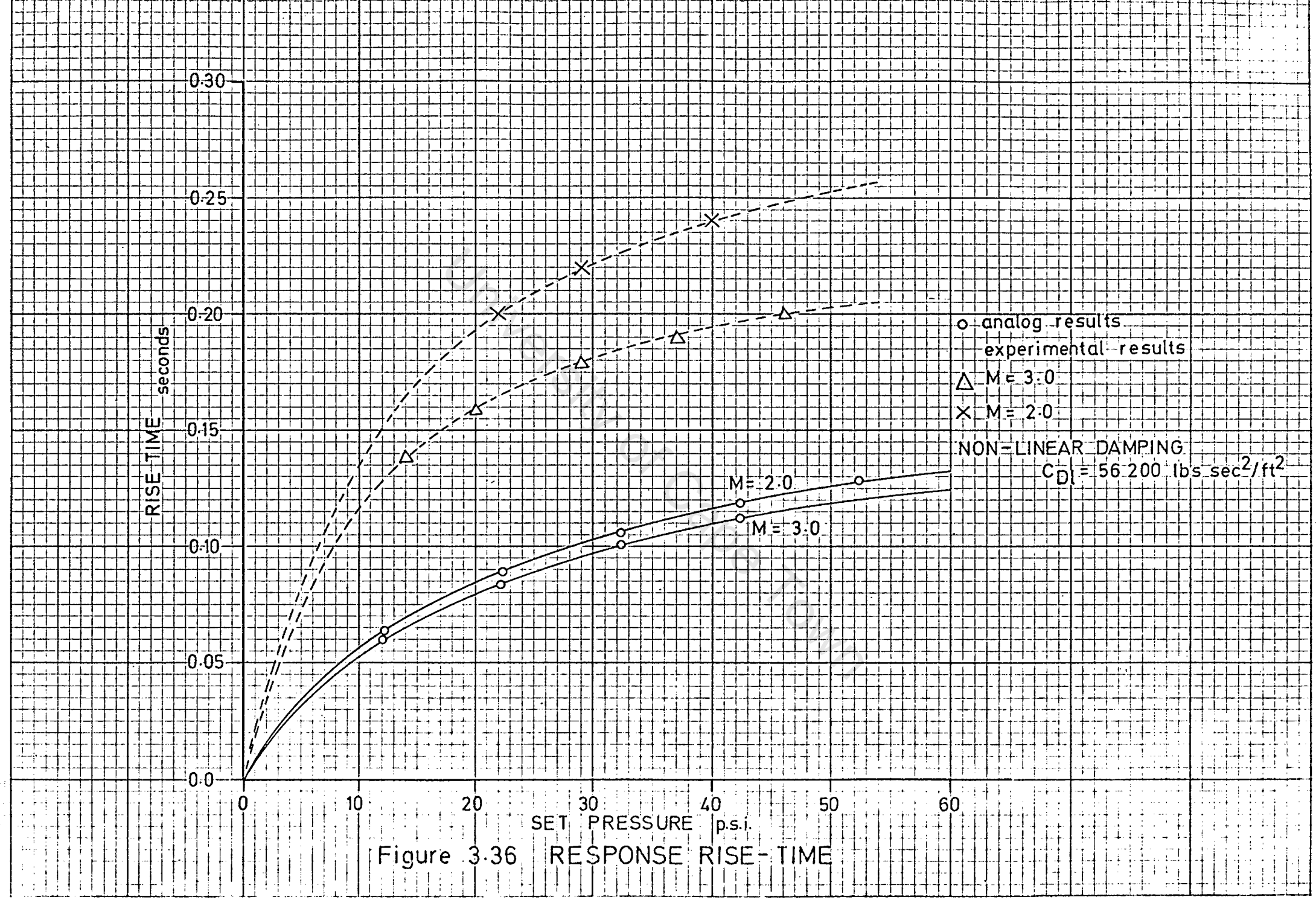

Figure 3·36 RESPONSE RISE-TIME

positive displacement of the valve, will tend to reduce the acceleration of the valve and hence its maximum velocity. This is confirmed in figures 3.35 and 3.36. The time for the settling chamber pressure to reach the value of the set pressure (i.e. the particular solution) is longer than predicted by the analogue simulation. As the damping increases, the maximum velocity to which the valve must be accelerated, is reduced and the influence of the shut-down piston on the response curves is less (i.e. The damping forces predominate over the inertia forces). This is clearly illustrated in figure 3.35. The experimental results approach the theoretical curves at high damping. As is expected, the increased settling chamber pressure gives rise to an increased rise time. The same trend is followed in both the actual and simulated systems although the rise time in the actual system is longer due to the increase in the effective mass of the valve.

Optimum valve performance

The choice in the degree of damping of the system is very important to the performance of the control system. The two possible extremes of this damping are listed below:

1. Very heavy damping:
   The response of the valve may be so sluggish that it cannot retain a constant settling chamber pressure. The period of transient response may be very long.

2. Very low damping:
   As shown in Chapter 3, part 4.4 on the analogue computer, hunting or controlled instability occurs for the non-linear damping system where the co-efficient of damping is low.

These extremes are illustrated in figure 3.37 for both the Mach 2.0 and 3.0 nozzles.

The system is considered to have reached steady state when the response pressure has settled down to within 95% of the set pressure. Although it was difficult to determine the delay time in practice, due to the adverse effect of the valve unbalance, this time could be estimated roughly.

These experimental results have also been plotted on figure 3.37. The analogue solutions indicate where possible controlled instability starts for each nozzle and the magnitude of these oscillations.

In the case of the Mach 2.0 nozzle, the delay time appears to follow the predicted curve quite well - although it is slightly shorter. Even though the 'hunting zone' was entered, the actual settling chamber pressure did not

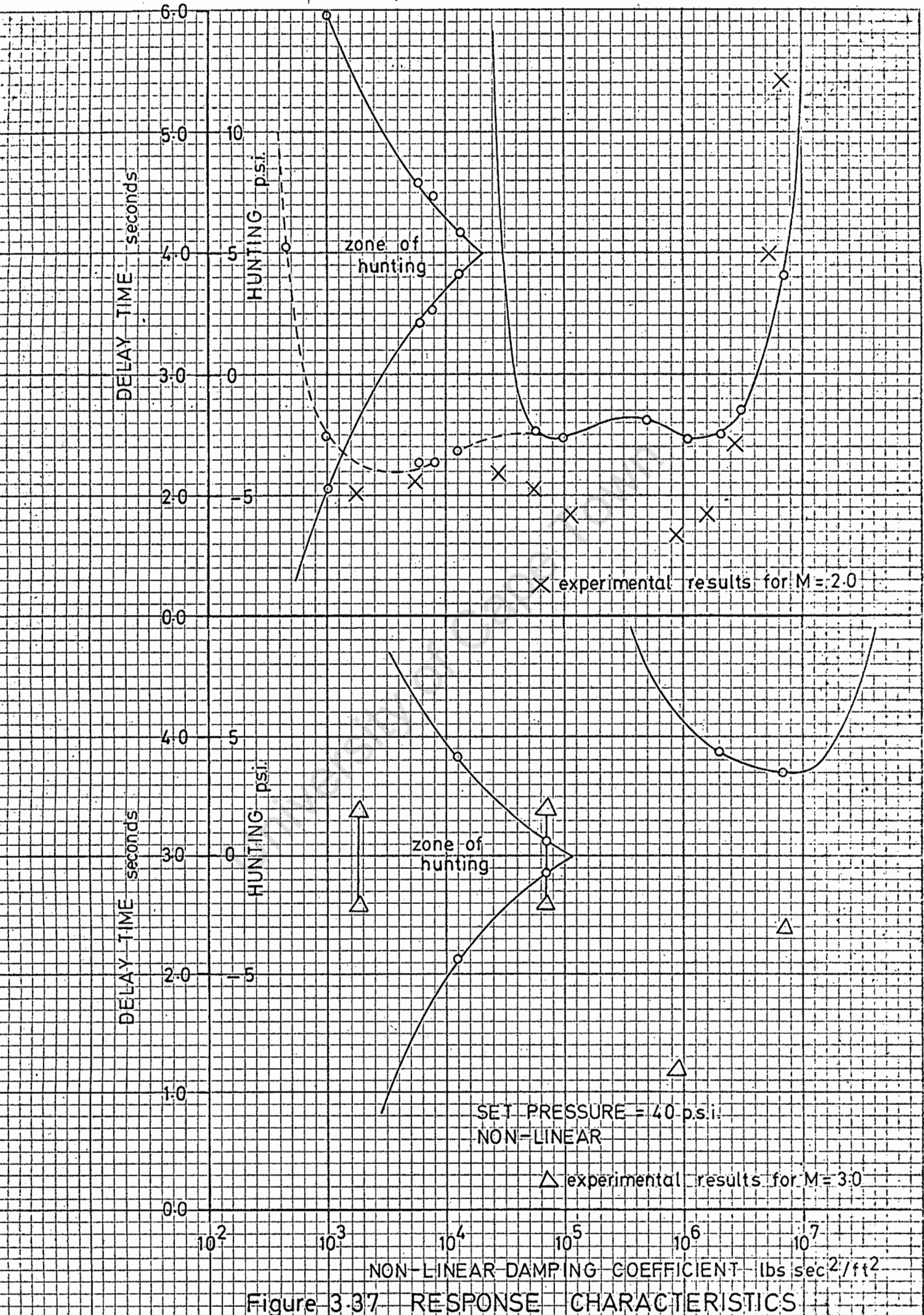

Figure 3·37 RESPONSE CHARACTERISTICS

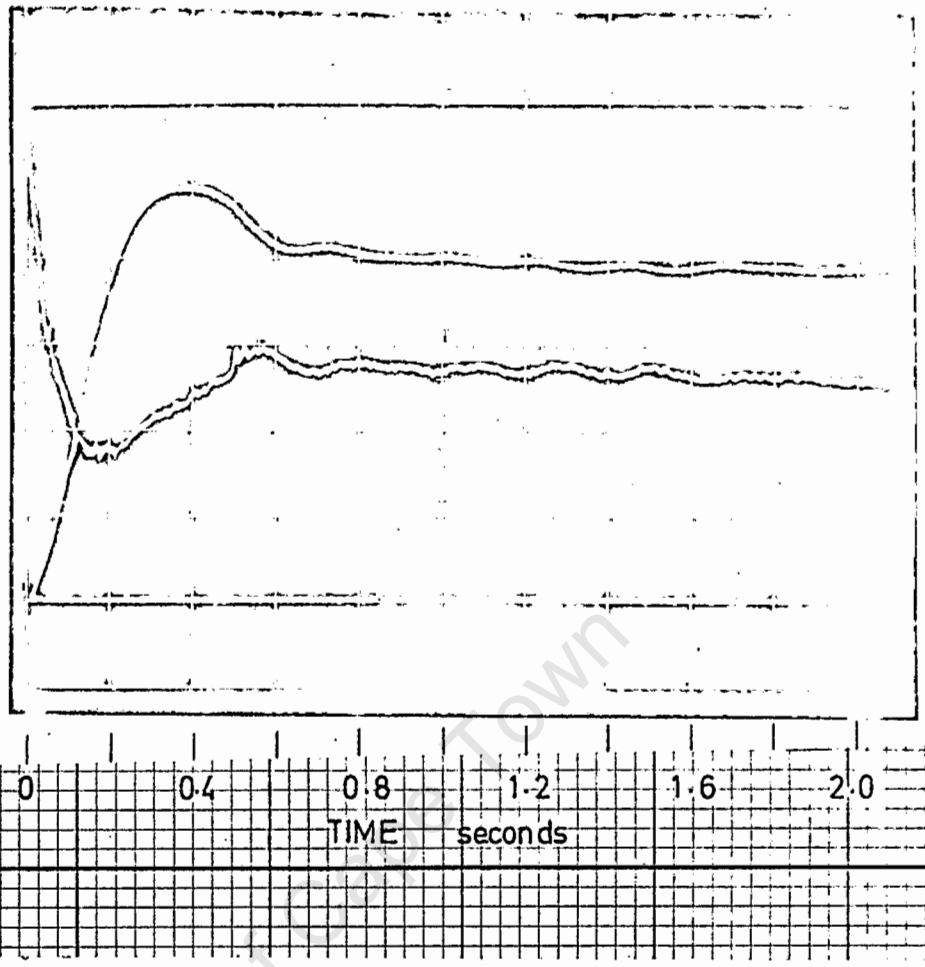

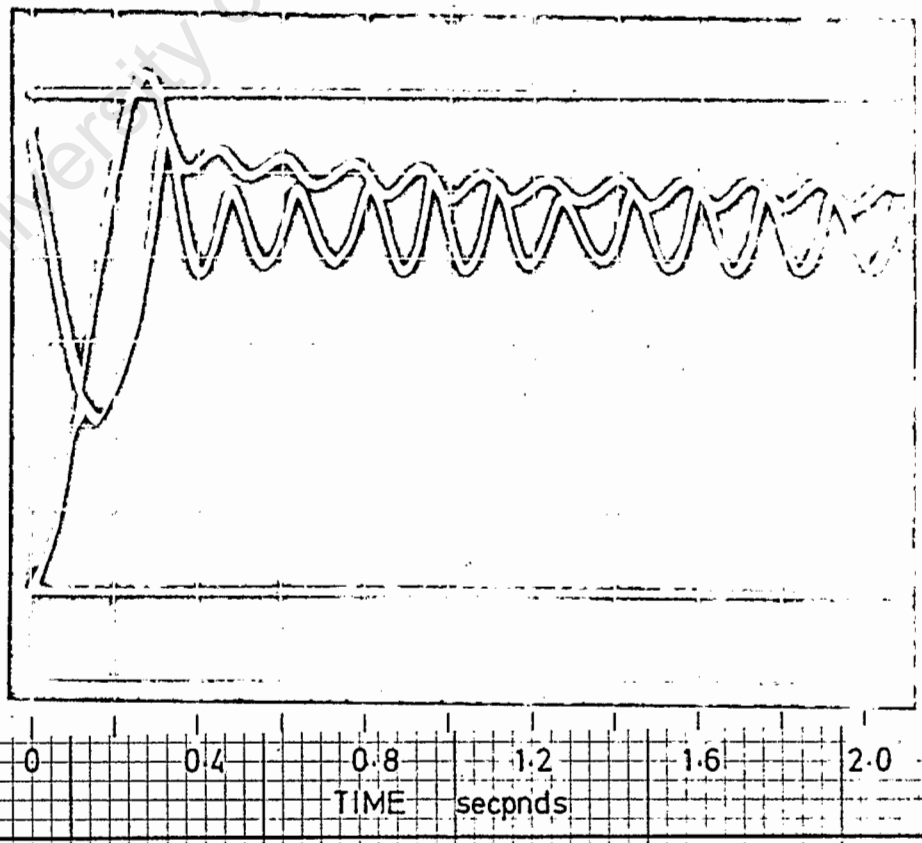

BYPASS NUMBER 8 (C_{Dnt} = 54·200 lbs sec^2/ft^2)
SET PRESSURE = 40 p.s.i.
MACH 3·0 NOZZLE
MACH 2·0 NOZZLE

ACTUAL RESPONSE CURVES
Figure 3·38

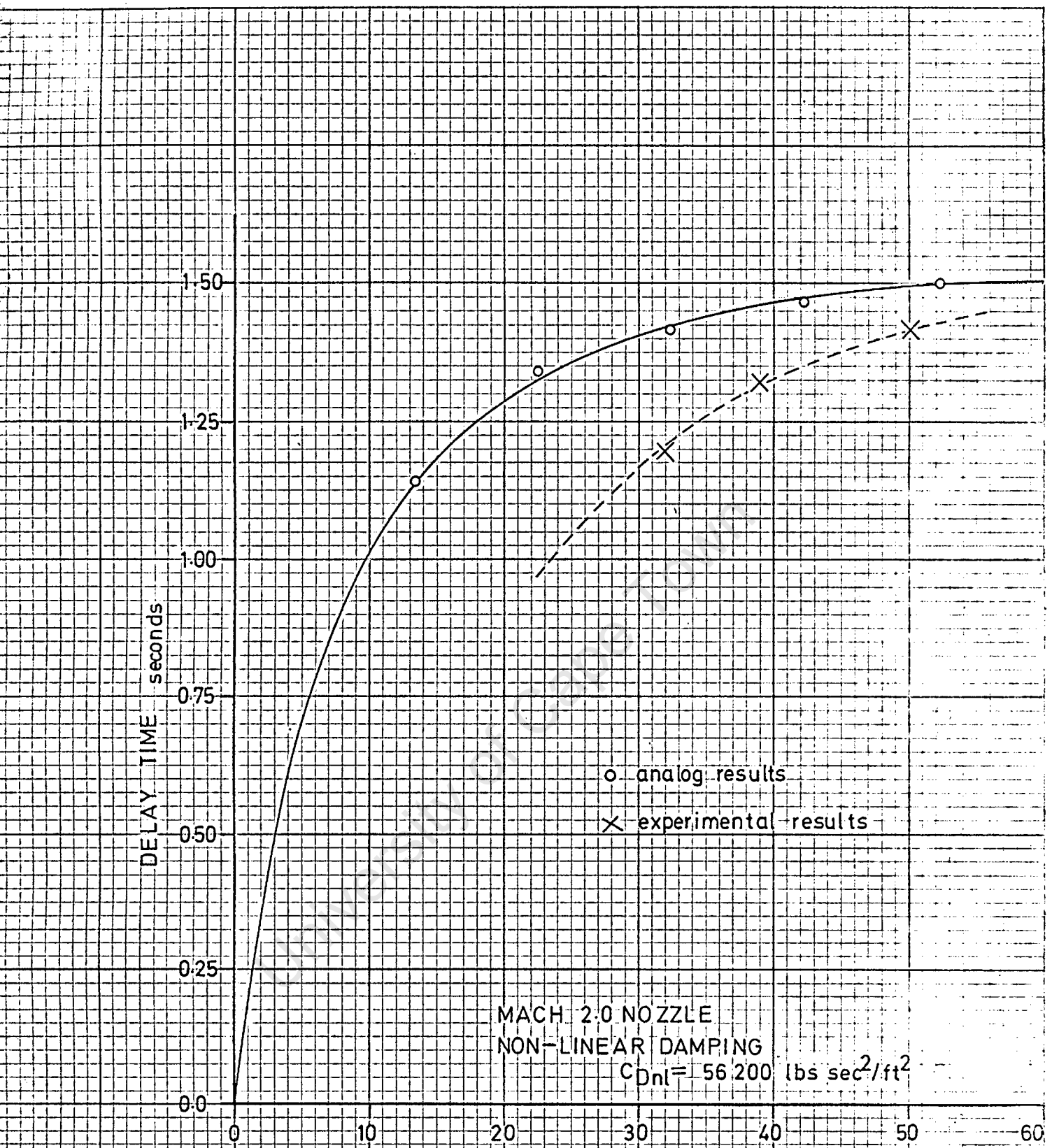

RESPONSE DELAY TIME

Figure 3·39

not show this unstable tendency. For the Mach 3,0 nozzle hunting occurred at the point at which it was expected. A further decrease in damping did not influence the amplitude of the oscillation to any extent. (the amplitude was about $\pm$ 2 psi of the settling chamber pressure).

A comparison may be made of the performance of the two nozzles in figure 3.38. For the same damping coefficient (equivalent to a bypass orifice number 8), the Mach 3,0 nozzle showed unstable characteristics whereas the Mach 2,0 nozzle did not. This verifies the conclusion deduced from the predicted performance curves.

The influence of increasing settling chamber pressure upon the delay time, for the Mach 2,0 nozzle, is illustrated in figure 3.39 . For the higher control valve diminishes and the experimentally obtained points approach the predicted results.

5.3 DISCUSSION OF VALVE CHARACTERISTICS

The influence of the neglected properties on the control system performance may be investigated using the experimental results. In addition the values of the co-efficients used in the theoretical analysis may be checked against the actual values.

Nozzle Flow Rate

The theoretical run time curves, in figure 3.40 for Mach 2.0 and 3.0 nozzles, have been derived from the same conditions given in Chapter 1, part 5.2. The experimental results superimposed upon these curves simply confirm the original assumptions in the derivation of run times (See Chapter 1).

Flow Rate through the Valve

The mass flow rate through the valve is given by equation 1,45 as:

$$\dot{M} = K_1 . Pd . X$$

Where K_1 is the valve flow co-efficient necessary in the analogue simulation. The mass flow rate has been assumed dependent upon the valve opening and storage drum pressure. These two assumptions should be adjusted to suit the actual conditions.

1. The mass flow rate through the valve is dependent upon the air pressure immediately upstream of the valve; this is somewhat less than the drum pressure.
2. The mass flow rate past the seats of the valve is dependent on the throat width, t, and not on the valve displacement. (See figure 3.41).

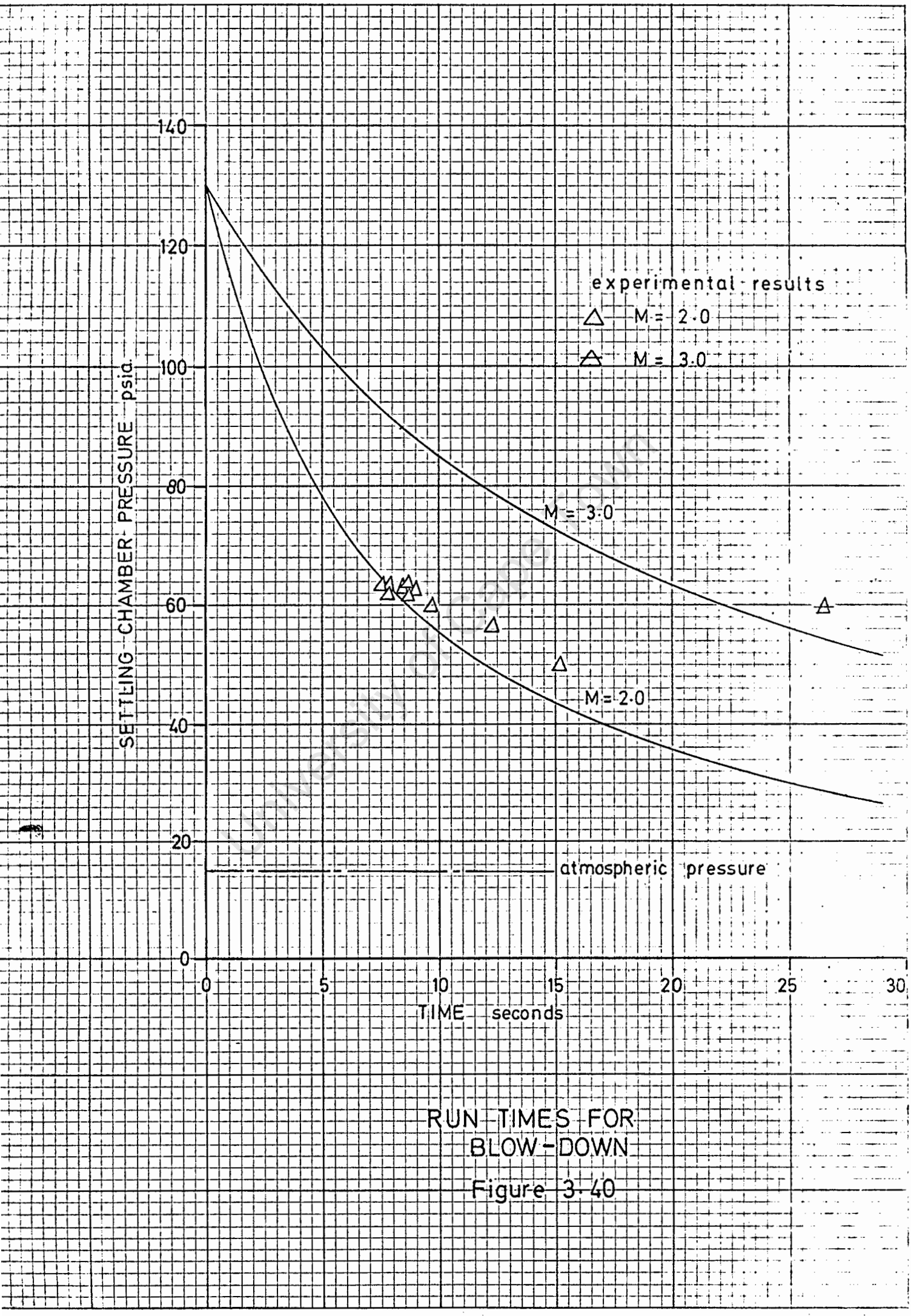

RUN TIMES FOR BLOW-DOWN

Figure 3·40

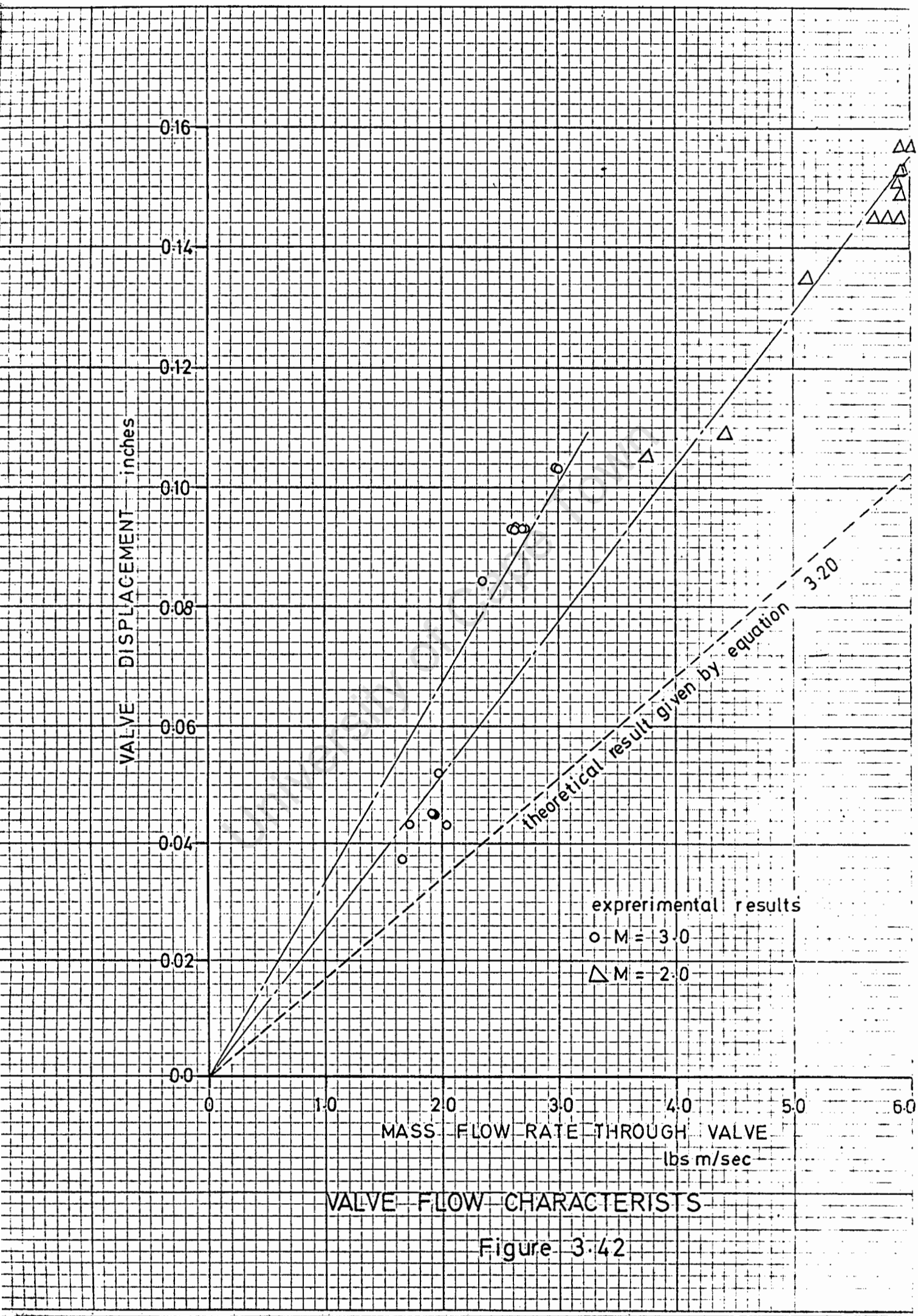

VALVE FLOW CHARACTERISTS

Figure 3·42

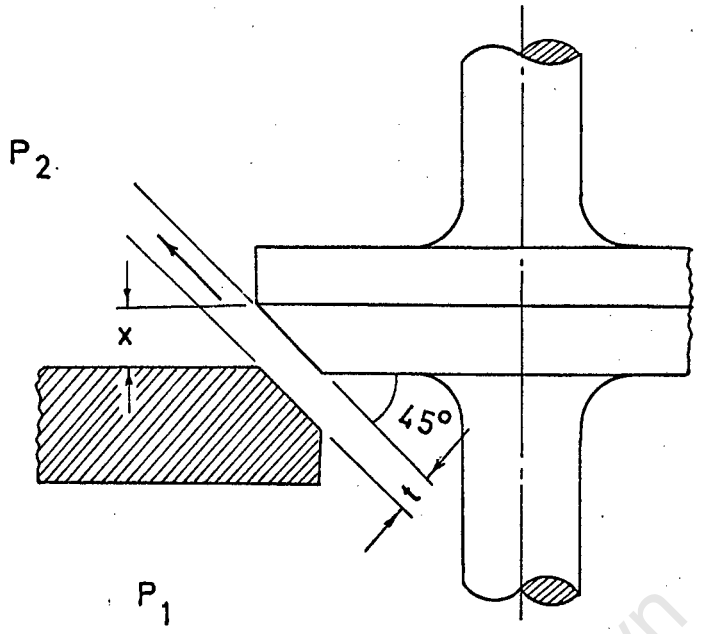

VALVE SEAT ARRANGEMENT

Figure 3.41

For a valve seat of 45^{o}, the actual throat width t is given as:

$$t = 0{,}707\ X \quad \ldots\ldots\ldots\ldots\ldots\ldots\ldots\ldots\ldots\ldots \quad 3.19$$

By considering a co-efficient of discharge for the valve not equal to unity and the supply duct pressure loss, the correct valve flow co-efficient may be obtained. The supply duct pressure loss is discussed in Chapter 1, part 1.2 and is given as approximately 20 lbs per sq.inch.

The mass flow rate through the valve is thus given by:

$$\dot{M} = K_1 C_D .\ 0{,}707\ X\ (P_i - 20) \quad \ldots\ldots\ldots\ldots\ldots\ldots\ldots \quad 3.20$$

This equation, together with the experimental data, is presented in figure 3.42. The difference in the slopes of the co-efficient curves for the two nozzles, indicates that the coefficeint of discharge through the valve is greater at the smaller valve openings.

Valve Characteristics

The performance of the valve and hence of the settling chamber pressure control system, is dependent upon the valve mass, its damping and the controlling forces. Deviations from the theoretical solution could occur as a result of errors in the assumed values of any one of these factors.

1. Mass:

   The mass of the shut-down piston increases the inerita of the valve. Figures 3.34 and 3.44 compare the theoretical and actual response curves for a heavily damped and underdamped system respectively.

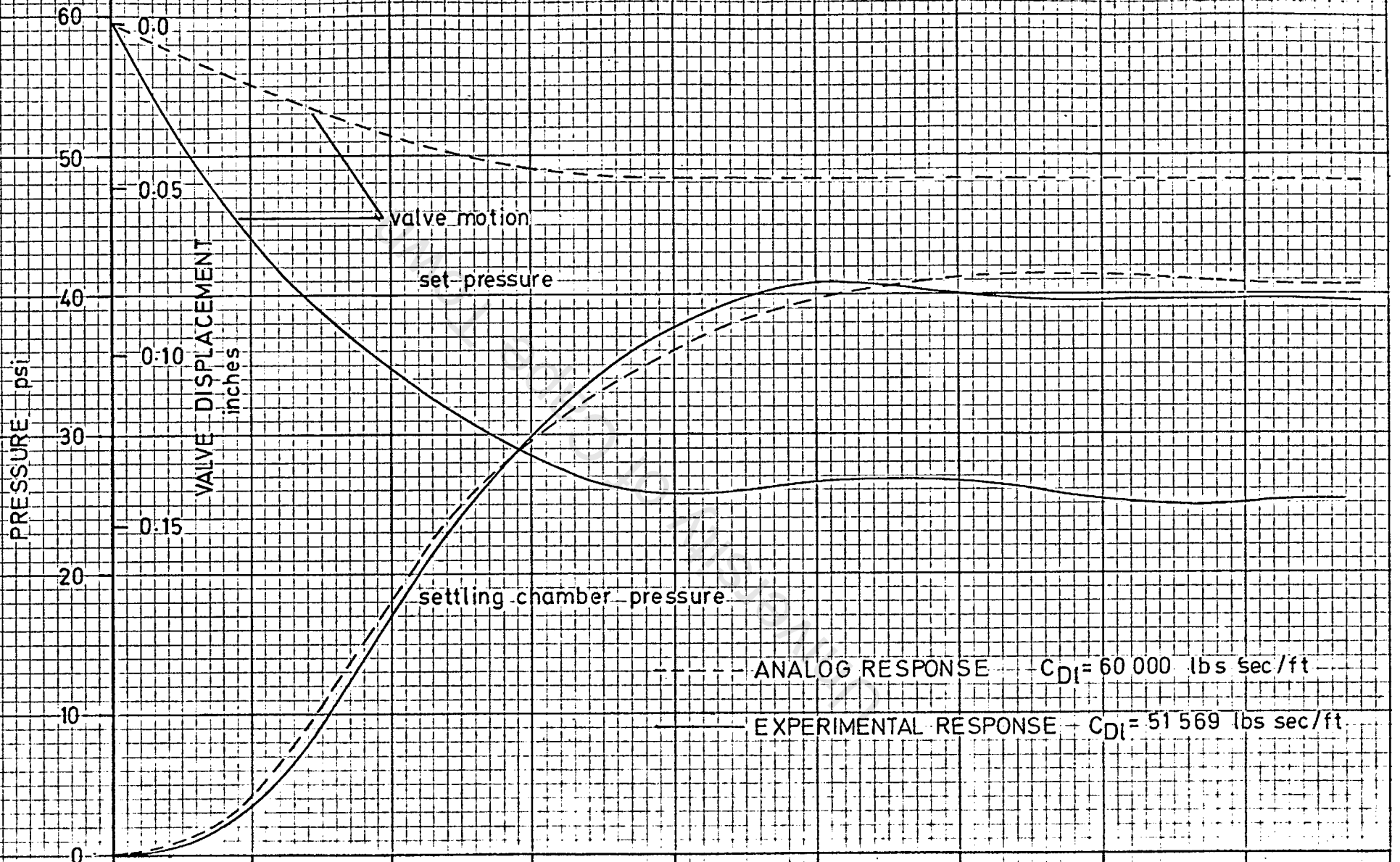

Figure 3.43 RESPONSE CURVES

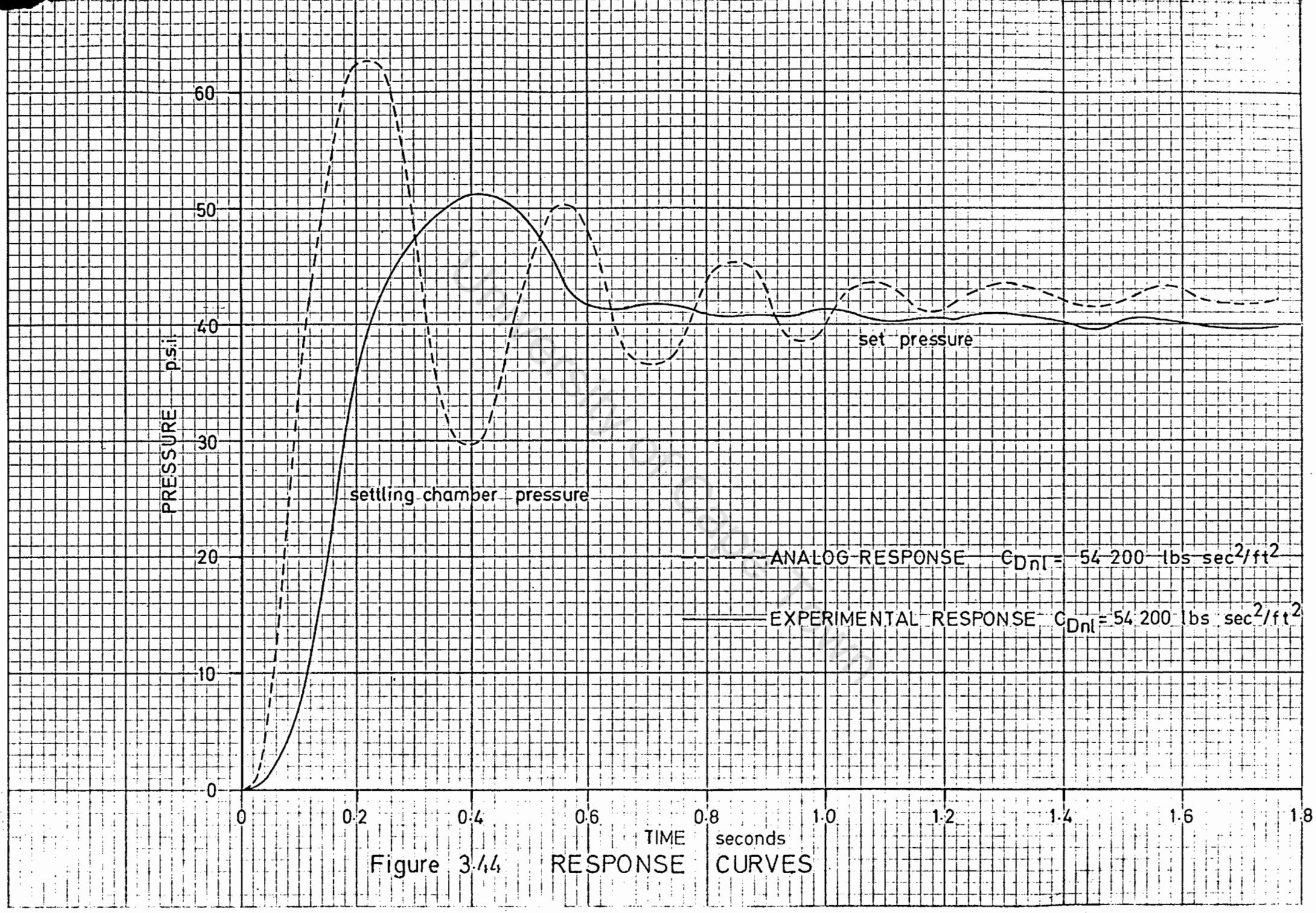

Figure 3.44 RESPONSE CURVES

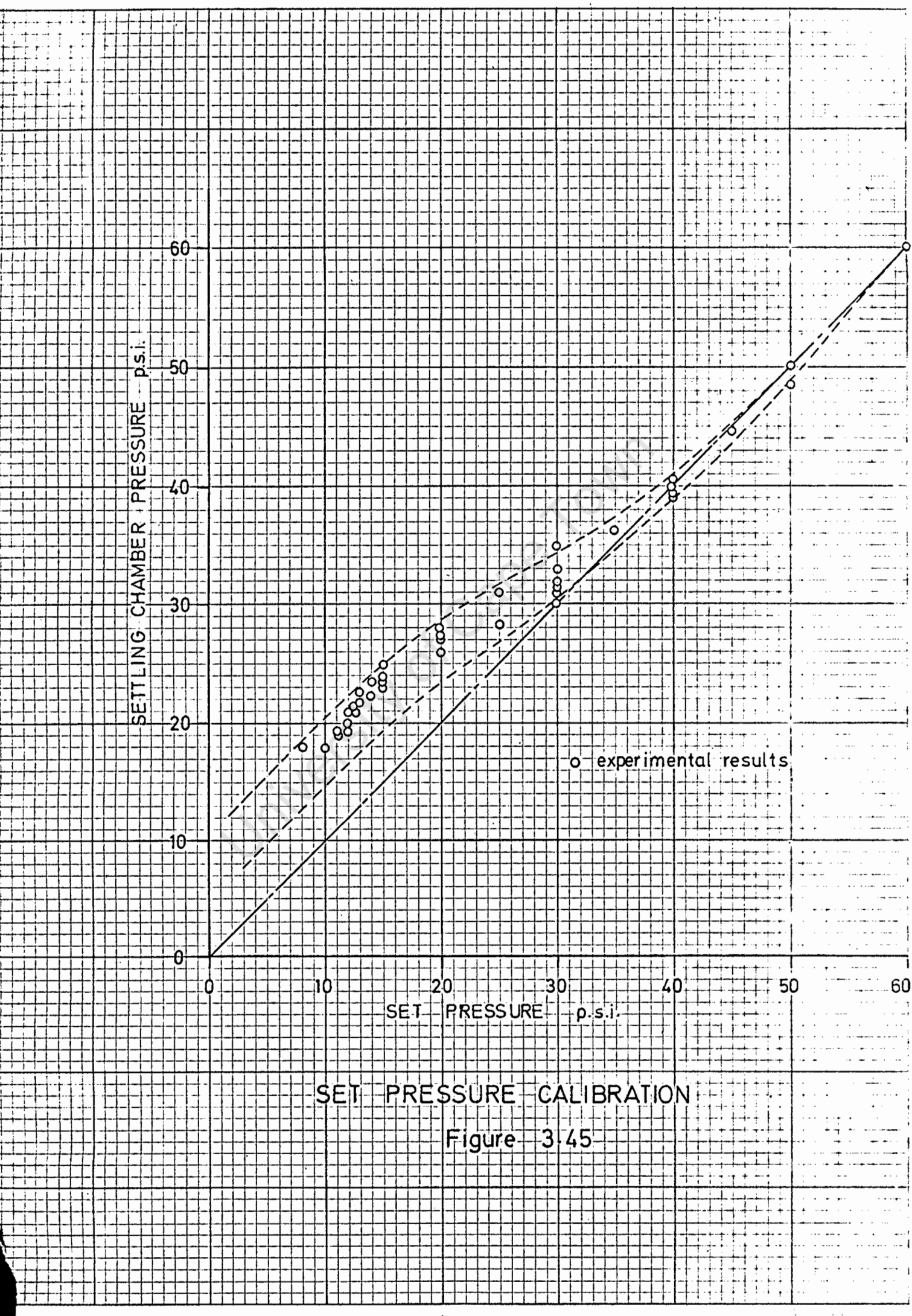

SET PRESSURE CALIBRATION

Figure 3.45

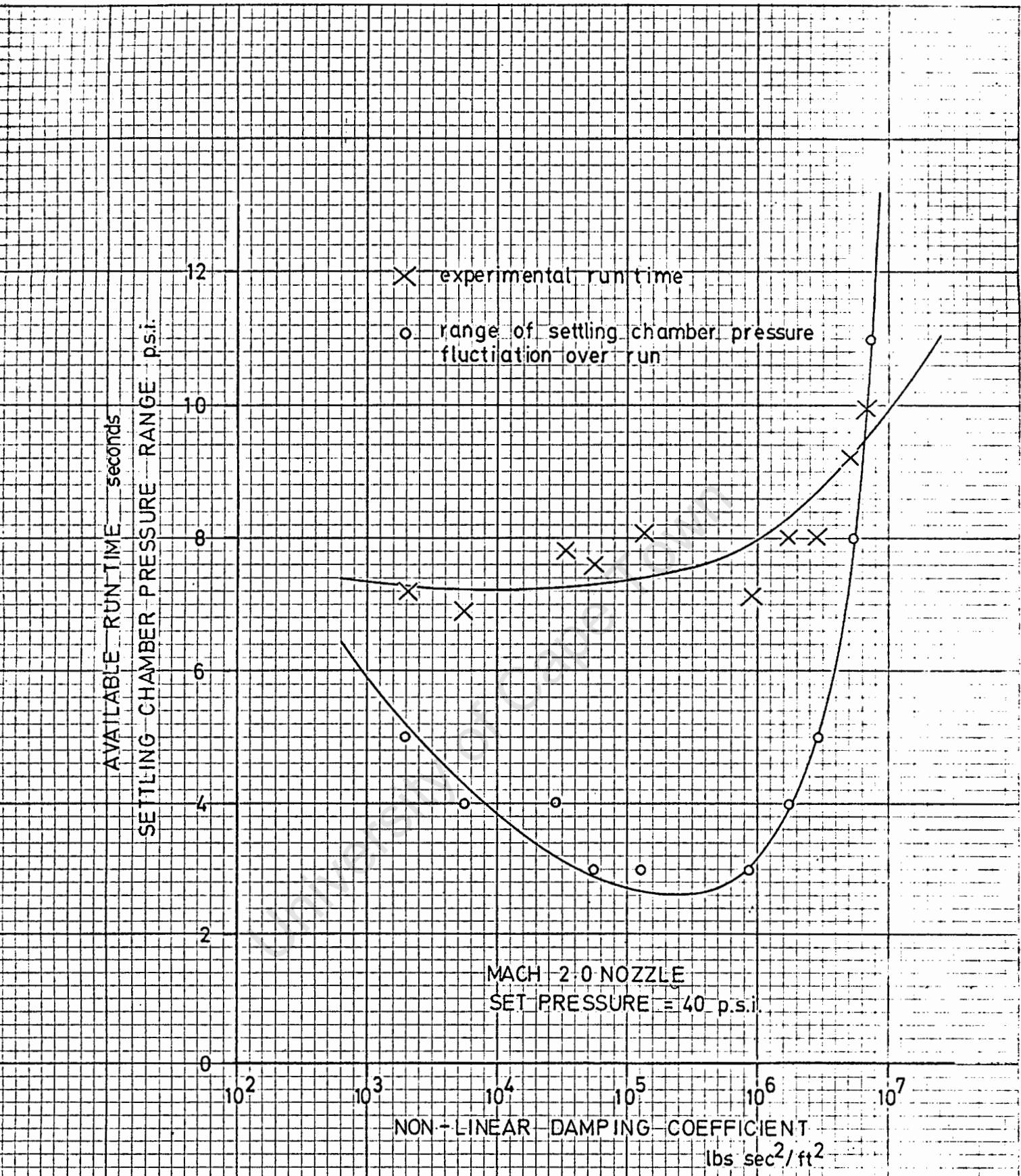

ACTUAL SYSTEM RUN CHARACTERISTICS

Figure 3·46

The additional mass of the shut-down piston, in the second case, reduces the overshoot and increases the rise time. For the overdamped system, the pressure response curves are very similar, indicating little influence of the additional mass. The difference in the displacement curves is explained under 'flow rate through valve'.

2. Damping:

The damping co-efficients are a reasonable measure of the actual degree of damping as shown in part 1.5.

3. Controlling forces:

The controlling force results from a pressure difference across the valve diaphragm. Unfortunately, the equilibrium of the pressures across the diaph-diaphragm is upset by the unbalance of the forces on the valve seats and the initial static friction of the shut-down piston.

The resistance of the shut-down piston is relatively small in comparison with the controlling forces and it only affects the system during the first downward displacement of the valve.

The magnitude of the unbalance forces on the valve seats are relatively large and it varies during a blow-down (See gigures 3.30, 3.31 and 3.32) Figure 3.45 shows the relationship of set pressure to actual pressure. The deviation from the linear curve is a measure of the unbalance of the valve and the range of the experimental results is due to the change of this unbalance during a run.

Figure 3.46 shows the magnitude of the change in settling chamber pressure during a complete run period. The minimum degree of deviation for this pressure occurs at a non-linear damping coefficient of 200,000 lbs sec^2/ft^2.

5.4 CONCLUSIONS

The modifications to the valve control system have improved its performance and flesibility. The response characteristics of the settling chamber pressure are controllable and the desired stagnation pressure may be set by remote adjustment.

The most suitable damping for this control system lies within the range of non-linear damping coefficients between 200,000 and 1,000,000 lbs sec^2/ft^2. This degree of damping is produced by bypass orifice numbers between 4 and 5.

At this damping, the deviation of the settling chamber pressure during a complete run period, for a Mach 2.0 nozzle and set pressure of 40 psig, is about 2,5 psi. The delay time, from flow initiation until the desired settling chamber

pressure is reached, is about 0,8 seconds.

APPENDIX 1

1.1 WIND-TUNNEL SPECIFICATIONS

Test-Section Area, A_1 = 8 sq. inches.

Wind-Tunnel Width, w = 2 inches.

Storage Drum volume, Vd = 165 cubic feet.

Initial Storage drum pressure, P_{di} = 150 lb/in^2 gauge

Initial Storage drum temperature, T_{di} = 545^oR

Final Storage drum temperature, T_{df} = 520^oR

Supply duct loss at termination of flow, P_l = 25 lbs/in^2

Gas constant, R = 53,3 ft lbf/lb ^oR

Gravitational acceleration, g_c = 32.2 ft/sec^2

Ratio of specific heats for aie, γ = 1,4.

1.2 THE THEORY OF CHARACTERISTICS

Small disturbances in a two-dimensional, supersonic flow are propagated in the form of pressure waves along Mach lines, These lines are of constant perturbation potential, and the vector change in the velocities produced by the pressure wave must have a direction normal to the Mach wave direction.

The lines may either be left-running or right-running, belonging to families II and I respectively.

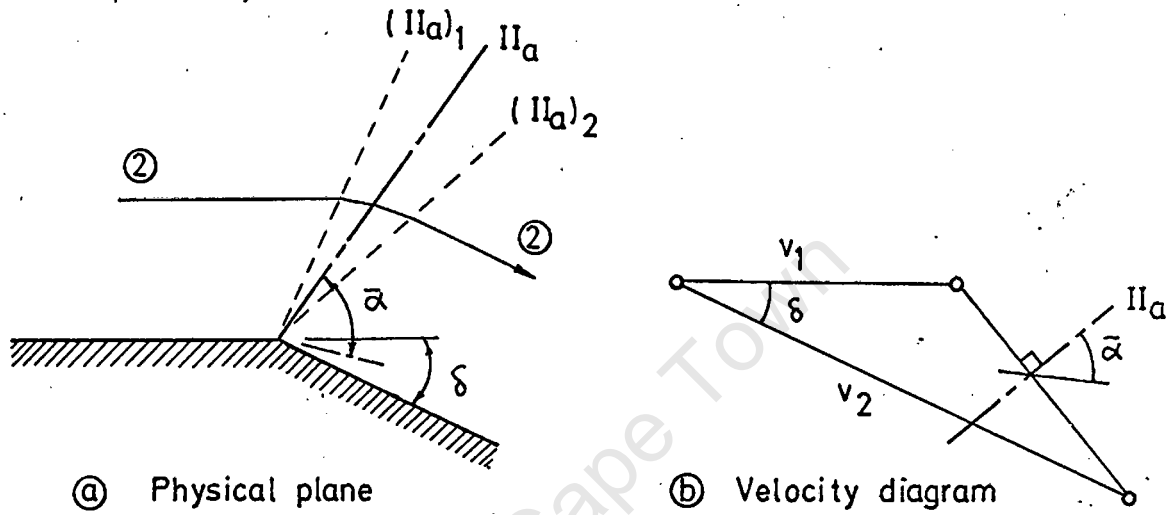

Figure 1.7

These considerations are illustrated in figure 1.7, the Mach wave in this case being left-running.

From figure 1.7(a), the initial effect of the corner is propagated along the left-running Mach line (IIa), having an angle α_1 to the initial flow. Tentatively, the velocity V_2 can be obtained knowing the corner angle δ. But the left-running Mach wave $(IIa)_2$ has an angle α_2 when related to the downstream flow. The accuracy of the first approximation can be improved by simply taking the Mach line IIa at the mean Mach angle $\bar{\alpha}$ to the mean flow direction.

In this way, after several itterations, a better value of the stream properties in region 2 can be found. In real flow, the fluid velocity direction changes gradually within the Mach fan - an approximation can be achieved by introducing a number of finite steps.

This is illustrated in figure 1.8, by assuming the corner to be a gradual curve. The curved wall, as an approximation, shall be replaced by a series of straight sections. From each corner a Mach wave is propagated so that it changes the flow direction to that of the wall. As described above, the Mach lines, II, are found from the mean flow conditions between regions. With stepwise increments, the complete flow field can be described. Flow, where only pressure waves of one family appear, is known as flow with waves of one family,

simple-wave flow, Prandtl-Meyer flow or corner type flow (3).

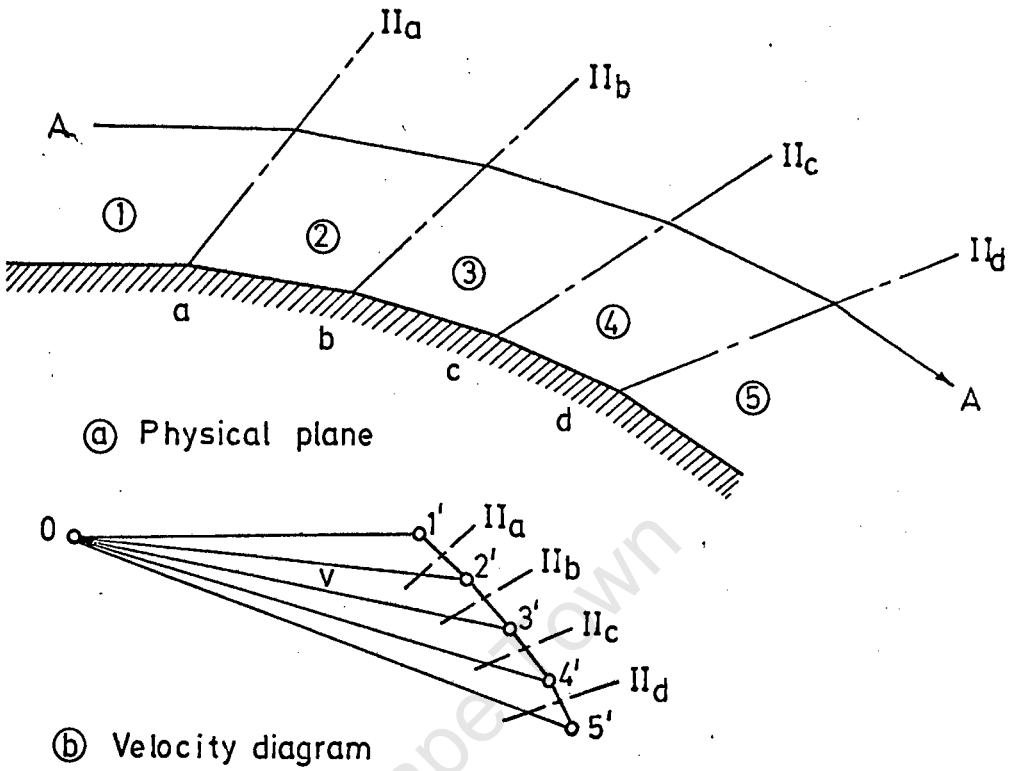

Figure 1.8

Figure 1.8(b) denotes the velocity vectors in fields 1, 2, 3, 4 and 5. The respective image points on the velocity diagram are 1', 2', etc. It is seen here that the velocity vector, and the stream direction (θ) are polar co-ordinates in the velocity or hodograph plane. As the velocity can be plotted at any point in the hodograph plane, then a single line in the hodograph is a representation of the complete streamline.

i.e. The hodograph streamline 1', 2', 3', 4', 5' is the representation of the physical streamline AA.

Hodograph Characteristics

A plot of the complete field of hodograph streamlines, for both left and right-running waves, enables us to obtain an exact solution to a complicated flow pattern.

Left Running Wave:

Imagine a Mach wave of family II turns the flow through a positive angle d and with corresponding changes in stream properties.

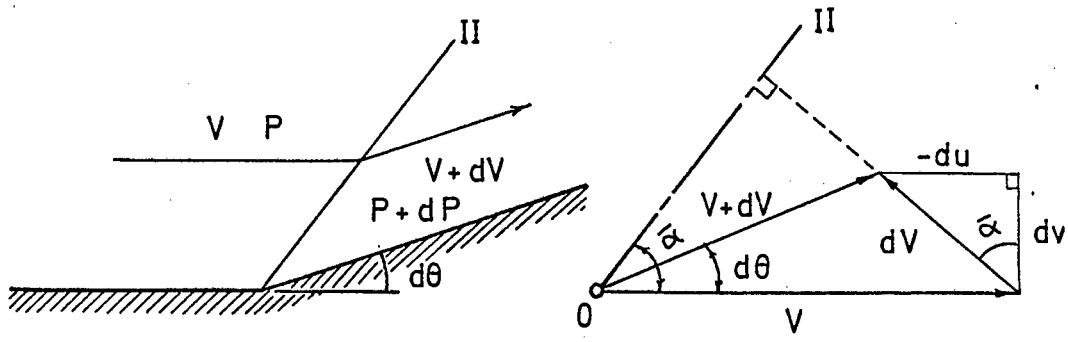

ⓐ Physical plane ⓑ Velocity diagram

Figure 1.9

du and dr are the cartesian increments in the velocity as the flow is changed by the Mach line of constant perturbation potential. Note that du is in the limit, the algebraic increment in velocity dv (3).

From figure 1.9(b), we get:

$$dv = v\,d\theta \quad ; \quad du = dv$$

$$\therefore du/dv = \tan\alpha = 1/\sqrt{M^2 - 1}$$

$$\text{or } \frac{1}{v}\frac{dr}{d\theta} = -1/\sqrt{M^2 - 1} \quad \ldots\ldots\ldots\ldots\ldots\ldots\ldots\ldots \quad 1.5$$

But from (3):

$$\frac{dr}{r} = \frac{dM^2}{2M^2\left(1 + \frac{\gamma - 1}{2} M^2\right)}$$

Therefore, substituting into equation 1.5:

$$\therefore \quad d\theta = \frac{\sqrt{M^2 - 1}\; dM^2}{2M^2\left(1 + \frac{\gamma - 1}{2} M^2\right)} \quad \ldots\ldots\ldots\ldots\ldots\ldots\ldots \quad 1.6$$

Integration of this equation gives the change in flow direction in terms of Mach number.

$$\therefore \quad = -\sqrt{\frac{\gamma + 1}{\gamma - 1}}\ \text{arc tan}\ \sqrt{\frac{\gamma - 1}{\gamma + 1}(M^2 - 1)} + \text{arc tan}\ \sqrt{M^2 - 1}$$

$$+ \text{constant} \quad \ldots\ldots\ldots\ldots\ldots \quad 1.7$$

1.3 HODOGRAPH FLOW DIAGRAM

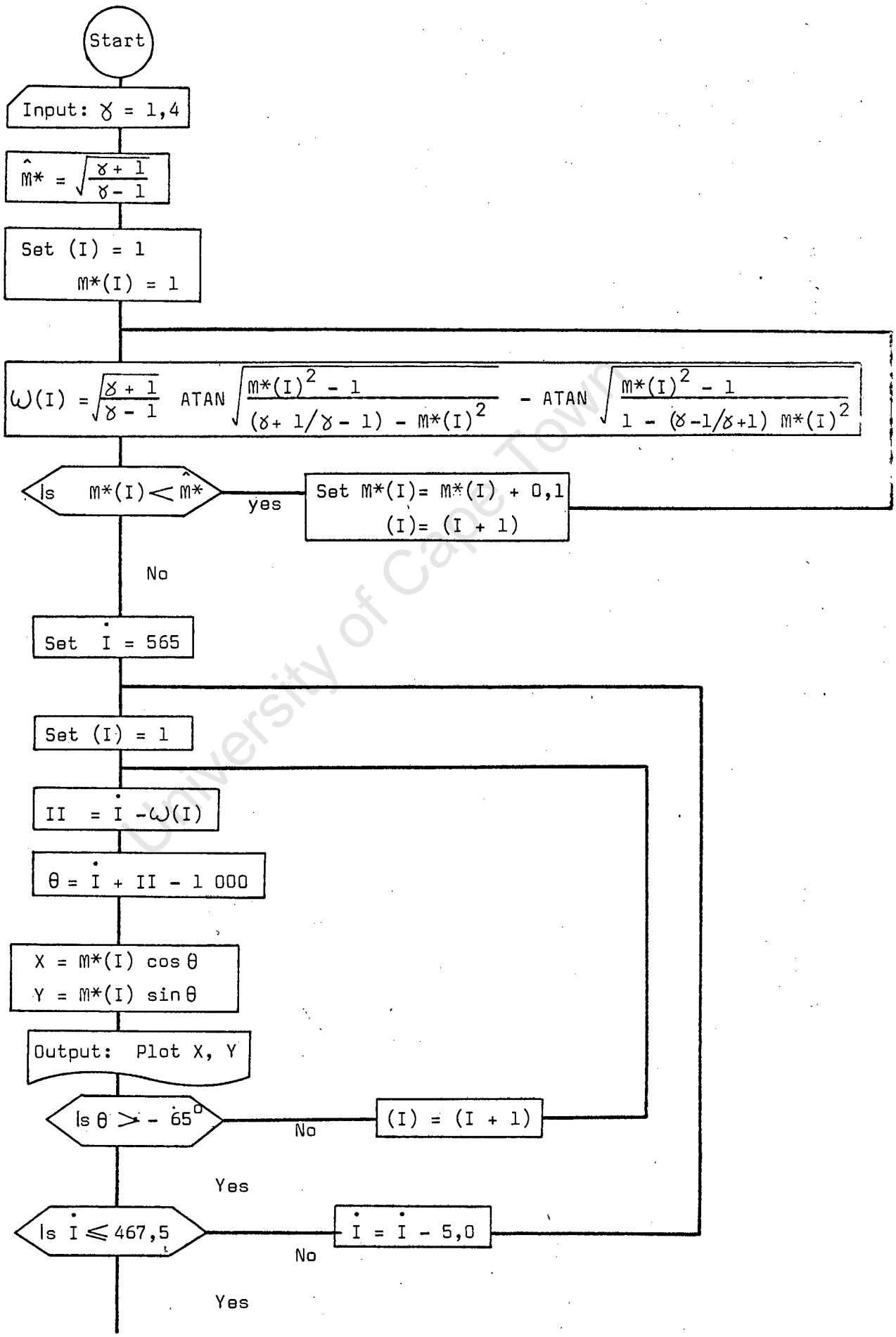

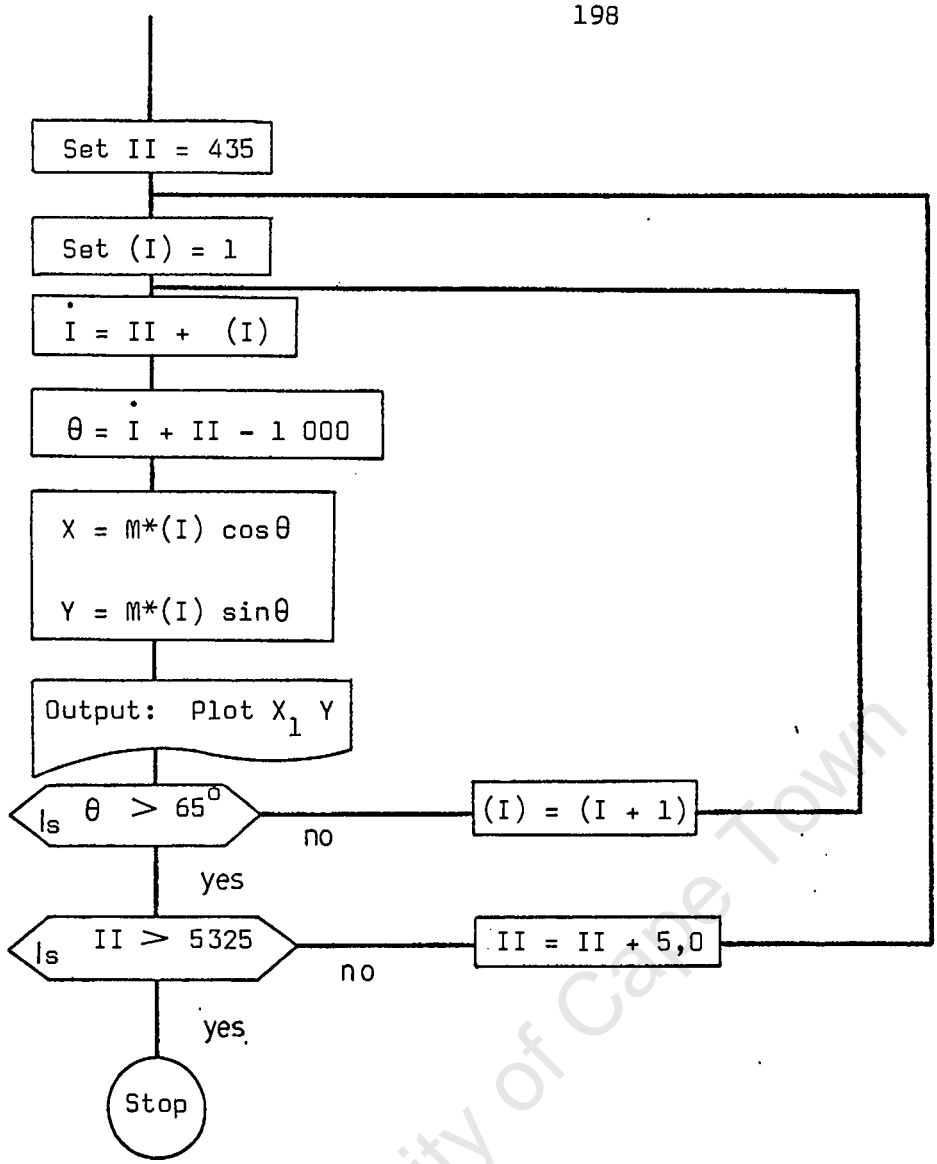

INSTRUCTION PROGRAM

```
C
C       HODOGRAPH CHARACTERISTICS APPLICABLE TO NOZZLE DESIGN
C
      REAL M(200),MAL(200),K,LL,LIM
      DIMENSION W(200),DEGRE(4)
      K=1.4
C     INSTRUCTIONS FOR GRAPH AXES
      CALL FPLOT(2,0.,0.)
      CALL SCALF(10.0,10.0,-0.5,-1.5)
      CALL FGRID(0,0.,0.,1.0,1)
      CALL FGRID(0,1.0,0.,0.1,10)
      CALL FPLOT(-2,0.,0.)
      THETA=45.0
  315 XAX=COS(THETA/57.3)
      YAX=SIN(THETA/57.3)
      CALL FPLOT(0,XAX,YAX)
      IF(THETA+45.0)300,300,310
  310 THETA=THETA-1.0
      GO TO 315
  300 CALL FPLOT(0,0.,0.)
```

```
C       EVALUATION OF W IN TERMS OF M* AND M
        I=1
        M(1)=1.0
        AA=(K+1.0)/(K-1.0)
        AB=SQRT(AA)
  120   AC=(M(I)**2.0)-1.0
        AD=AA-(M(I)**2.0)
        AE=1.0-((M(I)**2.0)/AA)
        AF=SQRT(AC/AD)
        AG=SQRT(AC/AE)
        BA=AB*57.3*ATAN(AF)
        BB=57.3*ATAN(AG)
        W(I)=BA-BB
        BC=(2.0*(M(I)**2.0))/(K+1.0)
        MAL(I)=SQRT(BC/AE)
        IF(M(I)-2.0)100,110,110
  100   I=I+1
        M(I)=M(I-1)+0.01
        GO TO 120
  110   L=I
C       PLOTTING OF CURVES
        CI=518.0
        LIM=0.3
  320   CALL FPLOT(1,0.,0.)
        J=(-2)
        DO 4 I=1,L
```



```
        CII=CI-W(I)
        THETA=CI+CII-1000.0
        X=M(I)*COS(THETA/57.3)
        Y=M(I)*SIN(THETA/57.3)
        CALL FPLOT(J,X,Y)
        J=0
        IF(Y+LIM)325,325,4
    4   CONTINUE
  325   CALL FCHAR((X+0.01),Y,0.10,0.10,0)
        WRITE(7,500)CI
  500   FORMAT(F4.0,'I')
        IF(CI-500.0)330,330,340
  340   CI=CI-1.0
        LIM=LIM+0.04
        GO TO 320
  330   CII=482.0
        LIM=0.3
  350   CALL FPLOT(1,0.,0.)
        J=(-2)
        DO 5 I=1,L
        CI=CII+W(I)
        THETA=CI+CII-1000.0
        X=M(I)*COS(THETA/57.3)
        Y=M(I)*SIN(THETA/57.3)
```

```
      CALL FPLOT(J,X,Y)
      J=0
      IF(Y-LIM)5,360,360
    5 CONTINUE
  360 CALL FCHAR((X+0.01),Y,0.10,0.10,0)
      WRITE(7,510)CII
  510 FORMAT(F4.0,'II')
      IF(CII-500.0)370,380,380
  370 CII=CII+1.0
      LIM=LIM+0.04
      GO TO 350
C     FOR NOZZLE ANGLES OF 6,9,18 DEGREES
  380 DEGRE(1)=6.0
      DEGRE(2)=9.0
      DEGRE(3)=18.0
      DO 7 I=1,3
      CALL FPLOT(1,0.,0.)
      Y=2.1*(SIN(DEGRE(I)/57.3)/COS(DEGRE(I)/57.3))
      CALL FPLOT(2,2.1,Y)
      CALL FCHAR(2.1,Y,0.10,0.10,0)
      WRITE(7,700)DEGRE(I)
  700 FORMAT(F5.1,' DEGREES')
    7 CONTINUE
      CALL FCHAR(-0.05,-0.05,0.10,0.10,0)
      WRITE(7,710)
  710 FORMAT('ORIGEN')
      LL=0.96
      I=1
  750 CALL FCHAR(LL,-0.05,0.10,0.10,0)
      WRITE(7,720)MAL(I)
  720 FORMAT(F7.3)
      IF(M(I)-1.95)730,740,740
  730 I=I+10
      LL=LL+0.1
```



```
      GO TO 750
  740 CALL FCHAR(1.1,0.3,0.5,0.5,0)
      WRITE(7,760)
  760 FORMAT('I')
      CALL FCHAR(1.1,-0.3,0.5,0.5,0)
      WRITE(7,770)
  770 FORMAT('II')
      CALL FCHAR(0.0,-1.0,0.25,0.25,0)
      WRITE(7,780)
  780 FORMAT('HODOGRAPH CURVES APPLICABLE TO NOZZLE DESIGN')
      CALL FCHAR(0.1,-1.1,0.15,0.15,0)
      WRITE(7,785)
  785 FORMAT('AXES IN TERMS OF THETA AND MACH NUMBER M')
      CALL EXIT
      END
```

1.4 NOZZLE DESIGN LIMITS

For the following discussion, assume that the first Mach line is reflected twice. If the expansion section curvature is finite, then an infinite number of reflections would occur between points 6 and 7 in figure 1.12. Hence to meet the stipulation that only two backward reflections occur, points 7 and 5 must coincide at a corner.

Rewriting equations 1.9 and 1.10:

$$\theta_I = -\omega(M^*) + 2I - 1\,000$$

$$\theta_{II} = +\omega(M^*) + 2II - 1\,000$$

From figure 1.12(b);

$$\theta_6 = \theta_4 = \theta_1 = 0$$

Substituting into the above equations:

$$\therefore |\theta_5| = \omega_5 - \omega_6 = \omega_4 - \omega_5$$

$$|\theta_3| = \omega_1 - \omega_3 = \omega_3 - \omega_4$$

These may be simplified to:

$$\omega_1 - \omega_3 + \omega_5 - \omega_6 = \omega_3 - \omega_4 + \omega_4 - \omega_5$$

$$\therefore \omega_1 - \omega_6 = \omega_3 - \omega_5 + \omega_3 - \omega_4 + \omega_4 - \omega_5$$

$$= 2\omega_3 - 2\omega_5$$

$$= (2\omega_3 - 2\omega_4) + (2\omega_4 - 2\omega_5)$$

$$= 2|\theta_3| + 2|\theta_5|$$

Furthermore, $\omega_6 = 0$

$$\therefore \omega_1 = 2|\theta_3| + 2|\theta_5|$$

$$\text{and } \frac{|\theta_3|}{\omega_1/2} = 1 - \frac{|\theta_5|}{\omega_1/2} = 1 - 2\frac{\omega_5}{\omega_1} \quad \ldots\ldots\ldots\ldots\ldots\ldots\ldots\ldots \quad 1.11$$

Also, from the geometry of the nozzle:

$$|\theta_3| - |\theta_5| \geqslant 0$$

But from 1.11:

$$|\theta_3| - |\theta_5| = \frac{\omega_1}{2} - 2|\theta_5|$$

And $|\theta_5|$ must be greater than zero:

Hence, these two equations give:

$$\frac{\omega_1}{2} - 2|\theta_5| \geqslant 0$$

$$\text{or} \quad 0 \leqslant |\theta_5| \leqslant \frac{\omega_1}{4} \; ; \quad 0 \leqslant \omega_5 \leqslant \frac{\omega_1}{4} \quad \ldots\ldots\ldots\ldots\ldots\ldots\ldots\ldots \quad 1.12$$

Substitute into equation 1.11:

$$\therefore 1 \geqslant \frac{|\theta_3|}{1/2} \geqslant \frac{1}{2} \quad \ldots\ldots\ldots\ldots\ldots\ldots\ldots\ldots \quad 1.13$$

1.5 TABLES FOR SEMI-GRAPHICAL NOZZLE DESIGN

TABLE 1.1 for figure 1.19(b)

Field	I	II	ω	θ	α	$\theta+\alpha$	$\theta-\alpha$
1	500	500	0^o	0^o	90,00	90,00	-90,00
2	501	500	1^o	1^o	69,57	68,57	-66,57
3	502	500	2^o	2^o	62,00	64,00	-60,00
4	503	500	3^o	3^o	58,18	61,18	-55,18
5	504	500	4^o	4^o	55,20	59,20	-51,20
6	505	500	5^o	5^o	52,74	57,74	-47,74
7	501	499	2^o	0^o	62,00	62,00	-62,00
8	502	499	3^o	1^o	58,18	59,18	-57,18
9	503	499	4^o	2^o	55,20	57,20	-53,20
10	504	499	5^o	3^o	52,74	55,74	-49,74
11	505	499	6^o	4^o	50,62	54,62	-46,62
12	502	498	4^o	0^o	55,20	55,20	-55,20
13	503	498	5^o	1^o	52,74	53,74	-51,74
14	504	498	6^o	2^o	50,62	52,62	-48,62
15	505	498	7^o	3^o	48,75	51,75	-45,75
16	503	497	6^o	0^o	50,62	50,62	-50,62
17	504	497	7^o	1^o	48,75	49,75	-47,75
18	505	497	8^o	2^o	47,08	49,08	-45,08
19	504	496	8^o	0^o	47,08	47,08	-44,08
20	505	496	9^o	1^o	45,57	46,57	-44,57
21	505	495	10^o	0^o	44,18	44,18	-44,18
22	506	500	6^o	6^o	50,62	56,62	-44,62
23	506	499	7^o	5^o	48,75	53,75	-43,75
25	506	498	8^o	4^o	47,08	51,08	-43,08
28	506	497	9^o	3^o			
32	506	496	10^o	2^o	44,18	46,18	-42,18
37	506	495	11^o	1^o	42,89	43,89	-41,89
43	506	494	12^o	0^o	41,70	41,70	-41,70

11-15	54,62	51,75	53,19
15-18	51,75	49,08	50,42
18-20	49,08	46,57	47,82
20-21	46,57	44,18	45,37

TABLE 1,2 for figure 1,19(a)

Wave	Right-running Mach wave			Left-running Mach wave		
	Upstream $(\theta+\alpha)$	Downstream $(\theta+\alpha)$	Mean $(\theta+\alpha)$	Upstream $(\theta-\alpha)$	Downstream $(\theta-\alpha)$	Mean $(\theta-\alpha)$
1-2				-90,00	-66,57	-78,29
2-3				-66,57	-60,00	-63,29
3-4				-60,00	-55,18	-57,59
4-5				-55,18	-51,20	-53,19
5-6				-51,20	-47,74	-49,47
6-22				-47,74	-44,62	-46,18
7-8				-62,00	-57,18	-59,59
8-9				-57,18	-53,20	-55,19
9-10				-53,20	-49,74	-51,47
10-11				-49,74	-46-62	-48,18
11-23				-46,62	-43,75	-45,19
12-13				-55,20	-51,74	-53,47
13-14				-51,74	-48,62	-50,18
14-15				-48,62	-45,75	-47,19
15-25				-45,75	-43,08	-44,42
16-17				-50,62	-47,75	-49,19
17-18				-47,75	-45,08	-46,42
18-28				-45,08	-42,57	-43,82
19-20				-44,08	-44,57	-44,32
20-32				-44,57	-42,18	-43,37
21-37				-44,18	-41,89	-43,04
2-7	68,57	62,00	65,29			
3-8	64,00	59,18	61,59			
8-12	59,00	55,20	57,19			
4-9	61,18	57,20	59,19			
9-13	57,20	53,74	55,47			
13-16	53,74	50,62	52,18			
5-10	59,20	55,74	57,47			
10-14	55,74	52,62	54,18			
14-17	52,62	49,75	51,19			
17-19	49,75	47,08	48,42			
6-11	57,74	54,62	56,18			

1.7 FOELSCH'S METHOD OF NOZZLE DESIGN

Refer to figure 1.22, where radial source flow exists.

Consider two-dimensional flow of unit width. Therefore where $r > r_*$ (supersonic region), the streamlines are straight, diverging from the apparent origin O. From this source the uniform mass flow, per radian of angle, can be assumed constant.

i.e. $r\rho g$ = constant

The one dimensional Mach number - area relationship can be used to define the Mach number M at points a distance r from the source O.

$$\therefore \quad A(M) = \frac{rd\theta}{r_* d\theta} = \frac{1}{M}\left(\frac{1 + \frac{\gamma-1}{2}M^2}{\frac{\gamma+1}{2}}\right)^{\gamma+1/2(\gamma-1)} = \frac{r}{r_*} \quad \text{.....} \quad 1.19$$

From continuity, the mass flow rate from the apparent source (or more accurately from the nozzle throat) is equal to the mass flow rate through the nozzle.

$$\therefore \quad \rho_* q_* r_* \theta_i = \rho_* q_* y_*$$

$$\therefore \quad r_* = \frac{y_*}{\theta_i} \quad \text{.....} \quad 1.20$$

The co-ordinates on charateristic C_-^i, $(X', y')_1$ are given by:

$$X^1 = r\cos\theta \; ; \; y^1 = r\sin\theta \quad \text{.....} \quad 1.21$$

Also the Mach characteristic, QP, is of constant perturbation potential. Hence the flow parameters are also constant along this line.

i.e. $M = M_Q = M_P$; $\theta = \theta_Q = \theta_P$

$$\bar{\alpha} = \bar{\alpha}_Q = \bar{\alpha}_P; \; \rho + \rho_Q = \rho_P$$

$$q = q_Q = q_P$$

From the hodograph relationship given in equation 1.9 for left-running characteristic waves:

$$\theta_I = -\omega(M^*) + (2I - 1\,000)$$

Where I defines θ as being constant on Mach waves of family I.

$$\therefore \theta_I + \omega = \text{constant} \quad \ldots\ldots\ldots\ldots\ldots\ldots\ldots\ldots\ldots\ldots \quad 1.22$$

(The hodograph streamline I, is constant for left-running waves)

Hence $\theta_p + \omega_p = \theta_e + \omega_e = \theta + \omega$

Since $\theta_e = 0$ (parallel flow) and $\omega_e = \omega_1$, then:

$$\theta = \omega_1 - \omega \quad \ldots\ldots\ldots\ldots\ldots\ldots\ldots\ldots\ldots\ldots\ldots\ldots\ldots\ldots \quad 1.23$$

The angle that the C^+ characteristic makes with the nozzle axis, is given as $\theta + \bar{\alpha}$ for left-running waves.

Therefore the slope of this wave is given as:

$$\frac{dy}{dX} = \tan(\theta + \bar{\alpha})$$

Hence, the norizontal and vertical distances respectively from points X^1 and Y^1 to the nozzle contour is given by:

$$X - X^1 = \overline{QP} \cos(\theta + \bar{\alpha}) \quad \ldots\ldots\ldots\ldots\ldots\ldots\ldots\ldots\ldots\ldots \quad 1.24$$

$$y - y^1 = \overline{QP} \sin(\theta + \bar{\alpha}) \quad \ldots\ldots\ldots\ldots\ldots\ldots\ldots\ldots\ldots\ldots \quad 1.25$$

The mass flow rate across IQ is given by $r\rho q(\theta_i - \theta)$. But, from continuity, this same mass flow rate must cross PQ. This is given by:

$$\overline{QP}\,\rho\, q \sin\bar{\alpha}$$

(See figure 1,23)

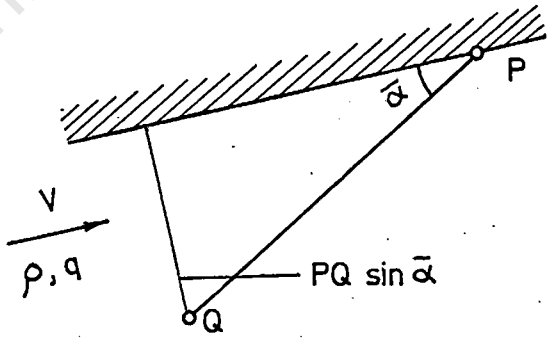

Figure 1.23

$$\therefore \overline{QP} \sin\bar{\alpha} = r(\theta_i - \theta) \quad \ldots\ldots\ldots\ldots\ldots\ldots\ldots\ldots\ldots\ldots \quad 1.26$$

From equations 1.19, 1.20 and 1.26, we obtain:

$$\overline{QP} = \frac{y_* A(M)}{\sin\bar{\alpha}} \left(\frac{\theta_i - \theta}{\theta_i}\right) \quad \ldots\ldots\ldots\ldots\ldots\ldots\ldots\ldots\ldots\ldots \quad 1.27$$

Finally, the Mach direction $\bar{\alpha}$ is given by:

$$\sin \bar{\alpha} = \frac{1}{M} \qquad \text{from (3)}$$

The final parametric equations defining the nozzle contour between $X_i \leqslant X \leqslant X_e$, are produced as follows.

From equation 1,24:

$$X = \overline{QP} \cos(\theta + \bar{\alpha}) + X^1$$

Substitute for $\overline{QP}$ and X^1 from equations 1,27 and 1.21 respectively:

$$\therefore = \frac{y_* A(M)}{\sin \bar{\alpha}} \left(\frac{\theta_i - \theta}{\theta_i}\right) \cos(\theta + \bar{\alpha}) + r \cos\theta$$

But from equations 1.19 and 1.20:

$$r = A(M) \frac{y_*}{\theta_i}$$

Substituting for r in the above equation:

$$\therefore X = \frac{y_* A(M)}{\sin \bar{\alpha}} \left(\frac{\theta_i - \theta}{\theta_i}\right) \cos(\theta + \bar{\alpha}) + \frac{Y_* A(M)}{\theta_i} \cos\theta$$

Here $\cos(\theta + \bar{\alpha}) = \cos\theta \cos\bar{\alpha} - \sin\theta \sin\bar{\alpha}$

And; $\sin \bar{\alpha} = \frac{1}{M}$

$$\cos \bar{\alpha} = \frac{\sqrt{M^2 - 1}}{M}$$

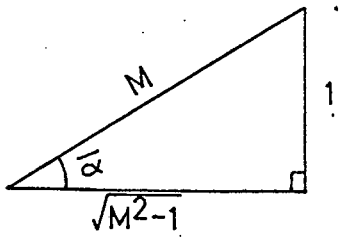

Substitute in the above equation:

$$\therefore X = \frac{y_* A(M)}{\theta_i} (\theta_i - \theta) \left\{ \sqrt{M^2 - 1} \cos\theta - \sin\theta \right\} + \frac{y_* A(M)}{\theta_i} \cos\theta$$

Rearranging this equation gives the X co-ordinate of the nozzle cancelling profile:

$$\frac{X}{y_*} = \frac{A(M)}{\theta_i} \left\{ \cos\theta + \left[\left(\sqrt{M^2 - 1} \cos\theta - \sin\theta \right)(\theta_i - \theta) \right] \right\} \ldots\ldots\ldots \quad 1.28(a)$$

Similarly, the corresponding y co-ordinate is given as:

$$\frac{y}{y_*} = \frac{A(M)}{\theta_i} \left\{ \sin\theta + \left[\left(\sqrt{M^2 - 1} \sin\theta + \cos\theta \right)(\theta_i - \theta) \right] \right\} \ldots\ldots \quad 1.28(b)$$

Where $\theta = \omega_1 - \omega$

1.8 SUBSONIC INLET DESIGN

The acceleration of the air is chosen to follow a full cosine curve the maximum defined by a constant C.

i.e. $\frac{d\hat{v}}{dt} = C$ (See figure 1.26)

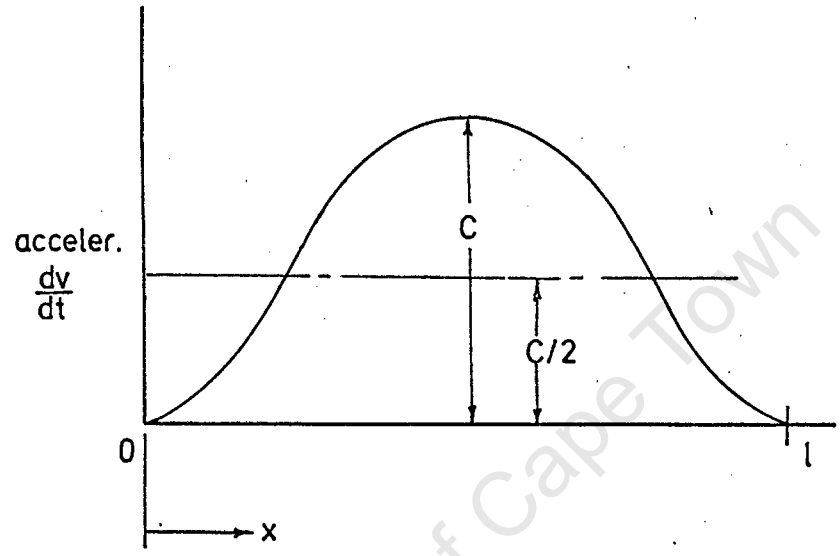

FIGURE 1.26

The acceleration at any point is:

$$\text{Acc.} = \frac{dv}{dt} = \frac{C}{2} \cos 2\pi \frac{X}{l} + \frac{C}{2}$$

$$= \frac{C}{2}\left(1 - \cos 2\pi \frac{X}{l}\right)$$

but $\frac{\partial v}{\partial t} = \frac{dv}{dX} \cdot \frac{dX}{dt} = \frac{dv}{dX} \cdot V$

$$\therefore \quad v \frac{dv}{dX} = \frac{C}{2}\left(1 - \cos 2\pi \frac{X}{l}\right)$$

or $$vdv = \frac{C}{2}\left(1 - \cos 2\pi \frac{X}{l}\right) dX$$

Integrate this equation between the boundary 1, and any point within the section:

$$\therefore \int_{v_1}^{v} vdv = \int_{X_1}^{X} \frac{C}{2}\left(1 - \cos 2\pi \frac{X}{l}\right) dX$$

For $X_1 = 0$,

For $X_1 = 0$,

$$\therefore \frac{1}{2}\left\{v^2 - v_1^2\right\} = \frac{C}{2}\left\{X - \frac{l}{2\pi}\sin 2\frac{X}{l}\right\} \quad \text{.....} \quad 1.32$$

To find the valve of the constant C, it is necessary to apply boundary conditions to equation 1.32.

i.e. $X_1 = 0; \quad v = v_1$

$X_2 = l; \quad v = v_2$

$$\therefore \frac{1}{2}\left\{v_1^2 - v_1^2\right\} = \frac{C}{2}\left\{(0) - \frac{l}{2\pi}(0)\right\}$$

or $$\frac{1}{2}\left\{v_2^2 - v_1^2\right\} = \frac{C}{2}\left\{l - \frac{l}{2\pi}\sin \cancel{2\pi}^{0}\right\}$$

$$\therefore \frac{C}{2} = \frac{1}{2l}\left\{v_2^2 - v_1^2\right\}$$

From the continuity equation:

$$Q = v_2 y_2 = v_1 y_1$$

$$\therefore C = \frac{Q^2}{l}\left\{\frac{1}{y_2^2} - \frac{1}{y_1^2}\right\} \quad \text{.....} \quad L.33$$

1.9 PROGRAMME FOR NOZZLE PROFILE

INSTRUCTION PROGRAM

```
C
C                NOZZLE PROFILE FOR UNIFORM FLOW AT THE REQUIRED
C                          MACH NUMBER
C
C                SETTING GRAPH AXES,SCALES AND REQUIRED CONSTANTS
C
      REAL LI,LT,LE,LS,LL,INF
      REAL N
      REAL M
      REAL L
      M=2.35
      P=1.4
      Q=15.0
      R=2.5625
      S=2.00
      K=1
      RT=2.0*R
      RS=R+S
      RR=R-S
      RU=R-0.5
C          PLOTTER ROUTINE
      CALL FPLOT(2,0.,0.)
      CALL SCALF(0.5,2.,-10.,-4.)
      CALL FGRID(0,0.,0.,1.0,30)
      CALL FGRID(1,0.,0.,0.25,22)
      CALL FGRID(2,0.,0.,1.0,15)
      CALL FGRID(0,0.,R,30.,1)
      CALL FGRID(2,0.,R,15.,1)
      CALL FGRID(0,0.,RT,1.0,30)
      CALL FGRID(2,0.,RT,1.0,15)
C          SCALE ROUTINE
      L=0.0
      N=-0.40
   30 CALL FCHAR(N,-0.25,0.10,0.10,0)
      WRITE(7,17)L
   17 FORMAT(F5.1)
      IF(L-30)23,24,24
   23 L=L+1.0
      N=N+1.0
      GO TO 30
   24 L=-1.0
      N=-1.40
  350 CALL FCHAR(N,-0.25,0.10,0.10,0)
      WRITE(7,170)L
  170 FORMAT(F5.1)
```

```
AGE   2

      IF(L+15)370,370,270
  270 L=L-1.0
      N=N-1.0
      GO TO 350
  370 L=0.25
      N=0.20
  460 CALL FCHAR(0.25,N,0.10,0.10,0)
      WRITE(7,380)L
  380 FORMAT(F4.2)
      IF(L-5.5)390,395,395
  390 L=L+0.25
      N=N+0.25
      GO TO 460
  395 CALL FCHAR(-2.0,-2.0,0.25,0.25,0)
      WRITE(7,20)
   20 FORMAT('SUPERSONIC NOZZLE PROFILE')
      V=M
      CALL FCHAR(0.0,-2.5,0.18,0.18,0)
      WRITE(7,19)V
   19 FORMAT('UNIFORM MACH NUMBER IS',F5.2)
      J=(-2)
      CALL FPLOT(J,30.0,RR)
      J=0
      WRITE(5,100)V
  100 FORMAT(1H ,'                              TEST SECTION MACH NUMBER IS',F5.2)
C     CONSTANT AREA RATIO
      AA=1.0/V
      AB=P+1.0
      AC=P-1.0
      AD=AB/(2.0*AC)
      AE=(AC/2.0)*(V**2.0)
      AF=(2.0/AB)*(1.0+AE)
      AG=AF**AD
      A=AA*AG
      HT=S/A
C     CONSTANT MACH ANGLE
      BD=(V**2.0)-1.0
      BE=SQRT(AB/AC)
      BF=SQRT((AC/AB)*BD)
      BG=SQRT(BD)
      BH=BE*57.3*ATAN(BF)
      BI=57.3*ATAN(BG)
      W=0.0175*(BH-BI)
      T=W
      U=T/4.0
C     EXIT POINT LE
      FA=U*SQRT(BD)
      FB=1.0+FA
      LE=(2.00*FB)/U

C              CANCELLATION SECTION
C
      WRITE(5,610)
  610 FORMAT(1HO,'CANCELLATION SECTION')
      WRITE(5,101)
  101 FORMAT(1HO,'X COORD. FLOW GAP  Y COORD.          M          A
     C     W')
C          AREA RATIO
```

```
AGE   3

  800 IF(K-2)2,2,700
  700 J=(-2)
      M=V
      CALL FPLOT(1,30.0,RS)
      CALL FPLOT(J,30.0,RS)
      J=0
      GO TO 2
    2 AA=1.0/M
      AB=P+1.0
      AC=P-1.0
      AD=AB/(2.0*AC)
      AE=(AC/2.0)*(M**2.0)
      AF=(2.0/AB)*(1.0+AE)
      AG=AF**AD
      A=AA*AG
C          MACH ANGLE
      BD=(M**2.0)-1.0
      BE=SQRT(AB/AC)
      BF=SQRT((AC/AB)*BD)
      BG=SQRT(BD)
      BH=BE*57.3*ATAN(BF)
      BI=57.3*ATAN(BG)
      W=0.0175*(BH-BI)
      Z=T-W
      B=COS(Z)
      C=SIN(Z)
      D=SQRT((M**2.0)-1.0)
      E=(A*HT)/U
      F=U-Z
C          COORDINATES
      CA=D*B
      CB=CA-C
      CD=CB*F
      CE=B+CD
      X=E*CE
      CF=D*C
      CG=CF+B
      CH=CG*F
      CI=C+CH
      YIN=E*CI
      Y=R-YIN
      IF(K-2)710,710,720
  720 YM=R+YIN
      CALL FPLOT(J,X,YM)
      GO TO 730
  710 WRITE(5,110)X,YIN,Y,M,A,W
  110 FORMAT(1H0,F7.3,3X,F6.3,3X,F6.3,12X,F5.2,4X,F5.3,4X,F7.3)
      CALL FPLOT(J,X,Y)
  730 IF(U-Z)10,10,11
   11 M=M-0.01
      GO TO 2
C
C                EXPANSION SECTION
C
C     INFLECTION POINT LI
   10 LI=X
      THROAT POINT LT
      EA=(HT/2.0)
```

```
'AGE   4

      EB=(LI/HT)
      EC=COS(U)
      ED=SIN(U)
      EE=3.0*(EC/ED)
      EF=EB-EE
      LT=-EA*EF
      IF(K-2)775,775,740
  740 GO TO 3
  775 WRITE(5,620)
  620 FORMAT(1HO,'EXPANSION SECTION')
      WRITE(5,202)
  202 FORMAT(1HO,'X COORD. FLOW GAP  Y COORD.')
      DA=LI-LT
      CST=(HT*(SIN(U)/COS(U)))/DA
    3 DB=X-LT
      DC=DB/(3.0*DA)
      DD=1.0-DC
      DE=DB/HT
      DF=CST*DD*(DE**2.0)
      YIN=HT*(1.0+DF)
      Y=R-YIN
      IF(K-2)750,750,760
  760 YM=R+YIN
      CALL FPLOT(J,X,YM)
      GO TO 770
  750 WRITE(5,201)X,YIN,Y
  201 FORMAT(1HO,F7.3,3X,F6.3,3X,F6.3)
      CALL FPLOT(J,X,Y)
  770 IF(X-LT)12,13,13
   13 X=X-0.25
      GO TO 3

                SUBSONIC INLET

   12 IF(K-2)810,810,780
  780 GO TO 790
  810 WRITE(5,630)
  630 FORMAT(1HO,'SUBSONIC INLET')
      SET=(1.0/(HT**2.0))-(1.0/(R**2.0))
      LS=Q-LT
      WRITE(5,250)
  250 FORMAT(1HO,'X COORD. FLOW GAP  Y COORD.')
  790 LL=Q
    9 PT=(LL/Q)-((1.0/6.2832)*SIN(6.2832*(LL/Q)))
      QT=SET*PT
      RT=QT+(1.0/(R**2.0))
      YIN=SQRT(1.0/RT)
      Y=R-YIN
      X=LL-LS
      IF(K-2)830,830,840
  840 YM=R+YIN
      CALL FPLOT(J,X,YM)
      GO TO 850
  830 WRITE(5,300)X,YIN,Y
  300 FORMAT(1HO,F7.3,3X,F6.3,3X,F6.3)
      CALL FPLOT(J,X,Y)
  850 IF(LL-0)15,15,16
   16 LL=LL-0.25
```

```
      GO TO 9
   15 IF(K-2)860,860,870
  860 K=4
      GO TO 800
C
C     GRAPH AXES AND SCALES
C
  870 CALL FCHAR(X,RU,0.10,0.10,0)
      WRITE(7,510)
  510 FORMAT('                                        SUBSONIC INLET').
      CALL FCHAR(LT,RU,0.10,0.10,0)
      WRITE(7,520)
  520 FORMAT('   EXPANSION SECTION')
      CALL FCHAR(LI,RU,0.10,0.10,0)
      WRITE(7,530)
  530 FORMAT('   CANCELLATION SECTION')
      CALL FCHAR(LE,RU,0.10,0.10,0)
      WRITE(7,540)
  540 FORMAT('      TEST SECTION')
      INF=57.3*U
      GAP=2.0*HT
      CALL FCHAR(14.0,-2.0,0.10,0.10,0)
      WRITE(7,550)INF,GAP
  550 FORMAT('INFLECTION ANGLE IS',F6.2,' DEGREES , THROAT GAP IS',F6.3,
     C' INCHES')
      WRITE(5,200)U,HT,LT,LI,LE
  200 FORMAT(1HO,'INFLECTION ANGLE',F6 .3,' RADIANS',//,1H ,'THROAT HEIG
     CHT',F6.3,' INCHES',//,1H ,'THROAT LENGTH',F6.3,' INCHES',//,1H ,'I
     CNFLECTION LENGTH',F7.3,' INCHES',//,1H ,'EXIT LENGTH',F7.3,' INCHE
     CS')
      CALL FGRID(1,X,RU,1.0,1)
      CALL FGRID(1,LT,RU,1.0,1)
      CALL FGRID(1,LI,RU,1.0,1)
      CALL FGRID(1,LE,RU,1.0,1)
      CALL FGRID(1,30.0,RU,1.0,1)
      CALL FCHAR(14.0,-2.5,0.18,0.18,0)
      WRITE(7,560)
  560 FORMAT('SCALE*')
      CALL FCHAR(17.0,-2.5,0.10,0.10,0)
      WRITE(7,570)
  570 FORMAT('HORIZONTAL AXIS*HALF FULL SIZE*INCHES')
      CALL FCHAR(17.0,-2.75,0.10,0.10,0)
      WRITE(7,580)
  580 FORMAT('VERTICAL AXIS*TWICE FULL SIZE*INCHES')
      CALL EXIT
      END
```

SAMPLE SOLUTION

TEST SECTION MACH NUMBER IS 2.35

CANCELLATION SECTION

X COORD.	FLOW GAP	Y COORD.	M	A	W
17.120	1.999	0.562	2.35	2.295	0.621
16.817	1.999	0.563	2.34	2.274	0.617
16.520	1.997	0.564	2.32	2.253	0.613
16.228	1.994	0.568	2.31	2.233	0.608
15.941	1.990	0.572	2.30	2.213	0.604

EXPANSION SECTION

X COORD.	FLOW GAP	Y COORD.
9.271	1.452	1.109
9.021	1.413	1.148
8.771	1.374	1.187
8.521	1.335	1.226
8.271	1.297	1.264

SUBSONIC INLET

X COORD.	FLOW GAP	Y COORD.
3.705	0.871	1.691
3.455	0.871	1.691
3.205	0.871	1.691
2.955	0.871	1.690
2.705	0.872	1.690

INFLECTION ANGLE 0.155 RADIANS

THROAT HEIGHT 0.871 INCHES

THROAT LENGTH 3.705 INCHES

INFLECTION LENGTH 9.271 INCHES

EXIT LENGTH 17.120 INCHES

1.10 PROGRAMME FOR BOUNDARY LAYER CORRECTION

INSTRUCTION PROGRAM

```
C
C          BOUNDARY LAYER CONSIDERATIONS ON NOZZLE PROFILE
C                    MACH NUMBER = 2.35
C
      REAL LE,LT,M,K,LEN,MAC,L,N,MOC
      DIMENSION X(200),Y(200),XCR(200),YCR(200)
C
C     CHARACTERISTICS FOR MACH NUMBER = 2.35
      M=2.35
      LE=17.12
      LT=3.705
      W=2.00
      HT=0.871
      T=545.0
      P=40.0
      RAT=0.4752
      RAD=0.15564
C     CONSTANTS FOR STANDARD AIR
      U=3.716E-07
      K=1.4
      G=32.2
      R=53.3
C     INSTRUCTIONS FOR PLOTTER SCALES
      CALL FPLOT(2,0.,0.)
      CALL SCALF(1.0,1.0,-2.,-15.)
      CALL FGRID(0,0.,0.,1.0,45)
      CALL FGRID(1,0.,0.,0.5,7)
      CALL FGRID(3,0.,0.,0.5,7)
      L=1.0
      N=0.60
   30 CALL FCHAR(N,-0.25,0.10,0.10,0)
      WRITE(7,10)L
   10 FORMAT(F5.1)
      IF(L-45)15,20,20
   15 L=L+1.0
      N=N+1.0
      GO TO 30
   20 L=3.5
      N=3.4
   50 CALL FCHAR(-0.75,N,0.10,0.10,0)
      WRITE(7,35)L
   35 FORMAT(F5.2)
      IF(L+3.50)45,45,40
   40 L=L-0.5
      N=N-0.5
      GO TO 50
```

```
PAGE   2    RORY COX

   45 CALL FCHAR(5.0,-10.0,0.25,0.25,0)
      WRITE(7,55)
   55 FORMAT('SUPERSONIC NOZZLE PROFILE FOR MACH NUMBER OF 2.35')
      CALL FCHAR(5.0,-10.5,0.20,0.20,0)
      WRITE(7,60)
   60 FORMAT('WITH BOUNDARY LAYER CONSIDERATIONS')
      CALL FCHAR(25.0,-11.0,0.20,0.20,0)
      WRITE(7,65)
   65 FORMAT('SCALE   FULL SIZE,INCHES')
C
C     CALCULATION OF REYNOLDS NUMBER IN TEST SECTION
      DEN=(RAD*P*144.0)/(R*T)
      V=M*SQRT(K*R*G*RAT*T)
      VIS=U*(RAT**0.76)
      LEN=(LE-LT)/12.0
      REN=((DEN*V*LEN)/(VIS*G))
      WRITE(5,100)
  100 FORMAT(1HO,'NOZZLE BLOCK COORDINATES FOR A MACH NUMBER OF 2.35',//
     C,1H ,'     WITH BOUNDARY ALLOWANCES')
      WRITE(5,110)DEN,V,VIS,LEN,REN
  110 FORMAT(1HO,'TEST SECTION DENSITY',E11.4,' LBS/CU FT',//,1H
     CELOCITY IN TEST SECTION',F7.1,' FT/SEC',//,1H ,'VISCOSITY OF
     CIR IN TEST SECTION ',E11.4,' SLUGS/FT SEC',//,1H ,'LENGTH FRO
     COAT TO TEST SECTION IS',F7.3,' FT',//,1HO,'REYNOLDS NUMBER
     CTEST SECTION IS',E13.6)
C
C     CORRECTION OF THE Y COORDINATES OF THE NOZZLE PROFILE
      WRITE(5,115)
  115 FORMAT(1HO,'COORD NUMBER  X COORD. BL THICK.  CORRECTED Y COO
     C         MACH NUMBER AT POINT X')
      J=(-2)
      READ(8,200)(X(I),Y(I),I=1,137)
  200 FORMAT(3F10.3,3F10.3)
      DO 2 I=1,137
      XCR(I)=X(I)+(15.0-LT)
      CALL FPLOT(J,XCR(I),Y(I))
      J=0
    2 CONTINUE
      CALL FPLOT(1,XCR(1),-Y(1))
      J=(-2)
      DO 3 I=1,137
      CALL FPLOT(J,XCR(I),-Y(I))
      J=0
    3 CONTINUE
      CALL FPLOT(1,0.00,3.0625)
      CALL FPLOT(2,43.0,3.0625)
      DO 4 I=1,137
      IF(XCR(I)-15.0)320,320,330
  330 IF(43.0-XCR(I))300,310,310
  300 GO TO 4
  310 MAC=1.0
      A=Y(I)/HT
      XA=2.0/(K-1.0)
      XB=(K+1.0)/2.0
      XC=2.0*(K-1.0)/(K+1.0)
  230 XD=MAC*A
      XE=XD**XC
      XF=XE*XB
```

```
      XG=XF-1.0
      XH=XA*XG
      MOC=SQRT(XH)
      ERR=MOC-MAC
      IF(ERR-0.001)210,220,220
  220 MAC=MOC
      GO TO 230
  210 YA=0.29/(REN**0.2)
      YB=0.088*MOC
      YC=YB+0.07
      YD=2.0*Y(I)
      YE=(W+YD)/W
      YF=YA*(X(I)-LT)*YC*YE
      YCR(I)=YF+Y(I)
      YBLOK=3.0625-YCR(I)
      WRITE(5,120)I,XCR(I),YBLOK,YCR(I),MOC
  120 FORMAT(I7,7X,F7.3,2X,F7.3,7X,F9.3,24X,F5.2)
      CALL FPLOT(J,XCR(I),YCR(I))
      GO TO 4
  320 YCR(I)=Y(I)
      YBLOK=3.0625-Y(I)
      WRITE(5,135)I,XCR(I),YBLOK,YCR(I)
  135 FORMAT(I7,7X,F7.3,2X,F7.3,7X,F9.3)
    4 CONTINUE
      CALL FPLOT(1,0.0,-3.0625)
      CALL FPLOT(2,43.0,-3.0625)
      DO 5 I=1,137
      IF(XCR(I)-15.0)340,340,350
  340 GO TO 5
  350 IF(43.0-XCR(I))360,370,370
  360 GO TO 5
  370 CALL FPLOT(J,XCR(I),-YCR(I))
    5 CONTINUE
C
C     GRAPH DETAILS
      CALL FGRID(1,15.0,-0.5,1.0,1)
      CALL FGRID(1,43.0,-0.5,1.0,1)
      CALL FCHAR(12.0,2.0,0.10,0.10,0)
      WRITE(7,70)
   70 FORMAT('UPPER NOZZLE BLOCK')
      CALL FCHAR(12.0,-2.0,0.1,0.1,0)
      WRITE(7,75)
   75 FORMAT('LOWER NOZZLE BLOCK')
      CALL FCHAR(14.4,1.0,0.1,0.1,0)
      WRITE(7,80)
   80 FORMAT('NOZZLE THROAT')
      CALL FGRID(1,(15.0+(LEN*12.0)),-0.5,1.0,1)
      CALL FCHAR((16.0+(LEN*12.0)),0.5,0.1,0.1,0)
      WRITE(7,85)
   85 FORMAT('SUPERSONIC TEST SECTION')
      CALL FCHAR(35.0,-11.0,0.1,0.1,0)
      WRITE(7,90)REN
   90 FORMAT('REYNOLDS NUMBER IN TEST SECTION IS',E13.6)
      CALL FCHAR(35.0,-11.5,0.1,0.1,0)
      BT=3.0625-HT
      WRITE(7,95)BT
   95 FORMAT('MATERIAL REQUIREMENTS-I NOZZLE BLOCKS 43.0 X 2.0 X',F6.3,'
     C INCHES')
```

PAGE 4 RORY COX

```
      CALL EXIT
      END
```

SAMPLE SOLUTION

NOZZLE BLOCK COORDINATES FOR A MACH NUMBER OF 2.35

WITH BOUNDARY ALLOWANCES

TEST SECTION DENSITY 0.3086E-01 LBS/CU FT

AIR VELOCITY IN TEST SECTION 1853.7 FT/SEC

VISCOSITY OF THE AIR IN TEST SECTION 0.2111E-06 SLUGS/FT SEC

LENGTH FROM THROAT TO TEST SECTION IS 1.117 FT

REYNOLDS NUMBER IN THE TEST SECTION IS 0.940874E 07

COORD NUMBER	X COORD.	BL THICK.	CORRECTED Y COORD.
2	43.000	0.790	2.271
3	42.000	0.800	2.262
4	41.000	0.810	2.252
5	40.000	0.819	2.242
6	39.000	0.829	2.232
7	38.000	0.839	2.223
8	37.000	0.848	2.213
9	36.000	0.858	2.203
10	35.000	0.868	2.194
11	34.000	0.878	2.184
12	33.000	0.887	2.174
13	32.000	0.897	2.164
14	31.000	0.907	2.155
15	30.000	0.916	2.145
16	29.000	0.926	2.135
17	28.415	0.933	2.129
18	28.111	0.936	2.126
19	27.814	0.941	2.121
20	27.522	0.947	2.115

1.11 PROGRAMMES FOR NOZZLE CALIBRATION

INSTRUCTION PROGRAM FOR EQU. 1.42

```
      STATIC PRESSURE CALIBRATION
      REAL MACH
      REAL K
      K=1.4
      WRITE(5,200)
  200 FORMAT(1H1,'WALL STATIC PRESSURE MEASUREMENTS')
      WRITE(5,210)
  210 FORMAT(1H0,'STAG.PRESSURE    DISPLACEMENTS    MACH NUMBER',//,1H ,
     C'   LBS/SQ.IN       HOR.X  VER.Y')
      DO 10 N=1,3
      READ(8,100)X,Y,PCS,PS,PB
  100 FORMAT(F5.2,F5.2,F10.2,F10.2,F10.2)
      P=(0.492*(PB-PS))
      RAT=PCS/P
      AA=2.0/(K-1.0)
      HA=(K-1.0)/K
      AB=(RAT**HA)
      HB=AB-1.0
      HC=AA*HB
      MACH=HC**0.5
      WRITE(5,110)PCS,X,Y,MACH
  110 FORMAT(1H0,F10.3,8X,F5.2,F6.2,7X,F6.3)
   10 CONTINUE
      CALL EXIT
      END
```

SAMPLE SOLUTION

MACH NUMBER SOLUTION 3

WALL STATIC PRESSURE MEASUREMENTS

STAG.PRESSURE	DISPLACEMENTS	MACH NUMBER
LBS/SQ.IN	HOR.X VER.Y	
40.240	15.00 20.00	1.800
55.340	16.00 20.00	2.222
56.780	17.00 20.00	1.659

INSTRUCTION PROGRAM FOR EQU. 1.43

```
      REAL M
      REAL MACH
      REAL K
C
C          PITOT PRESSURE CALIBRATION
C
      K=1.4
      WRITE(5,200)
  200 FORMAT(1H1,'PITOT PRESSURE RAKE MEASUREMENTS')
      WRITE(5,210)
  210 FORMAT(1HC,'STAG.PRESSURE    DISPLACEMENTS    MACH NUMBER',//,1X,
     C'   LBS/SQ.IN        HOR.X VER.Y')
      DO 10 N=1,3
      READ(8,100)X,Y,PP,PCS
  100 FORMAT(F5.2,F5.2,F10.2,F10.2)
      RAT=PCS/PP
      M=1.0
      AA=(K+1.0)/(2.0*K)
      AB=(K-1.0)/(2.0*K)
   16 AC=((M-1.0)*(M**2.0))+2.0
      AD=((K*1.0)*(M**2.0))
      AE=AC/AD
      AF=(AA*(RAT**(K-1.0))*(AE**(-K)))+AB
      MACH=AF**0.5
      EA=MACH-M
      IF(EA-0.01)110,110,120
  120 M=MACH
      GO TO 16
  110 WRITE(5,320)PCS,X,Y,MACH
  320 FORMAT(1H0,F10.3,8X,F6.2,F6.2,4X,F9.3)
   10 CONTINUE
      CALL EXIT
      END
```


SAMPLE SOLUTION

MACH NUMBER SOLUTION 2

PITOT PRESSURE RAKE MEASUREMENTS

STAG.PRESSURE LBS/SQ.IN	DISPLACEMENTS HOR.X	VER.Y	MACH NUMBER
58.670	15.00	20.00	2.772
23.800	16.00	20.00	3.235
59.670	15.00	20.00	2.776

INSTRUCTION PROGRAM FOR EQU. 1.44

```
      STAGNATION PRESSURE CALIBRATION

      REAL M
      REAL MACH
      REAL K
      K=1.4
      WRITE(5,150)
150   FORMAT(1H1,'STAGNATION PRESSURE CALIBRATION ON CENTRE-LINE')
      WRITE(5,200)
200   FORMAT(1H0,' HORIZONTAL DISPLACEMENT    MACH NUMBER      STAG
     CPRESSURES      ERROR',//,1H ,'    INCHES FROM THROAT
     C         CORRECT    RECORDED       PC-PR')
      DO 10 N=1,3
      READ(8,100)X,PS,PSS,PP,PPS
100   FORMAT(F5.2,F10.2,F10.2,F10.2,F10.2)
      P=(PS*PPS)/PSS
      RAT=P/PP
      M=1.0
      HA=(2.0/(K+1.0))
      HB=(-K+1.0)/K
      HC=(2.0*K)/(K+1.0)
      HD=(K-1.0)/(K+1.0)
      HE=1.0/K
      AA=RAT**HB
      AB=AA*HA
 16   AC=HC*(M**2.0)
      AD=(AC-HD)**HE
      AE=AB*AD
      MACH=AE**0.5
      BA=(MACH-M)
      IF(BA-0.01)110,110,120
120   M=MACH
      GO TO 16
110   BB=((K-1.0)/2.0)*(MACH**2.0)
      BC=(1.0+BB)**(K/(K-1.0))
      PCS=BC*P
      PE=PCS-PPS
      WRITE(5,210)X,MACH,PCS,PPS,PE
210   FORMAT(1H0,F14.2,15X,F6.3,10X,F6.3,4X,F6.3,6X,F6.3,' LBS/SQ.IN')
 10   CONTINUE
      CALL EXIT
      END
```


SAMPLE SOLUTION

MACH NUMBER SOLUTION 1

STAGNATION PRESSURE CALIBRATION ON CENTRE-LINE

HORIZONTAL DISPLACEMENT INCHES FROM THROAT	MACH NUMBER	STAGNATION PRESSURES CORRECT	RECORDED
1.50	2.562	52.442	57.200
1.60	2.502	72.732	49.700
17.00	3.083	76.615	54.230

1.12 THE PRINCIPLE OF SUPERSONIC DIFFUSERS

Consider perfectly isentropic supersonic flow whereby the fluid is accelerated to sonic velocity at the nozzle throat and then to the predetermined supersonic velocity in the wind-tunnel test-section. Complete static pressure regain is achieved by slowing down the flow isentropically to sonic velocity at the diffuser throat and then to the original stagnation pressure in the divergent duct. It follows that the nozzle and diffuser throats must be the same and that the wind-tunnel could run at design conditions indefinitely.

However, even for this theoretically perfect system, difficulties arise during start-up. In order to initiate flow in the tunnel, a pressure difference must be maintained across the system. As mentioned in, Chapter 1, part 1.2, as this pressure difference increases, a normal shock developes at the nozzle throat when this pressure difference becomes high enough, the shock propagates downstream through the diverging portion of the nozzle. Associated with this shock is a corresponding loss in stagnation pressure in the system. The result is such that the diffuser throat area must be increased to accommodate the flow for the worst condition of this normal shock. This worst possible cause, involving maximum loss in stagnation pressure, is that of a normal shock in the test-section (see figure 1.55(a)).

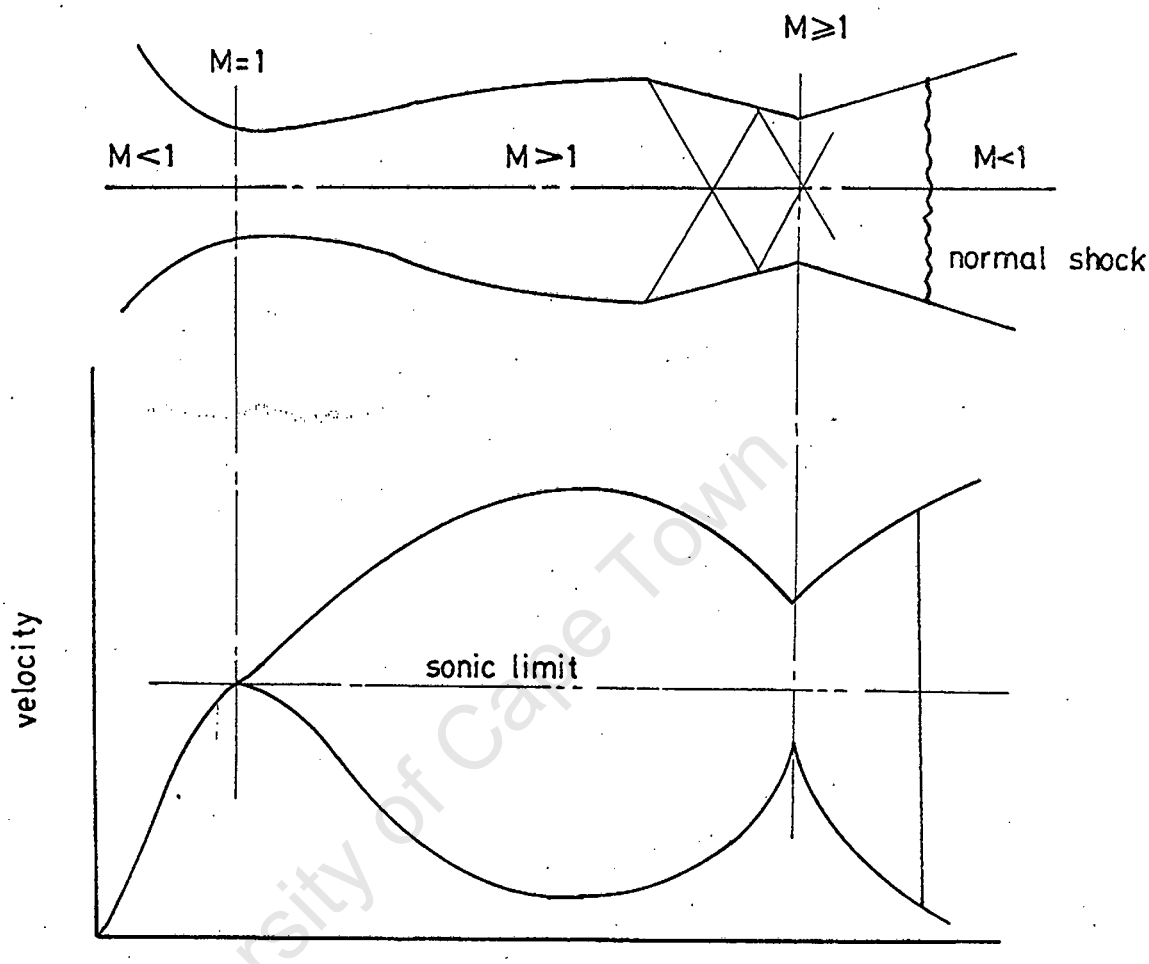

VELOCITY DIAGRAM

Figure 1·55

If the diffuser throat area is less than the critical amount the flow will chock and the shock will never reach the test-section.

For a correct diffuser throat area, the normal shock will 'jump' from the test-section to the equivalent area in the divergent portion of the diffuser. i.e. The shock is 'swallowed' by the diffuser (see figure 1.55 (b)).

In order to maximise the pressure recovery in the diffuser, the initial stagnation pressure can be reduced until the normal shock has been moved upstream to the diffuser throat, the position at which the shock strength is minimum.

1.12 FLOW PATTERN IN A PERFECT DIFFUSER

In practise, the flow within the supersonic diffuser is much more complicated than is initially assumed.

Firstly, the design of the diffuser is such that positive Mach waves are generated by the contraction of the diffuser inlet. These weak shocks reduce the flow velocity to the diffuser throat. Secondly, the subsequent expansion at the diffuser throat leads to a very complicated flow pattern in the divergent duct.

A study of this flow for a particular example is very useful in understanding the properties of stagnation pressure recovery.

Example:

Consider a wedge type, two-dimensional supersonic diffuser with an inlet Mach number of 2,35, a diffuser contraction angle of 3^{o} and an inlet height of 4 inches.

The flow patterns, resulting from these dimensions, have been fully developed for decreasing stagnation pressure in figures 1.56(a), (b) and (c) respectively.

(a) For a critical throat diffuser, the flow pattern developed for minimum 'start-up' is given in figure 1.56(a)

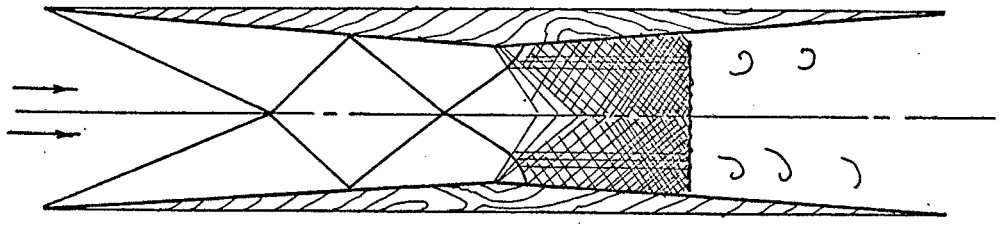

ⓐ starting conditions

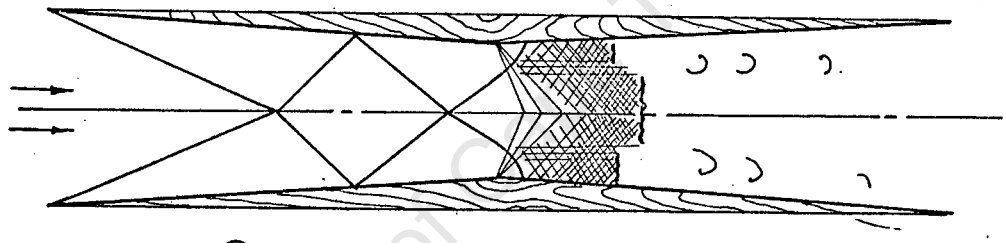

ⓑ reduced stagnation pressure

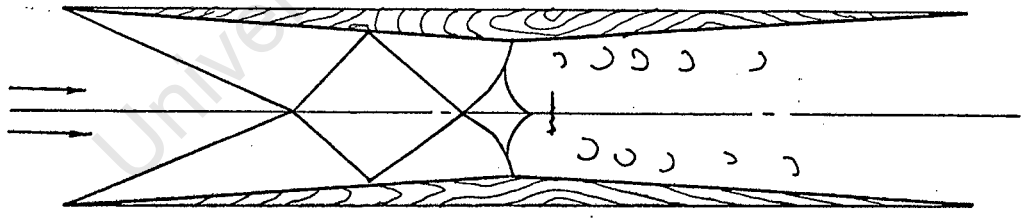

ⓒ complete pressure recovery

FLOW PATTERN IN DIFFUSER

Figure 1·56

The sharp cornered contraction, at the diffuser inlet, generates oblique shocks. These reflect backwards down the converging portion of the nozzle, reducing the flow velocity at each meeting.

A right-running expansion fan, formed at the diffuser throat, merges with the left-running oblique shock. (Considering the upper half). The oblique shock is strengthened by this iner-reaction and the curvature of this shock front generates vorticity. In the discrete wave pattern, this phenomenon is

represented by slip planes. Wavelets striking the slip planes are in part transmitted and part reflected. Thus more and more waves appear in the flow field, the net result being to distribute the non-uniformities on an ever finer scale. At large distances from the diffuser throat, the flow can be considered as uniform.

Eventually a normal shock will revert the whole flow to subsonic velocity.

(b) As the stagnation pressure is reduced, (see figure 1.56(b)), the normal shock moves upstream towards the diffuser throat. The flow irregularities caused by the shock-expansion fan inter-reaction are much greater here and the formation of the normal shock is likely to be upset.

(c) The maximum reduction in stagnation pressure, so that supersonic flow is still retained in the test-section is achieved when the normal shock is moved to the diffuser throat. This shock will merge with the oblique compression waves as in figure 1.56(c).

In the subsonic flow, the unsteadiness in the flow stream is quickly dissipated by turbulent mixing of the fulid.

1.3 BOUNDARY LAYER EFFECTS

Unfortunately, viscous effects present in fluids results in boundary layer development and subsequent alterations in the perfect flow patterns.

Unless separation occurs, or unless there are extraordinary pressure gradients, the potential flow external to the boundary layer is substantially independent of the boundary-layer flow. The only effect is that the flow streamlines are displaced outwards from the wall by the displacement thickness of the boundary layer.

But shock waves in the vicinity of solid boundaries tend to impose such large pressure gradients on the boundary layer, that the latter is distorted to a considerable extent. Also the effects of this inter-reaction is felt both upstream and downstream through the subsonic region of the boundary layer. Hence, where shocks must be considered together with a well developed boundary layer, a change in the original shock pattern will occur together with radical changes in the anticipated flow pattern.

Oblique Shocks

We shall consider that only a turbulent boundary layer exists at the point where shocks are present in the wind-tunnel.

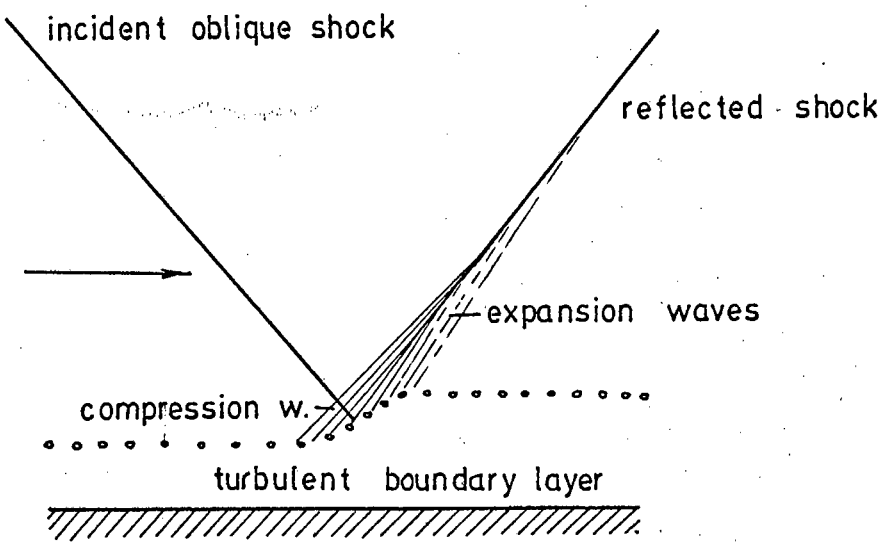

FIGURE 1.58

The incidence of an oblique shock upon the boundary layer leads to an increase in the pressure in the boundary layer upstream of the shock (see figure 1,58). This pressure rise leads to a thickening of the boundary layer, and the resulting streamline curvature generates compression wavelets that merge with the 'reflected shock'. The streamlines turn towards the original direction, this time generating expansion waves. These interact with the reflected shock reducing its strength slightly.

The points to be noted here are that the boundary layer thickness increases considerably after an oblique shock, and that the flow after this reflected shock has a slightly greater velocity than anticipated (3).

Normal Shocks

Normal shocks produce considerably greater pressure gradients than oblique shocks, so that the shock-boundary layer inter-reaction is intensified.

For a normal shock with a thick boundary layer, there is a series of bi-furcated normal shocks with the normal segment growing progressively shorter, until the stream is essentially subsonic (3) (See figure 1.59).

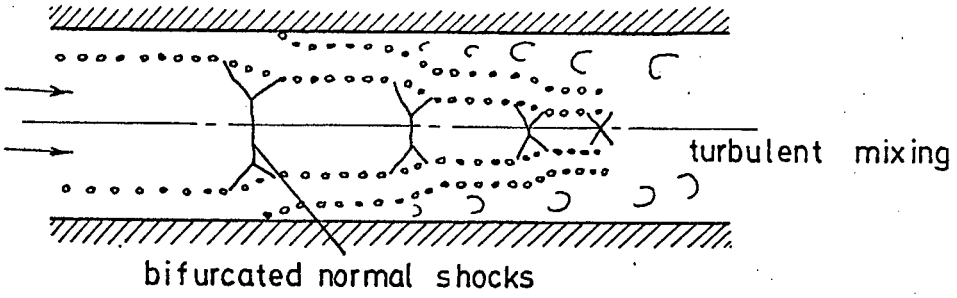

FIGURE 1.59

The duct cross-section is ultimately refilled by turbulent mixing of the fluid.

1.14 SUPERSONIC WIND-TUNNEL EFFICIENCY

A measure of the usefulness of the subsonic diffusers may be defined by their efficiency.

Figure 1.63 is the enthalpy-entropy diagram for a supersonic wind-tunnel without subsonic diffusion.

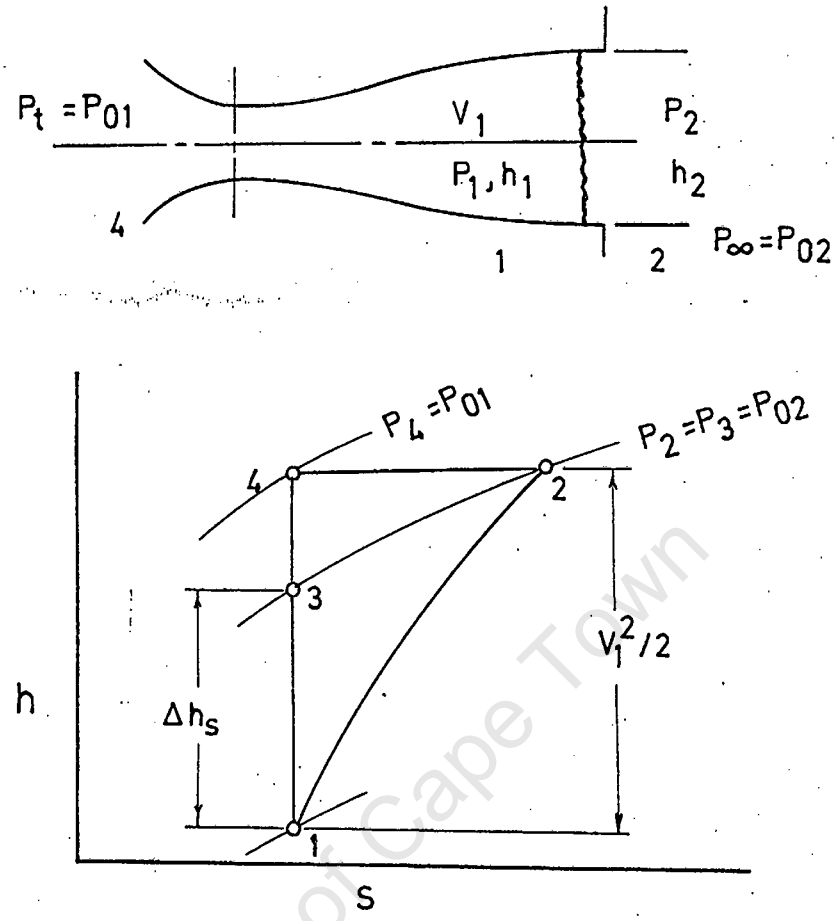

FIGURE 1.63

4 1: Isentropic acceleration of the fluid from zero velocity, with decreasing pressure and enthalpy.

1 2: Pressure regain, but with an increase in entropy across the normal shock.

The final enthalpy is the same as before, but there exists a loss in stagnation pressure. $(\Delta h)_s$ represents the enthalpy gain due to the normal shocks in the system.

The diffuser efficiency is given as:

$$\eta_d = \frac{(\Delta h)_s}{V_1^2/2} = \frac{h_3 - h_1}{h_2 - h_1} \quad \text{.....} \quad 1.51$$

The efficiency is defined as the ratio of the energy recovered by supersonic and subsonic diffusion, over the total kinetic energy of the fluid.

This may be rewritten as:

$$\eta_d = \frac{\left(\frac{\gamma-1}{2} M_1^2 + 1\right)\left(\frac{p_{o2}}{p_{o1}}\right)^{\frac{\gamma-1}{\gamma}} - 1}{\frac{\gamma-1}{2} M_1^2} \qquad \text{.....} \qquad 1.53$$

The equation in this form is very useful because the wind-tunnel efficiency is defined in terms of the test-section Mach number and the stagnation pressure ratio across the system

The enthalpy-entropy diagram for the complete sind-tunnel system is given in figure 1.64 assuming 100% efficient subsonic diffuser and neglecting boundary layer growth and oblique shock formation

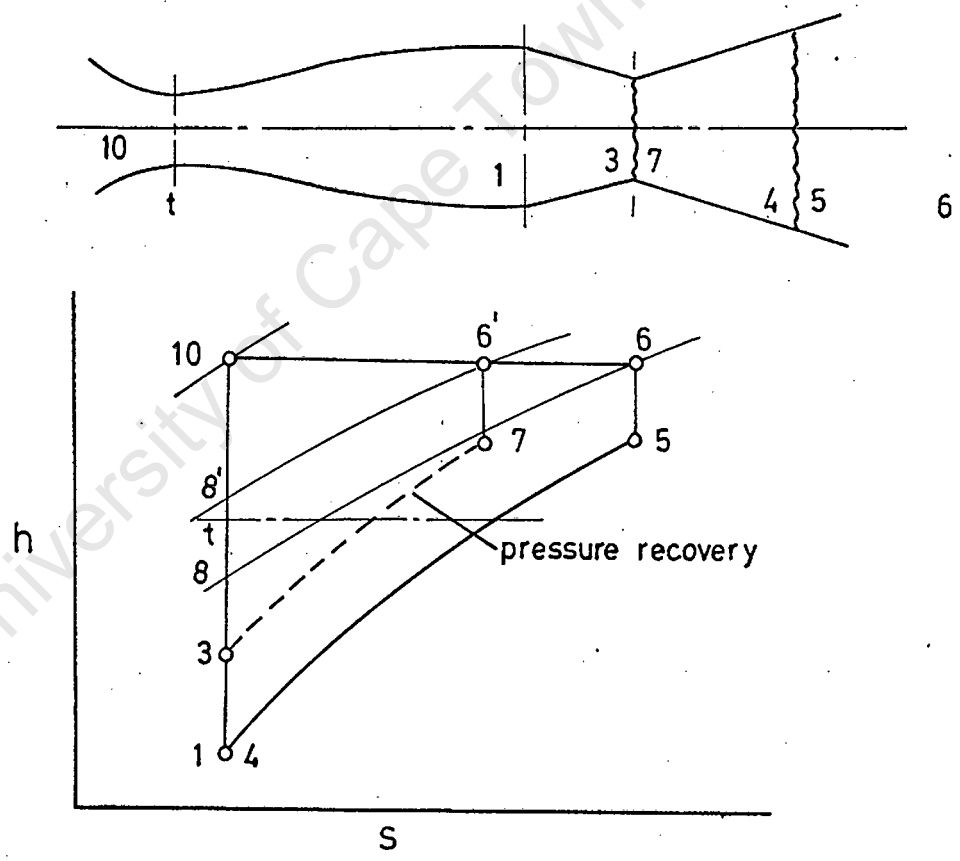

FIGURE 1.64

i.e. The flow in the system is isentropic except for the formation of the normal shock in the diffuser.

The entropy increase related to the stagnation pressure loss across this mormal shock is given as:

$$\frac{S_2 - S_1}{R} = -\log_e \frac{P_{o2}}{P_{o1}} \qquad \text{.....} \qquad 1.54$$

The factors that may influence the wind-tunnel efficiency in relation to the 'perfect' system are given below:

Oblique Shocks

An increase in entropy is associated with the oblique shock formation present because of the model support sting, the change in tunnel area after the test-section and the contraction of the diffuser inlet. The effect is to reduce the flow velocity and more points 2, 3 and 4 over to the right on the enthalpy-entropy diagram.

The final strength of the normal shock is reduced, but because the air velocity in the diffuser throat is also reduced, the degree of pressure recovery should not be adversely affected.

Boundary Layer

The entropy increase due to boundary layer growth moves points 1, 2, 3 and 4 to the right on the enthalpy-entropy diagram. There is also a decrease in the flow Mach number. (The free flow area is reduced by the displacement thickness of the boundary layer)

Although the reduced normal shock strength is advantageous, the necessary increase in the critical diffuser throat area, to allow this shock to pass, is a distinct disadvantage.

The result is that the degree of pressure recovery is greatly impared.

Subsonic Diffuser

It is very unlikely that the flow in the subsonic diffuser will be isentropic. Turbulence viscous effects and noise reducing screens, etc, will increase the stagnation pressure loss. Hence point 6, on the enthalpy-entropy diagram, will be moved to the right and the degree of subsonic static pressure recovery ($P_s - P_5$), will be reduced

APPENDIX 2

2.1 DEFLECTION EQUATION FOR A UNIFORMLY LOADED BEAM

+ ve bending moment
+ ve deflection

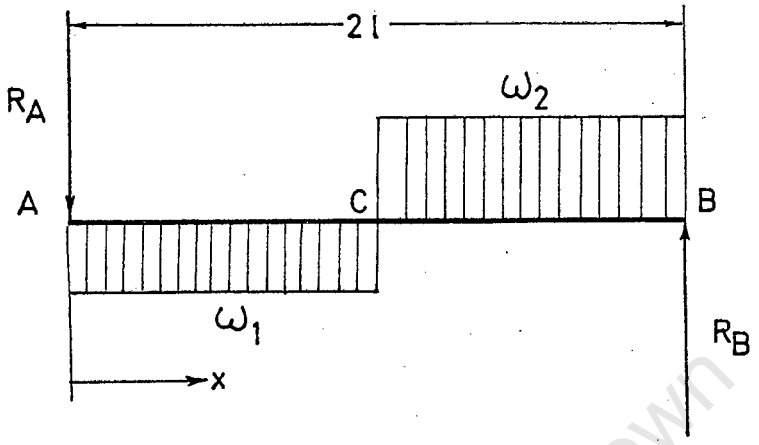

Taking moments about A:

$$\therefore \quad R_B = 2l + \omega_1 \frac{l.l}{2} = \omega_2 \frac{l\,3l}{2}$$

$$\therefore \quad R_B = \frac{3\omega_2 l}{4} - \frac{\omega_1 l}{4} \qquad \ldots\ldots\ldots\ldots\ldots\ldots\ldots\ldots \quad 1$$

Taking moments about B :

$$\therefore \quad R_A = 2l + \omega_2 \frac{l.l}{2} = \omega_1 l \frac{3l}{2}$$

$$\therefore \quad R_A = \frac{3\omega_1 l}{4} - \frac{\omega_2 l}{4} \qquad \ldots\ldots\ldots\ldots\ldots\ldots\ldots\ldots \quad 2$$

Derivation of deflection equations:

$0 < X < l$:

$$BM + \omega_1 X . \frac{X}{2} - R_A X = 0$$

$$\therefore \quad EI \frac{d^2y}{dX^2} = B.M = -\frac{\omega_1}{2} X^2 + R_A X$$

This equation must be integrated twice to find the deflection equation:

$$\therefore \quad EI \frac{dy}{dX} = (-\frac{\omega_1}{2}) . \frac{X^3}{3} + R_A . \frac{X^2}{2} + A \qquad \ldots\ldots\ldots\ldots\ldots \quad 3$$

$$EI\,y = \left(-\frac{\omega_1}{2}\right) \cdot \frac{X^4}{12} + R_A \frac{X^3}{6} + A_X + B \quad \ldots\ldots\ldots\ldots\ldots\ldots \quad 4$$

Where A and B are constants of integration.

$\underline{l < X < 2l}$

$$EI \frac{d^2y}{dX^2} = BM = \left(\frac{\omega_2}{2}\right) X^2 + (R_A - \omega_1 l - \omega_2 l)X + \frac{l^2}{2}(\omega_1 + \omega_2)$$

To simplify this equation let:

$$R_A - \omega_1 - \omega_2 = K_1$$

$$l^2/2\,(\omega_1 + \omega_2) = K_2$$

This equation is integrated twice to find the deflection equation:

$$EI \frac{dy}{dX} = \left(\frac{\omega_2}{2}\right) \frac{X^3}{3} + K_1 \frac{X^2}{2} + K_2 X + C \quad \ldots\ldots\ldots\ldots\ldots\ldots \quad 5$$

$$EIy = \left(\frac{\omega_2}{2}\right) \frac{X^4}{12} + K_1 \frac{X^3}{6} + K_2 \frac{X^2}{2} + CX + D \quad \ldots\ldots\ldots\ldots\ldots\ldots \quad 6$$

Where C and D are constants of integration.

$\underline{\text{Solutions of the constants of integration:}}$

The four unknown constants may be found by applying four boundary conditions to the above equations.

1. $y = 0$ at $X = 0$
2. $y = 0$ at $X = 2l$.
3. dy/dX same for equations 3 and 5 at $X = l$.
4. y same for equations 4 and 6 at $X = l$.

Applying the first boundary condition to equation 4:

$\therefore\ B = 0$

Applying the second boundary condition to equation 6:

$$\therefore\ 0 = \frac{16\omega_2 l^4}{24} + K_1 \frac{8l^3}{6} + K_2 \frac{4l^2}{2} + C2l + D$$

Substitute in the values of K_1 and K_2; and R_A:

$$\therefore D + 2Cl = -\frac{2}{3}\omega_1 l^4 \quad \ldots\ldots\ldots\ldots\ldots\ldots\ldots\ldots\ldots\ldots \quad 7$$

Applying the third boundary condition to equation 3 and 5 at $X = l$:

$$-\frac{\omega_1 l^3}{6} + R_A \frac{l^2}{2} + A = \frac{\omega_2 l^3}{6} + K_1 \frac{l^2}{2} + K_2 l + C$$

Eliminating K_1, K_2 and R_A gives:

$$A - C = \frac{l^3}{6}(\omega_1 + \omega_2) \quad \ldots\ldots\ldots\ldots\ldots\ldots\ldots\ldots\ldots\ldots \quad 8$$

Applying the final boundary condition to equations 4 and 6 where $X = l$.

$$\therefore -\frac{\omega_1 l^4}{24} + R_A \frac{l^3}{6} + Al = \left(\frac{\omega_2}{2}\right)\frac{l^4}{12} + K_1 \frac{l^3}{6} + K_2 \frac{l^2}{2} + Cl + D$$

Substitute in D from equation 7, and eliminate K_1, K_2 and R_A.

$$\therefore \quad A + C = \frac{\omega_2 l^3}{8} - \frac{13\omega_1 l^3}{24} \quad \ldots\ldots\ldots\ldots\ldots\ldots\ldots \quad 9$$

Final Solution:

From the three equations, (7, 8 and 9), the three unknowns A,C and D may be found:

$$A = \frac{7\omega_2 l^3}{48} - \frac{3\omega_1 l^3}{16}$$

$$C = -\frac{\omega_2 l^3}{48} - \frac{17}{48}\omega_1 l^3$$

$$D = \frac{1}{24}\omega_2 l^4 + \frac{1}{24}\omega_1 l^4$$

These constants may be substituted into equations 4 and 6 to give the deflection equations of the beam.

$0 \leq X \leq l$:

$$EIy = -\frac{\omega_1}{24} X^4 + \frac{R_A}{6} X^3 + \left(\frac{7}{48}\omega_2 l^3 - \frac{3}{16}\omega_1 l^3\right) X$$

$l \leq X \leq 2l$:

$$EIy = \frac{\omega_2}{24} \cdot X^4 + \frac{(R_A - \omega_1 l - \omega_2 l)}{6} \cdot X^3 + \frac{l^2}{4}(\omega_1 + \omega_2)X^2$$

continued

$$- \left(\frac{\omega_2 l^3}{48} + \frac{17\omega_1 l^3}{48} \right) . X + \left(\frac{\omega_2 l^4}{24} + \left(\frac{\omega_2 l^4}{24} \right) \right.$$

2.2 DEFLECTION EQUATION FOR A CONCENTRATED LOADED BEAM

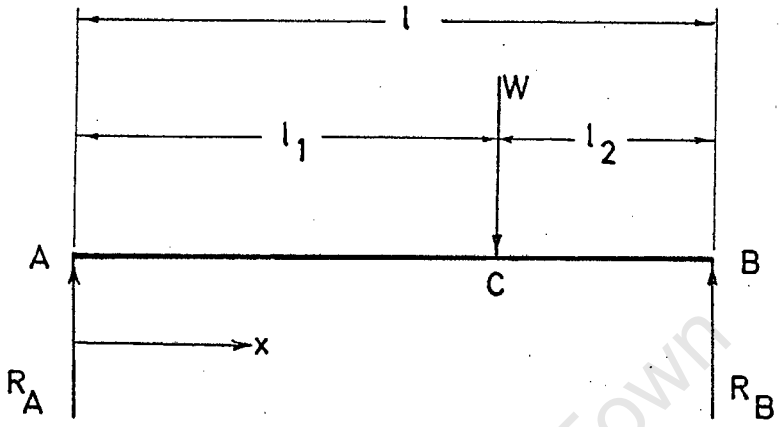

Taking moments about A:

$$\therefore \quad W l_1 = R_B l \quad ; \quad R_B = \frac{W l_1}{l} \quad \ldots\ldots\ldots\ldots\ldots\ldots\ldots\ldots \quad 1$$

Taking moments about B:

$$\therefore \quad W l_2 = R_A l \quad ; \quad R_A = \frac{W l_2}{l} = W\left(1 - \frac{l_1}{l}\right) \quad \ldots\ldots\ldots\ldots\ldots\ldots \quad 2$$

Derivation of deflection equations:

$0 < X < l_1$:

$$EI \frac{d^2y}{dX^2} = B.M = R_A X$$

Integrate twice to find the deflection equation:

$$EI \frac{dy}{dX} = \frac{R_A X^2}{2} + A \quad \ldots\ldots\ldots\ldots\ldots\ldots\ldots\ldots\ldots\ldots\ldots\ldots\ldots\ldots\ldots\ldots \quad 3$$

$$EI \, . \, y = \frac{R_A X^3}{6} + A_X + B \quad \ldots\ldots\ldots\ldots\ldots\ldots\ldots\ldots\ldots\ldots\ldots\ldots\ldots\ldots\ldots\ldots \quad 4$$

Where A and B are constants of integration.

$l_1 < X < l$

$$EI \frac{d^2y}{dX^2} = B.M = R_A X - WX + W l_1$$

$l_1 < x < l$

$$EI \frac{d^2y}{dx^2} = B.M = R_A x - wx + wl_1$$

Integrate twice to find the deflection equation

$$EI \frac{dy}{dx} = -(w-R_A)\frac{x^2}{2} + wl_1 x + C \quad \ldots\ldots 5$$

$$EIy = -(w - R_A)\frac{x^3}{6} + w l_1 \frac{x^2}{2} + Cx + D \quad \ldots\ldots 6$$

Where C and D are constants of integration.

Solutions of the constants of integration:

Applying the four boundary conditions to these equations to solve the four unknowns

1. $y = 0$ at $X = 0$
2. $y = 0$ at $X =$
3. dy/dX is the same for equations 3 and 5 at $X = l_1$.
4. y is the same for equations 4 and 6 at $X = l_1$.

Applying the initial conditions:

$\therefore B = 0$

Applying the second condition to equation 6:

$$\therefore D = (w - R_A)\frac{l^3}{6} w_1 \frac{l^2}{2} - Cl \quad \ldots\ldots 7$$

Applying the third boundary condition to equations 3 and 5 at $X = {}_1$:

$$A - C = R_A \frac{l_1^2}{2} - (w - R_A)\frac{l_1^2}{2} + wl_1^2$$

Substituting in R_A from equation 2.

$$\therefore A - C = \frac{wl_1^2}{2} \quad \ldots\ldots 8$$

Finally, applying the fourth boundary condition to equations 4 and 6 at $X = {}_1$:

$$\therefore Al_1 - C(l_1 - l) = -\frac{wl_1 l^2}{3} + \frac{wl_1^3}{3} \quad \ldots\ldots 9$$

Multiply equation 8 by l_1:

$$\therefore A l_1 - C l_1 = \frac{W l_1^3}{2}$$

Subtract this from equation 9:

$$\therefore C = \frac{W l_1 l}{3} - \frac{W l_1^3}{6l} \qquad \ldots\ldots 10$$

Similarly:

$$A = \frac{W l_1^2}{2} - \frac{W l_1 l}{3} - \frac{W l_1^3}{6l} \qquad \ldots\ldots 11$$

Final Solution:

The four know solutions to the constants of integration may be substituted into equations 4 and 6 to give the complete deflection equations.

$0 < X < l_1$:

$$EIy = \frac{R_A}{6} \cdot X^3 + W\left(\frac{l_1^2}{2} - \frac{l_1 l}{3} - \frac{l_1^3}{6l}\right) X$$

$l_1 < X < l$:

$$EIy = -\frac{W}{6}\,\frac{l_1}{l} \cdot X^3 + \frac{W l_1}{2} \cdot X^2 - W\left(\frac{l_1 l}{3} + \frac{l_1^3}{6l}\right).X + \frac{W l_1^3}{6}$$

2.3 PROGRAMME FOR MATRIX SOLUTION

INSTRUCTION PROGRAM

```
C
C          SOLUTION TO THE DEFLECTION MATRIX FOR THE STATICALLY
C          INDETERMINATE BEAM
C
      DIMENSION A(5,6),J(6)
      READ(8,100)((A(I,J),J=1,6),I=1,5)
  100 FORMAT(6F10.4)
      CALL JIM(A,5,6,NR,$50,J,5)
      WRITE(5,400)
  400 FORMAT(1HO,'     THE JACK LOADS REQUIRED TO NULLIFY DEFLECTION')
      WRITE(5,150)(I,A(I,6),I=1,5)
  150 FORMAT(1HO,'LOAD AT POINT ',I2,' IS',F8.4,' LBS')
      GO TO 250
   50 WRITE(5,200)
  200 FORMAT(1HO,'SOLUTION TO MATRIX REJECTED')
      GO TO 250
  250 CALL EXIT
      END
```

SOLUTION OUTPUT

```
      THE JACK LOADS REQUIRED TO NULLIFY DEFLECTION

LOAD AT POINT  1 IS-32.2928 LBS

LOAD AT POINT  2 IS-34.1568 LBS

LOAD AT POINT  3 IS 13.7290 LBS

LOAD AT POINT  4 IS 60.5596 LBS

LOAD AT POINT  5 IS 65.7151 LBS
```

APPENDIX 3

3.1 CONTROL UNIT SPECIFICATIONS

Shut-Down Piston:

Weight 1,75 lbs

Frictional Resistance 9,0 lbs.

Valve:

Weight 18,5 lbs

Diaphragm area 12,6 sq.inches

Travel 0,246 inches.

Damping Cylinder:

Bypass No.	Camping Coefficient C_D	Type
0	123,711	linear
1	91,418	$\frac{lb}{ft}$ sec
2	51,569	
3	1,664,441	
4	928,246	non-linear
5	216,128	
6	114,021	$\frac{lb}{ft^2}$ sec^2
7	74,260	
8	54,235	
10	29,372	
14	5,527	
Open	1,774	

Speed of sound in oil

$$c = \sqrt{\frac{E}{\rho}}$$

Where E = bulk modulus = 225×10^3 lbs per sq.inch

For a S.G of 0,86 for velocite, the density of the oil ρ_{oil} = 1,65 slugs per cubic ft.

$\therefore$ c = 4,430 ft per second

3.2 CONTROL COEFFICIENTS AND CONSTANTS

Valve:

A = diaphragm area = 12,57 sq.inches.

W = valve weight = 18,5 lbs.

g = gravitational acceleration = 32,2 ft/sec^2

K_1 = valve mass flow rate coefficient
= 4,7532 x 10^{-2} lbm ft/sec lbf.

C_D = damping coefficients (lbf sec/ft or lbf sec^2/ft^2)

Storage Drum:

R = universal gas content = 53,3 ft lbf/lb^oR

T_d = drum temperature = 550^oR

V_d = drum volume = 165 cu ft

P_i = Initial drum pressure = 150 p.s.i.g.

Settling Chamber:

V_s = settling chamber volume = 4.2 ft^3

T_s = settling chamber temperature = 550^oR

Nozzles:

K_2 = Nozzle mass flow rate coefficient.

Mach Numver	$K_2 \frac{lbm\ ft^2}{sec\ lbf}$
2,0	7,467 x 10-4
2,35	5,492 x 10^{-4}
2,5	4,789 x 10^{-4}
3,0	2,973 x 10^{-4}

3.2 SOLUTION TO CUBIC EQUATION

The solution to the cubic equation 3.11 may be achieved in two ways:

1. This equation may be rewritten as:

$$C_1X^3 + C_2X^2 + C_3X + C_4 = y$$

This is poltted in figure 3.1 for different damping coefficients. The three roots are found at y = 0.

This approach is satisfactory when all the roots are real and one is very large.

2. For the more accurate estimation of the roots, especially when the roots are imaginary, the small Olivetti desktop computer may be used.

The cubic equation must be rewritten as:

$$D^3 + C_{12} D^2 + C_{13} D + C_{14} = 0$$

Where : $$|C_{12}| = \left|\frac{C_2}{C_1}\right| \leqslant 10$$

$$|C_{13}| = \left|\frac{C_3}{C_1}\right| \leqslant 100$$

$$|C_{14}| = \left|\frac{C_4}{C_1}\right| \leqslant 1\ 000$$

These limitations to the magnitude of the input coefficients may be overcome by multiplying the variable D by a constant that sufficiently reduces these coefficients. The outputs of the computer, which are the roots of this equation, must be divided by the constant to bring them to their correct values.

The following table is a summary of the equation coefficients and the resulting roots:

Damping Coeft. $\frac{lbf}{ft}$ sec	C_{12}	C_{13}	C_{14}	Roots of Characteristic Equation
0	$0{,}005213 \times 10^2$	0	$11{,}98 \times 10^5$	-108,0; $+ 51{,}4 \pm 91{,}95_i$
100	$1{,}793 \times 10^2$	$9{,}074 \times 10^2$	$11{,}98 \times 10^5$	$- 203{,}7$; $+ 12{,}2 \pm 75{,}7_i$
1 000	$1{,}746 \times 10^3$	$9{,}074 \times 10^3$	$11{,}98 \times 10^5$	-1,741;
10 000	$1{,}741 \times 10^4$	$9{,}074 \times 10^4$	$11{,}98 \times 10^5$	$-2{,}41 \pm 26{,}12_i$ -17,405; $-2{,}605 \pm 7{,}87_i$

The instruction programme for the digital computer is given below for imaginary roots solution, together with an example of the output data.

3.4 SOLUTION TO RESPONSE EQUATION

Example 1: Damping coefficient 100,000 $\frac{lb}{ft}$ sec

From equation 3.12:

$$P_s = P_{total} + B_1 e^{-173{,}995t} + B_2 e^{-2{,}605t}$$

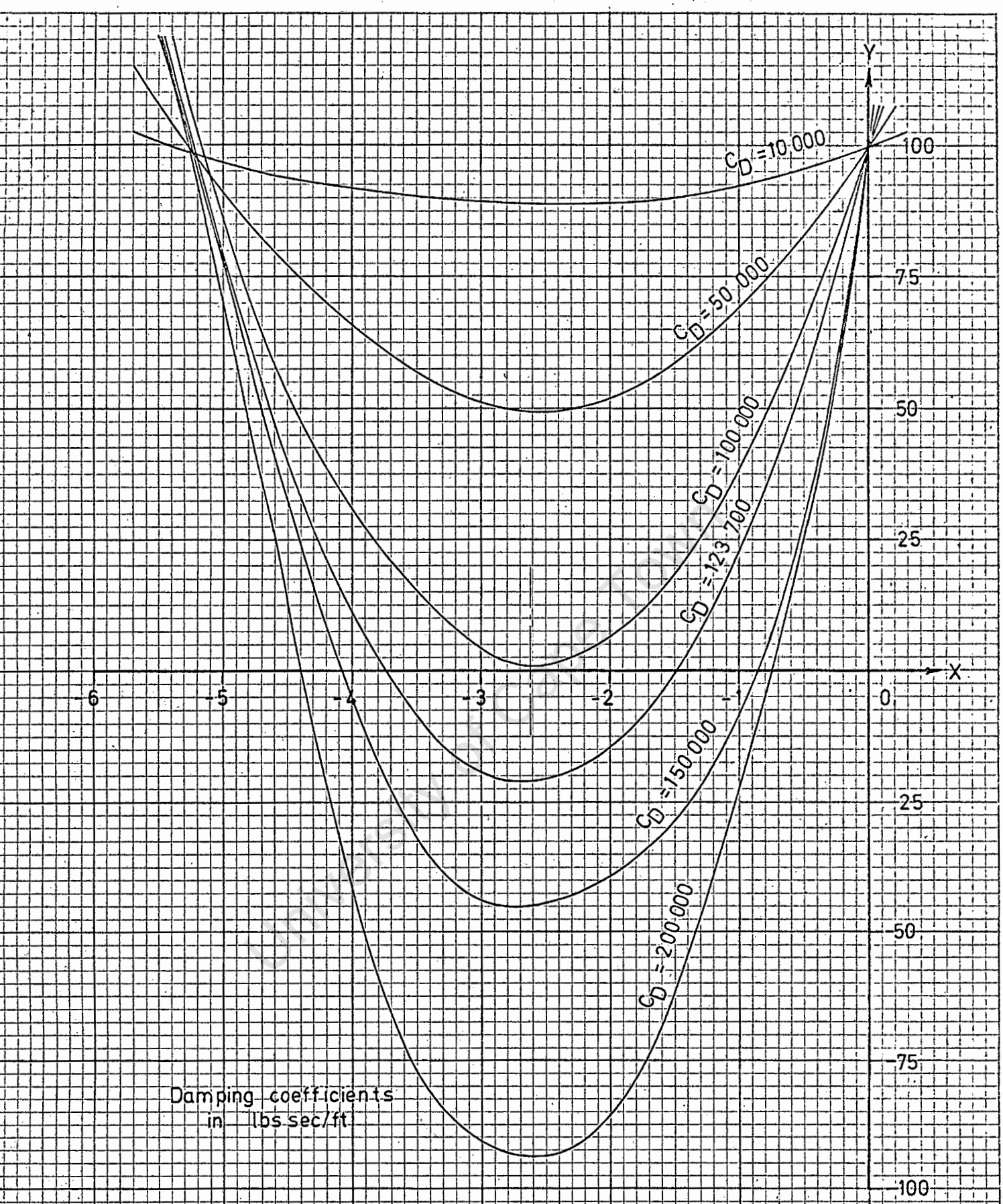

GRAPH OF THE CHARACTERISTIC EQUATION

$$C_1 x^3 + C_2 x^2 + C_3 x^1 + C_4 = y$$

FIGURE A3.1

OLLIVETTI INSTRUCTION PROGRAM

for solution to cubic equation

```
V
S
B↑
 S
C↑
 S
D↑
B↓
d÷
AX
B↕
b↑
 X
C-
A-
 -
B↕
A+
bX
C↕
 X
D-
C↕
C-
C↕
C√
B↓
 -
A√
 -
c↕
C↓
/V

c↕
 +
c↕
aV
d↓
A+
/0
aY
D↕
c↓
AX
dX
D+
c↕
AX
 X
A+
C-
A0
c÷
c↕
D↓
A÷
 ↕
 -
/Y
/0
c-
/Z
 ↕
/Z
B-
B↕
 Z

aZ
C↓
c÷
B↕
A7
D↓
d-
D↕
c↓
D÷
AX
C↑
B+
/W
A-
 -
A√
A0
C↓
b-
A0
/0
aW
c↓
b-
A0
/0
 V
 S
```

SAMPLE OUTPUT $C_D = 1000 \frac{\text{lbs sec}}{\text{ft}}$

			$C_D = 10000 \frac{\text{lbssec}}{\text{ft}}$
1·746	S	input coordinates	1·741
0·009074	S		0·0009074
0·001198	S		0·0000011[illegible]
-7·16903219	A0	converging itteration	-7·18112[illegible]
-4·24200945	A0		-4·2505[illegible]
-3·56416259	A0		-3·57206[illegible]
-3·50587875	A0		-3·51381[illegible]
-3·50539827	A0		-3·51334622
-3·50539821	A0		-3·51334616
output roots			
0·02611991	A0	imaginary roots imag.	0·00078[illegible]
-0·00240813	A0	real	-0·00026048
-1·74116375	A0	real root	-1·7404798[illegible]

Applying the boundary conditions to solve the two unknowns:

1. $P_s = 0$ at $t = 0$

$$\therefore \quad B_1 + B_2 = - P_{total} \quad \ldots\ldots\ldots\ldots\ldots\ldots\ldots\ldots\ldots\ldots\ldots\ldots \quad 1$$

2. $\frac{dP_s}{dt} = 0$ at $t = 0$

$$\therefore \quad - 173{,}995\ B_1 = 2{,}605\ B_2 \quad \ldots\ldots\ldots\ldots\ldots\ldots\ldots\ldots\ldots\ldots\ldots\ldots \quad 2$$

From this equation, it may be seen that $B_1 \lessapprox B_2$.

Therefore $B_1 \approx 0$ and $B_2 \approx P_{total}$

Substitute into the initial equation

$$\therefore \quad P_s = P_{total} - P_{total}\, e^{-2{,}605\ t}$$

Example 2: Damping coefficient 10,000 $\frac{lb}{ft}$ sed

From equation 3.12

$$P_s = P_{total} + B_1 e^{-17{,}405t} + B_2 e^{-(2{,}605 + 7{,}87_i)t} + B_3 e^{-(2{,}605 - 7{,}87_i)t}$$

This equation may be rewritten as:

$$P_s = P_{total} + B_1 e^{-17{,}405t} + Be^{-2{,}605} \sin(7{,}87t + \psi)$$

Applying the boundary conditions to solve the three unknowns B_1, B and ψ:

1. $P_s = 0$ at $t = 0$:

$$\therefore \quad B_1 + B \sin\psi = - P_{total} \quad \ldots\ldots\ldots\ldots\ldots\ldots\ldots\ldots\ldots\ldots\ldots\ldots \quad 3$$

2. $\frac{dP_s}{dt} = 0$ at $t = 0$:

$$\therefore \quad 0 = -17{,}405\ B_1 + (-2{,}605)\ B \sin\psi + (7{,}87)\ B \cos\psi \quad \ldots\ldots\ldots\ldots\ldots\ldots\ldots\ldots \quad 4$$

3. $\frac{d^2p_s}{dt^2} = 0$ at $t = 0$:

$$\therefore \quad 0 = (17,405)^2 B_1 + B \sin\psi \ (2,605^2 - 7,87^2)$$

$$+ B \cos\psi \ 2 \times (-2,605)\times(7,87) \quad \ldots\ldots\ldots\ldots\ldots \quad 5$$

These three equations may be used to solve for the three unknowns. The value of B_1 is very small and may be neglected.

The final equation may be written as:

$$p_s = p_{total} - \frac{p_{total}}{0,9494} \cdot e^{-2,605} \sin\left(\frac{180\times7,87}{}\ t^o + 71^o42'\right)$$

3.5 MAGNITUDE SCALE FACTORS

The maximum values of all the variables in the control analysis are given below together with the most suitable scale factors.

Maxima	Chosen scale factors
$\hat{p}_{sett} = 60$ p.s.i.g.	$a_{p_{sett}} = 0,1$
$\hat{\ddot{x}} = 1,090$ ft/sec^2	$a_{\ddot{x}} = 0,008$
$\hat{\dot{x}} = 3,37$ ft/sec	$a_{\dot{x}} = 2,83$
$(\hat{\dot{x}})^2 = 11,4$ ft^2/sec^2	$a_{(\dot{x})^2} = 0,8$
$\hat{x} = 0,0104$ ft	$a_x = 283,0$
$\hat{\dot{p}}_s = 1,140 \frac{lb}{in^2 sec}$	$a_{\dot{p}_s} = 0,008$
$\hat{p}_s = 100$ p.s.i.g.	$a_{p_s} = 0,08$
$\hat{p}_d = 150$ p.s.i.g.	$a_{p_d} = 0,05$

Where $a.|x|_{max} \leqslant 10$ volts.

REFERENCES

1. J. RUPTASH, "Supersonic Wind-tunnels - Theory, Design and Performance", U.T.I.A. Review, No. 5, 1952.

2. A.E. Puckett, "Supersonic nozzle Design", Journal of Applied Mechanics Dec. 1946

3. A.H. SHAPIRO, The Dynamics and Thermodynamics of compressible fluid flow, Volume I and II, Ronald Press Company, 1953.

4. E.W.E. Rogers and Miss B.M. Davis, "A Note on Turbulent Boundary Layer allowances in Supersonic Nozzle Design," A.R.C. Tech. Report, CP No. 333, 1957.

5. H. Altman, "An experimental investigation of the turgulent boundary layer in supersonic airflow", M.Sc. (Eng.) Thesis , Department of Mechanical Engineering, University of Cape Town, 1965.

6. P. Harrop, P.I.F. Bright, J. Salmon, M.T. Caiger, "The design and testing of Supersonic Nozzles", A.R.C. Tech Report, R + M No. 2712, May, 1950.

7. W.B. Fallis, G.W. Johnston, J.D. Lee, N.B. Tucker, J.H. Wade, "The Design and Calibration of the Institute of Aerophysics 16" x 16" Supersonic Wind-Tunnel", U.T.I.A. Report, No. 15, March, 1953.

8. J. Ludasiewicz, "Diffusers for supersonic wind-tunnels". Journal of the aeronautical sciences, September, 1953.

9. P. Dransfield, Engineering Systems and Automatic Control, Prentice-Hall Inc.

10. G.R. Peterson, Basic analogue computation, Collier-Macmillan Ltd.

11. R. Gayland, "Performance of a Supersonic Blowdown Wind-tunnel", B.Sc.(Eng) Thesis, University of Cape Town, 1962.

12. H. Altman, "Supersonic Wind-Tunnel", B.Sc. (Eng) Thesis, University of Cape Town, 1963.

13. J.E.A. John, Gas Dynamics, Allyn and Bacon.

14. G.K. Batchelor, F.S. Shaw, "A consideration of the design of wind-tunnel contractions", A.R.A. Report, No. 4, March, 1944.

15. L. Rosenhead (Chairman of the compressible flow tables panel), A selection of tables for use in calculations of compressible airflow, Oxford, 1952.

16. Mark's Standard Handbook for Mechanical Engineers, Baumeister.

17. E.P. Popov, Mechanics of Materials.

18. R.V. Giles, Fluid Mechanics and Hydraulics, Second Edition, Shawn Publication Company

19. Den Hartog, Mechanical Vibrations, 3rd Edition, McGraw-Hill book company.

20. D.B. Spalding, E.H. Cole, Engineering Thermodynamics, 2nd Edition, Edward Arnold (Publishers).

The following publications were generally referred to in the compilation of this thesis:

21. P.H. Oosthuizen, "The Design and construction of a small blowdown wind-tunnel", The South African Mechanical Engineer, November, 1965.

22. A.J. Van Wyk, "Wind-tunnel facilities at the national mechanical engineering research institute", C.S.I.R. Report, M.E.G. 983.

23. G. Deane, "Just a Detail", The Engineer, Sept. 4, 1964.

24. "Supersonic Design Studies - Co-operative Wind-Tunnel", Engineering, February 6, 1959.

25. W.A. Martin, "An experimental study of the Boundary Layer behind a moving plane shock wave", U.T.I.A. Report , No. 47. May, 1957.

26. S. Pai, Introduction to the theory of compressible flows, van Nostrand.

27. W.D. Snowball, "Blowdown Wind-Tunnel", B.Sc. (Eng) Thesis, University of Cape Town, 1963.

28. I.S. Smith, "Supersonic Wind-Tunnel", B.Sc. (Eng) Thesis, University of Cape Town, 1962.

29. F.H. Raven, Automatic Control Engineering, International student edition, McGraw-Hill book company.